VENTED GAS EXPLOSIONS

By

Rafiziana Md.Kasmani

Submitted in accordance with the requirements for the degree of Doctor of Philosophy

University of Leeds

School of Process, Environmental and Materials Engineering

Under the supervision of

Professor G.E.Andrews, PhD, B.Sc,C.Eng, M.I.MechE, SMAIAA, MASME, MSAE

and

Dr.H.N.Phylaktou, Phd, B.Eng

September 2008

The candidate confirms that the work submitted is her own and that appropriate credit has been given where reference has been made to the work of others

ABSTRACT

Explosion venting technology is widely accepted as the effective constructional protection measures against gas and dust explosions. The key problem in venting is the appropriate design of the vent area necessary for an effective release of the material i.e. the pressure developed during explosion did not cause any damage to the plant protected. Current gas explosion vent design standards in the USA (NFPA68, 2002) and European (2007) rely on the vent correlation first published by Bartknecht in 1993 (Siwek, 1996). NFPA 68 also recommends the correlation of Swift (Swift, 1983) at low overpressures. For a vent to give no increase in overpressure other than that due to the pressure difference created by the mass flow of unburnt gases through the vent, the vent mass flow rate is assumed to be equal to the maximum mass burning rate of the flame and this consideration should be used as the design mass flow through the vent. Two different methods (Method 1 and Method 2) have been proposed based on the S_u and S_u (E-1) to describe the maximum mass burning rate given as,

$$m_b = A_s S_u \rho_u = C_d \varepsilon A_v (2\rho_u P_{red})^{0.5} \quad (1)$$

$$m_b = A_s S_g \rho_u = A_s S_u (E-1) \rho_u = C_d \varepsilon A_v (2\rho_u P_{red})^{0.5} \quad (2)$$

The equation given in (2) is slightly different from (1) as is about 6.5 times the mass flow of the first method as it takes the effect of (E-1) where E is the expansion ratio.

A critical review were carried out for the applicability, validity and limitation on the venting correlations adopted in NFPA 68 and European Standard with 470 literature experimental data, covering a wide range of values for vessel volume and geometries, bursting vent pressure, P_v, L/D ratio, maximum reduced pressure, P_{red} and ignition location. The fuels involved are methane, propane, hydrogen, town gas, ethylene, acetone/air mixtures with the most hazardous near-stoichiometric fuel-air concentration. Besides, Molkov's equation (Molkov, 2001) which is regarded as alternative venting design offered in NFPA 68 and Bradley and Mitcheson's equation for safe venting design were also analysed on the experimental data for their validity and limitation as well as the proposed methods.

From the results, it is clear that Bartknecht's equation gave a satisfactory result with experimental data for K <~5 and Swift's equation (Swift, 1983) can be extended to wider range for P_{red} > 200 mbar, providing the parameter P_v is added into the equation. Method 2 gave a good agreement to most of the experimental data as it followed assumptions applied for correlations given by Bradley and Mitcheson for safe venting design (Bradley and Mitcheson, 1978a, Bradley and Mitcheson, 1978b).It is also proven that the vent coefficient, K is confident to be used in quantifying the vessel's geometry for cubic vessel and the use of As/Av term is more favourable for non-cubic vessels.

To justify the validity and applicability of the proposed methods, series of simply vented experiments were carried out, involving two different cylindrical volumes i.e. 0.2 and 0.0065 m^3. It is found that self acceleration plays important role in bigger vessel in determining the final P_{max} inside the vessel. Method 2 gave closer prediction on P_{max} in respect with other studied correlations.

The investigation of vented gas explosion is explored further with the relief pipe been connected to the vessel at different fuel/air equivalence ratios, ignition position and P_v. The results demonstrate that the magnitude of P_{max} was increased corresponding to the increase of P_v. From the experiments, it is found that peak pressure with strong acoustic behaviour is observed related to increase in P_v and in some cases, significant detonation spike was also observed, particularly in high burning velocity mixtures. It is found that substantial amount of unburnt gases left inside the vessel after the vent burst is the leading factor in increase of P_{max} for high burning velocity mixtures at centrally ignited. The associate gas velocities ahead of the flame create high unburnt gas flows conditions at entry to the vent and this give rise to high back pressures which lead to the severity in final P_{max} inside the vessel.

It was observed that end ignition leads to a higher explosion severity than central ignition in most cases, implying that central ignition is not a worst-case scenario in gas vented explosions as reported previously

CONTENTS

Abstract i

Contents iii

List of figures vii

List of tables xii

Nomenclature xiii

Acknowledgements xv

Publications by author xvi

CHAPTER 1 – VENTED GAS EXPLOSION –THE RESEARCH

1.0 Introduction 1

1.1 Venting gas explosions 2

1.1.1 General overview 2

1.2 Overview of the project studies 8

1.2.1 Simply venting gas explosions 9

1.2.1.1 Self-acceleration of spherical flames 12

1.2.1.2 Implication of the objectives to the present study 14

1.2.2 Vented gas explosion with relief pipe attached. 14

1.2.2.1 The influence of duct pipe diameter 17

1.2.2.2 Implication of the objectives to the present study 17

CHAPTER 2-EXPERIMENTAL SET-UP AND MEASUREMENT TECNIQUES

2.1 Test facility 19

2.2 Apparatus design considerations 19

2.2.1 Test vessels 21

2.2.2 Dump vessel 23

2.3 Construction details 23

2.3.1 Test vessels 23

2.3.2 Dump vessel 29

2.4 Vent cover selection 33

2.5 Instrumentation and data collection.....34
2.5.1 Instrumentation techniques.....34
2.5.1.1 Explosion pressure history.....35
2.5.1.2 Measurement of flame positions.....35
2.5.1.3 Thermocouples.....36
2.5.1.4 Flame speed calculation.....37
2.5.2 Data acquisition.....39
2.6 Identification hazards and safety measures.....39
2.6.1 Vessel failure.....40
2.6.2 Transmission of the explosion to auxiliary equipment.....40
2.6.3 Release of combustible gas into the Test room.....41
2.7 Operating procedures.....41
2.7.1 Fuel entrainment.....41
2.7.2 Ignition procedure.....42
2.7.3 Vessel purging.....42
2.8 Ancillary equipment.....42
2.8.1 Isolation valves and pipe works.....43
2.8.2 Mixture pressure monitoring system.....43
2.8.3 Vacuum gate valve.....47
2.8.4 Evacuation system.....47
2.8.4.1 Vacuum pump A.....47
2.8.4.2 Vacuum pump B.....47
2.8.5 Ignition system.....48
2.8.6 Nitrogen purging system.....48

CHAPTER 3-VENTED GAS EXPLOSIONS: THEORY AND CRITICAL REVIEW

3.0 Introduction.....50
3.1 Parameter involved in empirical equations.....51
3.2 Venting mechanism.....53
3.3 Venting theory.....58
3.4 Comparison of Bartknecht and Swift correlations as been adopted in NFPA 68 using derived methods on the same basis.....71
3.5 Review of the published experimental data.....74

3.5.1 Comparison of Bartknecht and Swift's correlations with published experimental data. 76
3.5.2 The influence of turbulent enhancement factor, β 80
3.5.3 The influence of the vessel's geometry.....85
3.5.4 Comparison between K and A_s/A_v term for vessel's geometries 90
3.5.5 Evidence for an additional influence of vessel volume on P_{red} 93
3.6 Concluding remarks.....96

CHAPTER 4-SIMPLY VENTED GAS EXPLOSION: THE PRACTICAL

4.0 Introduction 98
4.1 General features of experimental tests.....99
4.2 General explosion development 102
4.2.1 Results and discussions on Test vessel 1 104
4.2.1.1 Maximum pressure, P_{max} as a function of equivalence ratio 104
4.2.1.2 Flame speeds.....108
4.2.2 Results and discussion on Test vessel 2.....116
4.2.2.1 Maximum pressure, P_{max} 116
4.2.2.2 Flame speeds.....119
4.3 Deflagration to detonation in test vessel.....122
4.4 Influence of vent coefficient, K, volume and burst vent pressure, P_v on P_{max} ..126
4.5 Comparison between theory and experimental data.....134
4.6 Concluding remarks.....138

CHAPTER 5-VENTED DUCT GAS EXPLOSIONS

5.0 Introduction 140
5.1 Phenomenology of vessel vented through the duct 143
5.1.1 Effect of the relief duct fitted to the test vessel 145
5.1.2 The influence of static bursting pressure, P_v on maximum pressure, P_{max} 149
5.1.3 The influence of ignition position.....153
5.1.4 The acceleration of flame towards the vent duct and associated vent velocities 157
5.1.5 The duct flame speeds and gas velocities.....176

5.2 The influence of equivalence ratio on P_{max} 179
5.3 Comparison with other experimental data 183
5.4 Concluding remarks 185

CHAPTER 6- VENTED DUCT GAS EXPLOSIONS WITH BIGGER DIAMETER PIPE ATTACHED

6.0 Introduction 187
6.1 Effect of duct diameter on P_{max} 189
6.2 Flame speeds analysis 203
6.3 Pressure loss and unburnt gas velocity 207
6.4 Concluding remarks 212

CHAPTER 7- CONCLUSIONS AND RECOMMENDATIONS FOR FUTURE WORKS

7.0 Summary of major findings 214
7.1. General effects of venting explosions 214
7.1.1 Comparison of theory and experimental results 215
7.1.2 Duct vented gas explosion 216
7.2 Recommendation for the future work 218

REFERENCES 221

APPENDIX 230

LIST OF FIGURES

Figure 1.1 Example of commercial vent covers and its application 12
Figure 2.1 Schematic picture of test facility and control room 20
Figure 2.2 Schematic drawing for Test vessel 1 and 2 26
Figure 2.3 Scaled drawing of Test vessel 3 with pipe attached 27
Figure 2.3a Scaled drawing of pipe section for Test vessel 3 28
Figure 2.3b Scaled drawing of pipe section for Test vessel 3 29
Figure 2.4 Dump vessel schematic designs 32
Figure 2.5Vent covers used in the tests. From top left: Melinex membrane, aluminium foil. From bottom left: 100g A4 paper and magazine paper 34
Figure 2.6 Typical thermocouple traces indicating the change in voltage output due to flame arrival 36
Figure 2.7 Exposed junction, mineral insulated type-K thermocouples inside the rig. 37
Figure 2.8 Flow diagram illustrating safety and operational procedure 44
Figure 2.9 Example of operating procedure for carrying explosion tests 46
Figure 3.1 Pressure behaviour versus time for a closed and vented explosions 53
Figure 3.2 The pressure-time variation in a vented explosion. Graph reproduced from Cooper et al (Cooper, Fairweather and Tite, 1986) 57
Figure 3.3 Bartknecht data for propane-air at different volumes at E = 10J, P_v = 100 mbars (Bartknecht, 1993). * is for methane-air at 30m^3 on 1/K. Reproduced from Andrews (Andrews, 2004) 60
Figure 3.4 Methane/air experimental data as a function of K 77
Figure 3.5 Propane/air experimental data as a function of K 78
Figure 3.6 Hydrogen/air experimental data as a function of K . 78
Figure 3.7 Town's gas experimental data as a function of K 79
Figure 3.8 Methane/air at various geometries without β 81
Figure 3.9 Propane-air in various geometries without β 81
Figure 3.10 Methane/air with turbulent factor, β 84
Figure 3.11 Town gas/air with turbulent factor, β 84
Figure 3.12 Propane/air with turbulent factor, β 84
Figure 3.13 Influence of vessel's shape on methane/air explosion o Sphere and

□ cubic 87

Figure 3.14 The influence of rectangular vessels on P_{red} for propane/air

◊ rectangular 89

Figure 3.15 The influence of various geometries on P_{red} for town gas/air

◊ rectangular, □ cubic, ○ sphere 89

Figure 3.16 The influence of the vessel's shape on P_{red}. Δ cylinder ○ sphere 90

Figure 3.17 Methane/air for P_{red} as a function of K 91

Figure 3.18 P_{red} of methane/air at various geometries as a function of A_s/A_v 92

Figure 3.19 K_G as a function of vessel size for propane/air (4%) measured

at an initial pressure of 1 atm (Chippett, 1984) 94

Figure 3.20 Effect of P_{red} on vessel volume at constant K 95

Figure 4.1 Typical pressure-time histories for centre and end ignition

in Test vessel 1 103

Figure 4.2 Typical pressure-time histories and flame position in Test vessel 2 103

Figure 4.3 Methane/air at different equivalence ratio, Φ 105

Figure 4.4 Propane/air at different equivalence ratio, Φ 106

Figure 4.5 Ethylene/air at different equivalence ratio, Φ 106

Figure 4.6 Maximum rate of pressure rise, dP/dt (max) at various equivalence

ratios for propane/air (above) and ethylene/air (below) 107

Figure 4.7 Hydrogen/air at different equivalence ratio, Φ 107

Figure 4.8 Flame speeds of methane/air at end and central ignition as

a function of equivalence ratio 109

Figure 4.9 Flame speed as a function of flame distance from the spark for open

venting 110

Figure 4.10 Flame speeds of propane/air at end and central ignition as

a function of equivalence ratio 112

Figure 4.11 Time of flame arrival at maximum pressure, when leaving

the vessel and at the corner region as a function of propane/air

equivalence ratio 113

Figure 4.12 Diagram on the flame movement at end ignition and the

unburnt gases left inside the vessel 113

Figure 4.13 Flame speeds of ethylene/air at end and central ignition as

a function of equivalence ratio 114

Figure 4.14 Flame speeds of hydrogen/air at end and central ignition as a function of equivalence ratio 115

Figure 4.15 Time of flame arrival at maximum pressure, when leaving the vessel and at the corner region as a function of equivalence ratio 116

Figure 4.16 Pressure-time history for different fuels at $\Phi = 1.0$

Figure 4.17 Pressure time history for maximum pressure inside the vessel (P_1) and pressure inside the dump vessel (P_6) at stoichiometric hydrogen/air 117

Figure 4.18 Maximum pressure P_{max} for different fuel/air mixtures as a function of equivalence ratio 118

Figure 4.19 Flame speeds for the studied gas/air as a function of equivalence ratio. Lewis no, Le and Markstein no, Ma taken from this sources (Clark and Smoot, 1985, Searby and Quinard, 1990, Tseng, Ismail and Faeth, 1993) 121

Figure 4.20 Maximum pressures with and without spike traces in hydrogen/air explosion in Test vessel 2 123

Figure 4.21 Hydrogen/air explosion at $\Phi = 0.54$ (16 % concentration) for Test vessel 1 at end and centre ignition 124

Figure 4.22 Ethylene/air explosion at $\Phi = 1.0$ (6.5 % concentration) for Test vessel 1 at end and centre ignition 124

Figure 4.23 Methane/air at different K for $\Phi = 1.05$ 127

Figure 4.24 The influence of K on P_{max} and predicted flame area, A_f for methane/air mixture 128

Figure 4.25 Hydrogen/air at stoichiometric concentration for different K 129

Figure 4.26 Influence of P_v on P_{max} for Test vessel 2 133

Figure 5.1 Pressure-time histories for simply vented and duct vented explosion for methane/air at $\Phi = 1.06$ for end ignition (initially open venting). dP/dt traces were given for both cases 146

Figure 5.2 Pressure records at selected positions along the test vessel for methane/air at $\Phi = 1.06$ for end ignition. ΔP_{2-3} is the pressure difference at the vent entrance, ΔP_{3-5} is pressure difference inside the pipe and ΔP_{5-6} is the duct exit pressure loss. T_{in} and T_{out} indicate the time flame enters and leaves the duct respectively 149

Figure 5.3 P_{max} v P_v on stoichiometric propane/air and methane/air for 1 m length duct 150

Figure 5.4 P_{max} v P_v for ethylene/air at $\Phi = 0.8$ and hydrogen/air at $\Phi = 0.54$ 152

Figure 5.4 Methane/air at $P_v = 178$ mbar 155

Figure 5.5 Propane/air at $P_v = 178$ mbar 156

Figure 5.6 Hydrogen/air at $P_v = 178$ mbar 156

Figure 5.7 Ethylene/air at $P_v = 424$ mbar 156

Figure 5.8 Reproduced from Cooper et al(Cooper, M.G, Fairweather, M and Tite, J.P, 1986). Flame propagation mechanism at the various phases of a vented explosion 162

Figure 5.9 Flame speed a function of the flame distance from the spark for $P_v = 0$ for methane/air and propane/air. $\Phi = 1.0$ for both gas/mixtures 160

Figure 5.10 Flame speed as a function of distance from the spark for $P_v = 0$ for ethylene/air ($\Phi = 0.8$) and hydrogen/air ($\Phi = 0.54$). Noted that only hydrogen line for NFPA 68 was drawn as there is no available data for ethylene in the guidance 165

Figure 5.11 Hydrogen/air at $\Phi = 0.54$ for end ignition. $P_v = 209$ mbar 167

Figure 5.12 Propane/air at $\Phi = 1.0$ for end ignition. $P_v = 178$ mbar 168

Figure 5.13 Propane/air at $\Phi = 1.0$ for end ignition. $P_v = 424$ mbar. Spiky pressure peak is observed in this test 168

Figure 5.14 Methane/air for $\Phi = 1.0$ at central ignition. $P_v = 424$ mbar 169

Figure 5.15 Influence of P_v on flame speed upstream of the vent for methane/air ($\Phi = 1.0$) and propane/air ($\Phi=1.0$) with end and central ignition 169

Figure 5.16 Influence of P_v on flame speed upstream of the vent for ethylene/air ($\Phi = 0.8$) and hydrogen/air ($\Phi = 0.54$) with end and central ignition 171

Figure 5.17 Methane/air for end and central ignition as a function of equivalence ratio 172

Figure 5.18 Propane/air for end and central ignition as a function of equivalence ratio 174

Figure 5.19 Ethylene/air for end and centre ignition as a function of equivalence ratio 175

Figure 5.20 Hydrogen/air for end and centre ignition as a function of equivalence ratio 176

Figure 5.21 Flame speed in the duct pipe for propane/air as a function of equivalence ratio at end ignition 178

Figure 5.22 Flame speed in the duct pipe for hydrogen/air as a function of equivalence ratio at end ignition 179
Figure 5.23 Methane/air at end (left) and centre (right) ignition at various P_v 181
Figure 5.24 Propane/air for end (left) and centre (right) ignition at various P_v 181
Figure 5.25 Ethylene/air for end (left) and centre (right) ignition at various P_v 182
Figure 5.26 Hydrogen/air at end (left) and centre (right) ignition at various P_v 182
Figure 5.27 Comparison between other published experimental data and current project. The data reported were 10 % methane/air, 4.5% propane/air, 5.2% ethylene/air and 16 % hydrogen/air and 5 % acetone/air. NFPA 68 correlation (NFPA68, 2002) and Bartknecht's equation (Bartknecht, 1993) are used for $0 < L_d > 3$ m 184
Figure 5.28 P_{red} as a function of L/D 185
Figure 6.1 Pressure time profile for methane/air at $\Phi = 1.08$ 190
Figure 6.2 Pressure time profile for hydrogen/air at $\Phi = 0.54$ 190
Figure 6.3 Pressure time profile for hydrogen/air at end ignition. $\Phi = 0.54$ 191
Figure 6.4 P_{max} of methane/air as a function of equivalence ratio 192
Figure 6.5 P_{max} of propane/air as a function of equivalence ratio 192
Figure 6.6 P_{max} of ethylene/air as a function of equivalence ratio 194
Figure 6.7 P_{max} of hydrogen/air as a function of equivalence ratio 195
Figure 6.8 Time of flame arrival as a function of equivalence ratio 196
Figure 6.9 Flow interactions for methane/air at end ignition. $\Phi = 1.08$ 197
Figure 6.10 Flow regimes in vessel before and after explosion-like combustion in duct, effect of the flame front distortion; a) narrow ducts b) large duct. Reproduced from (Ponizy, B and Leyer, J.C, 1999b) 199
Figure 6.11 Pressure time histories and flame arrival for ethylene/air at $\Phi = 0.8$ 200
Figure 6.12 Pressure inside the duct for ethylene/air as a function of equivalence ratio 202
Figure 6.13 Pressure time histories and flame arrival for propane/air at $\Phi = 0.8$ for end ignition 203
Figure 6.14 Average flame speeds measured (a) in second half of the vessel (between T_1 and T_3 as in Fig.2.3b) and (b) in the vent duct (between T_4 and T_9) as a function of equivalence ratio for methane/air 203
Figure 6.15 Flame speeds measured a) in second half of the vessel (between T_1 and T_3 as in Fig.2.3b) and b) inside the duct

(between T_4 and T_9) as a function of equivalence ratio for hydrogen/air 205

Figure 6.16 Schlieren cine photographs of cellular flame development during explosion of H_2/air mixture, $\Phi = 0.26$. Reproduced from Bradley and Harper (Bradley, D and Harper, C.M, 1994) 208

LIST OF TABLES

Table 2.1 Test vessel design details 24

Table 2.2 Dump vessel design details 30

Table 2.3 List of P_{stat} of vent covers used 33

Table 2.4 Procedure in calculating the flame speeds from raw data 38

Table 3.1 Studied correlations for venting of gas explosions 71

Table 3.2 Comparison constant value derived for Method 1 and 2 with respect to Swift's C, fuel characteristic constant 72

Table 3.3 List of predicted β with respect with Bartknecht's C_3 constant 73

Table 3.4 K_G value used for vent area calculation. All data were excerpted from Bradley and Mitheson (Bradley and Mitcheson, 1978b) except for acetone-air data (Molkov, Dobashi, Suzuki and Hirano, 2000) 75

Table 3.5 Summary on average turbulent factor, β for different vessel's shape and fuels 83

Table 4.1 Summary of the experimental tests 101

Table 4.2 Summary of different gas/air properties at highest flame speeds.

Values of Table 4.3 Time of flame arrival for Test vessel 1 122

Table 4.3 Time of flame arrival for Test vessel 1 125

Table 4.4 Summary of experimental P_{max} for Test vessel 1 and 2 for K = 16.4. The ignition position is end ignition 130

Table 4.5 Summary of experimental average flame speed, S_{favg} for Test vessel 1 and 2 for K = 16.4. The ignition position is end ignition 132

Table 4.6 Experimental data and calculated equations for test vessels at Φ = 1.0 136

Table 4.7 Percent error deviation for experimental and calculation result 136

Table 4.8 Comparison of methane/air mixture with different P_v for Test vessel 2 137

Table 5.1 Explosion data for 4.0% propane/air, 9.5% methane/air, 5.2% ethylene/air and 16% hydrogen/air mixtures. Flame speed, S_f in the vessel refers to the speed from the spark towards the vent (Tv_4-Tv_2) while flame in the duct is the average value obtained along the duct (T_{out}-T_o). S_t is the turbulent burning velocity as S_f/E where E is the adiabatic expansion ratio. K_G is (dP/dt) $V^{1/3}$ and K_{Gmax} is based on the maximum dP/dt from pressure transducer P_1, which occurs after the flame has exited the duct. K_{Gvent} is based on the rate of pressure rise just prior to the flame entering the duct pipe and is proportional to the mass burning rate upstream of the vent.* Spiking pressure trace 163

Table 5.2 Predicted flame radius when the vent burst for gas/air 166

Table 6.1 Summary of experimental results (highest P_{max} either end or central ignition) with predicted values from Eq.5.1, 5.2, 5.3 and 5.4 where P_{red} without duct obtained from the simply vented experimental data 199

Table 6.2 Calculated unburnt gas velocity at the duct entrance, inside the duct pipe and at the duct pipe exit for studied fuel/air mixtures 210

NOMENCLATURE

A_s Total surface area of the vessel, m^2

A_v Vent area, m^2

BR blockage ratio

Br_t turbulent Bradley number

C_d orifice discharge coefficient

C_{ui} speed of sound, m/s

dP/dt maximum rate of pressure rise

E expansion ratio

K Vent coefficient ($= V^{2/3}/A_v$)

Ka Karlovitz number

K_G mixture reactivity index, bar-m/s

L/D length to diameter ratio

Le Lewis number

Ma Markstein number

Mach Mach number

m_b mass rate of burning

P_{red} reduced maximum pressure, bar

P_{max} maximum overpressure, bar

Pr Prandtl number

P_v vent bursting pressure, bar

R gas constant (82.0552×10^{-6} m^3bar/Kmol)

Re Reynolds number

S_f flame speed, m/s

S_g unburnt gas velocity, m/s

S_u laminar burning velocity, m/s

S_T turbulent burning velocity, m/s

T temperature, K

V volume, m^3

Π_{red} dimensionless maximum pressure (P_{red}/P_i)

Π_v dimensionless vent bursting pressure (P_v/P_i)

Greek symbols

β turbulent enhancement factor

γ ratio of specific heat at constant pressure and volume (= 1.4)

ρ_u unburnt gas density

ρ_b burnt gas density

χ/μ deflagration-outflow-interaction number

ε expansibility factor

Φ equivalence ratio

ΔP pressure differential

ACKNOWLEDGEMENTS

Firstly, I would like to thank and extend my heartfelt gratitude to my supervisor, Prof. G.E.Andrews for giving me the opportunity to undertake this study. His constant involvement, advice, brilliant thoughts and encouragements throughout this project is gratefully appreciated and acknowledged.

Thank is also expressed to R.A.Boreham, for his help and technical expertise for completing this project. I would like to thank my other supervisor, Dr.Roth Phylaktou, Ms S.K Willacy for her help and motivation and fellow postgraduates for guidance throughout this project.

Most especially a special thank to my parents and family for a constant support and encouragement in completion of this project and thesis. Not forgetful to Nadiah, Liz, Toby, Emma, Danial, Brian and Bev for welcome distraction from study and making my life in Leeds more meaningful.

And to God, who made all things possible.

PUBLICATION BY THE AUTHOR

Kasmani, R. M, Willacy, S. K, Phylaktou, H. N and Andrews, G. E. (2006), Self accelerating gas flames in large vented explosions that are not accounted for in current vent design, 2nd International Conference on Safety & Environment in Process Industry, Naples, Italy.

Kasmani, R.M, Andrews, G.E, Phylaktou, H.N, Willacy, S.K. (2007), Vented gas explosion in a cylindrical vessel with a vent duct, Third European Combustion Meeting (ECM 2007), Crete, Chania.

Kasmani, R.M, Andrews, G.E., Phylaktou, H.N. and Willacy, S.K.(2007), Influence of static burst pressure and ignition position on duct-vented gas explosions, 5th International Seminar on Fire and Explosion Hazards, Edinburgh, UK.

Willacy, S.K., Phylaktou, H.N., Andrews G.E., Kasmani, R.M. and Ferrara, G. (2006), Stratified Propane-Air Explosions of Global Concentration Outside Normal Flammability Limits, 2nd International Conference on Safety & Environment in Process Industry, Naples, Italy.

CHAPTER 1

VENTED GAS EXPLOSION – THE RESEARCH

1.0 Introduction

The potential explosion hazard resulting from deflagration of gases in processing system is a reality which must be recognised and considered when designing plants and processes. When the potential explosion hazard is not properly addressed, the result would be catastrophic; both in terms of risk of injury to personnel and property loss as well as equipment damage.

Several techniques have been developed to prevent the destructive damage to plants in industries. One of the most recognized and widely used explosion protection strategy is venting. Current gas explosion vent design standards in the USA (NFPA68, 2002) and European (2007) rely on the vent correlation first published by Bartknecht in 1993 (Siwek, 1996). NFPA 68 also recommends the correlation of Swift (Swift, 1983) at low overpressures. The correlations apply to compact vessels, which Bartknecht defines as those with a length to diameter ratio, L/D < 2. The European Directive on 'Gas Explosion Venting Protective Systems' (2007) became mandatory after August 2007. The limit of L/D of 2 given in Bartknecht's equation as the upper limit for a compact vessel in order for the spherical flame propagation is still valid assumption for most of the flame travel.

Studies on vented gas and dust explosions have shown the evolution of venting area with pressure depend on the nature and state of the initial explosive mixture i.e. composition, initial pressure and temperature, pre-ignition turbulence and on the vessel characteristics i.e. dimension and shape, position of the ignition source, location, size, strength and shape of vent, presence of obstacles within the vessel. An understanding of the mechanisms by which pressure is generated in vented explosions is important in the design of explosion reliefs and to the investigation of incidents. Such knowledge provides the basic of the development of prediction methods for use in risk and hazard studies on an actual or proposed industrial plant.

The vented gaseous deflagrations have been studied extensively for many years to provide understanding of the phenomena. However the information on explosion venting is mostly empirical and related to experiments conducted with homogeneous,

quiescent gas-air mixtures. Yet, the different basic physical aspects of vented deflagrations have still not been studied sufficiently. For decades, venting experiments with various initial conditions and modelling model using lumped parameter as a venting parameter were done to understand the dynamics and physical process of venting. From the intensive works done by previous researchers (Bartknecht, 1993, Bradley and Mitcheson, 1978a, Bradley and Mitcheson, 1978b, Burgoyne and Wilson, 1960, Cousins and Cottons, 1951, Cubbage and Marshall, 1974, Cubbage and Simmonds, 1955, Cubbage and Simmonds, 1957, Donat, 1977, Zalosh, 1980), correlations were offered to be used in order to design the required vent area; unfortunately they are strictly applied within the limits of the experimental range investigated. Hence, the key knowledge about the physical and dynamic mechanism of venting with or without the relief pipe needs to be understood in order to reduce the potential of explosion severity.

1.1 Venting gas explosions

1.1.1 General overview

Early work on explosion relief was done by Cousins and Cottons (Cousins and Cottons, 1951) which used propane and hydrogen in four vessels having a range of L/D ratios of 1.41 to 22.1. They studied the effect of vent burst pressures and vent ratio on maximum reduced pressure inside the vessel at different initial conditions. The work concluded that initial condition and strength of vent burst pressure caused the increase of maximum pressure inside the vessel during venting and gave recommendation for vent area design. Another early study was carried out at the Midlands Research Station (MRS) of the Gas Council by Cubbage and Simmonds(Cubbage and Simmonds, 1955, Cubbage and Simmonds, 1957). Their thorough work concerned with the explosion venting of industrial drying ovens using town gas as the fuel. The experiments were done on oven which were approximately cubical and with variety of vent condition coupling the influence of vent cover inertia. The significant of their work resulted in two peaks of pressures from the explosion which later been used to correlate the vent area requirement with the reduced pressure obtained. The magnitude of each pressure peak has also been quantified in terms of vent ratio relief panel failure pressure, mass

per unit area of the relief, location of ignition as well as shelf arrangement (obstacles). Low breaking burst pressures lead to large flame elongation, and hence larger flame area and result to higher expected vessel pressures whereas at high breaking pressure the effect of flame distortion is reduced.

Other experimental studies which have yielded data sets against the correlations that can be tested include those of Harris (Harris, 1967), Harris and Briscoe (Harris and Briscoe, 1967), Pritchard et al (Pritchard, Allsopp and Eaton, 1995) and Zalosh (Zalosh, 1980). From these works, it has led to the development of a number of empirical and semi-empirical methods and of the scaling laws. The correlation methods have been widely used since it is obviously desirable, for design purposes, to be able to access the effectiveness of the explosion relief in a given situation by calculation rather than experiment.

The introduction of gas nomograms based on Bartknecht (Bartknecth, 1981) has been recognised to be most commonly used in predicting the required vent area as they are simple to use and can be extrapolated to the maximum limit, i.e. volume up to 1000 m^3. However, the nomograms do not compare well with actual experimental data, introducing serious errors as the graphs being difficult to read accurately and gave over-predicting values for interpolation and extrapolation operation. Besides, they can only be used with confidence for four typical fuel-air mixtures, over a narrow range of bursting pressures as being investigated by Simpson (Simpson, 1986) while only semi-empirical recommendations are given for their extrapolation to different conditions. Simpson also noted that the low pressure extrapolation of Bartknecht's nomograms would only conservatively yield high relief area estimates. Since the nomograms introduced more errors, equations are more favoured and nomograms take second place.

The most used and recommended correlation for venting gas deflagration is adopted by NFPA 68 which based on the works of Swift (Swift, 1983) and Bartknecht (Bartknecht, 1993). Bartknecht 's correlation is given as the vent area, A_v, as a function the vessel volume, $V^{2/3}$ multiplied by a complex term that includes the mixture reactivity K_G, reduced overpressure in the vented explosion, P_{red} and static vent burst pressure, P_v. The ratio of $V^{2/3}/A_v$ has been referred to in the explosion venting literature (Harris, 1983) as the vent coefficient, K. The $V^{2/3}$ dependence of overpressure on the test vessel

volume is a characteristic of spherical or compact vessel explosions, where the flame remains mostly in spherical shape during venting process and this is the mandatory limit for L/D = 2 in European Standard (2007) and NFPA 68 (NFPA68, 2002). If the spherical flame propagates at a constant rate irrespective of the vessel volume, there should be no other dependence of P_{red} on volume other than K. However, Bartknecht's equation rely only on his set of experimental data at different volumes and vent area (Bartknecht, 1993). At a fixed gas or mixture reactivity and fixed volume, Bartknecht correlated the experimental results as shown in Eq.1.1 where a and b given in Table 1.1.

$$A_v = aP_{red}^{-b} \tag{1.1}$$

Table 1.1 Value of a and b for Eq. 1.1

Gas	K_G	a	b
Methane	55	0.164	0.5720
Propane	100	0.200	0.5797
Town gas	140	0.212	0.5900
Hydrogen	550	0.290	0.5850

When the a values been plotted as a function of the gas mixture reactivity, K_G, it gave

$$A_v = (0.1265 \log K_G - 0.0567) P_{red}^{-0.5817} V^{2/3} \tag{1.2}$$

$$K_G = (dP/dt) V^{1/3} \text{ bar-m/s} \tag{1.3}$$

where (dP/dt) is maximum rate of pressure rise and V is volume (m^3). It should be noted that the constants used in Eq.1.2 were determined for V = 10 m^3 and the value of K_G given in Table 1.1 were not taking into account on the volume effect nor the value of b.

The correlation developed by Bartknecht (Bartknecht, 1993) can only be applied on its own limitation as the equation is the empirical derived from his experimental works and no other published venting data included as noted by Siwek (Siwek, 1996) in his study on published correlations in vented gas and dust/air- mixtures. In order to validate the equation developed, other data should be included so that the equation can be used globally with confidence.

NFPA 68 adopted Swift's equation (Swift, 1983) to apply for design and scale-up of venting system purposes and it seem that the results obtained were in good agreements with experimental data obtained by Donat (Donat, 1977) and Harris and Briscoe (Harris and Briscoe, 1967). Again, there is a limitation in using this approach as it can be applied on certain conditions i.e. P_{red} is not more than 200 mbar and only suits to low-strength enclosures. Meanwhile, Swift's correlation is given as A_v as a function of cross-sectional area of the enclosure, A_s multiplied to reactivity terms which include the burning velocity, S_u and turbulent enhancement factor, β. The use of the vented vessel surface area in vent correlations was first introduced by Runes (Runes, 1972) as the maximum possible flame area and was used to calculate the maximum flame mass burning rate.

In Bartknecht's correlation (Bartknecht, 1993) the gas/air reactivity is given by the mixture reactivity index, K_G and burning velocity, S_u by Swift's correlation (Swift, 1983) which also used in most models of turbulent explosions and previous vented gas explosion correlations (Zalosh, 1980). The K_G is not constant for a given gas but varies with composition, temperature, pressures and vessel size. It is easily shown that K_G is directly proportional to the burning velocity, S_u in the latter stages of a spherical closed vessel explosion as correlated by Kumar (Kumar, Bowles and Mintz, 1992) and Nagy (Nagy and Verakis, 1983) and hence the two parameters to quantify the reactivity are directly related.

Some confusion has been caused by the fact that correlation formulae resulting from these two different approaches, S_u and K_G in Swift and Bartknecht's correlations respectively, imply different results to predict the vent area. More specifically, the introduction of the venting deflagration index, K_G has been seen by some as counterintuitive and therefore, judged incorrectly. The dependent of K_G on volume appeared to be a reflection of the tendency of the flame ball to increase its effective surface area through instabilities in the flame sheet structure; the flame sheet geometry departs from an initially smooth spherical form to one of the greater effective surface area across which combustion continues at S_u which prevails at the local conditions of temperature and pressure (Pritchard, Allsopp and Eaton, 1995). The same observation

of volume dependence on K_G was also made by Chippet (Chippett, 1984) on his work on propane/air mixtures.

Meanwhile, the use of S_u as the fuel characteristic is preferred as it is independent of equipment geometry but is more difficult to measure than K_G. Cubbage and Simmonds (Cubbage and Simmonds, 1955, Cubbage and Simmonds, 1957), Cubbage and Marshall (Cubbage and Marshall, 1974) and Bradley and Mitcheson (Bradley and Mitcheson, 1978a, Bradley and Mitcheson, 1978b) used S_u as the basis of the their venting correlation in order to establish the relationship between the pressure developed in the combustion phenomena during venting. Theoretically, the flow pressure of unburnt gases through the vent is proportional to the square of the product of burning velocity and vent ratio. Thus, the higher the burning velocity of the gas involved, the higher will be the maximum pressure generated in the enclosure (i.e. S_u for hydrogen is 3.1 m/s and S_u for propane is 0.45m/s). However, the fundamental burning velocity refers significantly to the maximum rate of propagation of a flame into a quiescent gas mixture of the appropriate (near-stoichiometric) concentration, and initially at ambient conditions of temperature and pressure. In determining the burning velocity, some works had scattered values for high reactivity gases i.e. ethylene and hydrogen (Andrews and Bradley, 1972). This theoretical ideal situation did not encounter in gas explosion; turbulent is generated as the unburnt gas is pushed ahead of the flame front when the vent is opened which can give rise to the additional back pressure or driven past the obstacles or over surfaces. The effect of turbulence is well known and been investigated by various past researchers (Molkov, Dobashi, Suzuki and Hirano, 2000, Munday, 1963, Yao, 1974). Thus, because of this fundamental problem, the use of K_G is suggested by NFPA 68 in order to determine the required vent area for protecting the process vessel/enclosures. And yet, since less data of K_G are published, only data given by Bartknecht work (Bartknecht, 1993) and NFPA 68 (NFPA68, 2002) recommended be used as a reference.

Other correlations have been developed by several researchers in order to improve the design requirement and agree with experimental work i.e. Runes, Rust and Simpson Rasbash and Cubbage and Marshall (Lees, 1996) but, it was either fragmentary or obtained under different conditions. Since all correlations only applied to certain condition and with a limit of validity, Bradley and Mitcheson (Bradley and Mitcheson,

1978a, Bradley and Mitcheson, 1978b) have compared the results obtained by lumped-parameter model of vented explosions to the experimental data but yet, only a quantitative agreement was observed. The work was regarded more complete since it also offers a sound theoretical basic in predicting vent area; however the criteria they developed have been shown inadequate for large volumes with obstacle-generated turbulence (Swift, 1983). Further critical examinations of various existing equations and especially of their extrapolation within and beyond their recommended validity range have been presented by Molkov *et al* (Molkov, Dobashi, Suzuki and Hirano, 2000) who also developed a new so-called 'universal correlation' for vent area calculation. Razus *et al* (Razus and Krause, 2001) reviewed the empirical correlations developed for vent sizing based on the reduced pressure parameter. Following the authors, equation by Bradley and Mitcheson (Bradley and Mitcheson, 1978a, Bradley and Mitcheson, 1978b) and Molkov (Molkov, Korolchenko and Alexandrov, 1997) gave relatively close predictions to experimental data for most common hydrocarbon-air mixture.

Since published correlations are used to predict the overpressure developed in deflagration vented vessel with a validity restricted to certain limits of parameter characteristic for the vessel, the vent and the explosive mixture, there are no generally accepted correlations to guide the determination of vent areas for gaseous as being established for dust/air system i.e. VDI 3673.

Nevertheless, relevant experimental data are mostly limited to small aspect-ratio vessels usually cubical in shape (Cooper, Fairweather and Tite, 1986, Cubbage and Simmonds, 1955, Cubbage and Simmonds, 1957, McCann, Thomas and Edwards, 1985, Thorne, Rogowski and Field, 1983) and very little on other geometries. They both studied the physical and gas dynamics process in vented explosion in order to discuss the effecting factors result the number of pressure peaks obtained inside the enclosures; however, the effect of vessel and volume shape were still not be accounted.

Further, a special deficiency of experimental observations exists for elongated large-aspect-ratio vessels, which are typical for industrial applications. The large scale methane-air explosion test performed at Rusfoss, Norway by Moen et al (Moen, Lee, Hjertager, Fuhre and Eckhoff, 1982). The test found that obstacles even relatively small, have a dramatic influence on the violence of the explosion and pointed out that initially

quiescent explosive mixture criterion was totally inadequate for large scale explosion in obstacle environment. Flame propagation in such vessels has been proved to be very different from those with small-aspect-ratio spherical vessels.

Yet, therefore, some confusion concerning the application of the various equations to practical situations, both as to which is the most appropriate equation to use in a given circumstances and also as to the range of values of the various parameters for which the equation are valid. It is worth noting that the disparity between the experimental vents area - ranging from small to larger-closed to-room enclosures and correlated values are due to the uncertainty on the fundamental basis of vented explosion and lack of published experimental data that would render the development of vent sizing design.

Modelling on venting explosion has been carried and still, disparity between models proposed is huge. Complex computer codes requires considerable input data and accurate thermo physical properties as well as access to super-computer facilities are of little use in the system design (Zalosh, 1995). Their utility in exploring less complex flame laws however, is not in question. Design techniques should be quick and easy to use, accurate, conservative yet realistic and provide results that accord with experience.

1.2 Overview of the project studies

Since the published guideline of NFPA 68 (NFPA68, 2002) and European Standard (2007) has only included Bartknecht's equation for L/D = 2 which only his own data was used in developing the correlation, there is no guaranteed that empirical correlations could provide practical and safe venting design for industrial purposes. Further, the variation of fuel/air mixtures concentration is not widely studied, where many experimental done in stoichiometric concentration

The published gas venting data from 1920s to date were complied and collected with different volumes, gas reactivity, ignition position, shapes and different initial conditions. From the reported data, the comparison between Bartknecht's and Swift's equation were made as those equations were offered in NFPA 2002 and European Standard (2007). Further, those data were analysed to be compared to Bradley and

Mitcheson's equation (Bradley and Mitcheson, 1978a, Bradley and Mitcheson, 1978b) as well as Molkov's equation (Molkov, 2001). Theoretically, for a vent to give no increase in overpressure other than due to the pressure difference created by the mass flow of unburnt gas through the vent, the vent mass flow rate is considered to have an equal to the maximum mass burning rate of the flame. In the simplest case, the incompressible flow equation can be used for low P_{red} while treating the vent as an orifice with discharge coefficient, C_d which depends on the design of the vent and K. Based on this approaches, two different methods were proposed named as **Method 1** and **Method 2.** Method 1 assumes that the maximum overpressure occurs when the vent unburnt gas flow rate is at a maximum and is equal to the maximum mass burn rate at the flame front whereas Method 2 based on the assumption of the maximum overpressure occurs when the vent unburnt gas flow rate is at a maximum and this is equal to the maximum unburnt gas displaced flow by the flame front.

The difference of these two methods was the use of S_u and S_u (E-1) terms in the equations. The simple approaches were evaluated with additional of compressibility factor and turbulence factor to simulate the real explosions. These two methods were compared with the published experimental data to justify the applicability, validity and limitation with respect to the practical application. The detail discussion on the effect of volume and shape of the vessels, turbulent enhancement factor, β and K were made in order to investigate the important factors influencing the P_{red} in the development of gas venting explosions. Further, to demonstrate the applicability of the proposed methods to the practical application, series of vented gas explosions in two cylindrical volumes were carried out, mainly for medium and small scale volumes i.e. 0.2 and 0.0065 m^3.

1.2.1 Simply venting gas explosions

By performing the experiments with simply venting, the physics and dynamics of explosive mechanism were investigated. The project focused on the two different volumes of cylindrical vessel ; medium and small size volume to highlight the occurrence of self-acceleration effect in medium vessel compared to small vessel which is not taken into account in venting design guide.

Intensive works in venting gas explosion had been done by Cubbage and Simmonds (Cubbage and Simmonds, 1955, Cubbage and Simmonds, 1957) on industrial drying oven for variety of fuel gases and flammable vapours in enclosures up to 14 m^3 volume. They reported that there are two distinctive peak pressures obtained from the pressure-time profile explosion development. Hence, from this results, the correlation which contains terms expressing the effect of fuel/air mixtures characteristics and the volume enclosures in which the explosion occurs. This equation can be applied to any fuel/air mixtures since the effect of the combustion characteristics of different gases on the pressure generated is allowed for by the value of burning velocity, S_u.

Bartknecht's (Bartknecht, 1993) work on venting has been adapted in NFPA 68 guidelines for venting design. His works involved vessel volume up to 60 m^3 vessel and used only four different fuels which were methane, propane, hydrogen and town's gas. These experiments that been evaluated were carried out with restricted conditions and the equation can only be applied if the requirements fit. Some of the conditions needed to be fitted into the equation are P_v is between 0.1 to 0.5 barg and L/D of 2 which the current project closely followed. It is the aim of the current project to fit the condition required in order to investigate the parameters that not been taken into account in the equation developed. In a vented explosion without a vent pipe, the peak overpressure is related to two main pressure peaks, the first is related to the vent static burst pressure and the second to the pressure loss of unburnt gas through the vent. The second pressure peak increases as the vent coefficient, K (= $V^{2/3}/A_v$), increases and the first pressure peak dominates when the static burst pressure is high. In the present work a relatively high K of 16.4 (1/K = 0.061) was used and the overpressure without the vent pipe was dominated by the pressure loss of unburnt gas through the vent. The Bartknecht's correlation (Bartknecht, 1993) for vent area is in terms of 1/K and for a static bust pressure of 100mb the correlation takes the form of Eq. 1.2.

$$1/K = [0.1265\log K_G - 0.0567]/P_{red}^{0.5817} \quad (1.4)$$

K_G is the reactivity parameter given by the maximum rate of pressure rise in a 5-litres spherical closed vessel multiplied by the cube root of the volume. Bartknecht also gives the venting correlation for propane, methane, hydrogen and town's gas/air with 100 mbar vent burst pressure respectively as:

$$1/K_v = 0.197/P_{red}^{0.5820} \quad (1.5)$$

$$1/K_v = 0.164/P_{red}^{0.5820} \quad (1.6)$$

$$1/K_v = 0.291/P_{red}^{0.5820} \quad (1.7)$$

$$1/K_v = 0.220/P_{red}^{0.5820} \quad (1.8)$$

It will be shown that these predictions are grossly in error and even with a vent pipe the overpressures come no where near these values. When the experimental data of Bartknecht is examined (Kasmani, Willacy, Phylaktou and Andrews, 2006, NFPA68, 2002), it is clear that the exponent of P_{red} is fitted to the data with $1/K > 0.2$ or $K < 5$ and the correlations should never be used for higher K. This is not recognized in NFPA 68 or in the European guidance on venting. The limitation on the correlation is stated as $P_{red} < 2$ bar and the experimental data shows that this is effectively a limit of K of 10. It is found that in cubic vessels, this condition is not valid as the flame have touched the wall well before 2 bar overpressure was reached. However, none of the experimental data for $P_{red} > 0.8$ bar fits the correlation and all is lower than the correlation. This effectively gives the validity of the correlation at $K < 5$ and $P_{red} < 0.8$ bar and this is the incompressible vent flow regime. When the nearest Bartknecht's data point to the present results is used, which is a 1 m^3 vessel with $1/K = 0.058$ and the overpressure with a 100 mbar vent burst pressure was 2.5 bar for propane/air. It is clear in the Bartknecht's experimental data, there is a volume effect additional to that in K that is not included in the correlation (Kasmani, Willacy, Phylaktou and Andrews, 2006) and is likely associated with flame self-acceleration due to the development of cellular flames. This effect was also important in the present work.

In this work, the effect of fuel/air mixtures concentration at different ignition position will be investigated as little attention is given in this aspect. As stated in ATEX Directive (94/9/EC) , venting equipment should be protected based on worst case scenario and it is found that stoichiometric concentration at centrally ignited is not always the worst case.

Further, the use of vent cover i.e. lightweight relief panel, rupture membrane or explosion door has proven to have effect on explosion pressure generation inside the vessels/enclosures i.e. back pressure due to inertia of the vent cover (Molkov,

Grigorash, Eber, Tamanini and Dobashi, 2004). This commercial vent cover can be affected by the inertia of construction elements moving by overpressure during the explosion. The example of commercial vent cover available for venting is shown in Fig.1.1.

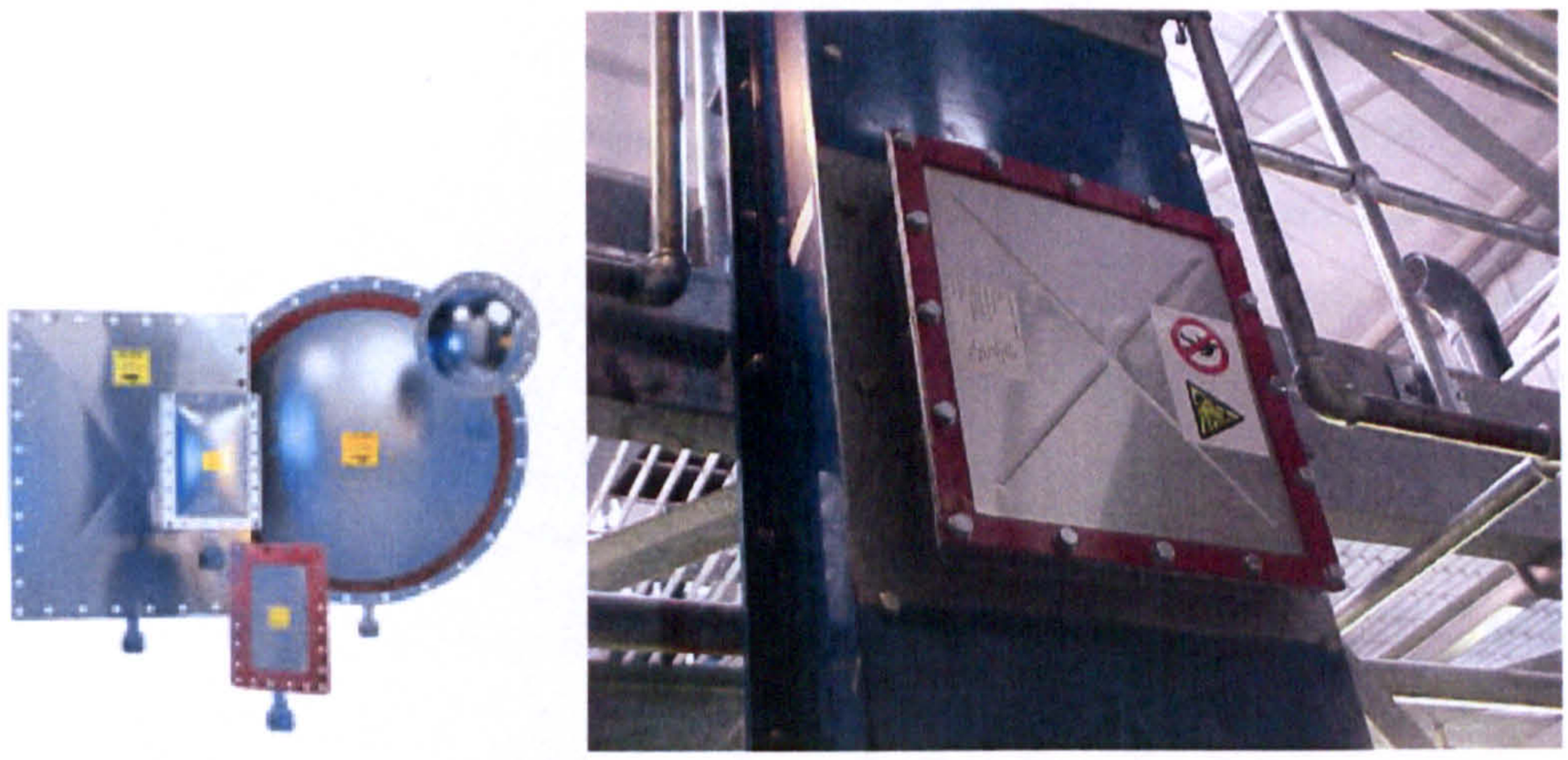

Figure 1.1 Example of commercial vent covers and its application.

The effect of inertia has been studied extensively in order to quantify the effect of inertia to the P_{red} during venting (Bartknecht, 1985, Cubbage and Simmonds, 1955, Molkov, Grigorash, Eber and Makarov, 2004). However, in this present work, the effect of vent cover inertia can be neglected as the material used is easily broken and not impending the flame propagation during venting explosion.

1.2.1.1 Self-acceleration of spherical flames

Although the laminar burning velocity and hence the flame speed in a spherical flame at constant pressure is normally assumed to be a fundamental constant a particular gas/air mixtures. However, experiments in vessel of different size has shown that this is not the case (Chippett, 1984, Pritchard, Allsopp and Eaton, 1995). The spherical flame speed has been demonstrated to vary with the flame radius, accelerating when the flame is small then having a period of near constant flame speed and at so-called ' critical flame radius', the flame starts to rapidly accelerate through a mechanism called ' self-acceleration' or flame cellularity. The net result is the K_G is a function of the vessel size. Harris and Wickens (Harris and Wickens, 1989) had done series of small and large scale

balloon tests on natural gas/air mixtures. They have shown conclusively that the high flame speeds of > 100 m/s are impossible to achieve in unobstructed explosion compared when the flame propagates through the unconfined explosion. In small volume balloon test, the flame speed of natural gas is found to be 3.1 m/s, close enough to the value given by Andrews and Bradley (Andrews and Bradley, 1973) of 2.6 m/s for a 50 mm diameter spherical flame in a 300 mm diameter closed cylindrical vessel. However, the increase value of flame speed in 3 m diameter of a large balloon in respect to its laminar burning velocity was observed in natural gas and ethylene i.e.7 and 15 m/s respectively. From the results, it can be said that all flames have a minimum distance that they propagate at the laminar flow rate before starting to self-accelerate due to the process of flame instability through the formation of cellular flames that have a greater total flame surface area than a smooth laminar flame. The detail of self-acceleration mechanism has been discussed by Bradley et al (Bradley, Cresswell and Puttock, 2001). In cellular flame, the magnitude of the increase in flame speed depends on the type of gas and the equivalence ratio of the mixtures. It is generally known that methane has a smaller acceleration than propane which in turn, is smaller compared to hydrogen. Hydrogen/air flame becomes cellular very easily as been shown by Andrews and Bradley (Andrews and Bradley, 1973) in 50 mm diameter of closed cylindrical vessel. They observed that the onset of flame cellularity occurs at the mixtures leaner than 25 % concentration.

Chippet (Chippett, 1984) introduced a method for the inclusion of the development of cellular flame in design procedures. In his correlation, η is considered as a factor for the increase in flame surface area due to cell formation. This is directly proportional to Prandtl number, Pr and Reynolds number, Re. Pe.Re is the flame stability parameter given by Istratov and Librovich (Istratov and Librovich, 1969) which predicts the critical conditions of the onset of flame instability and cell formation. It also postulated that η is essentially equivalent to the turbulent enhancement factor, β ($= S_T/S_U$). Thus, it is important to understand the flame self-acceleration and to include the parameter in explosion protection design.

1.2.1.2 Implication of the objectives to the present study

From the discussion above, the study was performed to gain better understanding of the physical processes which are important in the generation of the overpressures and to elucidate how this processes influence the severity of an explosion. Simplification on vent design is still preferred for venting design but it needs to be theoretical and practical basis which can be explained through the actual experimental results. Generally, this project's objectives are;

- To study the influence of K parameter on P_{red} in terms of vessels' shape and volume of the enclosures and the effect of bursting pressure, P_v.
- To quantify the influence of turbulent enhancement factor, β and flame self-acceleration on vented gas explosion for different gas reactivity and concentrations.
- To propose a simple approach in calculating the P_{red} and vent area, A_v using two different methods which crucial parameters involved in venting gas explosion development is included.

1.2.2 Vented gas explosion with relief pipe attached.

The study of the venting gas explosion of different fuel/air mixtures and concentrations were further examined in terms of the effect of duct pipe attached to the main vessel on P_{max}. Based on the experimental analysis of venting explosion with and without a pipe, it is known that the severity of the explosion is likely to be 2 or 12 fold increase with the presence of a duct with respect to simply vented vessels (Bartknecht, 1981, Ferrara, Benedetto, Salzano, Russo, 2006, Ponizy and Leyer, 1999a, 1999b, Siwek, 1996). The results of DeGood et al (DeGood and Chartrathi, 1991) and McCann et al (McCann, Thomas and Edwards, 1985) for various duct lengths supported these results. The surprising feature of these results is that the length of the duct is not a major parameter and only short and long ducts were separated by Bartknecht (Bartknecht, 1993). This is because the increase in the overpressure is dominated by duct entry and exit pressure losses; a duct would have to be about 100 pipe diameters long before the flow friction losses were equal to the combined inlet and exit pressure losses. The present work used

relatively a relatively short duct of 1m long and 0.162 m diameter (L/D = 6.2) but it exhibited all the features of explosion venting with a vent duct attached. In Bartknecht's work (Bartknecht, 1993) the 3 m long pipe was 0.5m diameter and hence the L/D was 6, close to that used in the present work. As pipe friction losses are a function of pipe L/D a dependence of the vent overpressure on the L/D would be expected rather than simply on the length of the duct, irrespective of its diameter. Particular emphasis was placed on the determination of flame speeds upstream of the duct, as well as flame speeds and gas velocities in the vent duct.

Further, the problem seems to be more complicated if the vent covers were placed at the vent. The effect of bursting vent on pressure development in vented explosion have been studied by several workers (Ferrara, Benedetto, Salzano and Russo, 2006, Pasman, Groothuizen and Gooijer, 1974, Ponizy and Leyer, 1999a, Ponizy and Leyer, 1999b, Cooper, Fairweather and Tite, 1986, Cubbage and Marshall, 1974), limit at stoichiometric fuel concentration. It is found that the peak pressure inside the vessel during duct-vented gas explosions did not result from the external explosion and not occur when the flame is propagating in the duct as reported by Kasmani *et al* (Kasmani, Andrews, Phylaktou and Willacy, 2007a, Kasmani, Andrews, Phylaktou and Willacy, 2007b). Vent rupture also generates a pressure wave which interacts with the flame front to distort it and hence increase its surface area and mass burning rate. These combined effects of turbulence and pressure waves created by the vent bursting result in acceleration of the flame prior to the vent duct and also increase the flow velocity, turbulence and flame speed in the vent duct. Tests with ducted explosion vents generally display Helmholtz oscillations, that is the pocket of burned gas within the vessel undergoes bulk motion towards and away from the vent opening, due to the mass of the duct contents and the compressibility of the gas in the primary enclosure that acts as a spring (McCann, Thomas and Edwards, 1985). The occurrence of a sharp pressure peak in the vent duct is also mentioned by Kordylewski and co-worker (Kordylewski and Wach, 1988) and maximum pressure effect in the vessel was found to occur with a particular duct length, equal to about 12 diameters. It is known now that the intensification of the combustion in the vessel is driven by an impulse generated during the burn-up in the initial part of the duct, shortly after the flame penetrates into it (Ponizy and Leyer, 1999a, Ponizy and Leyer, 1999b, Ponizy and Veyssiere, 2000)

When relatively narrow ducts are used with a sharp vessel-duct area change, the flame front entering the duct can be temporarily extinguished due to stretch (caused by the inlet vena contraction effect, which locally increases centreline velocities by 64 %) and cooling through turbulent mixing with unburned gas (Iida, Kawaguchi and Sato, 1985, Ponizy and Leyer, 1999a, Ponizy and Leyer, 1999b) which brings about stronger burn-up (i.e. with higher pressure amplitudes) during re-ignition (Ponizy and Veyssiere, 2000).

The increase in P_{red} with the addition of a vent duct is so large that vent ducts cannot be used without increasing the vent area and duct size to achieve a reduction in the overpressure. However, there is insufficient design data for gases to enable this to be done effectively and the physics of the process for gas explosion venting is not well understood. This contrasts with the situation for dust explosions, where a substantial experimental data base exists (Lunn, Crowhurst and Hey, 1988). The aim of the present work was to explore the physics of the venting process with a vent duct attached with various duct diameters to investigate the effect of the vent static burst pressure and the duct diameter size for central and end ignition for an explosion vessel at the limit of applicability of compact vessel venting correlations with a length to diameter ratio, *L/D* of 2. It is shown that generally, reverse flow in ducts of larger diameters will result in large scale mixing in the vessel which in turns generates higher pressure increase in the vessel (Ponizy and Leyer, 1999a, Ponizy and Leyer, 1999b). It is considered that it is the variation of the mass burn rate and flame speed of the flame approaching the vent that has a strong influence on the vent flow and on the subsequent combustion behaviour. A major feature of the explosions is that there are substantial proportions of the original flammable mixture in the test vessel after the flame has exited the vent duct. This is larger for central ignition than for rear ignition. Kasmani *et al* (Kasmani, Willacy, Phylaktou and Andrews, 2007) also shown that the faster mass burn rate approaching the vent as P_v increases causes sonic flow in the vent and hence choked flow. This prevents there being any outflow from the duct until the pressure has risen in the vessel to drive the burnt gases out. In some cases, this condition leads to a period of mixed burnt gas and unburnt gas venting with micro explosions and detonations in the vent duct. This phenomena has been detailed by Ferrara et al (Ferrara, Willacy, Phylaktou, Andrews, Benedetto and Mkpadi, 2005, Ferrara, Willacy, Phylaktou, Andrews, Benedetto and Salzano, 2005).

1.2.2.1 The influence of duct pipe diameter

The influence of vent ducts on gas explosions was investigated with the aim of determining whether the use of a vent duct of large area than that of the vent, would reduce the very large increases in overpressure that occur when vent ducts are used. In the presence of a vent duct, an increase of venting area and duct diameter has been found to not always result in a decrease in the peak over pressure (Ponizy and Leyer, 1999a).

The main reason for the increase in the overpressure when long vent ducts are attached to vents is due to the phase in the explosion when the flame is in the vent pipe with unburnt gas mixture ahead of it. The expansion of the burnt gases in the vent pipe greatly accelerates the unburnt gas flow and this increases the vent pipe friction, inlet and exit pressure losses (Lunn, Crowhurst and Hey, 1988). These effects are a function of the dynamic pressure in the vent pipe. In principle the dynamic pressures in the vent pipe can be reduced by simply using a larger vent diameter than that for the vent, rather than increasing both the vent and vent pipe sizes. For example, if the vent pipe was twice the diameter of the vent then the vent pipe dynamic pressure would be reduced by a factor of 16, if the vent mass flow rate remained constant. Some evidence that a larger vent pipe diameter would reduce the overpressure with no change in the vent size was provided by Nagy (Nagy and Verakis), which is quoted in NFPA 68 (2002). From the experiments performed on dust explosions with vent pipes (Lunn, Crowhurst and Hey, 1988), Hey (Hey, 1991) has suggested that the technique of using a larger vent duct diameter than the vent diameter is effective if the duct area/vent area is about ~ 2-2.5 and when P_{red} is less than 0.5barg. It is considered that this approach would be a simpler method of designing for safe vent pipes and the present work investigated for gas explosions a vent pipe that was close to twice the vent diameter, as recommended by Hey (Hey, 1991).

1.2.2.2 Implication of the objectives to the present study

From the discussion stated above, it is crucial to investigate and study the important phenomena occurred during the explosion development in vented gas explosion with the

relief pipe attached to the primary vessel. It is the aim of the present study to quantify the relationship of the P_{max} with ignition position, equivalence ratio and vent bursting pressure P_v as well as the duct pipe diameter and length in order to highlight the most leading factors of the rapid increase in P_{max} at the presence of the duct in vented gas explosion with respect to the simply vented explosion.

CHAPTER 2

EXPERIMENTAL SET-UP AND MEASUREMENT TECHNIQUES

2.1 Test facility

The research has been carried out in Room B11 which has been designated as the 'Explosion Hazards-High Pressure Test Facility'. The site is shown schematically in Fig. 2.1. Safety considerations have been top priorities to make sure that all tests were carried out in a safety manner. Two separated rooms have been designed: 'Control room' and 'Test room'. Access between the two rooms was via an interlocked door that formed part of the safety system controlling the ignition circuit. The dump-vessel, test vessels and instrumentation equipments were located in the Test room. Data logging hardware was situated in this area and was electronically linked to a computer network in the Control room. Data collection was synchronised with ignition using specialised software known as FAMOS.

2.2 Apparatus design considerations

2.2.1 Test vessels

In this project research, three test vessels were used. Test vessel 1 was constructed from cylindrical vessel with internal diameter of 0.5 m and length of 1.0 m with vent area of 0.021 m^2 and the volume of 0.2 m^3. For Test vessel 2, the cylindrical vessel with internal diameter of 0.126 m and length of 0.315 m was used. Further, for Test vessel 3, different length and diameter of pipes were connected to the main vessel at constant vent area of 0.021 m^2 for vented gas explosion with relief pipe tests. Table 2.1 gives details for the test vessels used.

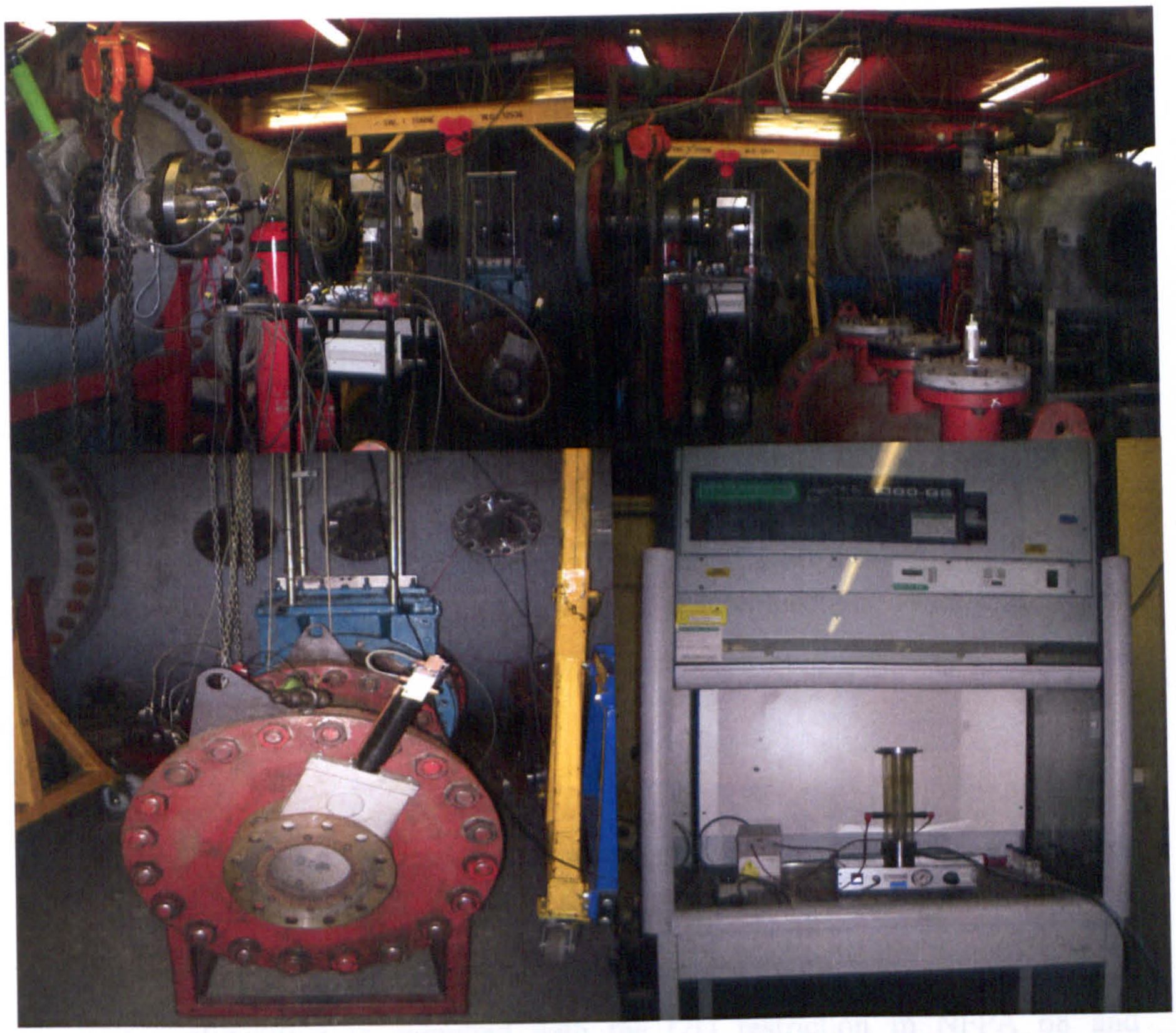

Test Room

Control room

Figure 2.1 Schematic picture of test facility and control room

The previous works (Bartknecth.W, 1981, Bradley and Mitcheson, 1978b, Bradley and Mitcheson, 1978a, Chippett, 1984, Cubbage and Simmonds, 1955, Cubbage and Simmonds, 1957, Donat, 1977, Zalosh, 1980) have shown that the evolution of pressure with time in venting gas explosion depends on the nature state of the initial explosive mixture, i.e. composition, initial pressure and temperature, pre-ignition turbulence and on the vessel characteristics i.e. dimension and shape, position of the ignition source, location, size, strength and shape of the vent, presence of the obstacles within the vessel. Further, the addition of the relief pipe to the vessel can significantly increase the violence of the explosion and the pressure in the vessel to the factor of 10 or more in which the explosion is vented directly to the atmosphere (Bartknecth, 1981, Kordylewski and Wach, 1988, Molkov, Baratov and Korolchenko, 1993, Ponizy and Leyer, 1999a, Ponizy and Leyer, 1999b). The test configuration was employed for the following reasons;

- The present project was aimed at investigating the physical and gas dynamics processes governing the generation of pressure peaks, P_{red}. Further, the influence of the vent cover fitting at the vent on Pred will also be studied.
- This configuration is complied with the L/D restriction in NFPA 68 and therefore, the results of this study will be compared to the published venting correlations offered by NFPA 68 and Draft of the European Standard.

2.2.2 Dump vessel

In order for safe vented explosions to be carried out in the laboratory, the test vessels were connected to a large dump-vessel that acted as an expansion chamber. Both burnt and unburnt gas could then be safely vented and continued before vessel purging. An important feature was the fact that pre-test conditions both inside and outside the test vessels could be accurately controlled. The overall dimensions and therefore volume of the dump vessel were also important variables along with the various vent diameters and pipe fitting. This design process was governed by the following factors;

- The internal length and diameter of the dump vessel had to be such that its volume was greater than that of the test vessel by the factor that allowed the

simulation of open-to-atmosphere explosions. If this was the case then the presence of the dump vessel would have little or no effect on the explosions development in the test vessel.

- Combustion of a gas mixture prepared in the test vessel would result in a pressure increase in the total system volume, V_T that was made up of the test vessel volume, V_t and the dump vessel, V_d such that,

$$V_T = V_t + V_d \tag{2.1}$$

Assuming adiabatic combustion at a constant pressure of 1 atm,

$$V_b = 7.5V_t \tag{2.2}$$

where V_b is the burnt gas volume assuming an adiabatic expansion factor of 7.5. Applying the ideal gas law,

$$P_2 = P_1 \frac{V_1}{V_2} \tag{2.3}$$

where

P_2 = absolute system pressure after combustion (atm)

P_1 = 1 atm

V_1 = system volume after combustion ($V_b + V_d$) (m^3)

V_2 = system volume before combustion ($V_t + V_d$) (m^3)

$$P_2 = 1x\frac{7.5V_t + V_d}{V_t + V_d} \tag{2.4}$$

Hence, the total system overpressure, P_{sys} is given by;

$$P_{sys} = \frac{6.5V_t}{V_t + V_d} \tag{2.5}$$

This calculation was performed for each test vessel volume and values of P_{sys} are listed in Table 2.1.

2.3 Construction details

2.3.1 Test vessels

The Test vessel 1 was made up from the existing 0.5 m diameter and 1 m length cylindrical test vessels that have been designed to BS1560 and rated at 28 bars as illustrated in Fig. 2.2. The vessel was drilled with tapped bosses welded on at positions along their length, to allow instrumentation in the form of thermocouples and pressure transducers to be fitted. A removable blank plate was used to close one end of the vessels. This was centrally drilled and tapped to allow a spark plug, hose connected to the barometer and hose connected to vacuum pump to be fitted. At the other end of the vessel, a 0.162 m diameter was drilled to simulate the vent area of 0.012 m^2. A certified hydraulic pressure test had been carried out on the test vessels before commissioning the tests. A scaled drawing of test vessel is shown in Fig. 2.2 and major dimensions and pressure rating are listed in Table 2.1.

The Test vessel 2 was made up from 0.162 m diameter and 0.315 m length cylindrical test vessels that have been designed to BS1560 and rated at 35.5 bars (Fig. 2.3). The vessel was drilled with tapped bosses welded on at positions along their length, to allow instrumentation in the form of thermocouples and pressure transducers to be fitted. A removable blank plate was used to close one end of the vessels. This was centrally drilled and tapped to allow a spark plug, hose connected to the barometer and vacuum pump to be fitted. Series of test on Test vessel 2 were carried out to investigate the effect of vent area on explosion development. The single-hole orifice plate was used to simulate the objective on varying the vent area which placed at the end of the vessel just before the gate valve and it gives,

$$A_v = (1 - BR)xA \tag{2.1}$$

where A_v is the vent area, BR is the blockage ratio of the orifice plate and A is the area of the plate.

For venting with relief pipes, 1 m pipe length has been connected to the other end of the Test vessel 1 for a constant vent area of 0.012 m^2 which been called a Test vessel 3 (Fig. 2.3). For 1 m pipe, there were two different internal diameter pipe fitted, i.e. 0.162 m and 0.315 m. Vessel support was in the form of moving frames fabricated in-house from L-section mild steel. Further, the test vessel was tied with the cradle of the crane to ease the movement to facilitate quick replacement of vent cover and pipe length without major rig dismantlement.

The open ended nature of the test vessels necessitates a method of isolation during fuel-air mixture preparation. This involved the closing of the gate valve (see Equipment Specification section) that has been bolted between the flange at the open-end of the test vessel and the flange of the dump vessel or the flange of the pipe if the pipe was connected to the test vessel. A compressed air supply with a line pressure of 10 bars was provided for valve operation which via solenoid valve, could be manually controlled by a switch in the Control room.

Table 2.1 Test vessel design details

	Test vessel 1	**Test vessel 2**	**Test vessel 3**
Internal diameter (nominal) (m)	0.5	0.162	0.5
Length (nominal) (m)	1.0	0.315	1.0
Wall thickness (m)	0.127	0.034	0.127
Design pressure (bar)	28	35.5	28
Flanges			
Class (BS1560,1970)	300	300	300
Flange thickness (m)	0.068	0.0365	0.068
Number of bolts	20	12	20

Bolt-hole diameter (m)	0.042	0.022	0.042
Bolt-hole PCD (m)	0.670	0.2699	0.670
Diameter of bolts(m)	0.038	0.019	0.038
Pipe section			
Internal diameter(m)	-	-	0.162/0.315
Section length (m)	-	-	1/1
Wall thickness(m)	-	-	3.4/3.4
Design pressure(m)	-	-	35.5/35.5
Length-to-diameter ratio(L/D)	-	-	6.17/3.17
Assembled test-vessel			
Length-to-diameter ratio(L/D)	2.0	1.94	2.0
Volume, V_t (m3)	0.2	0.0065	0.22/0.28
Ratio to total system volume to test volume, V_T/V_t	260	8000	235/187
System overpressure due to adiabatic combustion, P_{sys} (mbar)	24.9	0.812	27.5/34.6

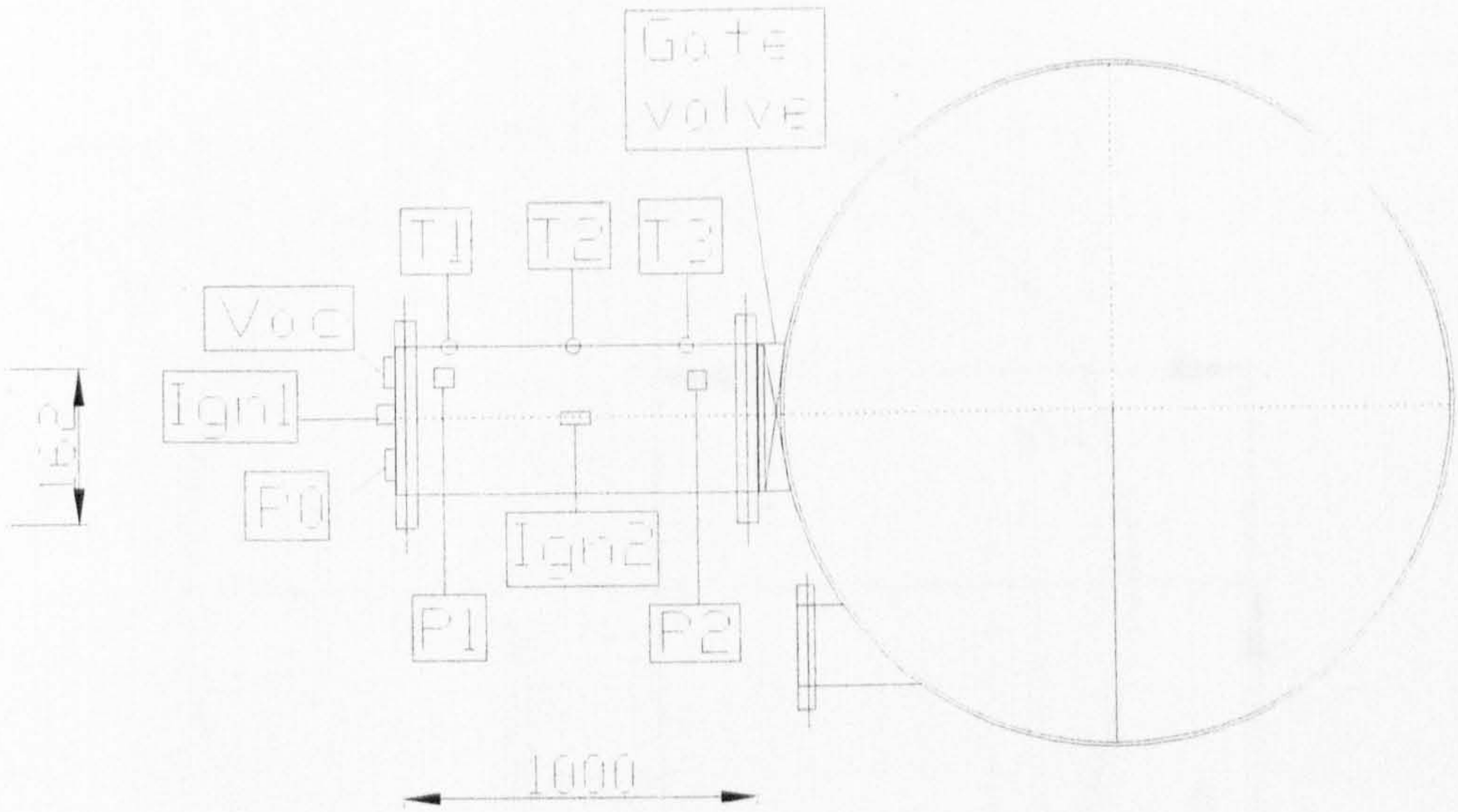

Test vessel 1

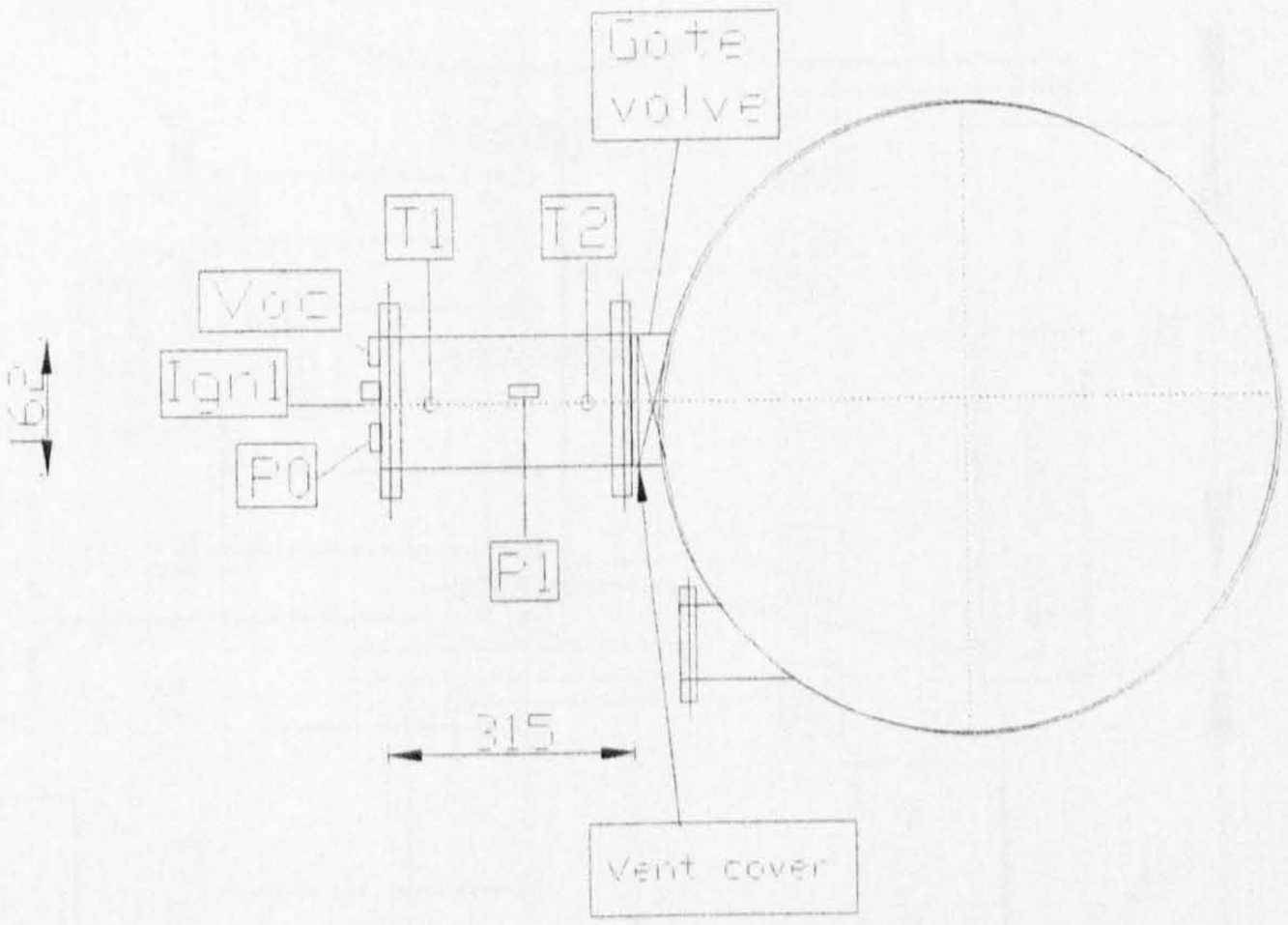

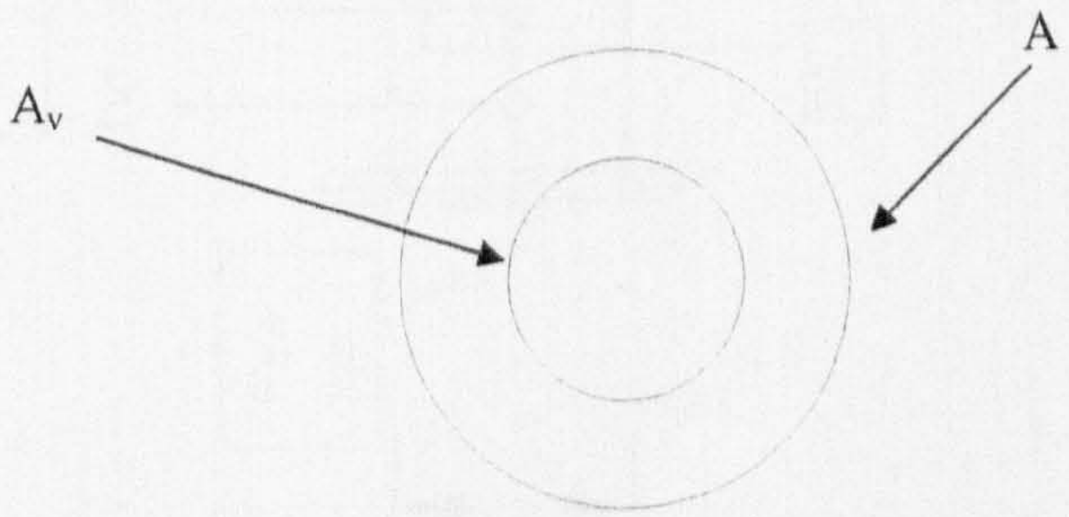

Test vessel 2

Figure 2.2 Schematic drawing for Test vessel 1 and 2

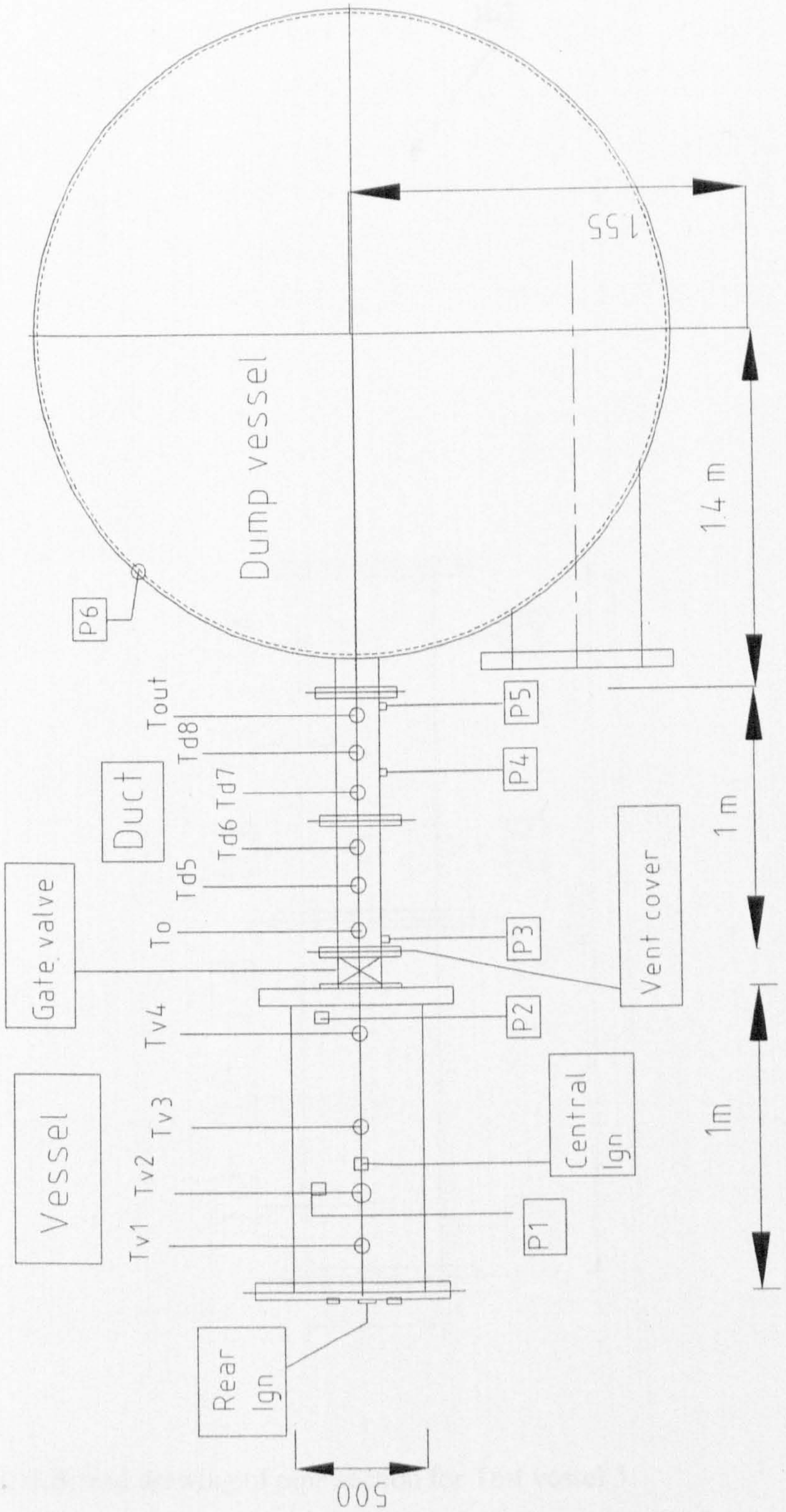

Figure 2.3 Scaled drawing of Test vessel 3 with pipe attached

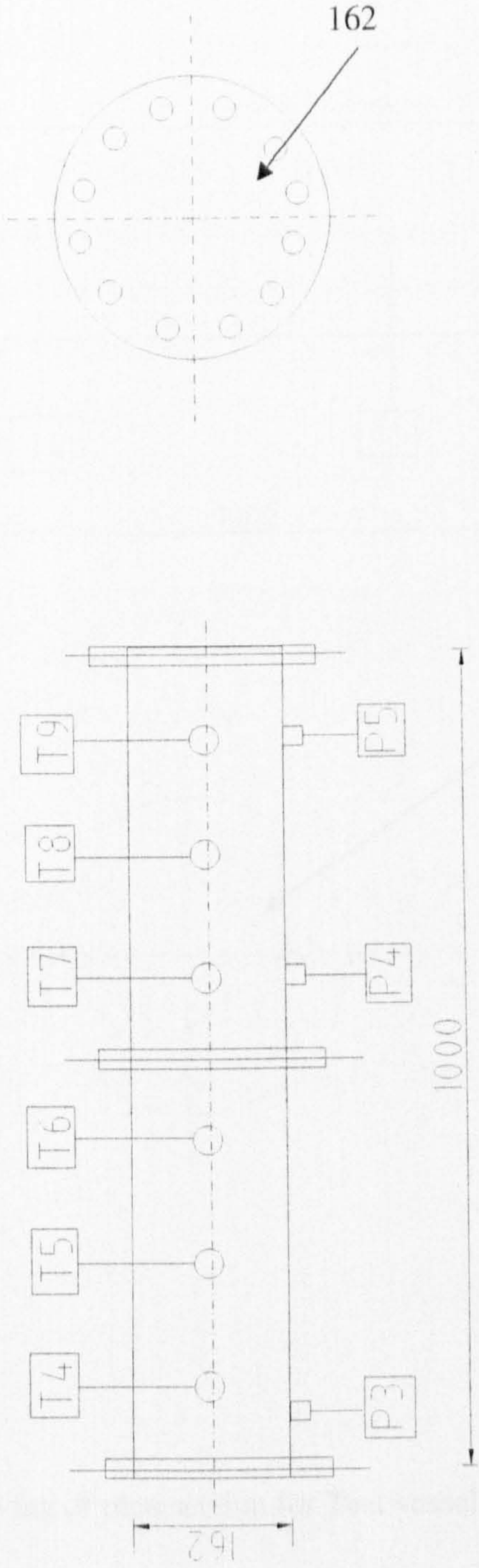

Figure 2.3a Scaled drawing of pipe section for Test vessel 3.

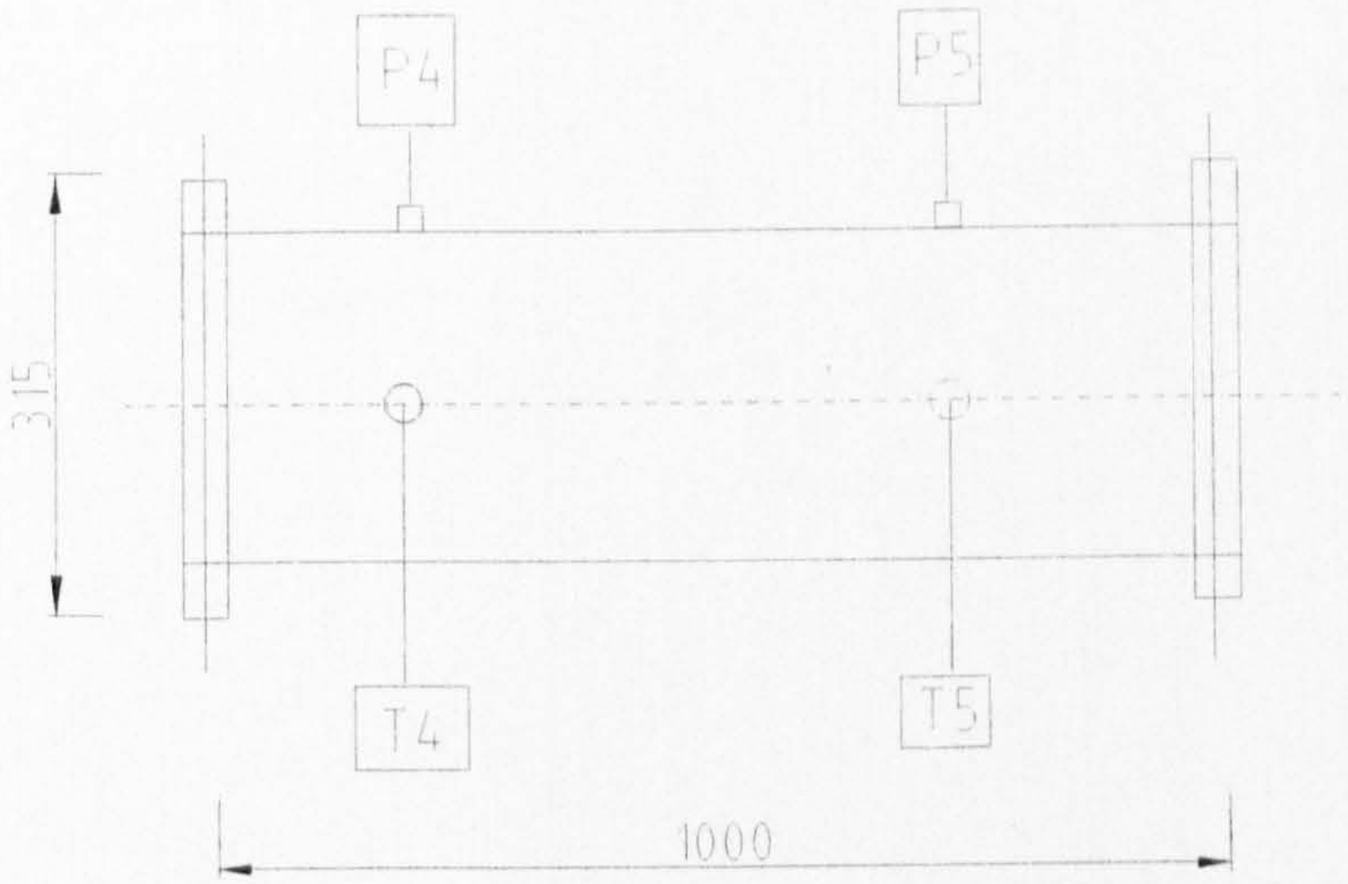

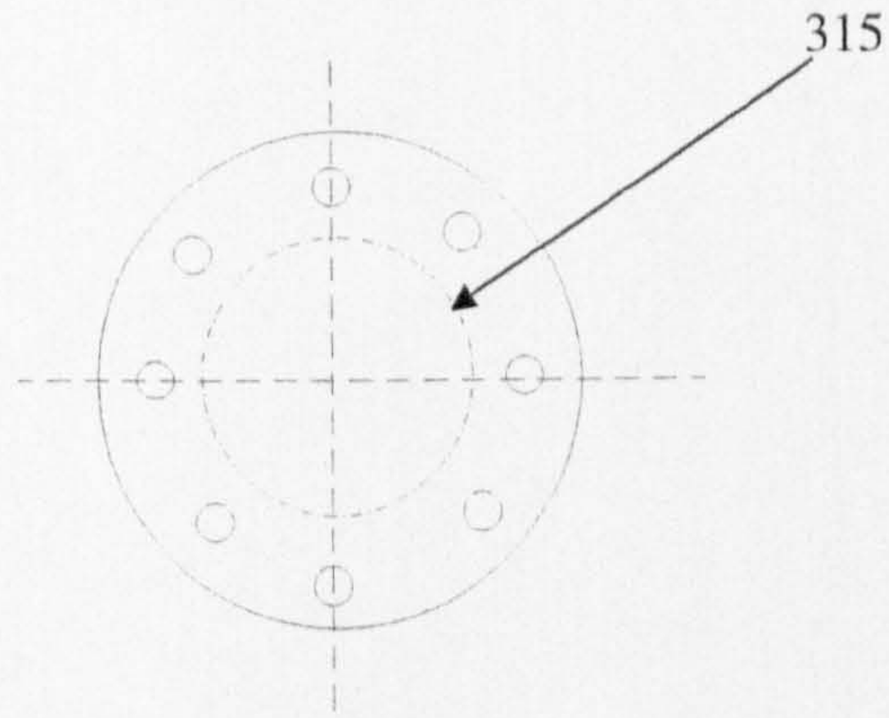

Figure 2.3b Scaled drawing of pipe section for Test vessel3.

2.3.2 Dump vessel.

The dump vessel was designed in-house as a cylindrical shell with dished ends. Flanges openings were included at various positions, with diameter matched that of the test

vessels. Their locations were determined by considering possible future research as well s the requirements of the present project.

Space restrictions limited the major linear dimensions of the dump vessel to 8 m in length and 2.5 m in diameter. This gave a volume of approximately 40 m3. Single piece torispherical dished ends of nominally 10 mm thickness were welded at both ends of the vessel. The large 1500 mm diameter flanged openings were supplied with flat blanks to close the vessel. Figure 2.4 shows scaled drawings of the dump-vessel and major dimensions are listed in Table 2.2.

Instrumentation ports were fitted so that the explosion pressures could be monitored at various distances from the test vessel exit. Fittings were tapped bosses welded on the dump-vessel back wall, opposite the test vessel connection points. Ports were also located in the dump vessel front-wall above the test vessel exit points.

Blanking plates were drilled and tapped to allow connection of pipe work to facilitate evacuation via an external vacuum pump or the introduction of compressed air. Pressure rated ball valves were used to isolate connection ancillary equipment from the dump vessel prior to ignition in the test vessel. Before explosion testing was started, a certified hydraulic pressure test was carried out by pressuring the water filled vessel to 11.25 baro.

Table 2.2 Dump vessel design details

Shell	
Internal diameter (m)	0.247
Length (m)	0.672
Shell thickness (m)	0.015
Torispherical (2:1) Dished ends	
Outer diameter (m)	2.500
Nominal plate thickness(m)	0.010

Assembled structure						
Total length (m)	0.800					
Design pressure (bar)	9					
Certified pressure(hydraulic test) (baro)	11.25					
Flanged openings						
Type	Nominal bore	Neck thks	Flange	Number bolts	Bolt-hole PCD (m)	Rating
N1	1.524 m O/DIA	20 plate	Special	52	1.759	Special
N2	0.508 m O/DIA	10 plate	RFSO	20	0.635	BS 4504 40/3
N3	0.162 m	SCH 40	RFSO	12	0.2699	BS 1560 class 300
N4	0.0762 m	SCH 40	RFSO	8	0.1683	BS 1560 class 300
N5	¼ '' BSP	COUPLING			-	Special

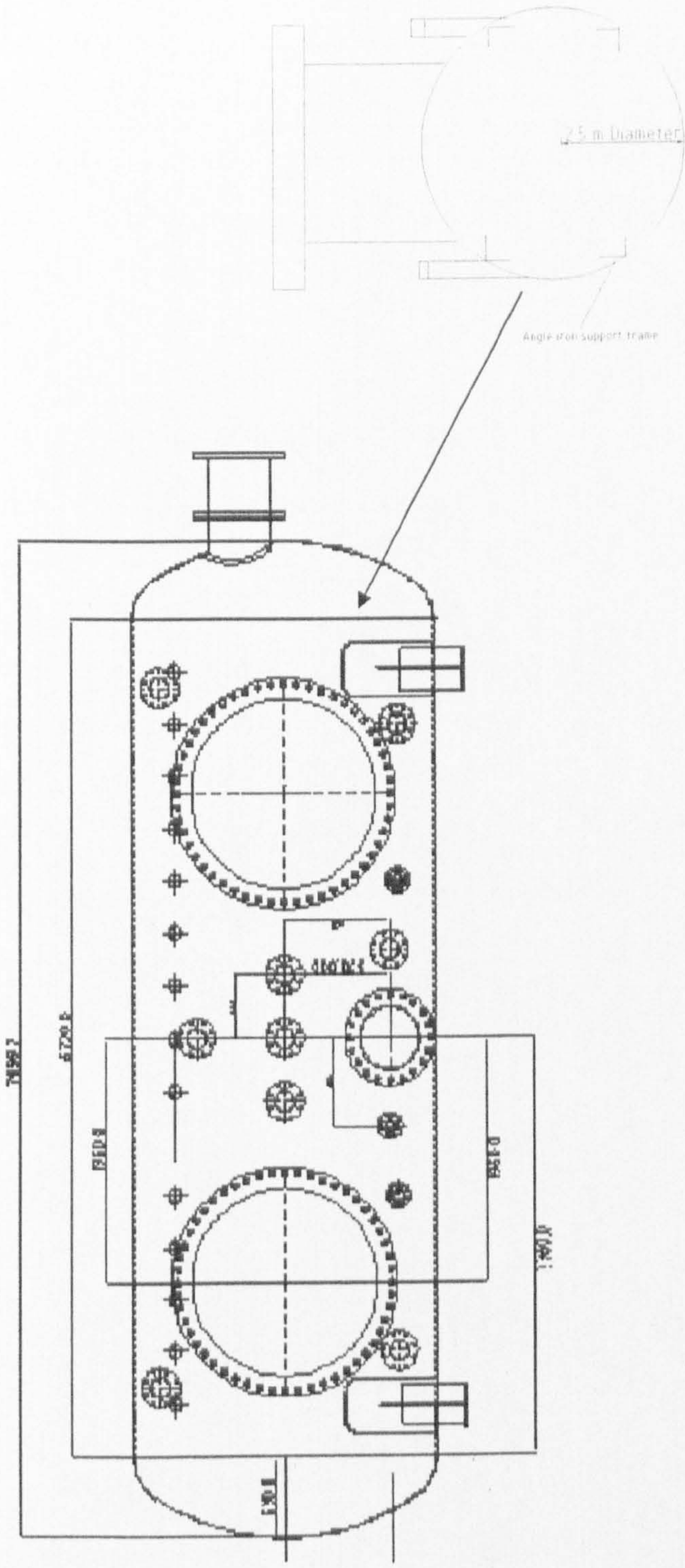

Figure 2.4 Dump vessel schematic designs

2.4 Vent cover selection

The vent covers were selected with a range of vent bursting pressure, P_{stat} in between 0.1 to 0.5 barg. Four vent covers were used; magazine paper, aluminium foil, Melinex membrane or Mylar film and 100g A4 paper. The vent cover was clamped between two steel plates before it placed at the end of the test vessel. Using compressed air, the vent bursting pressure, Pstat was determined experimentally. The lists of the vent cover used and its P_v were listed in Table 2.3

Table 2.3 List of P_v of vent covers used

Material	**Pv (expt)**	**Thickness (mm)**	**Average mass/area (kg/m^2)**
Magazine paper	0.097	0.5	0.014
Aluminium foil	0.178	0.21	0.011
Melinex membrane	0.209	0.20	0.004
100g A4 paper	0.424	0.12	0.02

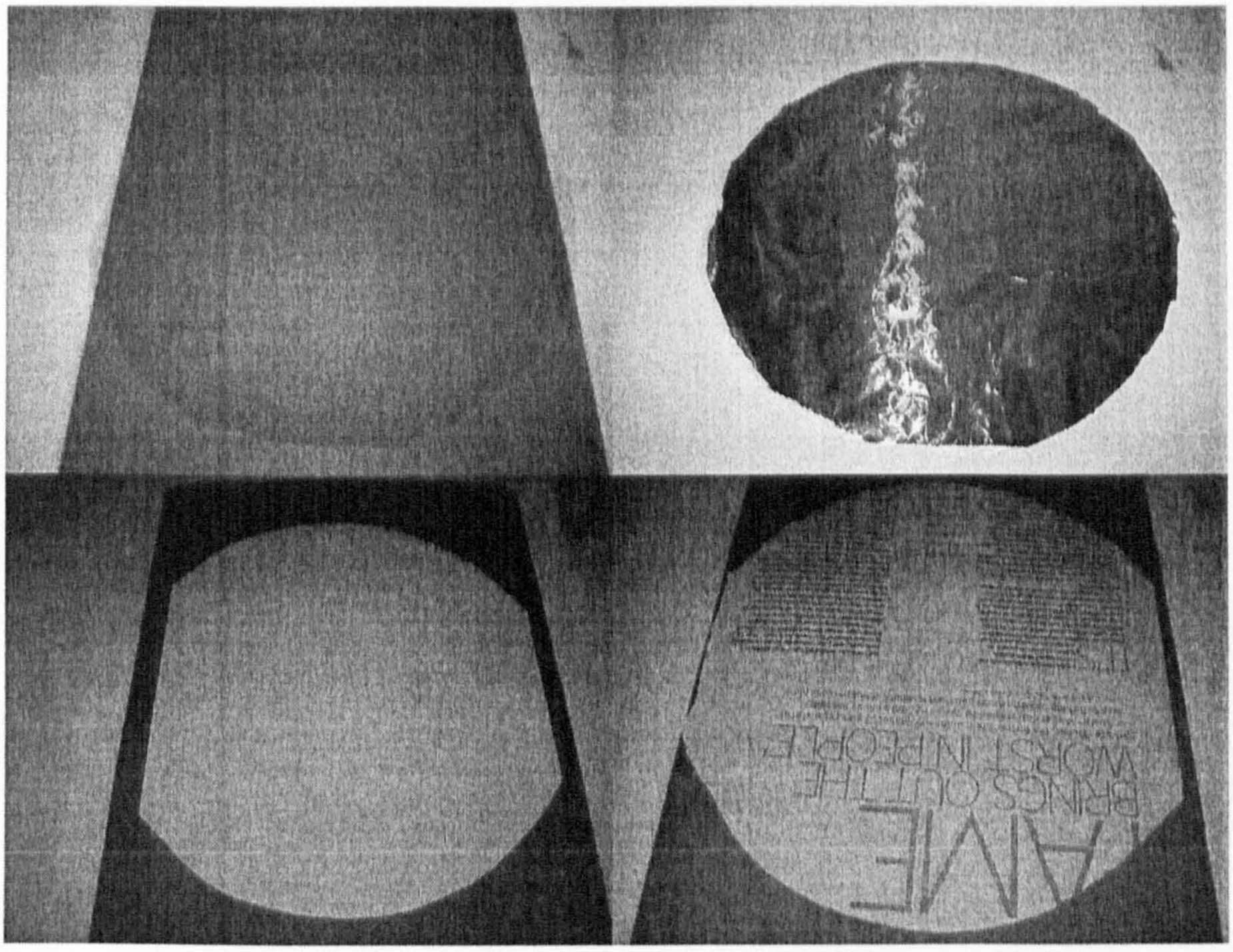

Figure 2.5 Vent covers used in the tests. From top left: Melinex membrane, aluminium foil. From bottom left: 100g A4 paper and magazine paper

2.5 Instrumentation and data collection

2.5.1 Instrumentation techniques

Important parameters studied in the general analysis of gas explosions are the flame speeds and maximum pressure attained during explosion development. Most experimental studies have included transducers to measure explosions overpressure. Various types have been employed including those of diaphragm and piezo-electric operation. For this present project, the relatively high pressure generated and large scale experimental rig meant that there were safety considerations to rule out the visualisation technique to monitor flame travel.

2.5.1.1 Explosion pressure history

As described earlier, threaded bosses were welded along the test vessels walls at drilled positions as locations for explosions monitoring equipment. The instrument employed then became an integral part of the test apparatus and therefore would be subject to the same internal pressure. The instrumentation therefore had to be robust enough to withstand the explosion pressures without losing its sensitivity. Absolute explosion pressures were measured in the test vessels and the dump vessel using Keller type-PAA/11 piezoresistive pressure transducers. They had a 5 bar measurement range with a maximum pressure measurement rating of 10 bar. They had high sensitivity combined with stability and shock resistance. Test vessel pressure transducers were located in the ignition-end flange and along its length as shown in Fig. 2.2, 2.3 and 2.3b.

All the pressure transducers were calibrated using a standard hydraulic dead-weight calibrator. This was performed with the transducers connected to the data acquisition system. Calibration of this integrated system eliminated any errors that might arise from the electronic circuit connecting the instrumentation to the data logging system.

2.5.1.2 Measurement of flame positions

A thermocouple junction placed in the path of a flame travel will register its arrival as a change in voltage potential across the junction. This is recorded as a distinct change in the analogue output of the thermocouple. Accurate measurement of the time of this signal change relative to that measured from an adjacent probe allowed the average flame speeds to be calculated at the midpoint between the two probes. This thermocouple technique has been used to monitor the flame arrival in previous explosion studies (Gardner, 1998) and the system was validated by comparison to photographic records of explosions in a closed spherical vessel. Figure 2.6 shows examples of thermocouple signals as displayed on a computer screen from which flame arrival time measurement were taken using a movable cursor. This thermocouple technique was a primary method of flame monitoring used in this study.

The thermocouple tips had an inherent thermal mass; however since all the thermocouples were at the same specification, it was assumed that they had the same response time. It should be noted that the thermocouples were not used to measure the temperature but merely detecting any change in temperature. The time delay or response time, usually refers to the time lag for full response to the stimulus and therefore, is not relevant at this point.

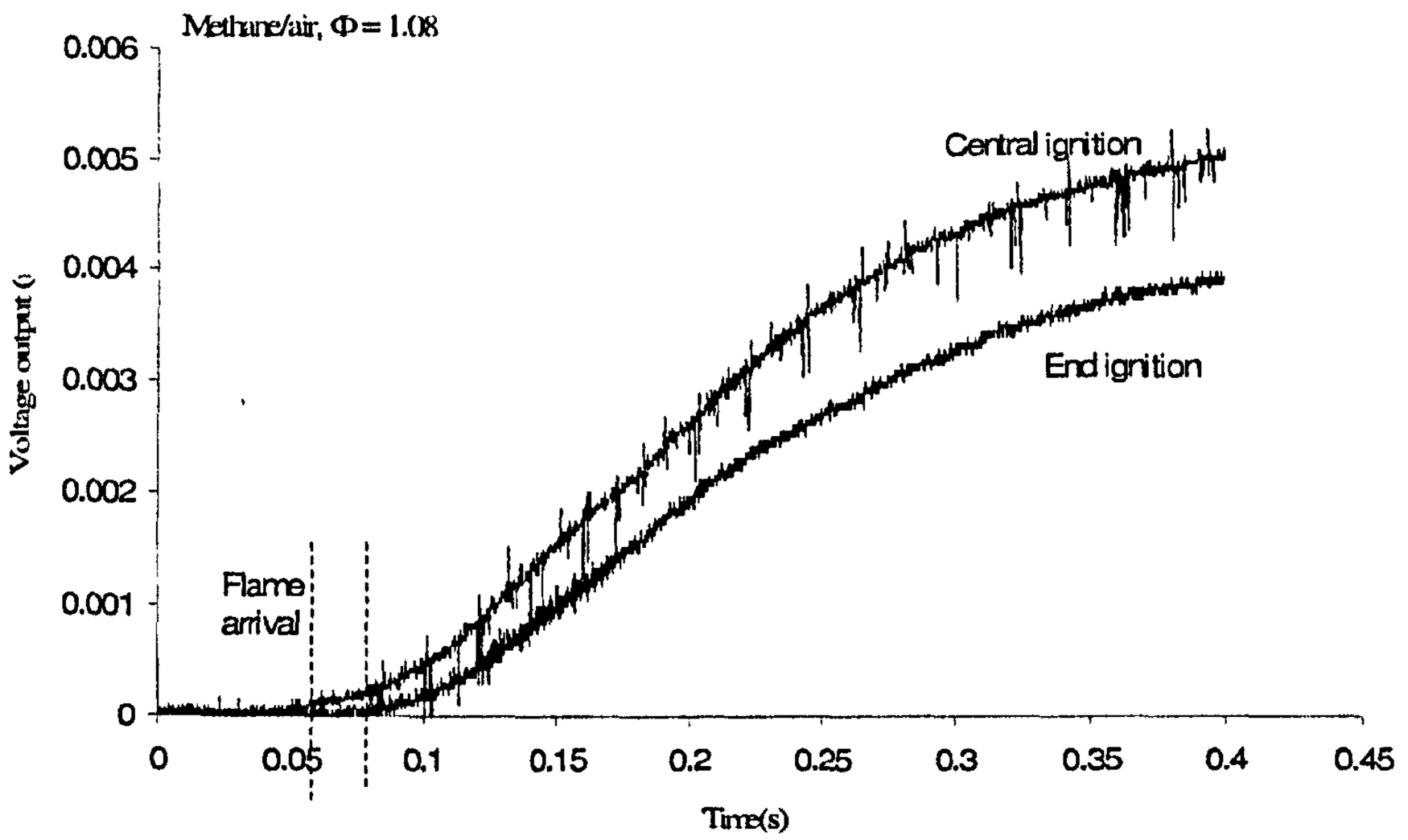

Figure 2.6 Typical thermocouple traces indicating the change in voltage output due to flame arrival.

2.5.1.3 Thermocouples

Exposed junction, mineral insulated type-K thermocouples as illustrated in Fig. 2.7 which been supplied by Fitmec Ltd. Oldham were used. The main body had a diameter of 3 mm and was located through the vessel wall so that the exposed 0.6 mm-diameter conduction wires were on the axial centreline of the test vessel. Each test vessel was fitted with up to twelve thermocouples along its length. Threaded Swagelock compression fittings were used to seal the units in tapped BSP bosses. The thermocouples were located through the vessel walls and so would be subject to high dynamic loads resulting from high velocity gas flow impact, before and after the flame arrival. In order to limit the bending and maintain accurate positioning of the

thermocouples, support structures were built into test vessels as well as along the pipes that were used.

The support consisted of a 1 mm diameter connecting wire, suspended above the axial centreline of the vessel from the thin metal strips at the end of the vessel. The percentage linear blockage of each strip was less than 0.4 %. Circular washers were used to hold the thermocouples 15 mm above their exposed junction.

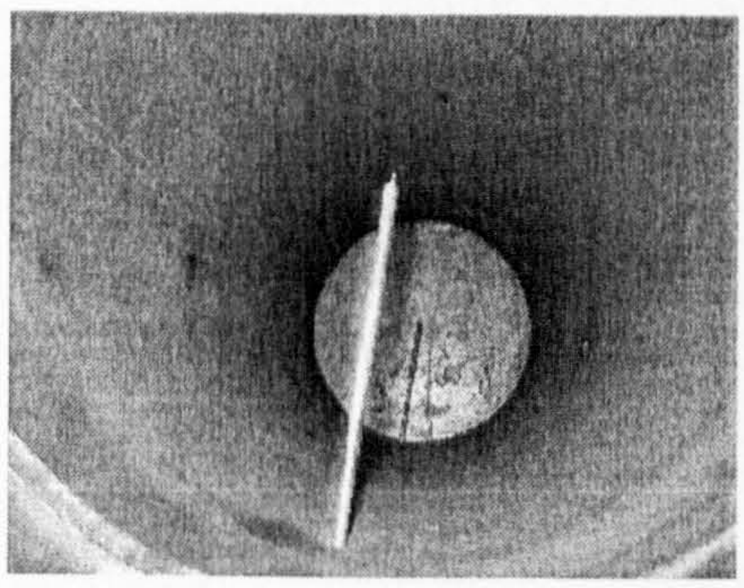

Figure 2.7 Exposed junction, mineral insulated type-K thermocouples inside the rig.

2.5.1.4 Flame speed calculation

By dividing the distance between two thermocouples with the time difference in flame arrival, the average flame speed between the two thermocouples could be calculated and assigned to the midway position. This method of flame speed calculation was possible from saved raw data from the thermocouples upstream of the test vessels. From raw data, all thermocouples were normalised using computer command in FAMOS.

During the initial stage, flame speeds were relatively low but will dramatically increase towards the downstream of the vessels and to the connecting pipe. Using the flame speeds method described above, the flame speeds were calculated at some positions. In order to extract precise results, a technique was employed to eliminate the excessive flame speed fluctuations. The method involved 'smoothing' the distance-time data by successive calculations of the flame speed at the midpoint of two adjacent points. The smoothing process is illustrated in Table 2.4.

Table 2.4 Procedure in calculating the flame speeds from raw data

Thermocouple distance-time smoothing method			
Raw data			
Flame arrival time, t	T/C position, x	Flame speed	Flame position
$t_{0,0}$ (ignition)	$x_{0,0}$		
$t_{1,0}$	$x_{1,0}$	$(x_{1,0}-x_{0,0})/(t_{1,0}-t_{0,0})$	$(x_{1,0}-x_{0,0})/2 + x_{0,0}$
$t_{2,0}$	$x_{2,0}$	$(x_{2,0}-x_{1,0})/(t_{2,0}-t_{1,0})$	$(x_{2,0}-x_{1,0})/2 + x_{1,0}$
$t_{3,0}$	$x_{3,0}$	$(x_{3,0}-x_{2,0})/(t_{3,0}-t_{2,0})$	$(x_{3,0}-x_{2,0})/2 + x_{2,0}$
$t_{4,0}$	$x_{4,0}$	$(x_{4,0}-x_{3,0})/(t_{4,0}-t_{3,0})$	$(x_{4,0}-x_{3,0})/2 + x_{3,0}$
$t_{n,0}$	$x_{n,0}$	$(x_{n,0}-x_{n-1,0})/(t_{n,0}-t_{n-1,0})$	$(x_{n,0}-x_{n-1,0})/2 + x_{n-1,0}$
Smoothing data			
$t_{0,1}= t_{0,0}$	$x_{0,1}= x_{0,0}$		
$t_{1,1} = (t_{0,0} +t_{1,0})/2$	$x_{1,1} = (x_{0,0} + x_{1,0})/2$	$(x_{1,1} -x_{0,1})/(t_{1,1} - t_{0,1})$	$(x_{1,1} -x_{0,1})/2 + x_{0,1}$
$t_{2,1} = (t_{1,0} +t_{2,0})/2$	$x_{2,1} = (x_{1,0} + x_{2,0})/2$	$(x_{2,1} -x_{1,1})/(t_{2,1} - t_{1,1})$	$(x_{2,1} -x_{1,1})/2 + x_{1,1}$
$t_{3,1} = (t_{2,0} +t_{3,0})/2$	$X_{3,1} = (x_{2,0} + x_{3,0})/2$	$(x_{3,1} -x_{2,1})/(t_{3,1} - t_{2,1})$	$(x_{3,1} -x_{2,1})/2 + x_{2,1}$
$t_{n,1} = (t_{n-1,0} +t_{n,0})/2$	$x_{n,1} = (x_{n-1,0} + x_{n,0})/2$	$(x_{n,1} -x_{n-1,1})/(t_{n,1} - t_{n-1,1})$	$(x_{n,1} -x_{n-1,1})/2 + x_{n-1,1}$

As mentioned earlier, Fig. 2.6 shows flame position against time of flame arrival data for 9.5 % CH_4/air in a simply vented test for open venting in Test vessel 1 between thermocouples at the centre and at the exit of the vessel where the high flame speeds were generated. The data series represent successive 'smoothed' values using the method described in Table 2.4. These thermocouple to flame speeds procedures needed

to get precise and accurate flame arrival time as well as the flame speeds for the tests done.

2.5.2 Data acquisition

The short duration of the highly transient explosions meant that accurate analysis required high speed data collection from the various instrumentations positioned throughout the test geometry. Processing the large number of recorded data was aided by specialised analysis software.

Initiation of data captured and the time of ignition were synchronised using Wind speed Wavecap software which allowed parameters such as sampling frequency and pre- and post- trigger sampling times to be varied.

Instrumentation was wired to a 34-channel Microlink 4000 system which designed for capturing high speed waveform with a sampling frequency of maximum 200 kHz per channel. The system monitored the 34 analogue inputs comprising pressure transducers and thermocouples. Analogue/digital conversion used 2 bit ADC, giving a resolution of 1 part in 2^{12} (= 4096). The voltage measurement range for pressure transducer was between 0 to 100 mV. For a pressure measurement range of 0-5 bar, the resultant transducer resolution was ±1.2 bar. The stored digital data was transferred to the computer network in the Control room. From this, subsequent signal conditioning and analysis was carried out using FAMOS software.

2.6 Identification hazards and safety measures

Hazards identification and handling were based on the experiences gained over the long-term, safe operation of similar cases and on advises and input received from University Health and Safety Officers. A number of possible hazard generation mechanisms were identified and associated safety measures were incorporated into the design and operation.

2.6.1 Vessel failure

The design features of the vessel in this study were listed in Table 2.1 and 2.2. All test vessels were pressure tested and certified to withstand pressure above 8 baro. This is the maximum adiabatic overpressure that can be generated by any fuel-air explosion initially at 1 bar. The possible transition to detonation combustion was also taken into consideration. The actual design pressure for each test vessel was higher than the overpressure associated with detonation.

The large volume dump-vessel was hydraulically tested at 11.25 baro. In accordance with the relevant regulation for the design of large pressure vessels, a pressure relief valve was fitted. The opening pressure of this valve was set at the design pressure of the vessel.

2.6.2 Transmission of the explosion to auxiliary equipment

The preparation of fuel-air mixture involved auxiliary equipment such as external pumps and monitoring systems which all specification will be described in later section. A safety operation procedure was designed to ensure that all procedures will be followed and applied for each test. In order to isolate the test vessel just prior to ignition, various ball-valves were closed and fuel-lines disconnected. The spark ignition circuit incorporated safety features that involved the closure of several electrical contacts. This is described in detail in later section. An important part of the circuit was a mixture inlet line safety interlock. The filling line had to be disconnected from the test vessel and then connected to the electrical interlock before ignition took place. The gas cylinder bottle was therefore isolated from the vessel before ignition.

2.6.3 Release of combustible gas into the Test room

This hazard was not specified to this facility but was also applicable to any University area where combustible gases were present and handled. In the event of an accidental explosion within the Test room, it was expected that the blast would be relieved to the outside through the large window along the external wall. This large vent area was expected to reduce the pressure below level that might damage the partitioning walls that isolated the Control room. The glass windows were covered with a clear membrane that was specially designed to limit the glass pigmentation.

2.7 Operating procedures

Due to large number of operations and safety checks involved in a single explosion test, an Operating Procedure form was devised that had to be completed during each test. This form contains all experimental steps that needed to be followed as well as the safety procedures. A flow diagram is shown in Fig. 2.8 that illustrates the safety procedures and guidelines that account for any deviations from the operational procedure. As part of the experimental programme, three repeat tests were performed at each condition and these demonstrated good reproducibility, with peak pressures varying by less than ±5% in magnitude.

2.7.1 Fuel entrainment

In order to create a combustible mixture of known composition, the volume of both fuel and air introduced into the test vessel had to be known accurately. The theory of partial pressure was applied to an accuracy of 0.1 mbar (0.01% of composition). The final pre-ignition mixture pressure was set at ambient pressure (~ 1 atm) for all tests. For example, to make up a mixture with 10% fuel/air ratio, the test vessel was evacuated to a vacuum pressure that allowed fuel to be introduced before letting the ambient air to fill in the test vessel to reach ambient pressure.

2.7.2 Ignition procedure

All isolating valves were closed and the mixture inlet line was disconnected from the test vessel and connected to a safety interlock. The data acquisition software was armed and ignition circuit integrity was indicated by light on the ignition control panel after the opening of the gate valve. The 'fire' button was pressed and this activated the spark plug and by this, it triggered the data collection system. Once the sampling time was over, the raw transducers data were displayed using FAMOS software. Output signals were recorded to check whether a pressure rise had occurred in the system and the maximum overpressure is not exceeded the critical adiabatic pressure of the fuel/air.

2.7.3 Vessel purging

Purging involved evacuation of both test vessel and the dump vessel using vacuum pump B (refer to later section). Once a sufficiently low vacuum pressure was attained, air was allowed to enter the system for more than ten minutes. This procedure was to ensure that the system atmosphere matched that of the outside ambient air. The test facility was then ready for the next test preparation.

2.8 Ancillary equipment

The preparation and ignition of fuel/air mixture inside the test vessel and its subsequent purging involved various equipments with associated pipe works and valves. As described in the previous section (refer to section 2.7), the procedures involved including the evacuation of the test vessel, mixture preparation and recirculation and control of the dump vessel pressure. Isolation of all ancillary equipment was required before ignition and the test vessel had to be isolated from the connected pipe (if venting with relief pipe geometry was carried out) and dump vessel during mixture preparation.

2.8.1 Isolation valves and pipe works

All valves that attached to the test vessel and the dump-vessel are needed to be closed prior to the ignition in order to stimulate the confined vessel condition. The fuel connecting pipe, the pipe attached to the vacuum pump and the pipe attached to the barometer should be disconnected prior to ignition. Step-by-step test procedure is shown in Fig 2.9.

2.8.2 Mixture pressure monitoring system

The theory of partial pressure was used to prepare a mixture of an accurately known composition. This required accurate knowledge of the test vessel pressure under vacuum. A Diametric type 600 Barocel pressure sensor was used to monitor the test vessel pressure during mixture preparation. The unit was fitted into the test vessel filling line circuit so that the mixture pressure could be monitored at all times. Its principle of operation was to transducer absolute vacuum pressure into a dc output voltage precisely proportional to input pressure. Advanced design allowed pressure measurement over a wide range of input pressure with high accuracy and stability. The unit was connected to a Diametrics type 1500 digital pressure display. The combined system allowed the mixture pressure to be monitored to a resolution of ±0.05 mbar. For a final pre-ignition pressure of ~1atm, a 10% CH_4-air mixture could be prepared to an accuracy of 0.05%.

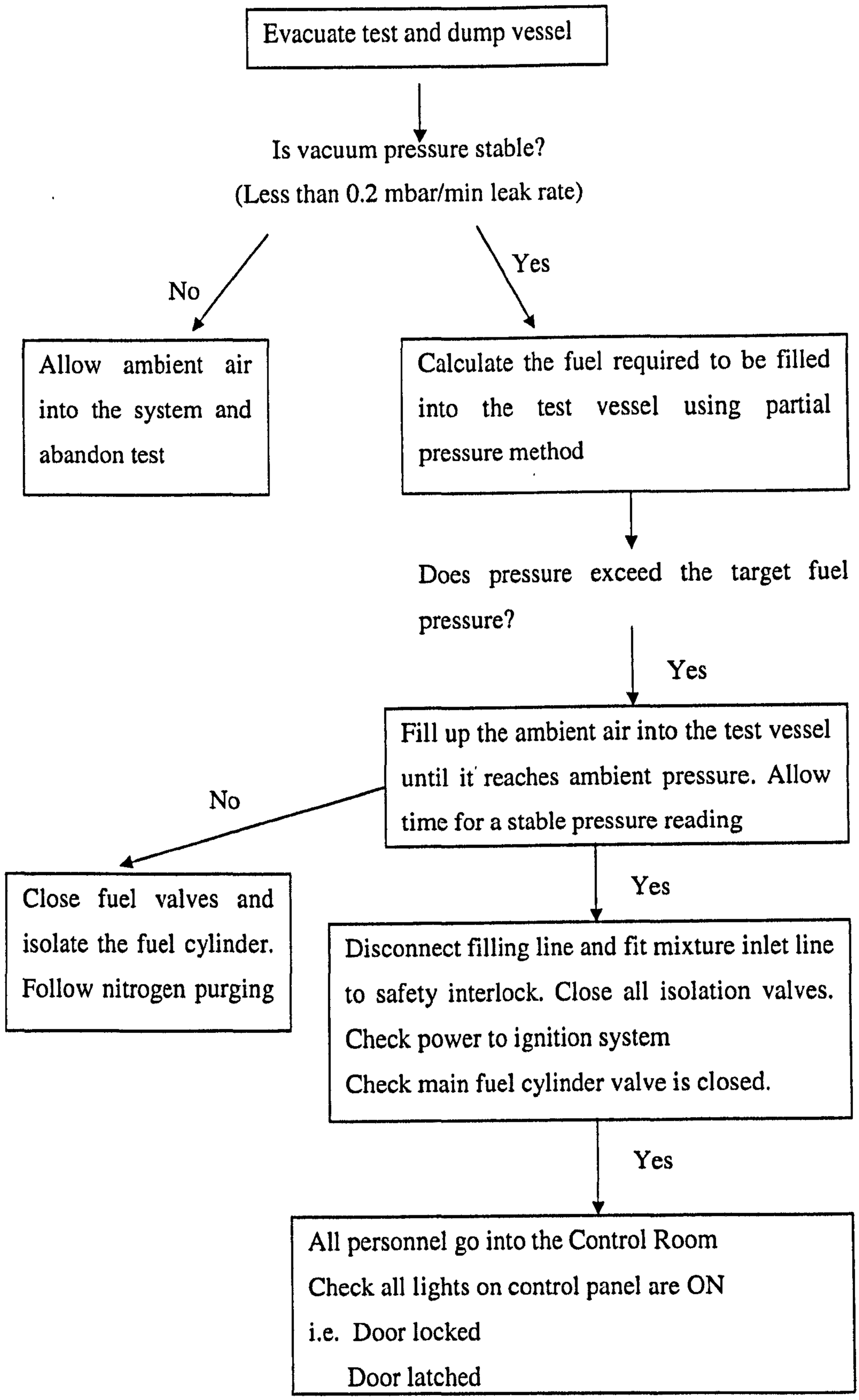

Figure 2.8 Flow diagram illustrating safety and operational procedure

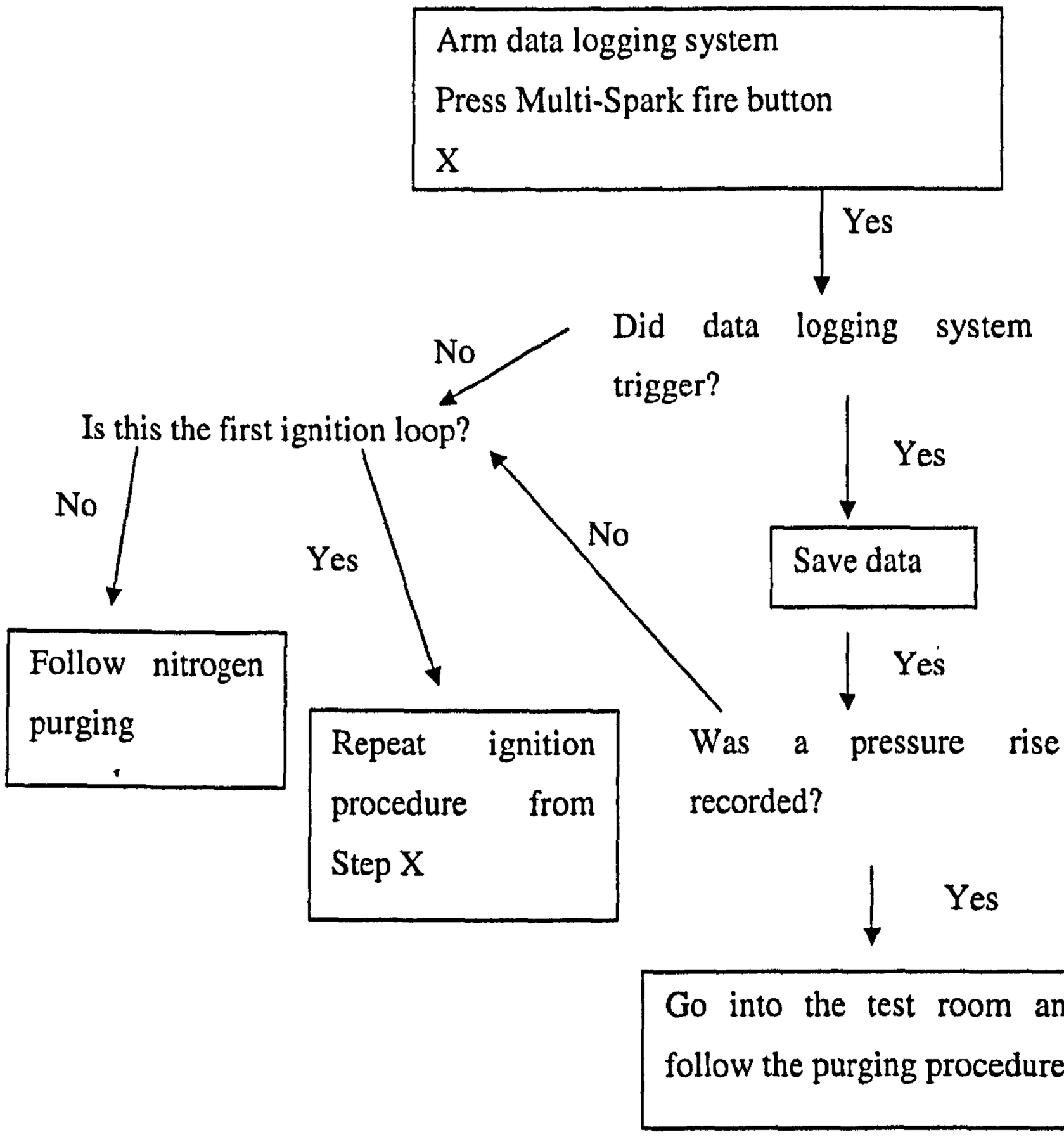

Figure 2.8 contd.

Date:		**Description:**	**Fuel:**
Test No:			**Concentration:**
Vent cover :			**ignition:**
Authorised by:			**injection:**

Procedure: **SIMPLY VENTED** Sheet: CH4, C3H8, **C2H4, H2 premixed, 0.315m-L x 0.162m-D CYLINDRICAL VESSEL**

Tick	Operation	Instruction	Action/Remarks
	Initial Start State		
	System purged		
	Pretest Conditons		
	Power to barocel		
	Load datalogging software		
	Close the gate valve		
	Vent cover in place		
	2WV to Test Vessel	**Ambient P** = (barocel)	
		Ambient T = C	
		Humidity = %	
		Timebase = uSec	
	Close GV1		
	Close V2		
	Open D5		
	Pretest checks		
	Power to spark		
	Audible test of spark		
	Open F1		
	Check bottle pressure		Ensure enough fuel >5 bar
	Open and Set regulator F2		Set to ~2bar
	Open and Set regulator F3		
	Operating State Connect & Evacuation		
	Connect		
	CP1 to V1		
	Open V1		
	CP2 to V3		
	2WV to Test Vessel		Check test vessel pressure
	Open D6		
	2WV to Dump Vessel		Check dump vessel pressure
	2WV to Test Vessel		
	Evacuation		
	Open CB1		
	Start Vac B	Vac to < 30 mbar	
	Close CB1		
	Stop Vac B		
	Is leak rate < 2 mbar/min?		if No: see S/P 1
Y / N	**Operating State CH4/ C3H8/ H2 filling**		
	Note & Record Vac P	% fuel required=	
		Vac P =	
		Fuel P required=	
		Total fill (vacP+fuel)=	
		Vf = litre	tf = second
	Open V3		
	Meter to total fill P	Actual pressure =	
	Close F1,F2,F3		
	Air filling		
	Close D5		
	Record required P	**Final pretest P =** **mbara**	(day ambient pressure)
	Crack V2 for initial air fill	Fill to 50 mbar less that pretest P	
	Close V2		
	Close V3	**Record pretest P (driver vessel)=**	**mbara**
		Record pretest P (dump vessel)=	**mbara**
	Close V1		
	Close D6		
	System Check		
	All valves Closed		
	Disconnect		
	CP1 from V1		
	CP2 from V3		
	Ignitor State : Sequence		
	All to control room		
	Lock doors		
	Start, Arm datalogger		
	Open GV1		
	Ignition	**Ignition Time =**	
	Data logging ends		
	Save data		
	Purging End State		
	Purging the test vessel		
	Connect CP1 to V1		
	Open V1		
	Open CB2		
	Start Vac B		
	Crack D5		
	Open V2		
	Open D2		
	Allow vac to run for >10 mins		
	Stop Vac B		
	Close CB2		
	Allow vessel pressure to reach ambient		
	CloseD2		
	Close V1		
	Disconnect CP1 from V1		
	Data check		
	Load test results		
Y / N	T/C & P data indicate ignition?	**Recorded (P0)(53671)=** **bara**	**bar over**
	if No: see S/P 2	**Recorded (P1)(63925)=** **bara**	**bar over**
		Recorded (P6)(53672) = **bara**	**bar over**
Y / N	is the maximum recorded pressure lower then the maximum predicted one?		if No: see S/P 3

Flame Arrival Times	
Thermocouple	Time
T4	
T5	

Comments:

Special Procedures (S/P) Sheet No.	**Cause/ Description**	**Authorised by Action**
1	Leak to atmosphere	Close all valves Abandon test Collect leak
2	No ignition ; Fault in igntion circuit	Vessel contains explosible mixture Connect N2 supply Isolate barocel Fill vessel to 1.5 bara Open CB1, Start Vac B Evacuate vessel to < 50 mbar Open V2, V3 & V4 (return vessel to ambient pressure) Re-integrate barocel Isolate N2 supply and follow purge procedure
3	Maximum pressures were underestimated;	go back to the risk-assessment stage get more accurate pressure predictions

Figure 2.9 Example of operating procedure for carrying explosion tests.

2.8.3 Vacuum gate valve

For all test vessels, a series 12 VAT vacuum gate valve with a nominal open diameter of 0.162 m was used to isolate the test vessel from the connected pipe and the dump vessel. It consisted of a light-weight aluminium body and gate with Viton seals. Shaft-feed-through was employed with pneumatic actuation. Valve operation was controlled by a solenoid valve in the compressed air supply line pipe.

2.8.4 Evacuation system

As mentioned earlier, mixture preparation in test vessel 1 and 3 involved evacuation of test vessel to certain vacuum pressure. The large vacuum pump B was used for this procedure as it involved bigger volume. For a smaller Test vessel 2, a smaller pump A was used for the same purpose.

2.8.4.1 Vacuum pump A

This was an Edwards EIM18 single direct drive, rotary vacuum pump. It has a nominal displacement rating of 340 l/min. the pumping mechanism was of the slotted rotor/sliding vane type. Direct drive was provided via a flexible coupling from a totally closed fan-cooled motor. It was controlled by an on/off switch located on the mixture preparation panel in Test room.

2.8.4.2 Vacuum pump B

This was an Edwards E2M175 to-stage rotary vacuum pump. It was an oil-sealed pump designed for reliable, long-term operation in both laboratory and industrial environment. It has a nominal displacement rating of 2967 l/min. the pumping mechanism was of the sliding vane type with high and low vacuum rotor and stator assembly. Direct drive was provided through a flexible coupling by a four-pole, three-phase motor to IP54 enclosure rating. The pump was water-cooled. Water flow was controlled by an electrical isolation valve. Power to the pump was via a main isolation valve and soft-starter.

2.8.5 Ignition system

A single conventional car spark plug was used to ignite the fuel-air mixture in the test vessels. Ignition was actuated from a standard combustion engine spark (16 J) via a high-capacitance discharge circuit. The circuit diagram is included the various safety interlocks. The system ensured that the following operations had to be carried out before spark ignition could be effected.

- The gate valve used to isolate the test vessels to pipe and dump vessel during the mixture preparation had to be opened prior to ignition. This action to ensure a vented explosion and avoid the high pressure attained inside the test vessel resulted from a closed-vessel explosion.
- The connecting door between the Control room and the Test room had to be closed and locked.
- The mixture inlet line had to be disconnected from the test vessel. This effectively meant isolation of the fuel supply prior to ignition.

Indication lights, fitted to the ignition panel at the Control room were monitored to check whether this action had been carried out. The data acquisition system was connected to the ignition circuit for triggering the fire button for data capture.

2.8.6 Nitrogen purging system

If the fuel-air mixture was not ignited might be due to the failure of the ignition spark plug or electrical faulty in ignition circuit, a relatively large volume of explosive mixture would remain inside the test vessel. Before any repairs could be made, the test vessel needed to be purged of the gas mixture. A nitrogen purging system is one of the special case circumstances that needed to be followed if this case happened. This procedure carried out by injecting high pressure nitrogen that would mix with the fuel. A standard pressure gauge on the Barocel could be monitored so that the volume of

nitrogen introduced was sufficient to inert the fuel-air mixtures. At the same time, simultaneous operation of vacuum pump B allowed the mixture to be safety purged and released to the atmosphere outside the Test room.

CHAPTER 3

VENTED GAS EXPLOSIONS: THEORY AND CRITICAL REVIEW

3.0 Introduction

The venting technique is a popular and effective prevention method to reduce explosion hazard in industrial containers of flammable gases, liquids and powders (Eckhoff, 1991). Venting is possible because most hydrocarbon-air mixtures have fundamental burning velocity, S_u normally less than 1 m/s although flame speeds may be considerably higher while the velocity of sound in air is around 340 m/s at normal temperature and pressure. This means that, pressure transmission may be regarded as effectively instantaneous but the rate of pressure rise will be relatively slow, subjecting the structure to be protected uniformly to a stress fixed by the amount of combustible material. Vent therefore may be located with equal value wherever feasible in a compartment or duct, providing the run-up distances from the point of ignition to the vent is similar (Anthony, 1978).

The implementation of venting has motivated several theoretical and experimental studies, the results of which have inspired the development of engineering standards i.e. NFPA 68 (NFPA68, 2002) and European Guide on venting (2007). The recommendation and guidelines provided by these publications are basically regards on the question of appropriate scaling of the correlation parameters as the analytical representations are invariably used to predict the vent area requirements for conditions that are beyond those covered by the experiments which support the design method.

Essentially, four quantities need to be known before a proper estimation of the vent area can be made (Lunn, 1992). These are:

- The reduced explosion pressure, P_{red}. This is the explosion pressure that should not be exceeded and which depends on the strength of the vessel. This is generally designated as P_{red} and has a unit of bar. P_{red} should not exceed two thirds of the bursting pressure, P_v. It may be that the strength of the vessel is not accurately known and such a lack of information must be an important consideration when deciding which method of vent area calculation to use.
- The vessel volume, V. Most of the basic methods for estimating vent areas are limited to compact enclosures with length to diameter (L/D) ratio less than 5.

- The mixture reactivity in terms of gas deflagration index, K_G or dust deflagration index, K_{ST} or burning velocity, S_u. It can be shown later the relationship between K_G and S_u and how K_G is dependent on vessel volume.
- Location of the ignition source and the turbulent factor. It had been depicted that end ignition gave higher P_{red} as the flame has longer travel distance compared to central ignition. Turbulence generated through the interaction of the gas flow ahead of the flame with obstacle inside the vessel. This is normally been taken into account by a turbulent factor, β where the turbulent burning velocity, S_T is in term of

$$S_T = 1 + \beta S_u \tag{3.1}$$

3.1 Parameter involved in empirical equations.

In venting, the pressure developed is dependent upon the vent coefficient, $K = V^{2/3}/A_v$ which expresses the effect of the vent opening area and the burning velocity, S_u of the gas-air mixture. However this parameters are not be used as straight forward. This concept has been applied by Cubbage and Simmonds (Cubbage and Simmonds, 1955, Cubbage and Simmonds, 1957), Cubbage and Marshal (Cubbage and Marshall, 1974) and Rasbash (Rasbash, Drysdale and Kemp, 1976). Bartknecht (Bartknecht, 1993) used K terms to express the vent flow pressure loss and vent bursting pressure in his correlation and K_G value to express the gas/air mixture reactivity. K_G is defined as

$$K_G = \left(\frac{dP}{dt}\right)_{max} V^{1/3} \quad \text{bar-m/s} \tag{3.2}$$

where dP/dt is the rate of pressure rise (bar/s) and V is the vessel volume (m^3). K_G is given as 50, 100, 140 and 550 bar-m/s for methane, propane, town's gas and hydrogen in 5 litre spherical vessel done by Bartknecht (Bartknecht, 1993). These values can only be used with the Bartknecht's correlation as K_G value is not to be constant but to increase with vessel volume as been investigated by Chippet (Chippett, 1984). Thus, K_G value should not be assumed constant and yet, be regarded to be representing the mixture reactivity. However, the use of burning velocity, S_u gives the same problem. In venting, it is assumed that S_u is constant throughout the explosion development so does

the flame speeds. This assumption is not valid as the higher compression pressure and temperature of the unburnt gases changes the burning velocity from that of the initial gas pressure and temperature. However, the change of S_u on these parameters is a small effect (~20% increase in S_u at the end of the explosion). Further, S_u is also dependent to the mixture reactivity, adding to the difficulties in quantifying the parameter. However, the assumption of constant S_u is not a bad approximation especially when S_u is taken as a little higher than the value at normal pressure and temperature.

A more completed theory of closed vessel flame propagation and the derivation of the relationship between rate of pressure rise and burning velocity, S_u was presented by Nagy et al (Nagy and Verakis, 1983).

$$\frac{dP}{dt} = \frac{3Su}{R} \cdot \frac{\gamma P_m^{2/3\gamma}}{P_o^{(2-1/\gamma-\beta)}} \cdot (P_o^{1/\gamma} - P_o^{1/\gamma})^{1/3} \left[1-\left(\frac{Po}{P}\right)^{1/\gamma}\right]^{2/3} P^{(3-2/\gamma-\beta)} \quad (3.3)$$

From Eq. 3.3, one can easily derive the dependent of K_G (from Eq.3.2) to S_u. Kumar at al (Kumar, Bowles and Mintz, 1992) also derived an equation for K_G as a function of S_u. This equation also assumes that S_u is the constant and does not vary with radius as well as pressure and temperature. The equation states as,

$$K_G = 4.84 S_u (P_m / P_i)^{1/\gamma} (P_m - P_i) \quad (3.4)$$

Further, using an assumption of only little pressure rise been experienced in the closed spherical vessel explosion in the first half of the flame travel and achieved its maximum about 98 % of adiabatic pressure rise in the last half of the travel given K_G value in term of,

$$K_G = 3.16 (P_m - P_i) S_u E \quad (3.5)$$

This formulation derived by Andrew (Andrews, 2004) with regards on the constant burning velocity through the flame travel. From Eq. 3.3 – 3.5, it is clear that the dependant of dP/dt on S_u. From this relationship, it can be seen that K_G = constant S_u. In dust explosion, the relationship of K_{st} and turbulent burning velocity, S_T existed and this can be related with laminar burning velocity for dust i.e. $S_T = \beta S_u$ as shown in Eq. 3.1.

These two parameters are mainly used to correlate the vent design by the researchers even not in direct order in order to meet minimum deficiency from experimental results.

3.2 Venting mechanism.

Experimental results or calculations for vented explosions are usually presented by expressing a term containing the peak (reduced) pressure, P_{red} as a function of a parameter describes the amount of venting. In contrast to the closed vessel, explosions in a vented vessel are characterised by the maximum reduced explosion overpressure, P_{red} instead of the maximum explosion overpressure, P_{max} (shown in Figure 3.1) and by the maximum reduced rate of pressure rise, $(dP/dt)_{red}$ instead of the maximum rate of pressure rise,$(dP/dt)_{max}$ (Siwek, 1996).The reduced explosion pressure or P_{red} is usually designed to be approximately two-thirds of the pressure required to rupture the vessel. In a given vessel, the 'reduced explosion pressure' will depend upon various factors such as the size/shape of the vessel, number and location of the vent, the opening vent pressure and inertia of the vent cover, the presence of obstructions inside the vessel, the explosive characteristics of the gas or dust etc.

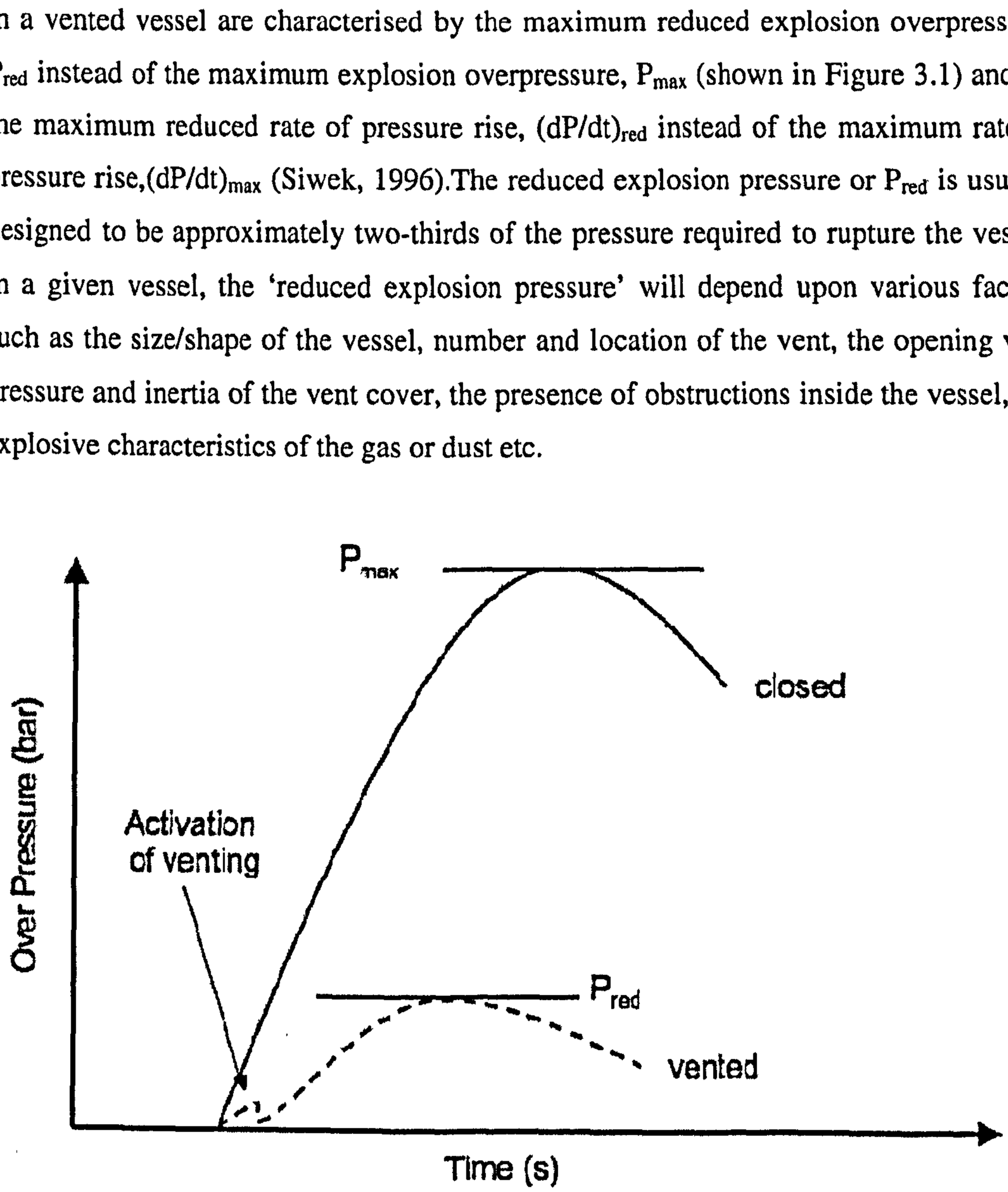

Figure 3.1 Pressure behavior versus time for a closed and vented explosions.

The basic principal of explosion venting provides for the rapid opening of a vent of sufficient area to allow unburned gas and explosion products to escape, thus limiting the pressure rise to an acceptable level. On the general basis, the reduced pressure attained in the vessel before venting must be less than the mechanical strength pressure of the containers. The vent opening must be correctly sized to allow the expanding gases to be vented at a rapid rate so as to limit the internal development of pressure. The acceptable pressure rise is determined by the requirement that the vessel should not rupture and in some cases, it should not deform. Essentially, a vented explosion can be considered to have three phases as shown in Figure 3.2:

- An initial confined explosion phase which occurs prior to removal of the vent cover

  At this stage, the rate of pressure rise will be determined by the rate of production of burnt gases which in turn depends upon the flame speed (Marked by **a**). Theoretically, flame will expand spherically before it distorted to semi-hemispherical shape and stretch towards the vent. The flame area is increasing and hence, the rate of mass burnt increases. The increasing of mass burnt rate will increase the flame speed and thus, higher dP/dt as well as the shorter time taken to reach a given pressure. It means that the first requirement of an effective explosion relief is that an open vent should be created at an early stage in the explosion process. By this means, the vent cover should have as low breaking pressure as possible.

- A vent removal phase. A situation when an open area is created through which gases can escape. In industrial practical, a vent cover is needed to seal the vessel in order to prevent the escape of fumes or combustion products but is designed to fail at a low pressure and allow an outflow of gases to be established at an early stage. The transition between the confined explosion phase and the vent removal characterised by P_I in Figure 3.2. After this phase, a significant decrease in explosion overpressure should result but since the flame front is still expanding, the rate of pressure rise, dP/dt is increasing and the pressure will rise. In order to minimise the pressure developed during venting, the breaking pressure, P_v should be low as possible. Lower breaking pressure leads to small flame elongation and hence, smaller flame areas and as a result lower P_{red}

whereas at higher breaking pressure, the effect of flame distortion is reduced as it takes longer time to break and hence would result on higher Pred (McCann, Thomas and Edwards, 1985). It should be noted that in higher P_v, the flame become cellular prior to removal of the relief panel.

- A venting phase. A phase during which gas flow out of the open vent is established. In this case, the pressure will rise again after the vent cover has been removed until the flame front reaches it maximum area which denotes as P_2 in Figure 3.2. Cubbage and Simmonds (Cubbage and Simmonds, 1955, Cubbage and Simmonds, 1957) thoroughly investigated the development of P_{red} in industrial ovens using town gas/air and methane/air mixtures by varying the location of the vents and different breaking pressure of vent covers. The significant result from their work was the double peak pressure profile attained. Double peak pressure-time profile occurs with low breaking vent pressure whilst single pressure peak profile occurs with vent cover having a high breaking pressure (Harris, 1983). A higher rise in vessel pressure is observed for lower venting pressures and this is explained by increased flame area and a longer period of unburned gas venting, which is less efficacious than burned gas venting (Bradley and Mitcheson, 1978b, Harris and Briscoe, 1967). Effectively, the total surface area of the flame front is greatly enhanced by the sudden opening of a vent, and this in turn increases the overall combustion rate of gases within the vessel. Thus, very strong second pressure peaks are often detected following the initial pressure drop when the vent opens.

Turbulence and stretching of the flame surface towards the vent opening can also result in an increase in the combustion rate (Buckland, 1980). The turbulence may be caused by increased gas flow velocities and by the opening of vent covers. Burgoyne and Wilson (Burgoyne and Wilson, 1960) have demonstrated that, all other things being equal, a vent which opens smoothly can give a lower P_{red} than does a diaphragm which burst abruptly at the same opening pressure. The very presence of a vent cover can increase turbulence in an explosion.

A further peak, P_3 might occur if the gas cools down sufficiently rapid to reduce the pressure in the vessel below ambient, causing re-entry of ejected unburnt gases. The

external explosion that gives rise to the P_3 is due to the fast flame propagation in the turbulent external vented premixed gases. This pressure increases as the vent area decreases or high K value as this will produce higher and turbulent jet velocity out from the vessel. Usually P_3 develops because the size and shape of the enclosures, the position of ignition source as well as the stretching and movement of the flame towards the vent as it opens, allowing burnt gas to be vented while combustion is still taking place inside. Transient pressure may also be affected by oscillation being set up in the system (Anthony, 1978) as represented by P_4. This oscillatory type combustion or Helmholtz oscillation will further increases the rate of combustion which that increase the internal pressure inside the vessel and this oscillation pressure gradually damped out as the flame expands. However, the burning rate during this phase is enhanced by the turbulence generated in the shear layer between the outflow burnt gas and unburnt gases within the vessel (Cooper, Fairweather and Tite, 1986). The strong interaction of the flame front, the shock/pressure wave and physical back flow into the vessel generally enhance the rate of combustion inside the vessel and further induced Taylor instability on the section of flame front surface farthest away from the vent. As the flame is continued to expand, it eventually encounters the walls of the vessel and this will suddenly decrease the flame area and hence the rate of pressure rise. Work by Solberg et al (Solberg, Pappas and Skramstad, 1980) confirmed the existence of third pressure peaks assembling the P_4 trace in $35m^3$ vessel in which the vent were initially covered. They found that a strong flow field will be generated at the opening of the vent which the flame will be strongly accelerated towards the vent and Taylor instability may develop at the worst case of central ignition.

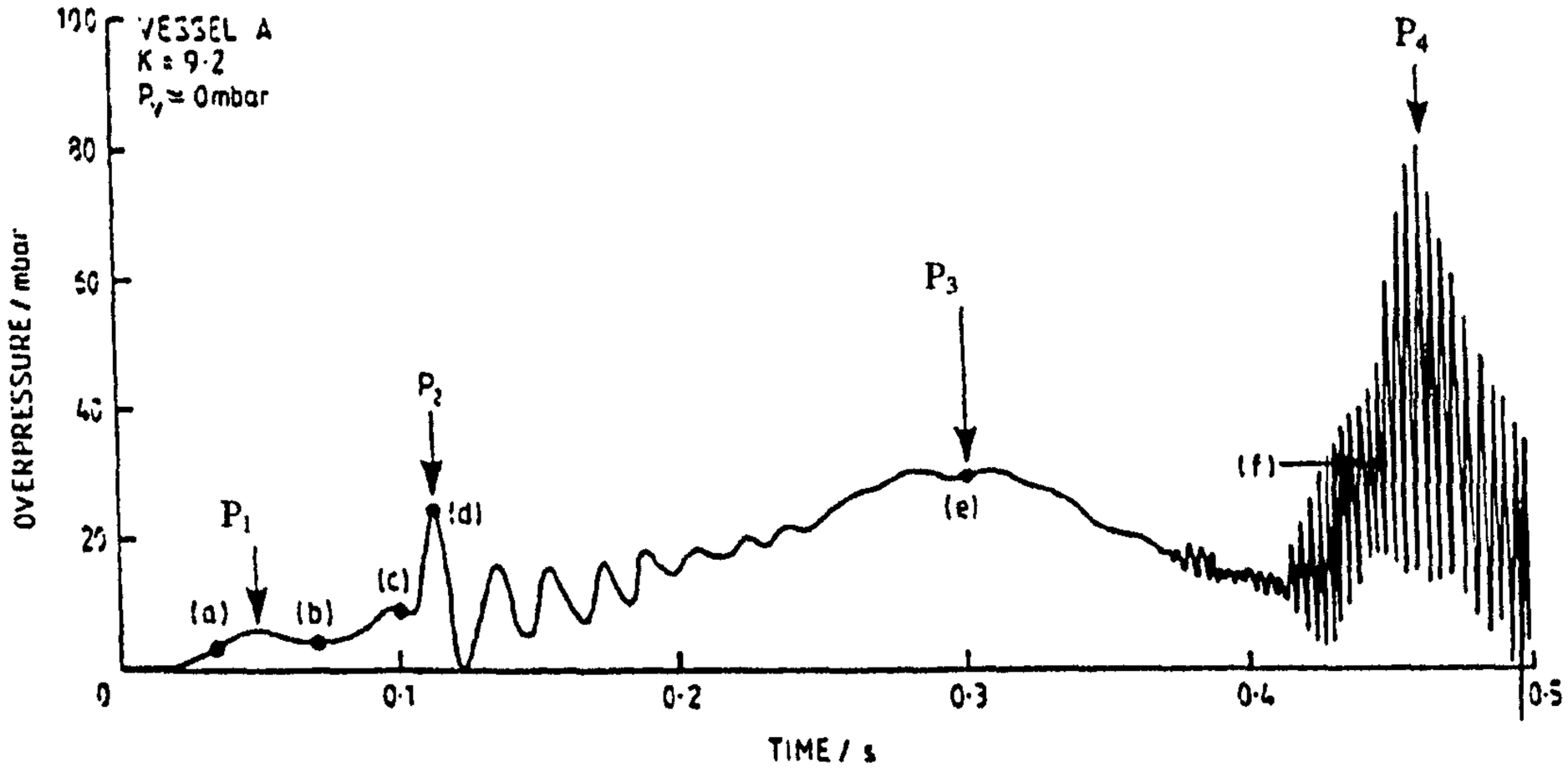

Figure 3.2 The pressure-time variation in a vented explosion. Graph reproduced from Cooper et al (Cooper, Fairweather and Tite, 1986)

The relative size of peaks P_1 and P_2 are determined by the size of the vent relative to the vessel, the magnitude of P_v, the flame speed and the scale and intensity of turbulence when the vent breaks. As the vent area of the vessel or enclosure is smaller, the pressure required for vent cover removal is increased. It is found that the bursting vent pressure, P_v is inversely proportional to the area of the vent cover (Cubbage and Marshall, 1974). Further, the smaller the A_v i.e. high K, the smaller is the vent area available upon its removal and the less rapid, therefore, the egress of combustion products were impeded. Due to inertia of the vent cover, a finite time is required immediately after P_v is reached to totally remove the vent cover sufficiently far from the enclosure for the flow of gases out of the enclosure and thus, the weight per unit area of the vent cover is another important factor influencing P_{red}. The heavier vent cover is not as effective as the lighter material in minimising the pressure developed (Cubbage and Marshall, 1974, Molkov, Grigorash, Eber, Tamanini and Dobashi, 2004).

An increase in P_v will cause P_1 to increase with respect to P_2; while high flame speed and high turbulence will cause P_2 to increase with respect to P_1. P_2 also increases with respect of P_1 as the vent size becomes smaller for a given vessel (Anthony, 1978). Further, at certain condition, there is only one peak is observed. The merging of P_2 with P_1 corresponds to a situation where dP/dt becomes negative after the operation of the vent which occurs when the vent is relatively large or flame speed is low. However, the

merging of P_1 with P_2 corresponds to the situation where dP/dt remains positive after the opening of the vent and this situation generally occurs when the vent is relatively small and flame speeds are higher.

Thus the explosion pressure developed in vented explosion depends on three quantities; the pressure required for vent to release, P_v the back pressure due to inertia of the vent cover and the back pressure caused by restriction to the gas flow through the vent and to these, the turbulent parameter must be added. These effects on P_{red} will become complicated function as other variables from those effects mentioned related to other dependent variables and all parameters need to be accounted in order to perform the appropriate design for venting.

3.3 Venting theory

For the purpose of correlating the theory and experimental results, P_2 will be assumed as the dominant overpressure as P_1 is usually regarded as the bursting burst pressure. The problem arises as most investigators of vented explosions do not report the pressure-time profile but simply report the maximum overpressure they attained in that particular experiments. Hence, it is normally not possible to know whether this is caused by P_1, P_2 or P_3.

However, understand the physics of vented explosion which regards the flow of the unburnt gases ahead of the flame vented out through the vent allows overpressure to be calculated. The procedure would allow the form of correlation which includes P_2 to be deduced and further, will then be compared to published experimental data in vented explosions. Thus it will be assumed that in most cases of vented explosion the maximum P_{red} is caused by the flow of unburnt gases through the vent and hence, P_2 should be taken as maximum overpressure based on the assumption made.

The most used and recommended correlation for venting gas deflagration is adopted by NFPA 68 (NFPA68, 2002) and European Gas Venting Guidance (2007)rely on the vent correlation developed by Bartknecht (Bartknecht, 1993) for high-strength enclosure and Swift's correlation (Swift, 1983) for low-strength enclosures, respectively. The

correlations apply for a compact vessel which Bartknecht defined as those with L/D < 2 although the draft European Standard (2007) has applied the correlations for L/D < 3. Bartknecht's correlation (Bartknecht, 1993) is given as the vent area, A_v, as a function the vessel volume, $V^{2/3}$ multiplied by a complex term that includes the mixture reactivity K_G, reduced overpressure in the vented explosion, P_{red} and static vent burst pressure, P_v. The $V^{2/3}$ dependence of overpressure on the test vessel volume is a characteristic of spherical or compact vessel explosions, where the flame remains mostly in spherical shape during venting process. If the spherical flame propagates at a constant rate irrespective of the vessel volume, P_{red} should be only dependence on A_v and $V^{2/3}$ or K. Bartknecht expressed his correlation as:

$$A_v = \left[\frac{0.1265 \log_{10} K_G - 0.0567}{P_{red}^{0.582}} + \frac{0.175(Pstat - 0.1)}{P_{red}^{0.572}} \right] V^{2/3} \tag{3.6}$$

where K_G is deflagration index (bar-m/s), P_v is the static burst pressure (barg), V is volume (m^3). Equation 3.6 is a dimensional relationship which yields A_v as a function of two terms i.e. the vent flow pressure loss for the first and the vent bursting pressure term for latter which gave a linear influence of P_v on A_v. There is no fundamental basic for Eq. 3.6 as it is a pure empirical correlation and relies on appropriate experimental data to determine the four adjustable parameters where the details of the data analysis have not been made public (Bartknecht, 1993). Again, the correlation developed by Bartknecht (Bartknecht, 1993) can be said empirical as the dependency of K_G with S_u as mentioned earlier. In his work, Bartknecht carried out venting explosion mainly in four different fuels which are methane, propane, town's gas and hydrogen at volume range between 1 to 60 m^3. If the equation is applied to a standard vent burst pressure of 100 mbar where the influence of P_v and weight of inertia of the vent, w can be assumed negligible, Eq. 3.6 can be transformed into:

$$\frac{1}{K} = \frac{0.1265 \log K_G - 0.0567}{P_{red}^{0.582}} = \frac{\text{constant}}{P_{red}^{0.582}} \tag{3.7}$$

Given a value of K_G for each gas as 55 for methane, 100 for propane, 140 for town's gas and 550 for hydrogen will give the constant as 0.164, 0.20, 0.212 and 0.290 respectively. As been discussed earlier, K_G increases with vessel volume but yet, Bartknecht has not been determined the K_G value at different vessel volume.

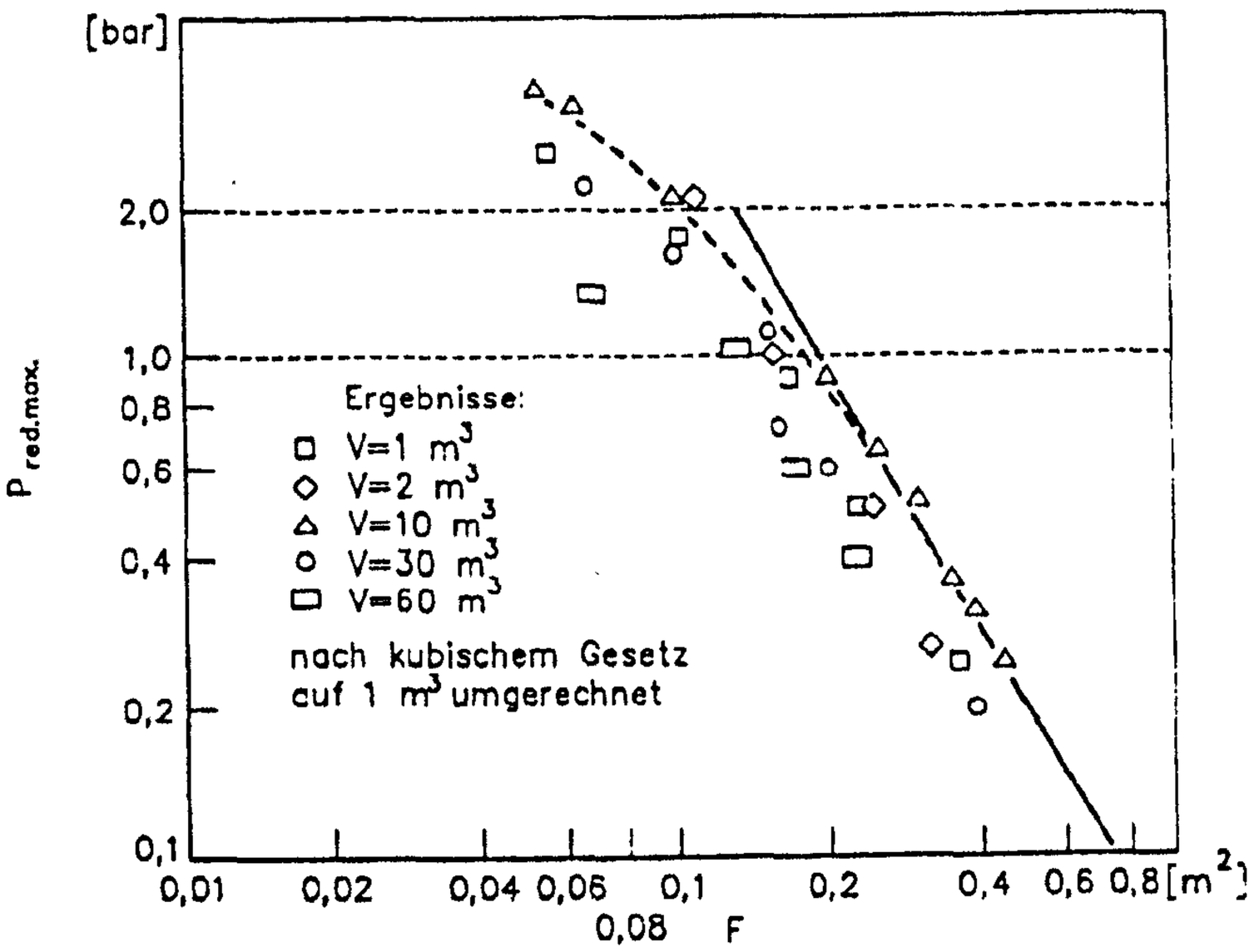

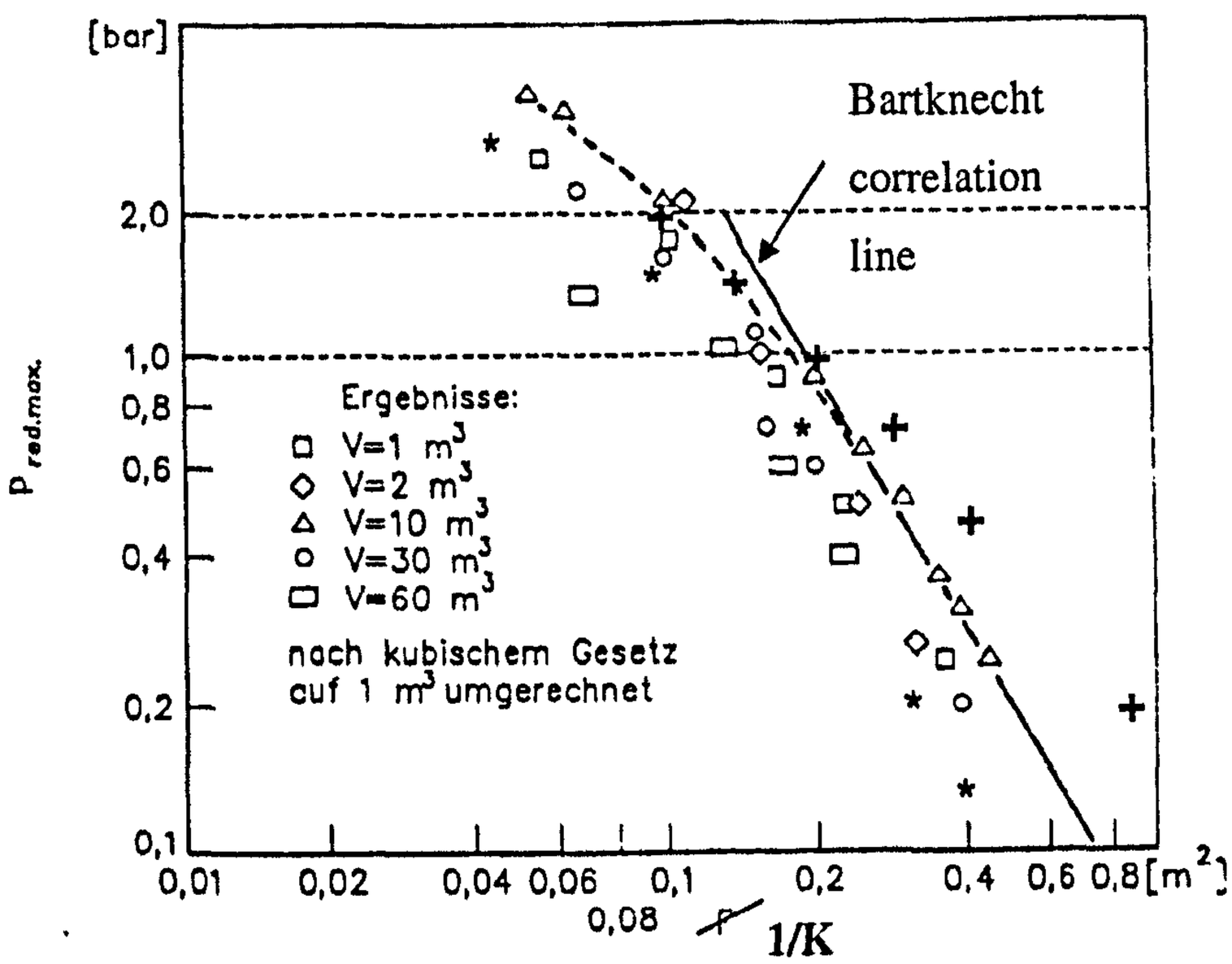

Figure 3.3 Bartknecht data for propane-air at different volumes at E = 10J, P_v = 100 mbars (Bartknecht, 1993). * is for methane-air at 30m^3 on 1/K. + is for propane/air at V = 2 m^3. Reproduced from Andrews (Andrews, 2004).

The correlation developed by Bartknecht (Bartknecht, 1993) can only be applied on its own limitation as the equation is the empirical derived from his experimental works and

no other published venting data included as noted by Siwek (Siwek, 1996) in his study on published correlations in vented gas and dust/air- mixtures.

Figure 3.3 shows the original data from Bartknecht for propane/air at different volume. From the figure, Bartknecht portrayed his correlation based on the experimental data obtained for V = 10 m^3. It suggested that the correlation developed by Bartknecht (Bartknecht, 1993) was purely empirical with no safety factor offered for venting design purposes. At the x-axis, it represented the vent area, denoted as F (m^2) and P_{red} for y-axis. However, when the result data is re plotted for V = 2 m^3, represented by the (+) sign, it is found that only one data agrees with the line that drawn from the correlation line. After re-analysed, it is found that F parameter at x-axis is a mistake and it should be corrected to 1/K. To justify the alterations, the methane experimental data, denoted as * sign from Bartknecht's work for methane/air at V = 30 m^3 were re plotted and it showed a poor agreement with the correlation line drawn. From the figure, it is implied that the same vent area is required irrespective of the vessel's volume which is obviously incorrect. Further, the results implied that lower overpressure attained for the same K in the largest volume i.e. 60 m^3

From Fig. 3.3, the overpressures are increasing with volume for vessel volume of 1 to 10 m^3 but decreasing for higher volumes. The self-acceleration mechanism can be the reasonable explanation for the increase overpressure for the first condition but there is no physical explanation for the latter case. As will be discussed later, the volume effect is not correctly correlated by the K parameter in Bartknecht's correlation.

NFPA 68 adopted Swift's equation to apply for design and scale-up of venting system purposes and it seem that the results obtained were in good agreements with experimental data obtained by Donat (Donat, 1977) and Harris and Briscoe (Harris and Briscoe, 1967). Again, there is a limitation in using this approach as it can be applied on certain conditions i.e. P_{red} is not more than 200 mbar and only suits to low-strength enclosures.

The Swift correlation has a form of:

$$A_v = \frac{CA_s}{P_{red}^{0.5}} \tag{3.8}$$

where C is the deflagration constant $(kPa)^{1/2}$ that determined by experiment or calculation enveloped the gas reactivity terms, discharge coefficient (typically 0.7) and turbulence factor (typically 5) and A_s is the vessel surface area (m^2). Further, the relationship between A_s and $V^{2/3}$ can be defined as A_s = constant $V^{2/3}$ where constant is equal to 4.84 for sphere, 6 for cubic, 6.3 for rectangular and 5.81 for cylinder with L/D = 2. In K term, Eq. 3.8 can be transformed into:

$$\frac{1}{K} = \frac{\text{constant}}{P_{red}^{0.5}} \tag{3.9}$$

The use of A_s instead of $V^{2/3}$ by Swift is followed by Bradley and Mitheson (Bradley and Mitcheson, 1978a, Bradley and Mitcheson, 1978b) as Swift predicts that a larger vent area is required for cubic vessel rather than spherical vessel at the same P_{red} and volume which is not in the case of Bartknecht's correlation. This means that A_s is the key parameter to include the influence of the vessel geometry/shapes on the overpressure. The simplicity and ease of use of Eq. 3.9 is questioned, underestimate the complexity of large-scale combustion phenomena and did not take into consideration the effect of vent opening pressure. Swift (Swift, 1983) based his design equation on theoretical development that indicates the independence of P_{red} of the vent opening pressure, if the turbulence enhancement itself is also independent of the vent opening pressure. The turbulence induced by the vent opening or the flow of unburnt gases over and around the obstacles are not yet realistically be demonstrated especially in large scale conditions as the previous investigators put constant to give effect on turbulence to fit with their experimental data and these values were differed from others and still, this root problem is not yet resolved.

The most classic and often referenced studies on vented explosion vent design has been published by Bradley and Mitheson (Bradley and Mitcheson, 1978a, Bradley and Mitcheson, 1978b). They made a detailed comparison of their theoretical results with an extensive compilation of the experimental data. Their presentation of the model results was in a form of plots for dimensional (in atmospheres) reduced explosion pressure,

ΔP_{red} versus a dimensionless vent parameter, $\overline{A}/\overline{S}$ as follows for initially closed venting i.e. with the vent cover on place;

$$P_{red} = 2.43(\overline{A}/\overline{S})^{-0.6993} \text{ for } P_{stat} \geq 1 \text{ barg} \tag{3.10}$$

$$P_{red} = 12.46(\overline{A}/\overline{S})^{-2} \text{ for } P_{stat} \leq 1 \text{ barg} \tag{3.11}$$

$$\text{with } \frac{\overline{A}}{\overline{S}} = C_d \frac{A_v C_{ui}}{A_s S_u}\left(\frac{\rho_u}{\rho_b} - 1\right)^{-1} \tag{3.12}$$

where C_{ui} is the speed of sound (m/s), ρ_u is the unburnt gas density (kg/m^3) and ρ_b is the burnt gas density (kg/m^3). The dimensionless vent parameter has been termed by Molkov (Molkov, 1995, Molkov, 2001) as turbulent Bradley number, Br_t where the only different from the original equation is the added deflagration-outflow-interaction number, χ/μ. The model suits ideally for spherical vessel flame propagation as it is the basis for the equations developed.

If the Eq. 3.10 and 3.11 changed to K term as followed in Bartknecht and Swift's equation above, it gives,

$$\frac{1}{K} = \frac{0.281 S_u (E-1)}{C_d C_{ui} P_{red}^{1.43}} = \frac{\text{contant}}{P_{red}^{1.43}} \tag{3.13}$$

$$\frac{1}{K} = \frac{3.53 S_u (E-1)}{C_d C_{ui} P_{red}^{0.5}} = \frac{\text{contant}}{P_{red}^{0.5}} \tag{3.14}$$

The equation developed by Bradley and Mitheson (Bradley and Mitcheson, 1978a, Bradley and Mitcheson, 1978b) assumed that the pressure rise will be enhanced by the venting of the unburnt gases rather than the burnt gases and this is taken as a 'worst case' scenario for a safe vent design. The pressure reduction enhanced by burnt gas venting is supported by Maisey (Maisey, 1965), Rasbash and Rogowski (Rasbash, 1986) and Yao (Yao, 1974).

Nevertheless, this approach is been questioned if there was a significant P_v (Lunn, ICheme, 1984 and 1990). The expanding flame front which associated with substantial

gas flow ahead of it and the presence of opening vent alters the flow patterns. These conditions generate intense turbulence towards the flame propagation in which increase the burning velocity and hence the maximum overpressure. At this particular condition where the postulated discrepancy between the theory and experimental results in a presence of turbulence associated with the increase in burning velocity, Bradley and Mitheson (Bradley and Mitcheson, 1978a, Bradley and Mitcheson, 1978b) recommended that a five fold increase in burning velocity above that of the laminar value would be necessary to fit the experimental data.

The recent alternative vent design correlation at increased pressure and temperature that is adopted by NFPA 68 and draft of the European Venting has been introduced by Molkov et al (Molkov, 1995, Molkov, 1999, Molkov, 2001, Molkov, Baratov and Korolchenko, 1993, Molkov, Dobashi, Suzuki and Hirano, 1999, Molkov, Grigorash, Eber and Makarov, 2004, Molkov, Grigorash, Eber, Tamanini and Dobashi, 2004, Molkov, Korolchenko and Alexandrov, 1997). They had called the correlations as a 'universal correlation' for prediction of reduced pressure and vent area. It is based on the modified correlation from the original correlation developed in 1993 and 1995.(Molkov, 1995, Molkov, Baratov and Korolchenko, 1993)

In the correlation, deflagration-outflow-interaction number or can be called turbulence-factor, χ/μ and Bradley-Mitcheson number, Br are introduced where the so-called deflagration-outflow-interaction number χ/μ was derived by fitting the calculated pressure-time curves to the experimental data from various author (Razus and Krause, 2001). The parameter represents the turbulent generated during the explosion development. The Bradley number and the deflagration-outflow interaction are follows:

$$\pi_{red} = Br_t^{-2.4} \quad \text{for } \pi_{red} < 1 \tag{3.15}$$

$$\pi_{red} = 7 - 6Br_t^{0.5} \quad \text{for } \pi_{red} > 1 \tag{3.16}$$

$$Br_t = \frac{\sqrt{E_o / \gamma_{uo}}}{\sqrt[3]{36\pi}} Br \frac{\mu}{\chi} \tag{3.17}$$

$$Br = \frac{A_v}{V^{2/3}} \frac{C_{ul}}{S_u (E-1)} \tag{3.18}$$

$$\frac{\chi}{\mu} = 0.9 \left[\frac{(1+10V^{1/3})(1+0.5Br)}{1+\pi_v} \right]^{0.37} \tag{3.19}$$

Where $\pi_v = \frac{P_v(bar \text{ absolute})}{P_i}$, E is the expansion ratio of ρ_u/ρ_b, γ is the specific heat ratio for unburned mixture, c_{ui} is the speed of sound (m/s) and Π_o is 'pi' number. As the same with other correlations, the original equations (Eq. 3.15 and 3.16) will be changed to K term. This gives as,

$$\frac{1}{K} = \frac{\sqrt[3]{36\pi}}{\sqrt{E/\gamma}} \cdot \frac{\chi}{\mu} \cdot \frac{S_u (E-1)}{C_{ui}} \cdot \frac{1}{P_{red}^{0.417}} = \frac{\text{constant}}{P_{red}^{0.417}} \tag{3.20}$$

$$\frac{1}{K} = \frac{\sqrt[3]{36\pi}}{\sqrt{E/\gamma}} \cdot \frac{\chi}{\mu} \cdot \frac{S_u (E-1)}{C_{ui}} \cdot \left(\frac{7-P_{red}}{6} \right)^2 = \text{constant} \left(\frac{7-P_{red}}{6} \right)^2 \tag{3.21}$$

The equation is valid for unobstructed enclosures but the author acknowledges its use for congested enclosures as well. The first attempt to quantify the level of turbulence generated in venting explosions has been made by Munday (Munday, 1963) with use of detailed models, experiments and best fit approach and from then, the works to include turbulence factor are progressing. Nevertheless, the value of turbulence factor is based on restricted, narrow range of exploited experimental data (Munday, 1963, Yao, 1974). Others used the dependence of turbulence factor on flame and vent outflow Reynolds number in order to take into account the changes of β during explosion (Chippett, 1984, Molkov, Dobashi, Suzuki and Hirano, 2000).

The disadvantage of using this approach is the difficulty to estimate the average values of β from such results. Furthermore Zalosh (Zalosh, 1995) stated that there is no clear correlation between β = constant or β = f (Re) approaches obtained by different authors. The author elaborated that the assumptions made in the formulation of detailed models concern: assumption about the composition of the vented gas, assumed flame geometry, the empirical parameters and correlation to account for turbulence enhanced combustion

and flame acceleration induced by flame instabilities. Further, this method requires users to determine turbulent Bradley number, B_{rt} and thermodynamic (γ_u, E_i, c_{ui}) as well as thermokinetic (S_{ui}) data before applying the formula below:

$$\frac{Br_t.\sqrt[3]{36\pi_0}.V^{2/3}}{c_{ui}.\sqrt{\frac{E_i}{\gamma_u}}} = \frac{A.(1+\pi_v)^{0.4}\left[1+0.5.\left(\frac{A.c_{ui}}{V^{2/3}(0.73S_{ui}).(E_i-1)}\right)^{\beta}\right]^{-0.4}}{\pi_{i\#}^{0.6}.\alpha.(1+10V^{1/3})^{0.4}.(0.73.S_{ui}).(E_i-1)} \tag{3.22}$$

As far as the author's concern, there are basically two different approaches of the explosion venting flow modelling applied. In order to obtain the mathematical expressions for flame flow and pressure development during venting explosions, it is necessary to establish the appropriate thermodynamic and physics fundamentals i.e. conservation of mass, gas law, energy balance etc. For a vent to give no increase in overpressure other than that due to the pressure difference created by the mass flow of unburnt gases through the vent, the vent mass flow rate is assumed to be equal to the maximum mass burning rate of the flame and this consideration should be used as the design mass flow through the vent. This approach in calculating the maximum vent flow could be said to overestimate the maximum flow as the assumption of the maximum flame area is very conservative.

Experiments made in the laboratory show equations for the gas flow through an orifice apply equally well to flow through a vent (Nagy and Verakis, 1983). Since the vent can be treated as an orifice, the incompressible flow equation through the orifice can be applied but somehow, the assumption of using this equation is only valid up to $P_{red} \leq$ 200 mbar then the full compressible flow orifice should be used.

This approach will be explained in two different methods. By **Method 1**, it is assumed that the maximum overpressure occurs when the vented unburnt gas flow rate is at a maximum and this equal to the maximum mass rate of burning at the flame front, m_b which has been applied by Swift (Swift, 1983), Munday (Munday, 1963) and Molkov (Molkov, 1995) before the modification made later in 2000. The equation is as follows:

$$m_b = S_u A_s \rho_u \tag{3.23}$$

where S_u is burning velocity (m/s), A_s is the internal surface area of the enclosure (m^2) and ρ_u is the unburnt gas velocity (kg/m^3). The assumption is valid as the flame approaches the wall at higher P_{red} as the flame area is closer to the wall. The maximum vent mass flow and pressure loss always occurs before the flame exits the vent at which during the period when the flame is expanding inside the vessel and pushing unburnt gases ahead of the flame due to the thermal expansion of the burnt gases. Once the flame exits the vent, the burnt gases are free to escape and expand outside the vent whereas the expansion inside the vessel ceases and hence the flame speeds inside the vessel will fall to S_u. Further, the burnt gas flow through the vent is at a low gas density and thus, will lower the pressure loss at the vent entrance. Thus, the prediction of the maximum venting overpressure is reduced to that of predicting the maximum unburnt gas flow through the vent and its associated flow pressure loss.

However, **Method 2** assumed that the maximum overpressure occurs when the vented unburnt gas flow rate, m_b is at a maximum and this equal to the maximum unburnt gas displaced flow by the flame front, S_g. This assumption has been applied for correlation developed by Runes (Runes, 1972) and Bradley and Mitheson (Bradley and Mitcheson, 1978a). The equation given is slightly different from Eq. 3.23 as is about 6.5 times the mass flow of the first method as it takes the effect of (E-1) where E is the expansion ratio. As S_g is close to flame speed, S_f in value, this approach is only slightly lower in mass flow rate than if it is based on flame speeds value.

$$m_b = S_g A_s \rho_u = S_u (E-1) A_s \rho_u \tag{3.24}$$

The approach of assuming the maximum flame area, A_f to be A_s as one of the characteristic in defining maximum burning rate maybe can lead to the overestimate of the overpressure. In spherical vessel, the flame would only propagates about half of the diameter at P_v = 100 mbar and hence the surface area is about a quarter of A_s. Taking A_s to calculate how much bigger the flame would take when venting occurs has been initiated by Runes (Runes, 1972). For a safe design of a vent, Runes (Runes, 1972) suggested that the important parameter needed to be considered is the required maximum burning rate and this can be given by the maximum flame surface area, A_f and by this assumption, Runes suggested that this could not be larger than the internal surface area of the enclosures, A_s.

For spherical flame propagation at central ignition, the mass burning rate of the flame, m_b equal to the incompressible flow equation through the orifice would give using **Method 1** and **Method 2** respectively;

$$m_b = A_s S_u \rho_u = C_d \varepsilon A_v (2\rho_u P_{red})^{0.5} \tag{3.25}$$

$$m_b = A_s S_g \rho_u = A_s S_u (E-1)\rho_u = C_d \varepsilon A_v (2\rho_u P_{red})^{0.5} \tag{3.26}$$

where C_d is discharge coefficient and ε is compressibility factor. It can be argued on the coefficient discharge, C_d value as the C_d value is always regarded as a constant of 0.61 for a sharp edge orifice but this would not apply for lower K value where C_d can increase up to 0.7 or more. In theory, C_d is dependent on the design of the vent and K. However, this does not change the fundamental characteristics of the flow, as in orifice plate flow metering compressibility is treated by adding an expansibility factor, ε, to the basic incompressible orifice flow equation, as shown in Eq. 3.25 and 3.26. The value of ε decreases as P_{red} increases and is 1.0 for incompressible flow and about 0.8 just prior to sonic flow at the nozzle. The compressibility equation is given by BS 1042 as:

$$\varepsilon = 1 - (0.41 + 0.35\frac{1}{K_v^2})\frac{P_{red}}{\gamma(P_i + P_{red})} \tag{3.27}$$

where γ is a specific gas constant and P_i is the initial pressure (bar). Another parameter that always assumed to be constant is the unburnt density where the value is taken as 1.2 kg/m^3. This is unjustifiable simplification as the density is the linear function of P_{red} in absolute pressure terms from the gas law. Thus it should be written as:

$$\rho_u = \frac{P_{red} MW}{RT} \tag{3.28}$$

where MW is the molecular weight of air (0.029 kg mol^{-1}), R is the gas constant (82.0552 x 10^{-6} m^3bar/Kmol) and T is the temperature (K). The result of taking the density as a function of P_{red} is to increase the mass burning rate and thus require a larger vent area for the same overpressure or a large overpressure for the same vent area.

Again, the problem arises as temperature is also assumed constant. During the initial portion of the explosion, the vented gases are cool. As the flame expands, the gases flowing through the vent will soon have the high temperature of the combustion reaction and based on the gas law, high temperature associated with high pressure attained. The assumption of constant temperature is not valid but the computation of the temperature rise due to compression is difficult without constant volume combustion. However, Lunn (Lunn, Crowhurst and Hey, 1988) has introduced approximate empirical method to estimate the compressed temperature as a function of P_{red}.

$$T = 298\left[(P_{red} + P_i)/P_i\right]^{0.286} \tag{3.29}$$

However, the rise in temperature due to the pressure rise is smaller than in pressure and by using a relatively high T of 300K, the error will be small and conservative as the density will be overestimated based only on P_{red}. Substituting Eq. 3.29 to Eq. 3.25 and Eq. 3.26 would give

$$\frac{A_v}{A_s} = \frac{0.00243 S_u}{\varepsilon C_d}\left(\frac{P_{red} + P_0}{P_{red}}\right)^{1/2} \tag{3.30}$$

$$\frac{A_v}{A_s} = \frac{0.00243 S_u (E-1)}{\varepsilon C_d}\left(\frac{P_{red} + P_0}{P_{red}}\right)^{1/2} \tag{3.31}$$

Noted that A_s and $V^{2/3}$ is in relation in terms of $A_s = C\ V^{2/3}$. The constant value is given in Table 3.2 below. For spherical vessel, $A_s = 4.84\ V^{2/3}$ and this will result to

$$\frac{1}{K} = \frac{0.0118 S_u}{\varepsilon C_d}\left(\frac{P_{red} + P_0}{P_{red}}\right)^{1/2} \tag{3.32}$$

$$\frac{1}{K} = \frac{0.0118 S_u (E-1)}{\varepsilon C_d}\left(\frac{P_{red} + P_0}{P_{red}}\right)^{1/2} \tag{3.33}$$

Equation 3.32 and 3.33 are suitable only when the flow through the vent is subsonic. When $P_{red} > 1.89\ P_0$, the flow is chocked and sonic flow is occurred. For spherical vessel it gives,

$$\frac{1}{K} = 0.0145 \frac{S_u}{T^{1/2}} \left(\frac{P_{red} + P_0}{P_{red}} \right) \tag{3.34}$$

$$\frac{1}{K} = 0.0145 \frac{S_u (E-1)}{T^{1/2}} \left(\frac{P_{red} + P_0}{P_{red}} \right) \tag{3.35}$$

However these approaches do not predict the influence of P_v and turbulence factor, β can be introduced in order to simulate the effect. For high P_v, the breaking of the vent will cause the pressure waves and generated turbulence where the net effect from these actions is increasing the rate of burning at the flame front. In computer modelling, the turbulence factor can be used to give an effective turbulence velocity, $S_t = \beta S_u$.

It seems that the underlying theory behind venting explosion makes other published correlations given by the previous investigators can be compared. It is important to compare the theory approach discussed above with the correlations offered by the vent design standards i.e. NFPA 68 and European Gas Venting Guidance 2006.

It is instructive to conclude that the reactivity term used by the vent design correlation is the burning velocity, S_u instead of the K_G values. In reality, the unburnt gases inside the vessel are not vented out at the same time when the burnt gases started to eject through the vent where the unburnt gases left and trapped at the corner region of the vessel in the case of non-spherical vessel. Once the burnt gases are vented, there is no further internal expansion of the flame and the flame speeds should be reduced to laminar burning velocity, S_u. At this state, the pressure will be associated with the subsequent combustion of the unburnt gases at S_u and the assumption for the maximum overpressure occurred at the maximum vent unburnt gas flow rate is valid. Below are the studied correlations along with the proposed equations to be compared to the published experimental data that will be discussed later.

Table 3.1 Studied correlations for venting of gas explosions

Correlation	Reference
$A_v = \left[\frac{0.1265\log_{10} K_G - 0.0567}{P_{red}^{0.582}} + \frac{0.175(Pstat - 0.1)}{P_{red}^{0.572}}\right] V^{2/3}$	Bartknecht (Bartknecht, 1993)
$A_v = \frac{CA_s}{P_{red}^{0.5}}$	Swift (Swift, 1983)
$P_{red} = 2.43(\overline{A}/\overline{S})^{-0.6993}$ for $P_{stat} \geq 1$ barg $P_{red} = 12.46(\overline{A}/\overline{S})^{-2}$ for $P_{stat} \leq 1$ barg	Bradley and Mitcheson (Bradley and Mitcheson, 1978a, Bradley and Mitcheson, 1978b)
$\pi_{red} = Br_t^{-2.4}$ for $\pi_{red} < 1$ $\pi_{red} = 7 - 6Br_t^{0.5}$ for $\pi_{red} > 1$	Molkov (Molkov, 1995)
$\frac{1}{K} = \frac{0.00243CS_u}{\varepsilon C_d}\left(\frac{P_{red} + P_0}{P_{red}}\right)^{1/2}$	Method 1
$\frac{1}{K} = \frac{0.00243CS_u(E-1)}{\varepsilon C_d}\left(\frac{P_{red} + P_0}{P_{red}}\right)^{1/2}$	Method 2

3.4 Comparison of Bartknecht and Swift correlations as been adopted in NFPA 68 using derived methods on the same basis.

To justify the applicability and validity of the proposed equations, it is useful to directly compare the derived methods with the correlations given in NFPA 68 i.e. Bartknecht's equation and Swift's equation. From Eq.3.7, Bartknecht's equation can be expressed as,

$$\frac{1}{K} = C_3 \, \mathrm{Pr}ed^{-0.5817} \tag{3.36}$$

where C_3 = 0.164 for methane, 0.200 for propane, 0.212 for town's gas and 0.290 for hydrogen. It should be noted that there is a relatively small dependency of K on mixture reactivity which is most unusual based on the fact that hydrogen is the high burning velocity mixture compared to methane and propane. For Method 1 and Method 2, Eq. 3.30 and 3.31 can be transformed in term of the constant value term as,

$$\frac{1}{K} = C_1 C_2 \varepsilon^{-1} \Pr ed^{-0.5} \tag{3.37}$$

where $C_1 = (\rho^{0.5}/(C_d 2^{0.5}) S_u$ for Method 1 and $C_1 = (\rho^{0.5}/(C_d 2^{0.5}) S_u (E-1)$ for Method 2. C_2 = 4.84 for sphere, 6 for cube, 6.3 for rectangular, 5.81 for cylinder with L/D = 2 and 5.54 for L/D=1. C_1 is the same derivation for Swift's C constant. If S_u = 0.4 m/s for methane, 0.45 m/s for propane and 3.1 m/s for hydrogen, C_d = 0.61 and ρ = 1.2 kg/m^3, it would give C_1 = 0.0016 for methane, 0.0018 for propane and 0.012 for hydrogen respectively for Method 1. For Method 2, with the same value of S_u, C_d and ρ for appropriate gases, C_1 = 0.0104 for methane with E = 7.5, 0.0126 for propane with E = 7.98 and 0.078 for hydrogen with E = 7.29. If these C_1 values were compared to Swift's C constant and C_3 in Bartknecht's equation, it will give the value as shown in Table 3.2.

Table 3.2 Comparison constant value derived for Method 1 and 2 with respect to Swift's C, fuel characteristic constant

Fuel	**C_1 Method 1 prediction**	**C_1 Method 2 prediction**	**C Swift's constant**	**C_3 Bartknecht's equation**
Methane	0.0016	0.0104	0.037	0.164
Propane	0.0018	0.0126	0.045	0.200
Hydrogen	0.011	0.068	Not available	0.290

Noted that it should be included C_2 for geometry's effect and for cube, it would give the combined constant C_1C_2 = 0.0097, 0.011 and 0.114 for methane, propane and hydrogen respectively for Method 1. Method 2 would give C_1C_2 = 0.062 for methane, 0.071 for propane and 0.41 for hydrogen. To get agreement for the turbulent effect or self acceleration factor, β, the ratio of C_3/C_1C_2 is calculated as Bartknecht's work used in larger vessel and it was suspected that self-acceleration is already present during the explosions. The list of predicted β is given in Table 3.3 below.

Table 3.3 List of predicted β with respect with Bartknecht's C_3 constant

Fuel	**C_1C_2 Method 1**	**C_1C_2 Method 2**	**C_3 Bartknecht**	**β Method 1**	**β Method 2**
Cube					
Methane	0.0097	0.062	0.164	16.9	2.6
Propane	0.011	0.071	0.200	18.2	2.8
Hydrogen	0.114	0.41	0.290	2.5	0.7
Sphere					
Methane	0.0078	0.050	0.164	21.0	3.3
Propane	0.0087	0.0569	0.200	23.0	3.5
Hydrogen	0.068	0.416	0.290	4.3	0.7
Rectangular					
Methane	0.01	0.066	0.164	16.4	2.5
Propane	0.011	0.08	0.200	18.2	2.5
Hydrogen	0.078	0.49	0.290	3.7	0.6
Cylinder for L/D = 2					
Methane	0.0093	0.061	0.164	17.6	2.7
Propane	0.010	0.073	0.200	20.0	2.7
Hydrogen	0.072	0.45	0.290	4.0	0.6

From the listed β value for both Method 1 and 2, it seems that Method 2 gives a good reasonable agreement for turbulent factor for methane and propane as the values closer to the turbulent factor given by other works (Munday, 1963, Pasman, Groothuizen and Gooijer, 1974, Yao, 1974) but not for hydrogen. Hydrogen using Method 1 and Method 2 give over prediction in respect to Bartknecht's results and these are unusual experimental result. It should be noted that Swift's equation gives β = 7 (Swift, 1983) for turbulent value during explosion and the predicted β values in Table 3.3 were lower than Swift's turbulent value. These β values will be compared with the best-fit β values from the tabulated experimental data later.

3.5 Review of the published experimental data.

A significant amount of data concerning vented explosion of methane-, propane-, hydrogen-, acetone-, ethylene-and town's gas-air mixtures were found in published literature. The reported 470 experiments were performed in a wide range of initial conditions: enclosures with various volumes (0.12 - 200 m^3) and shapes (cube, rectangular, cylinder and spherical) at various bursting vent pressure, P_{stat}(0 - 500barg) with different length-to-diameter ratio (L/D=1-4) and various location of ignition sources resulting scattered range of maximum reduced pressure, P_{red} (0.014-33.7 barg). The data near or at stoichiometric mixtures with air were studied. Experiments with central point ignition, point ignition near the vent and at the rear wall, as well as with plane and jet ignition, were processed. However, as stated in ATEX and European Guidelines for venting, it is said that central ignition produced worst case scenario and due to this, only experimental data at central ignition will be investigated. Some of the published results do not have sufficient internal details to calculate the internal surface area, A_s and thus, using $V^{2/3} \approx A_s$ is applied to data if the dimensions are not available. For those without detailed information on the geometry, an assumption of L/D = 2 is used for the calculation purposes. The list of constant used for the correlations' calculation presented in Table 3.4. K_G for calculation is excerpted from NFPA 68 (1978): K_G values for gases determined with 10J electric spark. The details of all experimental data are given in Appendix A (Table A.1).

Due to lack of agreements of the published correlations to be applied on the venting design purposes, the collected published experimental data will be compared to the main equations: Bartknecht and Swift's equation as been offered in NFPA 68, Bradley and Mitcheson as the equation offers for the safe venting approach and Molkov as been recommended to be one of the alternatives to be used for the venting design in NFPA 68 (2002). For other equations, it will be reviewed based on the necessity of the data comparison when situation permits. All graphs were plotted by P_{red} v K with respected correlations mentioned in Table 3.1. The data will be categorized according to the fuel/air type, the vessel shape and volume and P_v is between 0 to 500 mbar as this is the validity in using Bartknecht's equation. The reason to follow closely the Bartknecht's range of limitation/validity is due to the wide range of vessel volume to be applied

which V is up to 1000 m^3 where others are not. In case of P_v > 500 mbar, the different analysis will be formed in order to predict the suitability, availability and validity of those equations on the experimental data studied. All data sets are distinguished with shape of the vessel and different volume of the same vessel shape i.e. □ for cubic, ○ for sphere, ◊ for rectangular and Δ for cylinder. This is done to show whether there are independent volume effects which is not been accounted in K and if there is any differences due to the vessel's geometry, for the same K and volume

Table 3.4 K_G value used for vent area calculation. All data were excerpted from Bradley and Mitheson (Bradley and Mitcheson, 1978b) except for acetone-air data (Molkov, Dobashi, Suzuki and Hirano, 2000)

Fuel-air mixtures	**K_G (bar-m/s)**	**S_u (m/s)**	**C (bar)$^{1/2}$**	**ρ_u / ρ_b**	**γ_{uo}**	**γ_{bo}**
9.5 % CH_4-air	55	0.43	0.037	7.52	1.38	1.18
4.0 % C_3H_8-air	100	0.45	0.048	7.98	1.365	1.25
29.7 % H_2-air	550	2.70	-	7.29	1.40	1.25
6.53 % C_2H_4-air	243	0.68	0.048	8.06		
25% Town gas-air	150	1.22	-	6.64	1.38	1.18
Acetone-air	84	0.39	0.048	7.96	1.36	1.25

The relationship between A_s to $V^{2/3}$ as $A_s = C\,V^{2/3}$ is shown as follows:

Shape of the volume	Constant, C
Sphere	4.84
Cubic	6
Rectangular	4n + 2 where n = L/D
Cylinder	5.81 for L/D = 2
Cylinder	5.54 for L/D = 1

Further, since the applicability of Swift's equation is up to P_{red} ~ 100 mbar which is subsonic flow regime, the sonic flow will be applied for P_{red} > 900 mbar. The sonic flow applied when the pressure upstream of the vent reached a critical pressure, P_c which

equal to 900 mbar and the velocity of the gas flowing through the vent becomes sonic. The flow equation for sonic flow changes direct proportional between the mass flow and the upstream pressure, P_{red}. On the P_{red} v K graphs, in the case of Swift's equation, the Swift line with $Pred^{0.5}$ exponent is plotted up to $P_{red} < 900$ mbar and then the line with $Pred^{1.0}$ exponent is plotted for sonic flow.

To the author's knowledge, a quite recent comprehensive comparison on the published correlation on venting design has been made by Razus and Krause (Razus and Krause, 2001) . From their analysis, on the experimental data and by using cylindrical vessel with central ignition as fictitious examples of vented deflagration, they stated that NFPA 68 (NFPA68, 2002) and Bradley and Mitcheson correlations (Bradley and Mitcheson, 1978a, Bradley and Mitcheson, 1978b) gave highest P_{red} and suitable for a worst case consideration only. In a case where the static burst pressure, P_v is involved, equations given by Bradley and Mitcheson (Bradley and Mitcheson, 1978b) and Molkov (Molkov, 2001) seems to agree more on the experimental data for hydrocarbon/air yet the hydrogen/air needed more comprehensive experimental examination. Computational modelling on venting would not be considered in this case.

3.5.1 Comparison of Bartknecht and Swift's correlations with published experimental data.

To get more in-depth investigation on the discrepancy on both equations offered in NFPA 68, the published experimental vented explosion data for methane, propane, hydrogen and town's gas were shown in Fig. 3.4-3.7 with Bartknecht's and Swift's correlation. All data is been corrected to P_v = 100 mbar to allow the minimum P_v in Bartknecht's correlation to be applied The data points indicate the shape of the explosion vessel and different volumes of the same vessel shape as mentioned above i.e. □ for cubic. This is done to show whether there are independent volume effects which not correlated by K and whether there are any differences due to vessel shape, for the same V and K. The data sources are too numerous to be listed and not specifically identified in the graphs, as the object was to concentrate on vessel shape and volume. Figure 3.4 and 3.5 show that most of the data for spheres and cubic vessels are similar

and scattered around Bartknecht's correlation line. As mentioned earlier, Bartknecht developed his correlation based on the experimental data obtained from 10 m^3 cubic vessel volume of propane/air. However, as shown in Fig. 3.5, some of Bartknecht's data of propane/air at V = 60 m^3 are well below the correlation line which is not a general trend for cubic vessel. For hydrogen, only cubic vessels from Bartknecht's data were processed since other works did not have the same hydrogen concentration as Bartknecht i.e. 40 % v/v.

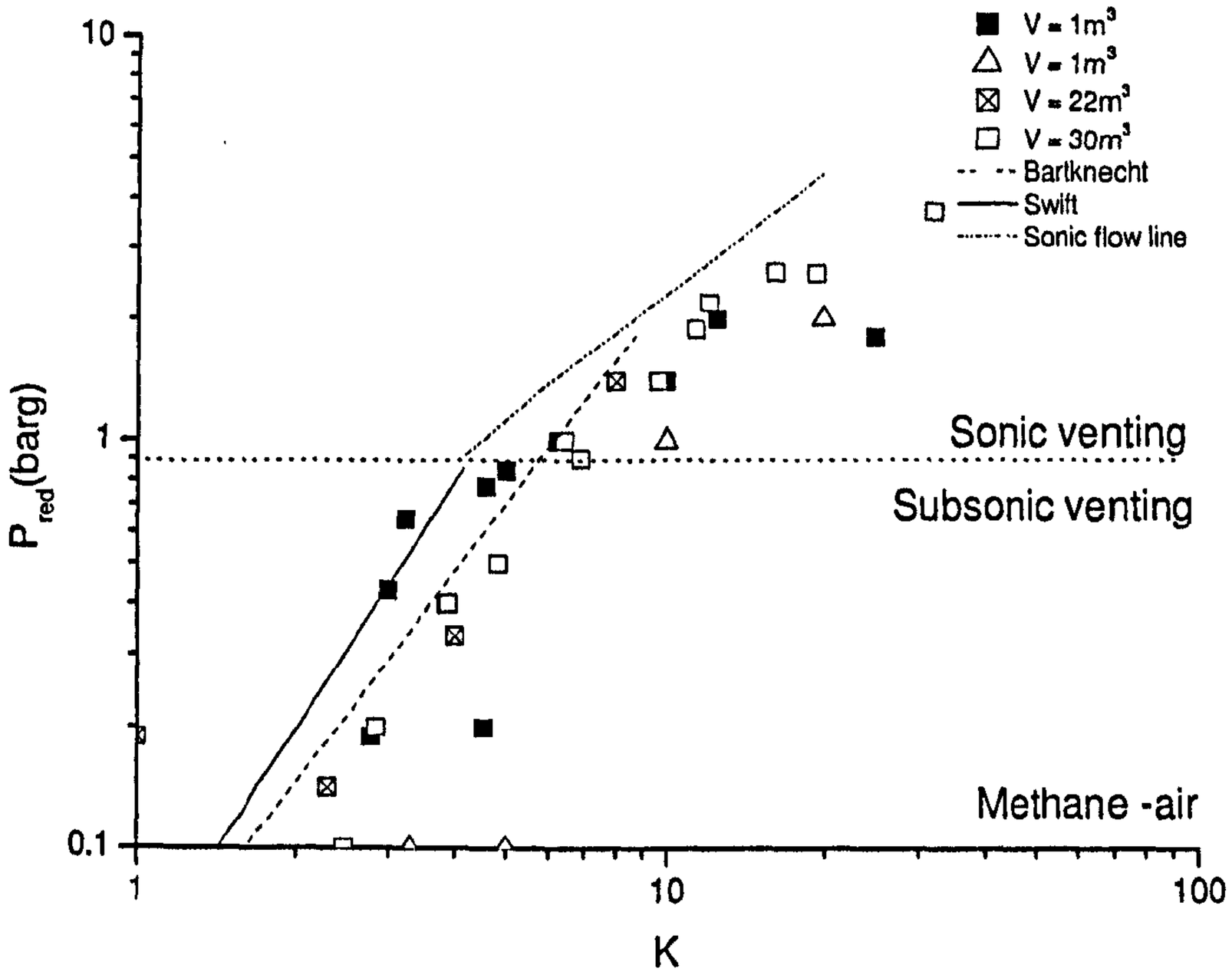

Figure 3.4 Methane/air experimental data as a function of K.

As been illustrated in Fig. 3.7, the rectangular vessels at lower K and subsonic flow gave poor fitting for both equations, suggesting that there is an influence of vessel's geometry in the development of venting gas explosion. The use of $V^{2/3}$ in vent coefficient probably not the best approach to represent the influence of vessel's geometry in venting gas explosion instead of total surface area of the vessel, A_s. Later, the discussion between the use of V2/3 and A_s will be discussed in details in order to determine the best approach to characterise the influence of vessel's geometry.

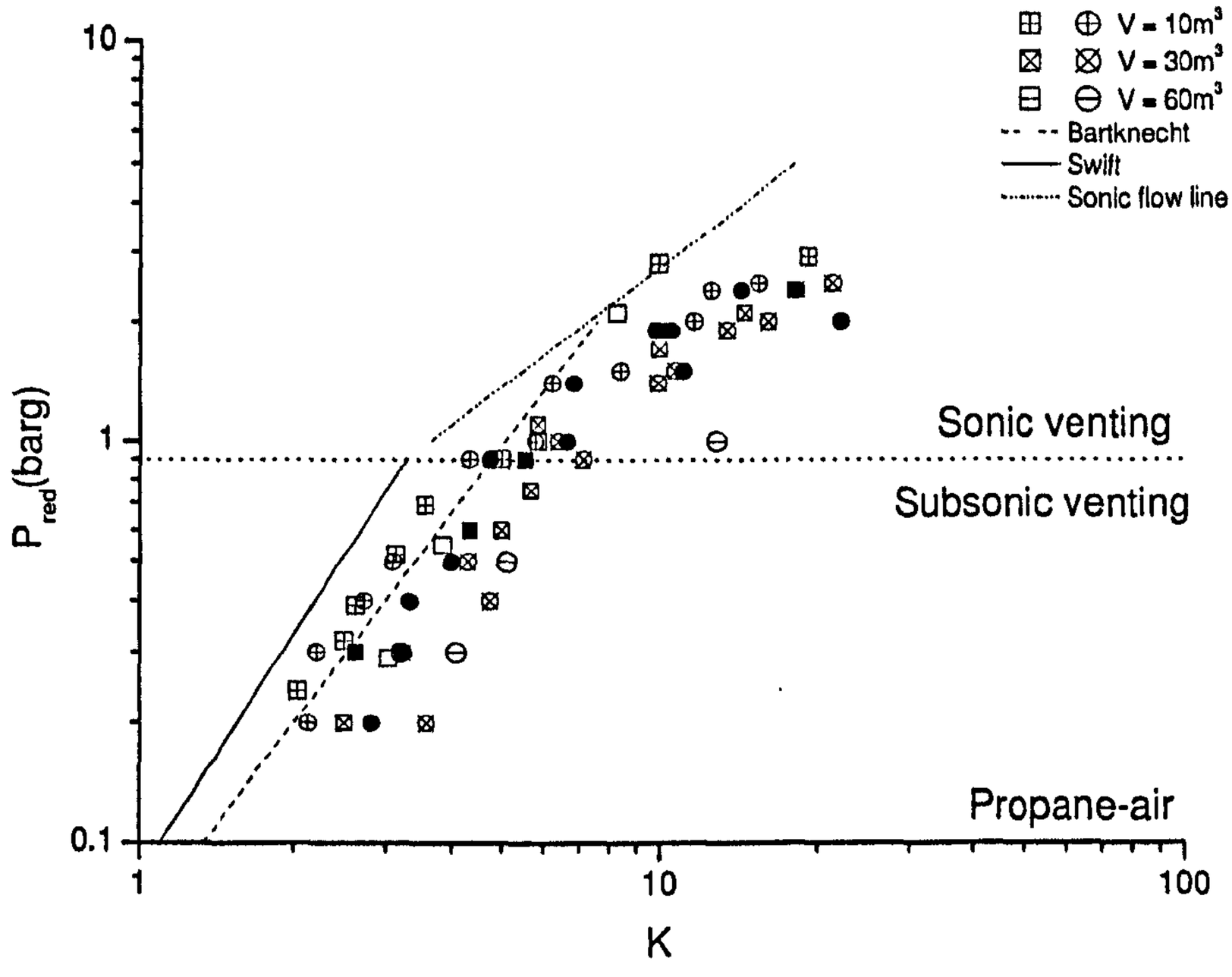

Figure 3.5 Propane/air experimental data as a function of K.

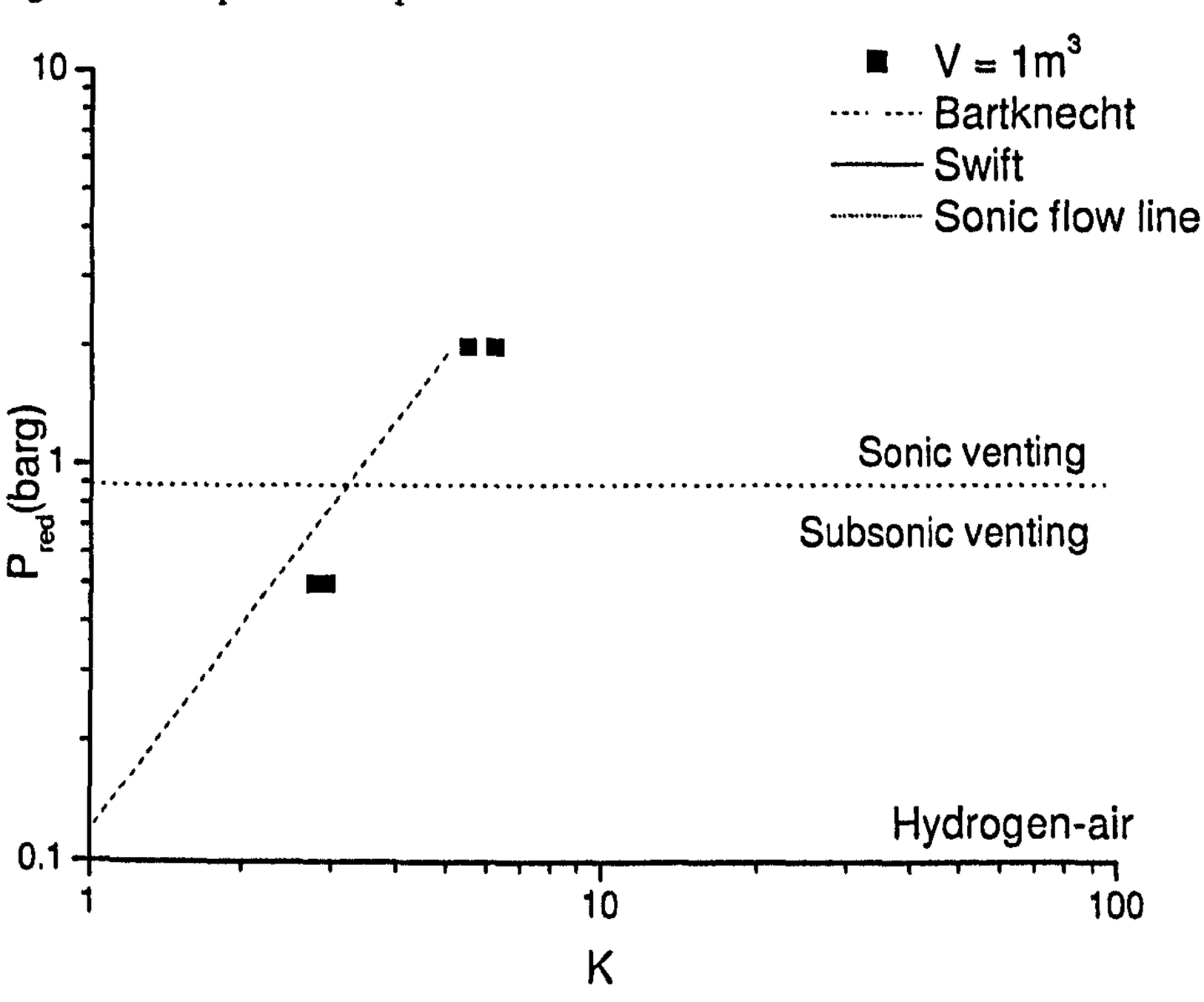

Figure 3.6 Hydrogen/air experimental data as a function of K

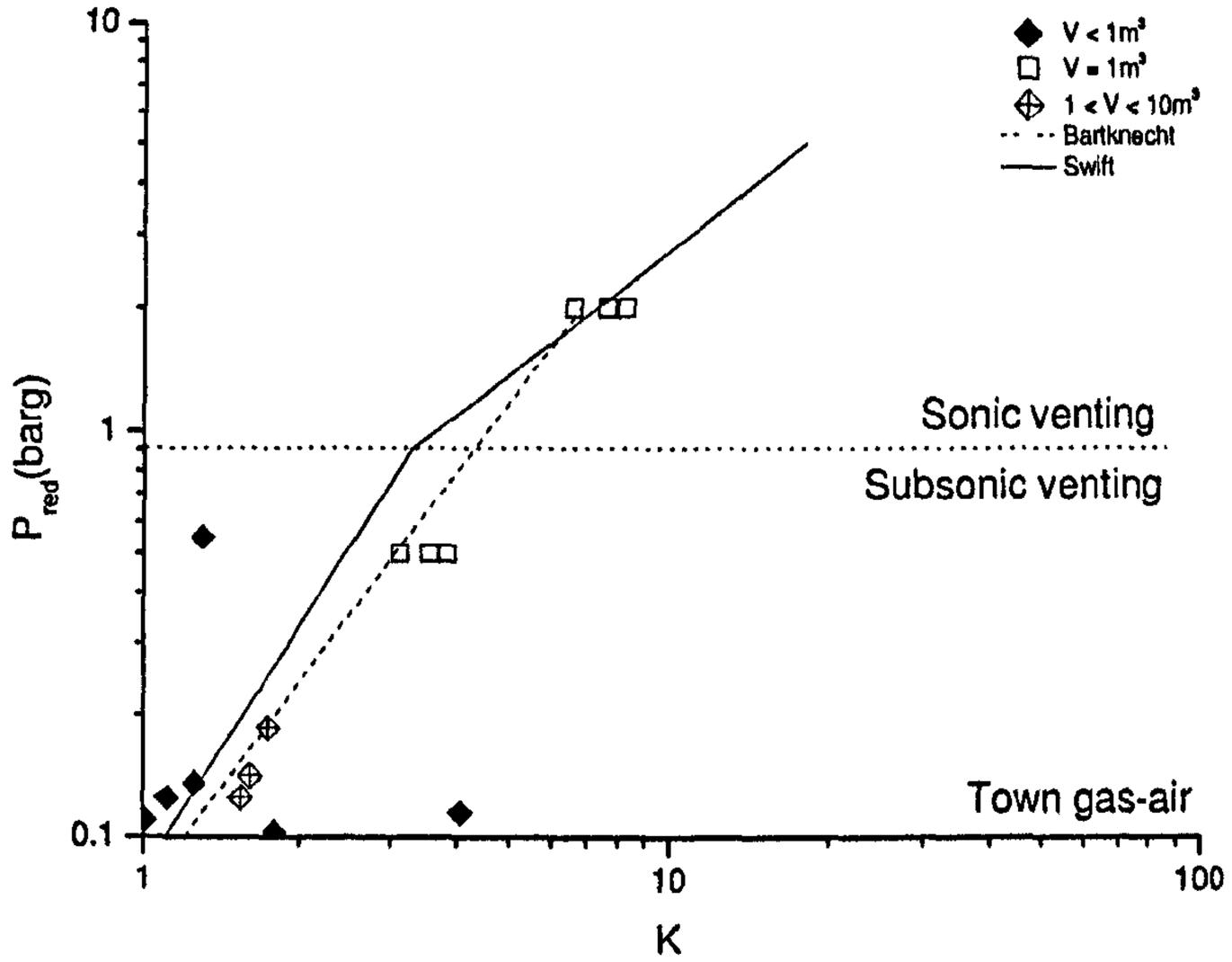

Figure 3.7 Town's gas experimental data as a function of K

Lacking of data at the same concentration as Bartknecht's work is the reason why only four data presented in Fig. 3.6. There are ~16 data points with higher P_{red} than Bartknecht's correlation which was only fitted to his own data set and included no other published data. The results show that Swift correlation has ~5 data points with higher P_{red} than predicted and hence would be a safer prediction than Bartknecht, thus it is recommended to be used and the limits on its applicability are also removed, providing a P_v term is added.

It is the main objective to compare all experimental data with the published correlations to show their validity and applicability. Further, the proposed theories based on **Method 1** and **Method 2** on venting will also be plotted on the graphs in order to make the comparison between the published correlations and how the equations fitted well with the published experimental data. It should be noted that there is no turbulence enhancement factor, β be added to the proposed equations (Method 1 and Method 2) in order to show at what extent the turbulence generated during the explosions. Afterwards, the turbulent enhancement factor, β will be added to the proposed equations that best fitted with most of the data. It is stated that Swift used $\beta = 7$ and Bradley and Mitcheson applied $\beta = 5$ to represent the turbulence generated during the explosion in order for correlation be well agreed with experimental data.

3.5.2 The influence of turbulent enhancement factor, β

At this stage, turbulence factor, β is not taken into account. As been mentioned previously, the level of turbulence induced in the vented explosion has to be determined experimentally as the determination of turbulent factor has not yet agreed to most of the practical application (Chippett, 1984, Molkov, Korolchenko and Alexandrov, 1997, Munday, 1963, Pasman, Groothuizen and Gooijer, 1974, Yao, 1974). The disadvantage of using the suggested approaches is the difficulty in estimating the average values of β from such results. When the vent area is low, it is not sufficient to vent the unburnt gas out from the vessel. The flame will be distorted, increasing the flame area. Thus, this criterion will increase the rate of pressure rise and hence, the pressure will build up rapidly. Decreasing the vent area, i.e. increasing the vent coefficient would initially increase the maximum pressure as the flame becomes unstable. During the onset of the venting, the flame will first start a Helmholtz oscillation; the pocket of burned gas within the vessel undergoes bulk motion towards and away from the vent opening. Consequence from these oscillations, the rate of volume production by combustion increases sufficiently for the internal pressure to increase, the oscillations themselves being gradually damped out as the flame expands. In this trend, turbulence was generated in the shear layer between the out flowing burned gas and the unburned gas within the vessel. The Helmholtz oscillations then induced Taylor instabilities. Taylor instabilities were more profound in larger vessel as discussed by Solberg et al (Solberg, Pappas and Skramstad, 1980).

From Fig.3.8 and 3.9, turbulent enhancement factor, $\beta = 1$ and $C_d = 0.61$ are used in order to correlate the same C_d constant using by other comparative equations. For Molkov's equation, $\frac{\chi}{\mu}$ is treated the same way since the equation is derived based on its own correlation as the constant parameters are not specified. It is illustrated that the turbulence factor is needed compulsorily to be added into the proposed equation in order to take into account the effect of static bursting pressure, P_v of the vent and the existed of the turbulence during the venting explosions.

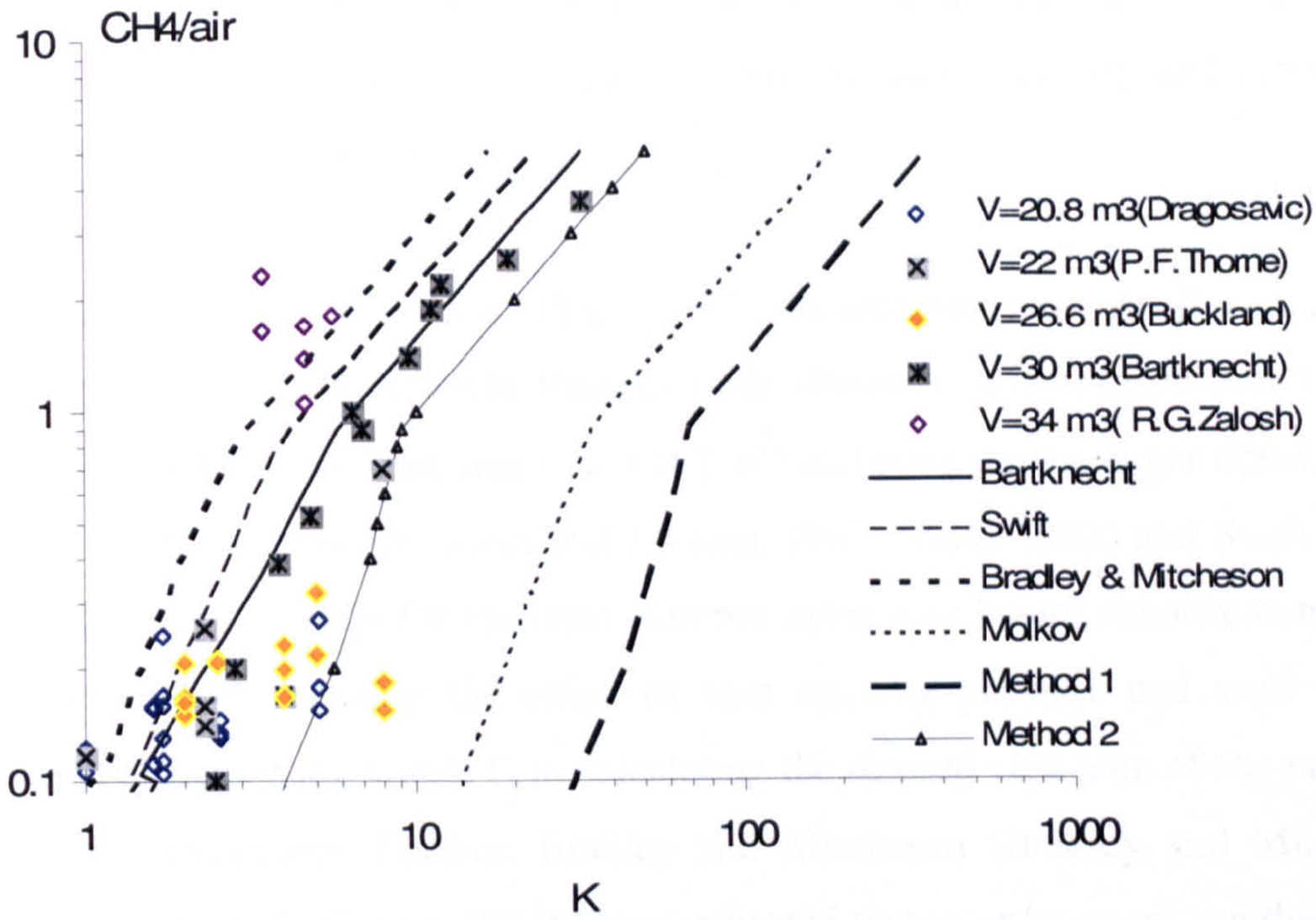

Figure 3.8 Methane/air at various geometries without β

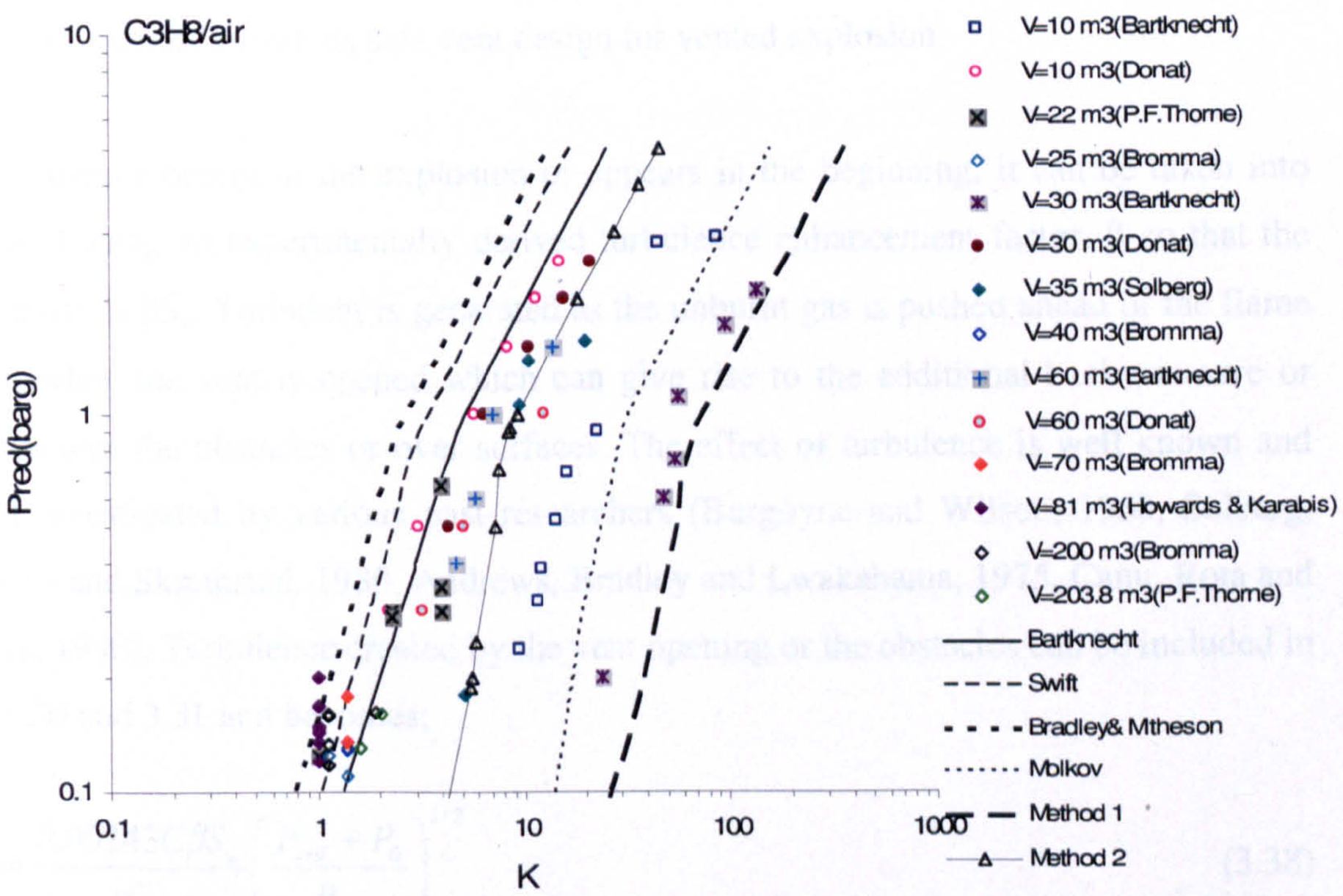

Figure 3.9 Propane-air in various geometries without β

From those figures above, it is clearly seen that Bradley and Mitcheson's equation has a good agreement with the experimental data compared to other studied equations, except for V = 34 m^3 at sonic venting with low K for methane/air. The implication of this is the adequate and safe protection in venting design can be applied for Bradley and

Mitcheson's equation but not in economic and practical application. It is crucial to develop the venting design equation that can provide safe, adequate and economical values in practical application.

For smoothly opening vents, Yao (Yao, 1974) recommended to use $\beta = 3$ and for bursting diaphragms, $\beta = 4$ while Pasman et al (Pasman, Groothuizen and Gooijer, 1974) gave $\beta = 3$ for small vent area ($A_v \leq 0.1\ m^2$) and $\beta = 1$ for the larger openings ($A > 0.1\ m^2$). Swift and Epstein (Swift and Epstein, 1987, Swift, 1983) and Swift (Swift, 1983) indicated that, except for the most extreme cases, a turbulent enhancement factor of 5 is sufficient to envelop the effect of vent opening pressure and used to give deflagration characteristic value, C in calculating the desired vent area of the protected equipments/containments. Further, Bradley and Mitcheson (Bradley and Mitcheson, 1978a, Bradley and Mitcheson, 1978b) also indicated that in order to get the theory and experiment to be in agreement, a turbulent factor of 5 would have to be assumed as being created by the vent. This recommendation applies on the initially covered vent in their correlation, known as safe vent design for vented explosion.

If turbulence occurs in the explosion or appears in the beginning, it can be taken into account using an experimentally derived turbulence enhancement factor, β so that the reactivity is βS_u. Turbulent is generated as the unburnt gas is pushed ahead of the flame front when the vent is opened which can give rise to the additional back pressure or driven past the obstacles or over surfaces. The effect of turbulence is well known and been investigated by various past researchers (Burgoyne and Wilson, 1960, Solberg, Pappas and Skramstad, 1980, Andrews, Bradley and Lwakabama, 1975, Canu, Rota and Carra, 1990). Turbulence created by the vent opening or the obstacles can be included in Eq.3.30 and 3.31 and becomes;

$$\frac{1}{K} = \frac{0.00243 C \beta S_u}{\varepsilon C_d} \left(\frac{P_{red} + P_0}{P_{red}} \right)^{1/2} \tag{3.38}$$

$$\frac{1}{K} = \frac{0.00243 C \beta S_u (E-1)}{\varepsilon C_d} \left(\frac{P_{red} + P_0}{P_{red}} \right)^{1/2} \tag{3.39}$$

Figure 3.10, 3.11 and 3.12 showed the examples on how the possible β had been processed in order to fit with the experimental data. The summary of the average turbulent factor, β for different vessel's geometry and fuels given by Table 3.5,

Table 3.5 Summary on average turbulent factor, β for different vessel's shape and fuels

Vessel's shape	**Methane**		**Propane**		**Hydrogen**		**Town's gas**		**Acetone**		**Ethylene**	
	β M1	β M2	β M1	β M2	β M1	β M2	β M1	β M2	β M1	β M2	β M1	β M2
Cubic	20	4	20	3	~20	5	-	-	-	-	-	-
Sphere	-	-	~20	4	-	-	-	-	20	3	-	-
Rectangular	20	4	~20	3	>20	10	10	2	-	-	7	2
Cylinder	20	3	-	-	15	3	-	-	-	-	-	-

The turbulent factor, β tabulated in Table 3.5 seems to agree with most of the previous experimenters but slightly lower that been given by Swift (Swift, 1983) and Bradley and Mitcheson (Bradley and Mitcheson, 1978a, Bradley and Mitcheson, 1978b). However, if the values in Table 3.5 is compared to values calculated using Bartknecht's constant in Table 3.3, it can be said that both values seems to have a good agreement. This implies that the vessel volume is the important role in determining the P_{red} in vented gas explosions as significant self-acceleration is induced in the larger vessel but having less effect in smaller vessel as been depicted by McCann et al (McCann, Thomas and Edwards, 1985) . It should be noted that the P_v effect is not counted in the **Method 1** and **Method 2** approaches and it is believed that the turbulent factor can be used to represent the effect of flame propagation by the vent flow due to the bursting vent.

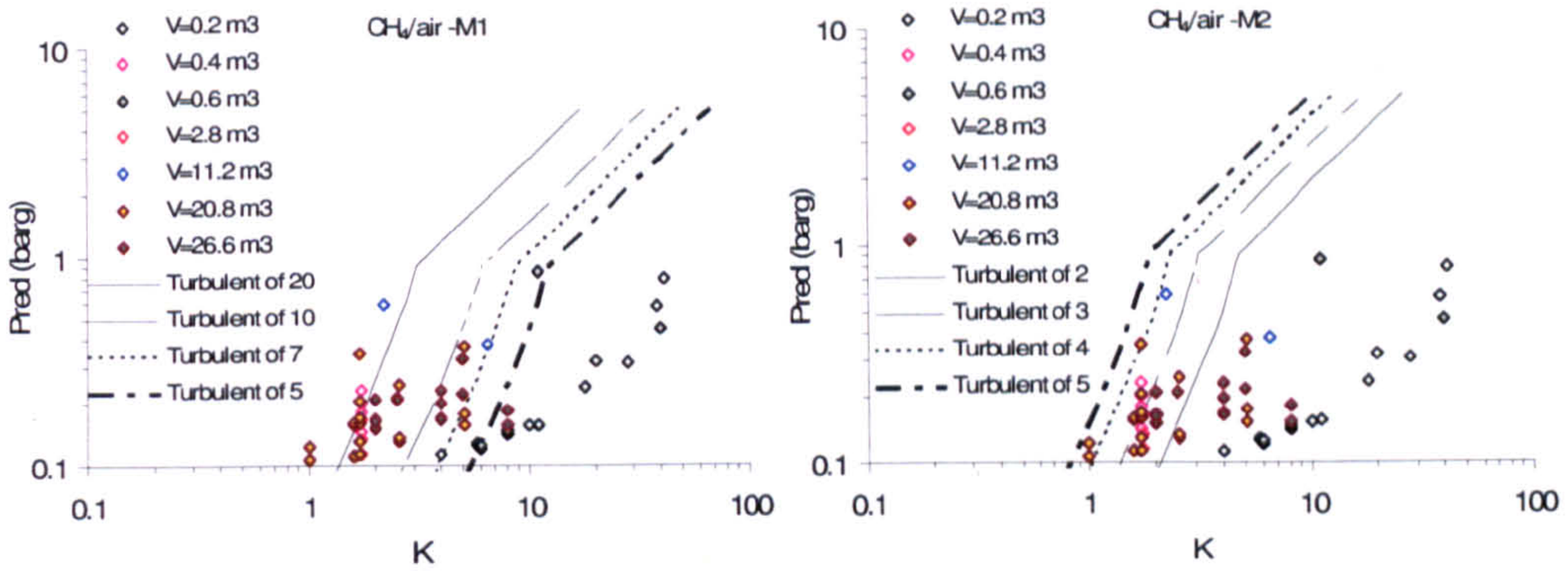

Figure 3.10 Methane/air with turbulent factor, β

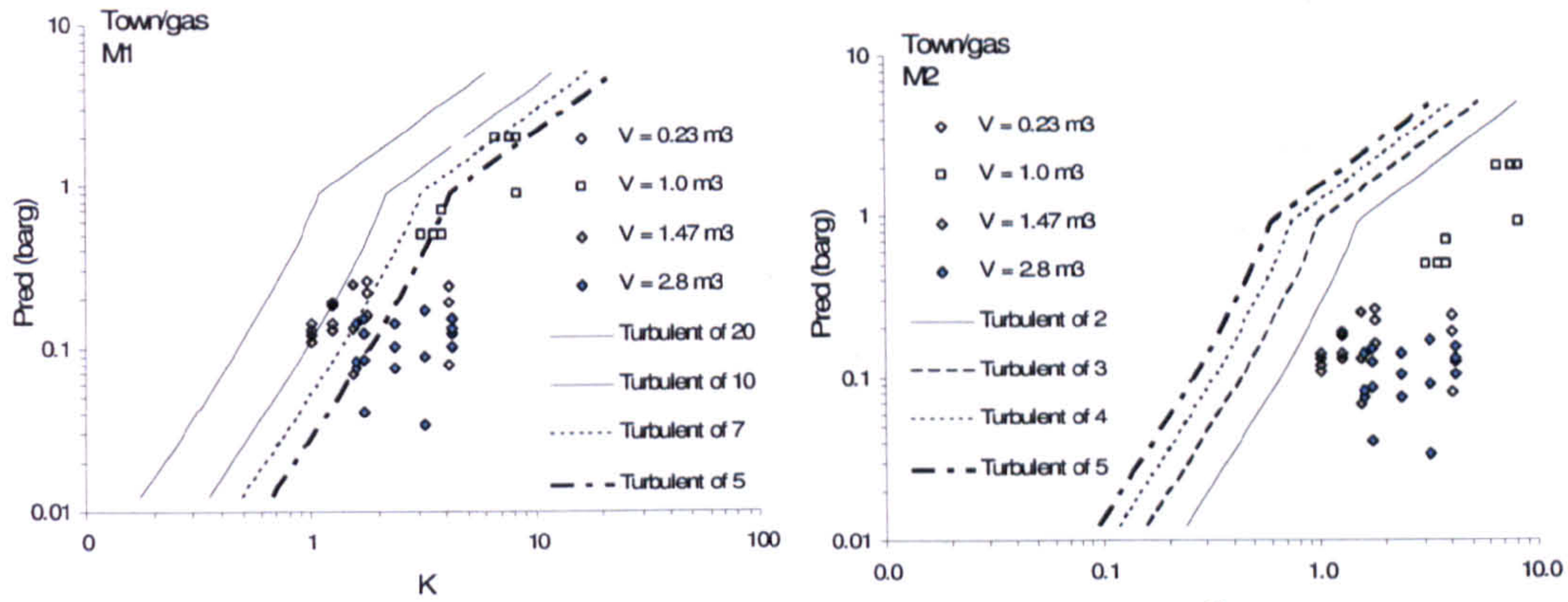

Figure 3.11 Town gas/air with turbulent factor, β

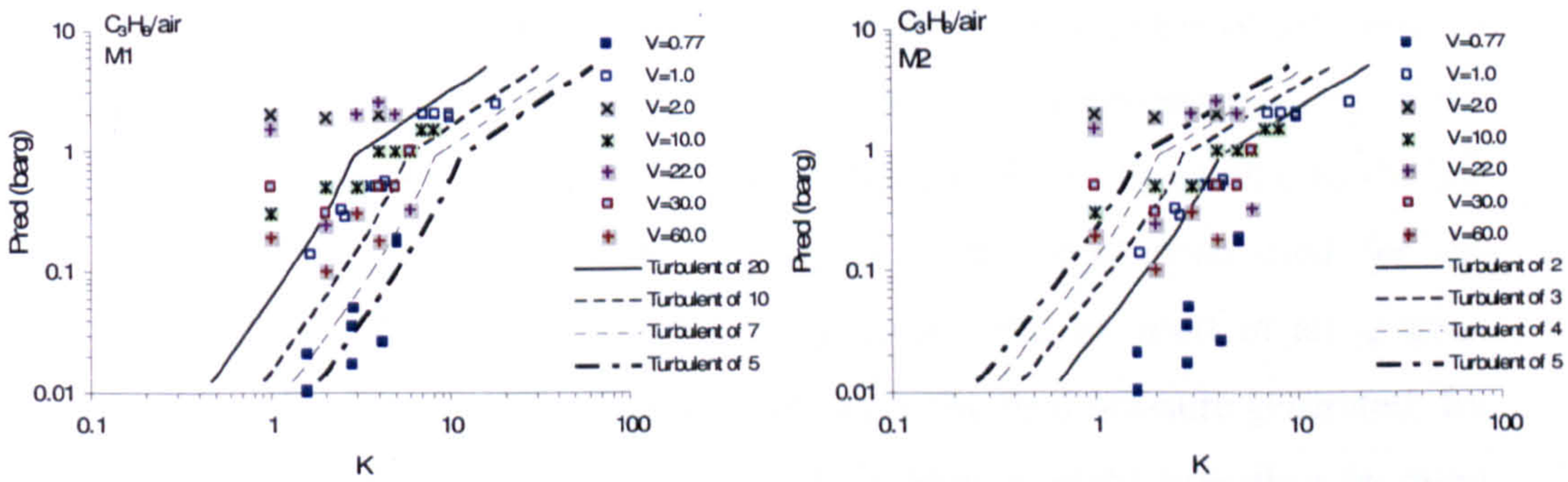

Figure 3.12 Propane/air with turbulent factor, β

However, it seems that **Method 1** with high β do not give satisfactory result to fit the experimental data. In this case, it can be argued on the application of S_u (E-1) and Su terms for demonstrating the unburnt gas ahead of the flame characteristic. This different approach to the maximum vent flow rate of unburnt gases is a crucial in vent prediction assumption as the difference is between S_g or S_f and S_u where usually a factor of 7 or 8 for hydrocarbon and hence (E-1) is ~ 6.5. As S_u (E-1) is close to S_f in value, **Method 2**

will give slightly lower vent mass flow rate where it is clear that based on flame speeds, S_f. The correction factors for expansibility and density as a function of vent area and P_{red} shown that the correlation fitted well with the data in the region compared to others.

Molkov (Molkov,Dobashi,Suzuki and Hirano, 2000, Molkov, 1995, Molkov, 2001, Molkov,Korolchenko and Alexandrov, 1997, Molkov,Grigorash,Eber,Tamanini and Dobashi, 2004) in his universal vent sizing correlation employed the inverse problem method to correlate the turbulence factor, χ and generalised discharge coefficient, μ. From author's understanding, the level of turbulence should grow with flame scale and vent area. Further, the maximum explosion overpressure should correlate with the square of the deflagration-outflow interaction number, $(\chi/\mu)^2$. Their work suggested that the deflagration-outflow-interaction number is dependant of fractal theory and with that criterion, Reynolds number is no longer needed in vented explosion correlations(Molkov, Dobashi, Suzuki and Hirano, 2000).

3.5.3 The influence of the vessel's geometry

Both explosion parameters are dependent on the design of the vessel. In general, the values of P_{red} and dP/dt are changed because of alterations in the amount of heat loss from the flame to the vessel walls. The geometrical term i.e. size/shape of the vessel is generally written as the ratio of the vent area to some other representative area of the system (the internal surface area of the vented enclosure, A_s or its volume to the 2/3 power). However, the vent coefficient, K method is the most often used for the assessment of vented gas explosion and this parameter will be used in all graphs' plotting. The size and shape of the enclosure influences the final pressure generated; for instance higher pressures will be generated in long narrow enclosures than in more nearly cubical ones but in practice, it is the characteristics of the explosion relief that will determine whether or not a plant is damaged by an internal explosion (Cubbage and Marshall, 1974). These two approaches in correlating the venting design do affect the prediction result on venting compared to experimental data. Bartknecht's correlation used the $V^{2/3}$ terms to describe a characteristic of spherical or compact vessel explosions, where the flame remains mostly in spherical shape during venting process on the dependence of overpressure on the test vessel volume. If the spherical flame

propagates at a constant rate irrespective of the vessel volume, there should be no other dependence of P_{red} on volume other than K. Meanwhile, Swift's correlation is given as A_v to be a function of cross-sectional area of the enclosure, A_s multiplied to reactivity terms which include the burning velocity, S_u and turbulent enhancement factor, β. The use of the vented vessel surface area in vent correlations was first introduced by Runes (Runes, 1972) as the maximum possible flame area and was used to calculate the maximum flame mass burning rate.

The use of A_s seems to be appropriated to link with the vessel's shape as if the vessel shape is substantially different from cubic or when L/D > ~ 2, the flame touches the wall before there has been a significant pressure rise and spherical flame propagation cannot be applied to model the explosion. In practise, maximum pressure usually but not always occurs when the flame contacts a wall of the vessel and the flame area begins to decrease (Nagy and Verakis, 1983). In non spherical vessels with central ignition, Ellis (Ellis, 1928) showed experimentally that the shape of the flame tends to assume the shape of the vessel. This observation is agreed by Nagy et al (Nagy and Verakis, 1983) with cylindrical vessel. In a large spherical vessel, the buoyancy of the hot gases may distort the flame development. If the ignition source is not centrally located, the flame front will contact the near wall before combustion is complete as the flame is allowed to expand in one direction resulting in an elongated flame with increasingly larger surface area and hence, faster expansion than centrally ignited flame. Consequently, the maximum rate of pressure and the maximum pressure will be less than when ignition is central because of greater heat losses. For central ignition, the flame will expand symmetrically in all directions in spherical shape. After some time, the flame begins to distort when first flames contacting the vessel wall and stretching towards the vent before changing its shape to a cylindrical flame.

From the data collected, it is observed those cubic and spherical vessels are the most vessels' geometry used in vented explosion. Assuming the flame initially behaves as a spherical shape, it is observed theoretically that the initial burnt mass are less than 10 % for cubic, cylinder for L/D = 2 and worst case for rectangular where only 2.5 % of the mass has burnt during the explosion process (in a case where P_{max} is assumed to be 8 bar) when the flame touches the wall. Since the mass burnt rate is proportion to rate of pressure rise (dP/dt), it will reduce the flame burning area and laminar burning velocity

and thus, decreases the P_{red}. At this point onwards, the heat losses from the burnt gases to walls are larger which also distributed to reduce P_{red}. Quenching of the flame just prior to reaching the vessel wall can be expected to have a significant effect on the K_G value in very small vessels. The reduced flame area after contacting with the walls influences the mass burnt rate which finally decreasing the amount of mass flow rate through a vent. Increasing L/D ratio, i.e. smaller D for constant L, less mass burnt rate is obtained which results to decrease P_{red}. Thus in large L/D vessel, the spherical flame portion of the flame propagation occupies a negligible part of the explosion event. This is why the standard cubical relationship involved in K_G or K_{st} (dust deflagration constant) parameters only apply to compact or near spherical vessels. For spherical vessel, 14% of initial mass or at overpressure of 1.12 bars for maximum pressure inside closed vessel is assumed to be 8 bars, has burnt when the flames first touch the vessel wall compared to about 7.5 % initial mass (overpressure = 600 mbars) burnt for cubic vessel. It was found that spherical vessels give higher P_{red} rather than cubic vessel due to a lower quenching effect to the vessel wall and since the mass burnt rate is proportion to rate of pressure rise (dP/dt), it gives rise to an accelerating flame front and an increased P_{red}. This scenario is shown in Fig. 3.13.

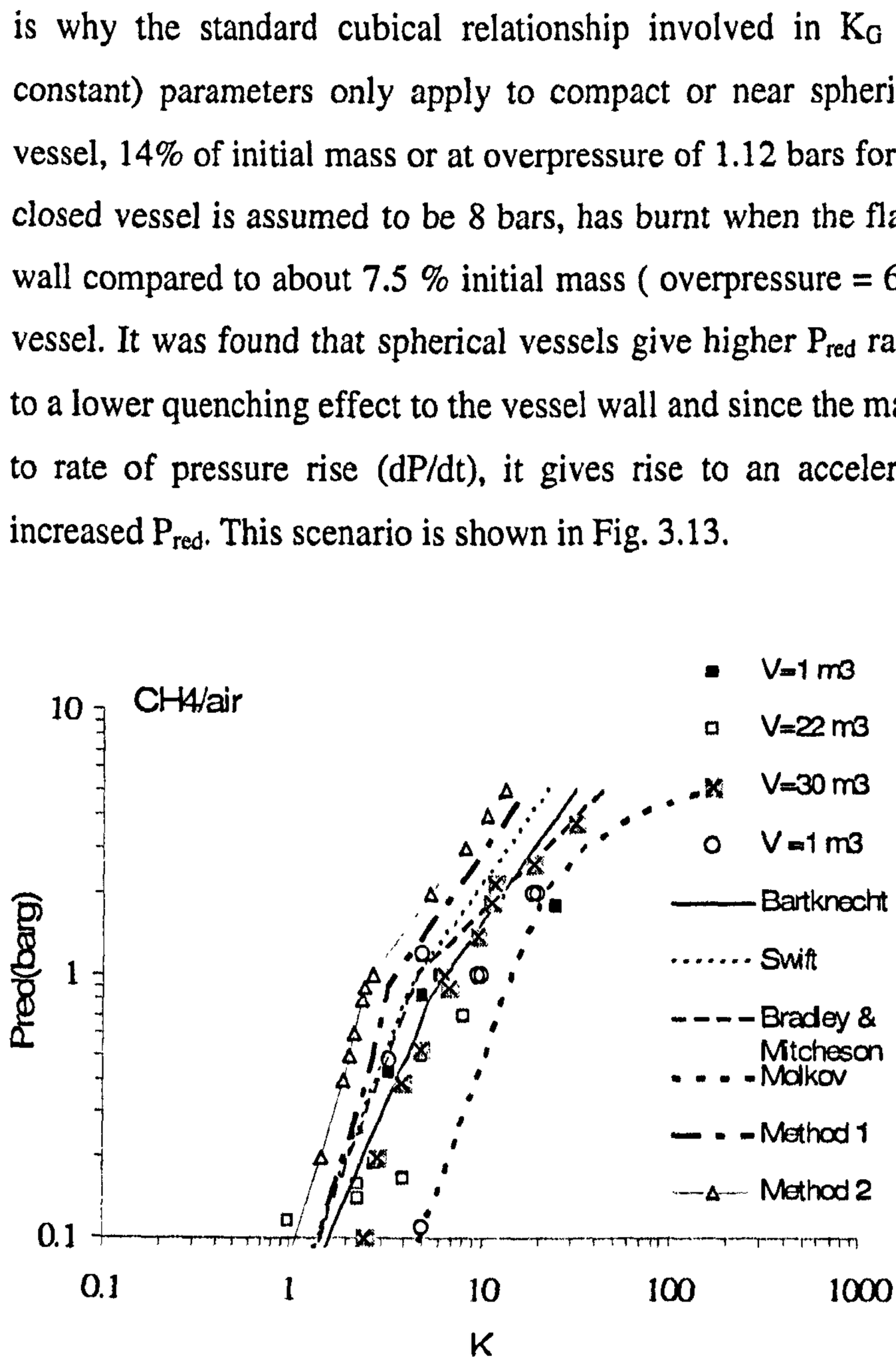

Figure 3.13 Influence of vessel's shape on methane/air explosion ○ Sphere and □ cubic

From Fig. 3.13, it is shown that the proposed equations **(Method 1 and Method 2)** gave satisfied correlation to fit most of the data when β is included. Even though Swift's

equation regarded to be applied for P_{red} < 200 mbars, it shown that the application of the equation can be extended. This is shown by most of the data fall under the Swift's line as previously mentioned in Section 3.4. In rectangular and cylinder vessel, the majority of the flame propagation is non-spherical as the flame is elongated to follow the vessel shape where ~ 2.5% of the mass has been burnt when spherical flames reaches the wall and hence, there are large heat losses subjective to convection heat. Since quenching rate is higher, the reduced flame area influences the mass burnt rate which finally decreases the amount of mass flow rate through a vent (Andrews, 2004). Thus for most practical situations, there will be large heat losses from the explosion and venting will occur after the flame has touched the vessel wall as shown in Fig. 3.14, 3.15 and 3.16 on non-spherical vessels data scattered outside the published correlation lines even at low K.

From Fig. 3.16, it was found that cylinder vessel data gave bit scattered plots for K> 1 from the proposed equations and published correlations. In a cylindrical vessel, the flame shape is divided into two periods. In the first period immediately after ignition, the flames were hemispheric and then half-spheroidal with sections parallel to the wall. In a very short period of time, nearly 80 % of the flame area vanishes because of the quenching of wall parallel parts. As a consequence, the amount of expanding burned gas is suddenly reduced, resulting a rapid decrease in heat release as well as P_{red} (Starke and Roth, 1986). The reduction of the flame area also contributed to the low peak pressure and dp/dt_{max}. Thus, for most practical situations, there will be large heat losses from the explosion and venting will occur after the flame has touched the vessel walls. Similar results also obtained by Leeds work on a larger cylinder (Phylaktou, Andrews and Herath, 1990). Their work showed that the point of deviation of the cylindrical vessel from spherical flame propagation is obtained at the time the flame touches the wall, causing lower dP/dt and peak pressure. It also concluded that the application of spherical flame propagation modelling can only be applied to spherical vessel if the full flame propagation is modelled (Phylaktou, Andrews and Herath, 1990)

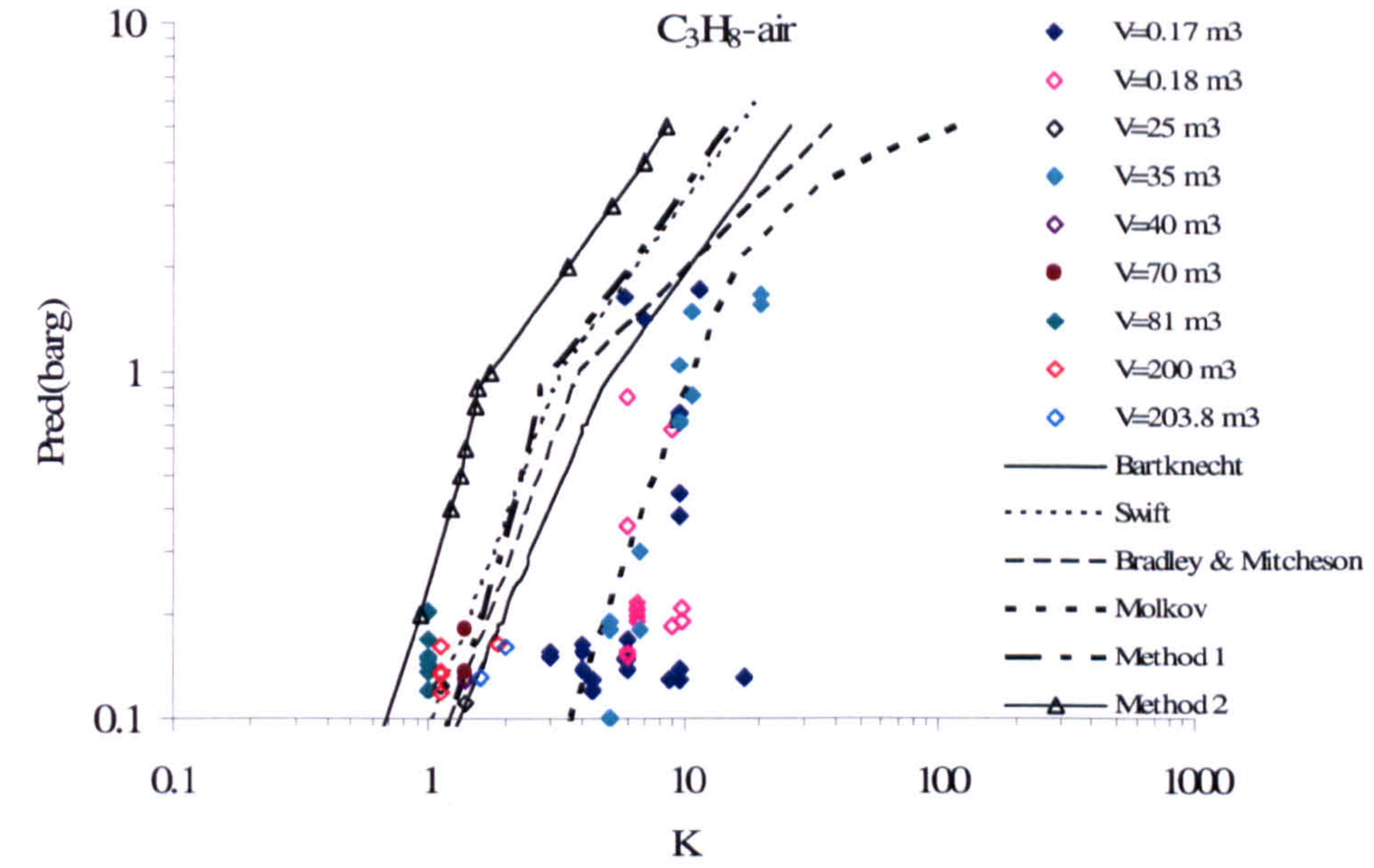

Figure 3.14 The influence of rectangular vessels on P_{red} for propane/air ◊ rectangular.

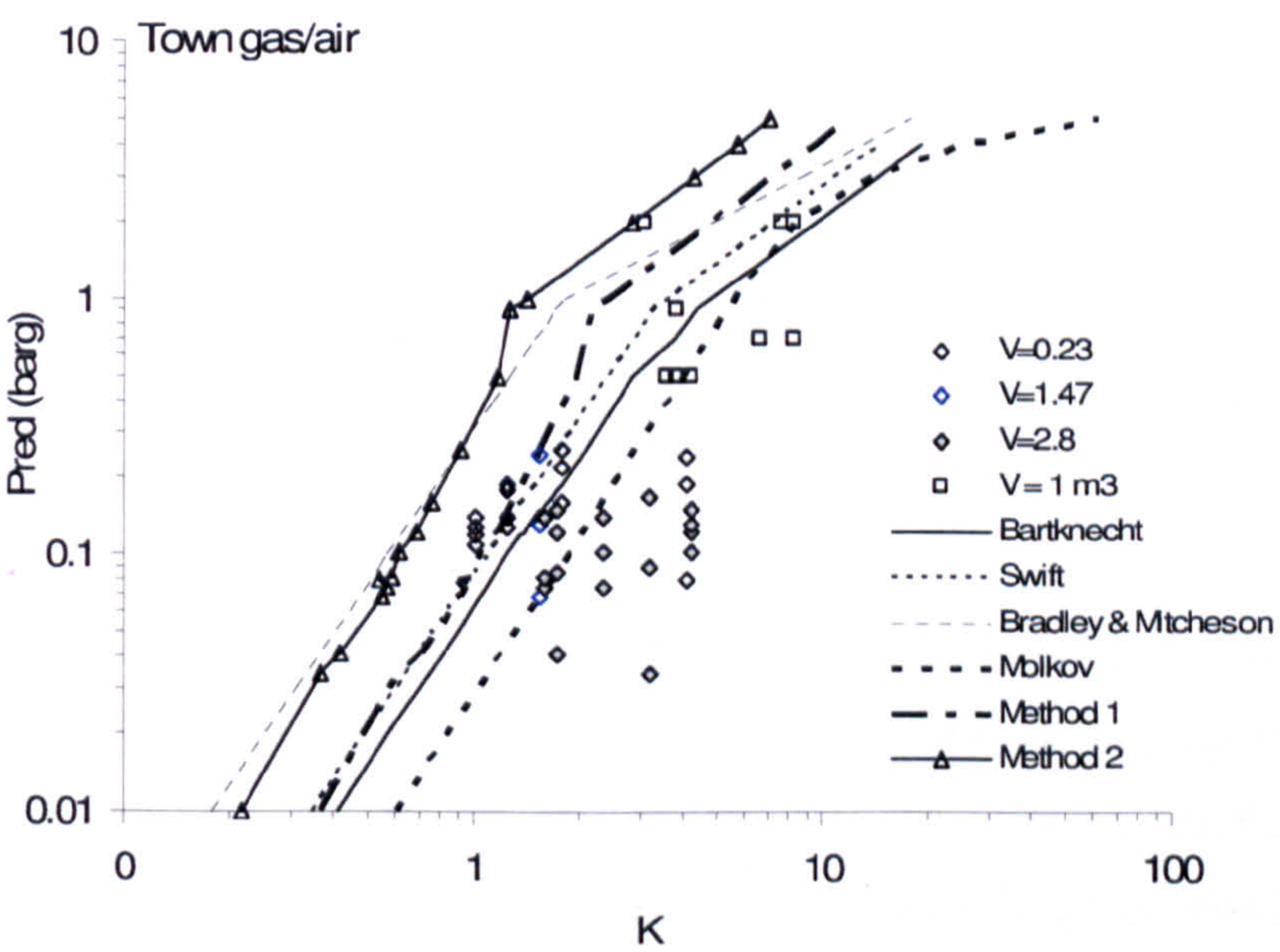

Figure 3.15 The influence of various geometries on P_{red} for town gas/air ◊ rectangular, □ cubic, ○ sphere

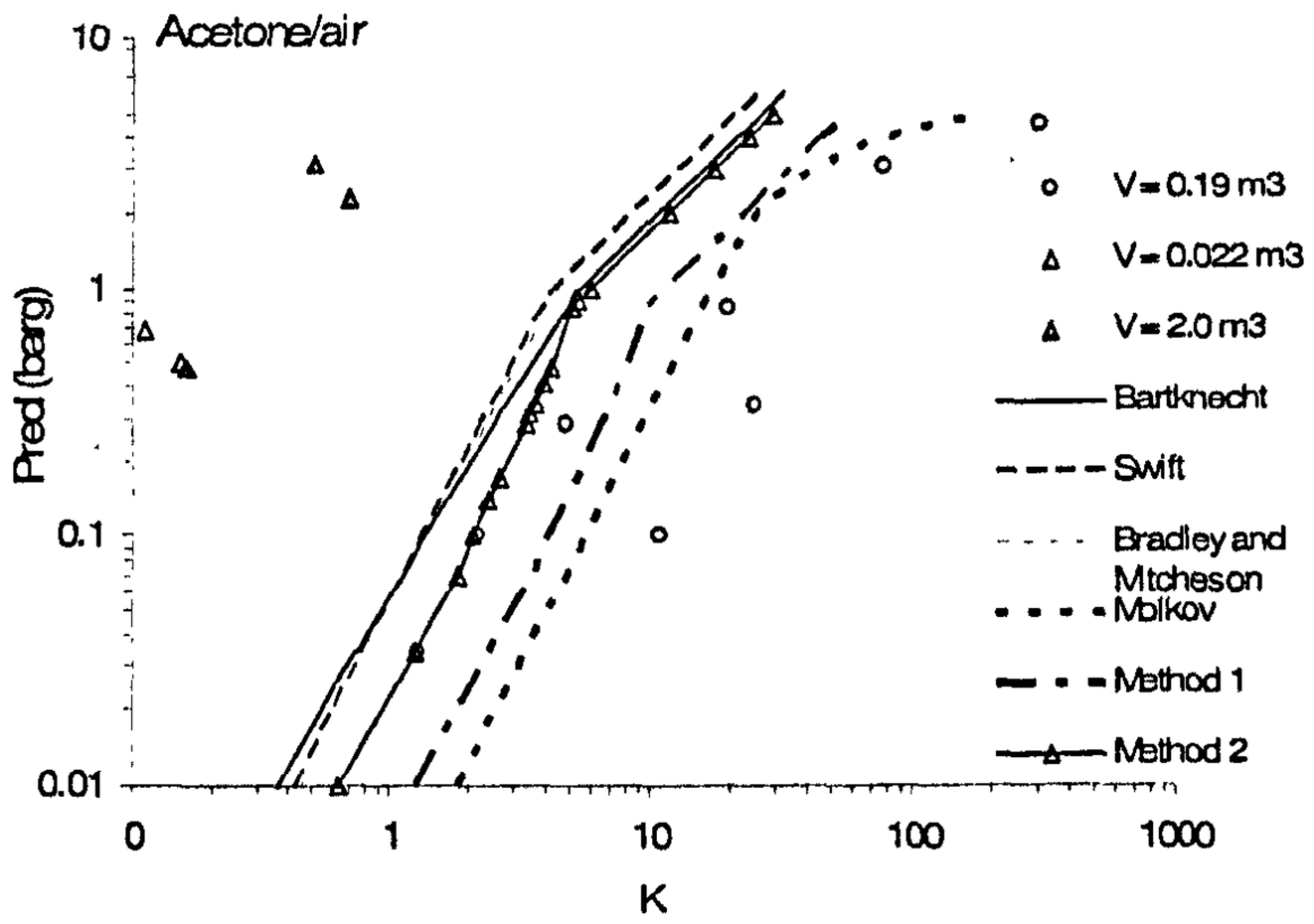

Figure 3.16 The influence of the vessel's shape on P_{red}. Δ cylinder ○ sphere

3.5.4 Comparison between K and A_s/A_v term for vessel's geometries

As been discussed above on how the use of $V^{2/3}/A_v$ (K) term is failed to give satisfactory results in non-cubic and non-spherical vessels, the term A_s/A_v will be replaced the K term in order to investigate the differences in using both terms for correlating the vessel's geometry in venting explosion. It should be noted that this analysis is only involved the whole set experimental data of methane/air in various geometries.

The data results will first be shown the P_{red} v K for cubic, rectangular and cylinder vessels as illustrated in Fig. 3.17. Again, turbulent enhancement factor, β is included accordingly for all correlation lines. From Fig. 3.17, it can be said that cubic vessel gave satisfactory results for all correlations but not with rectangular vessel. The data scattered around the correlation lines, but mostly around Method 2 and Bradley and Mitcheson's correlation lines. This suggests that both Method 2 and Bradley and Mitcheson can be applied for safe venting guide in venting design purpose. However, the cylinder data seems to fit well below the correlation lines.

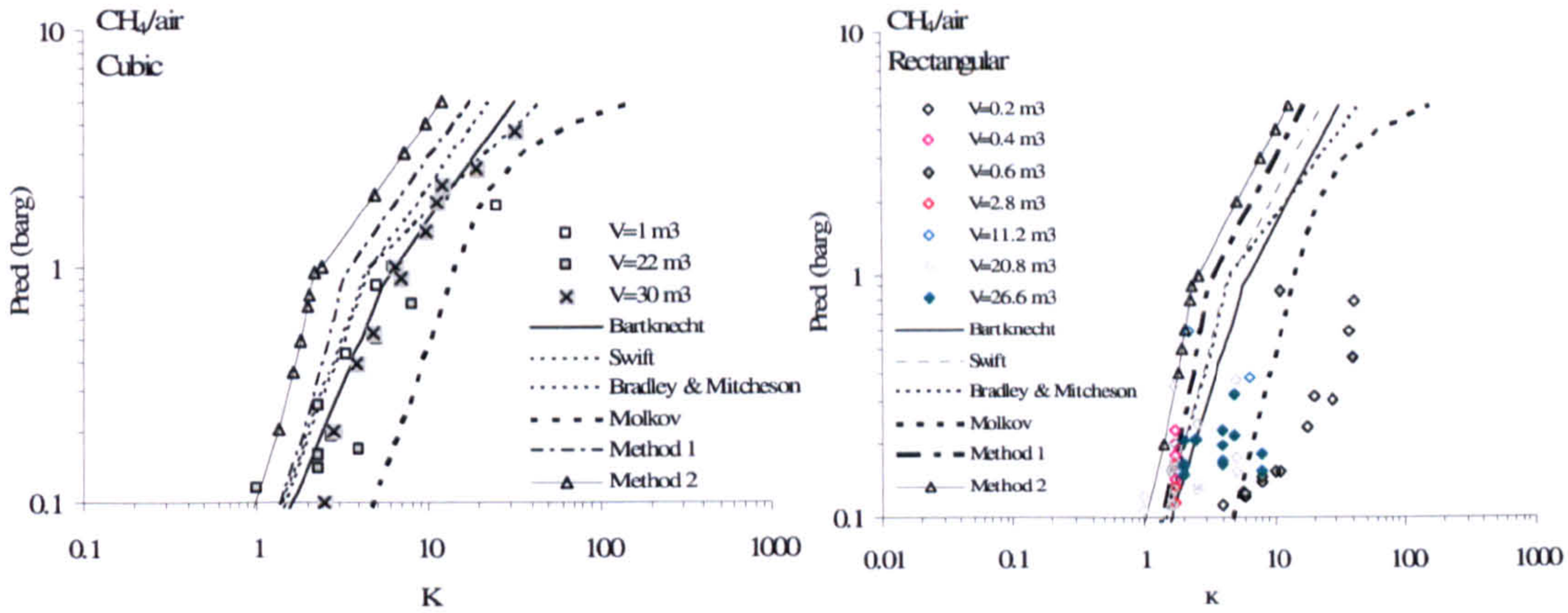

Figure 3.17 Methane/air for P_{red} as a function of K

When the same set of data was compared with P_{red} v A_s/A_v plots, it apparently gave better trend. The cubic data results seem not given good agreement when A_s/A_v term is applied for V = 30 m^3. All rectangular data fall below Bartknecht's correlation line, suggesting that the use of A_s term is more favourable in the case of non-cubic vessels as been postulated above. It also showed the same trend when applied to cylindrical vessel. From the analysis, it can be said that the K term is more favourable when it applied to cubic and spherical vessels as it fits the spherical flame propagation scaling law. The satisfactory results on correlating the influence of vessel's shape is given when A_s/A_v is applied for non-cubic and non-spherical vessels as been proved in Fig. 3.18. It can be recommended to use A_s term instead of $V^{2/3}$ term to get more precise results if the vessel's shape influence have to be taken into account in venting design.

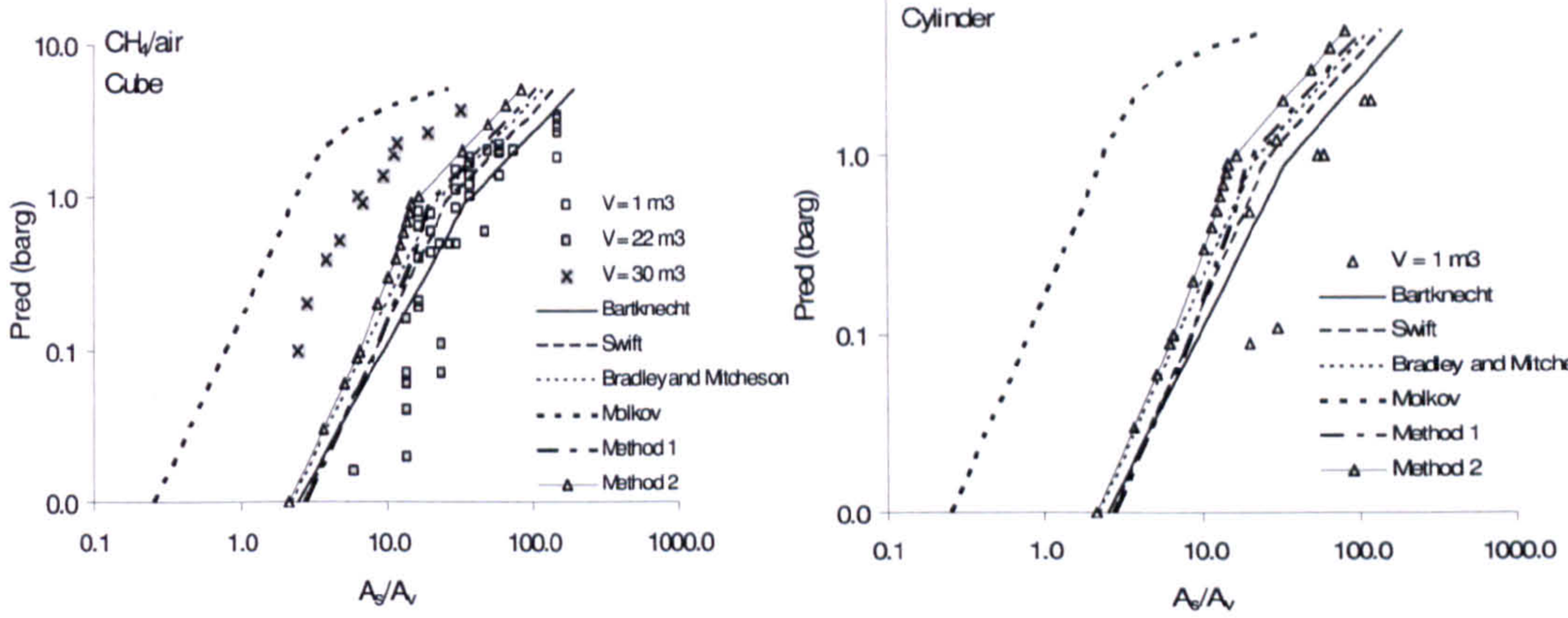

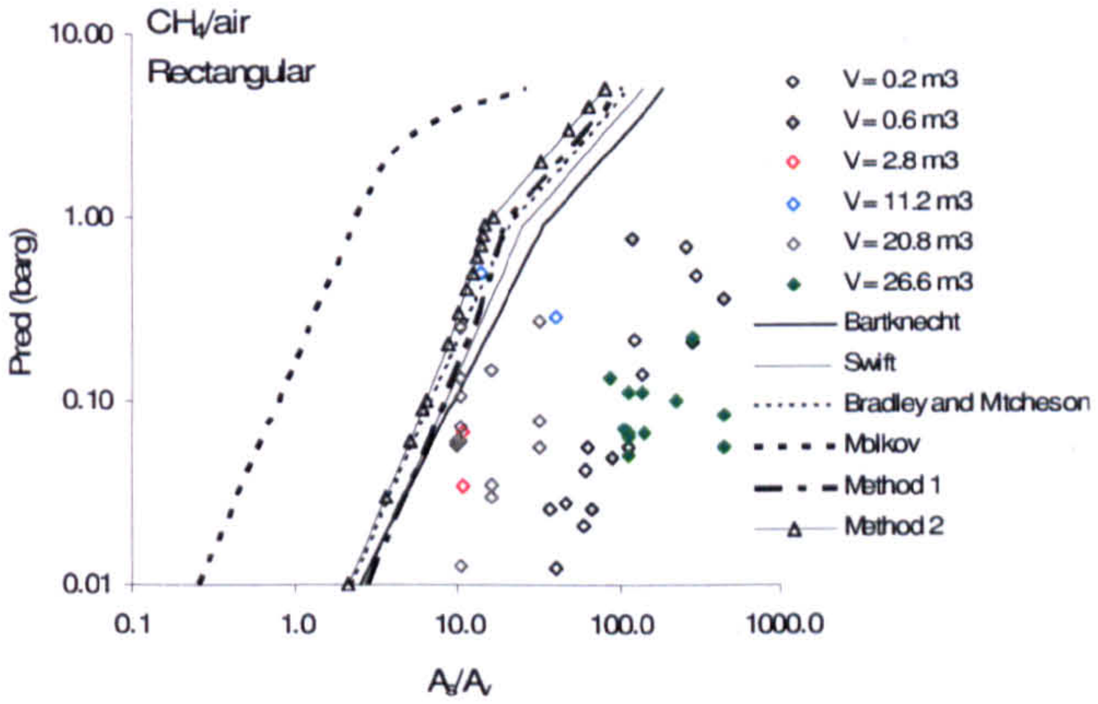

Figure 3.18 P_{red} of methane/air at various geometries as a function of A_s/A_v.

The data shows that P_{red} exponent should be 0.5 in the subsonic flow regime and unity exponent in the sonic flow regime are supported by the data. Bartknecht's 0.58 exponent is a compromise between the two regimes which not a good correlating exponent and does not fit the fluid mechanics of the vent flow. The main data scatter is due to the additional influence of volume. It can be summarised that the proposed equation (**Method 2**) for safe venting has more advantages compared to others. The analysis is based on the mass and momentum balance, only employing an empirical relationship to account for compressible flow and sonic flow. The use of S_u (E-1) and A_s terms for non-cubic and non-spherical vessels to correlate the important parameters involved in venting gas explosions seems to agree well with the published experimental data. The simplicity of this 'safe' venting correlation can be used for any required venting pressure and area, providing one of the values is given.

3.5.5 Evidence for an additional influence of vessel volume on P_{red}

The data for each volume tested over a range of K was plotted as P_{red} v K and later P_{red} at fixed K of 2, 4, 10 and 30. This allowed the influence of volume to be investigated at constant K. There is insufficient data to undertake these plots for town's gas and acetone. Figure 3.20 shows that for methane there is a very significant volume influence for $K < 4$ with no consistent effect at higher K. The higher K data is mainly in the sonic flow regime. At low K the increase in P_{red} with volume is probably due to the flame self acceleration effect, which extensively discussed in NFPA 68.

It is widely recognised that just as in the transition from laminar to a turbulent fluid flow, flame wrinkling occurs when the flame Reynolds number (Re) exceeds a certain value (3000-4000) i.e. which is a function of the flame expansion ratio, E (Groff, 1982). In smaller vessels, cellular instabilities does not appear until the late stages of the flame development just prior to the vent failure and thus, no significant effect on initial flame and pressure growth at low K. It means that in smaller vessel, the critical Reynolds number is not attained. Further, in smaller vessel, there will be less time for the coupling between the acoustic wave and the combustion wave to accelerate the burning rate effectively (Wingerden and Zeeuwen, 1983b, Wingerden and Zeeuwen, 1983a). Unfortunately, for larger vessel, the onset of flame cellularities would occurs in the early stages of the explosion, enabling to promote acceleration of the flame front and as a result to attain an increased rate of pressure rise (McCann, Thomas and Edwards, 1985). It should be noted that Bartknecht (Bartknecht, 1993) worked with large volumes (volume ranging from 1 to 250 m^3 cubic) so the self-acceleration flame had already occurred to the limit values and this is the reason which the correlation gave non-conservative prediction for A_v when applying to smaller vessel.

Further, Groff (Groff, 1982) explained that in larger vessel, hydrodynamic instabilities (transition of smooth spherical to polyhedral-cellular flame) will arise at some critical expansion ratio. This then accelerates the overall burning rate of the gas mixtures owing to the expanded flame surface area, thus increasing the maximum rate of pressure rise above that to be expected from the laminar system. Hydrodynamic flame acceleration effects (cell cellularities) produced will increase K_G values in larger vessels and wall quenching in the smaller vessels depress the K_G value. Therefore, the use of K_G values

as a simple scaling parameter for deflagrations is not valid (Chippett, 1984). Figure 3.19 shows example how K_G affects on size of the vessel.

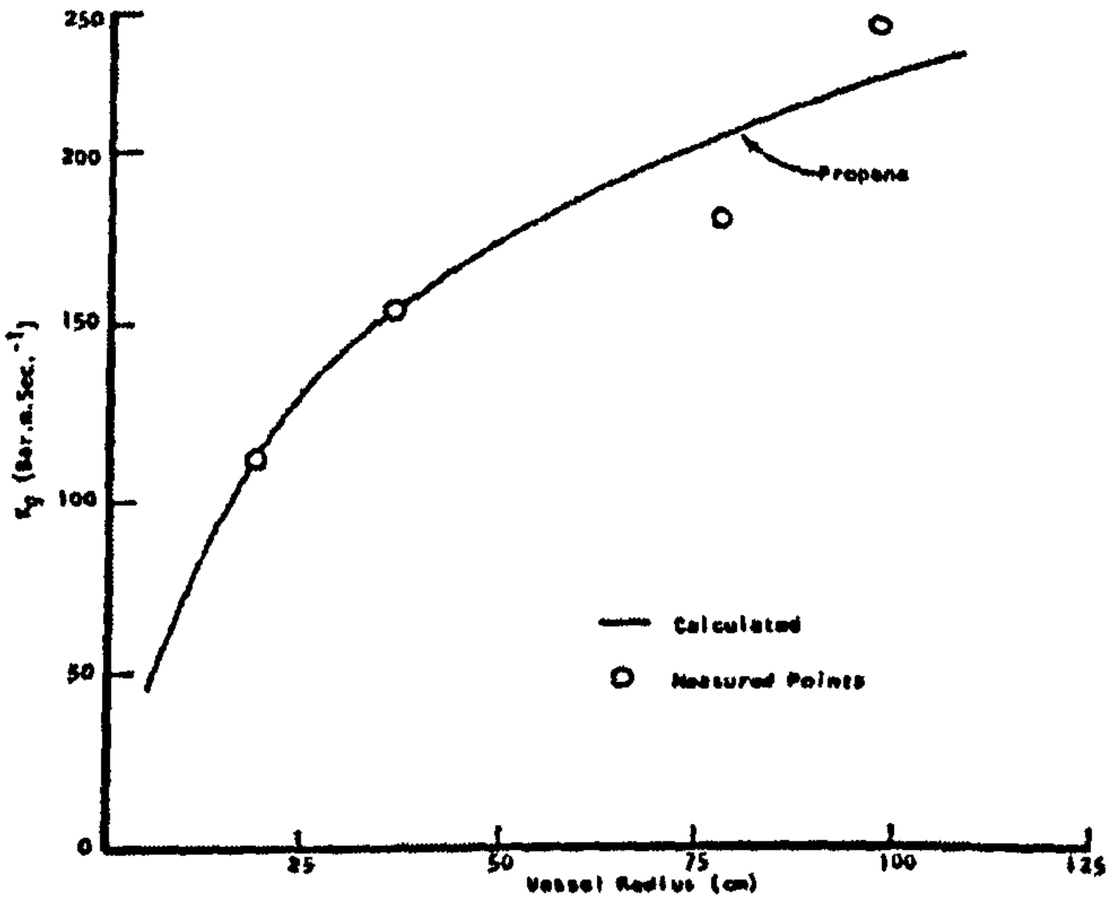

Figure 3.19 K_G as a function of vessel size for propane/air (4%) measured at an initial pressure of 1 atm (Chippett, 1984).

Larger flames form cells at a critical diameter and flame acceleration occurs. The net effect is an increase in S_u and K_G, which has not been accounted in Bartknecht or Swift correlation. In principle the effect is similar to vent induced turbulence and could be accounted by β term in the burning velocity equation. Hydrogen behaves in a similar way as methane at low K and little influence of volume in the sonic flow regime at high K as illustrated in Fig. 3.20. For propane, the additional volume effect is more complex. For $K < 4$ there is a consistent increase in P_{red} with volume, but for higher K there is a decrease in P_{red} as the volume increases at constant K. This latter trend is difficult to explain and in the original Bartknecht data (Fig. 3.3) shown a smaller vent area in the larger volumes (30 and 60 m^3) for the same overpressure. It can be postulated that it was due to the experimental errors. The likelihood of explosions resulting from stratified fuel-air mixtures is high, especially with regard to particularly buoyant or heavier than air leaks within structures; despite this the published literature on this topic is quite sparse. Current literature on stratified explosions deals predominantly with buoyant gases (DeHaan, Crowhurst, Hoare, Bensilum and Shipp, 2001, Liebman, Corry and Perlee, 1970).

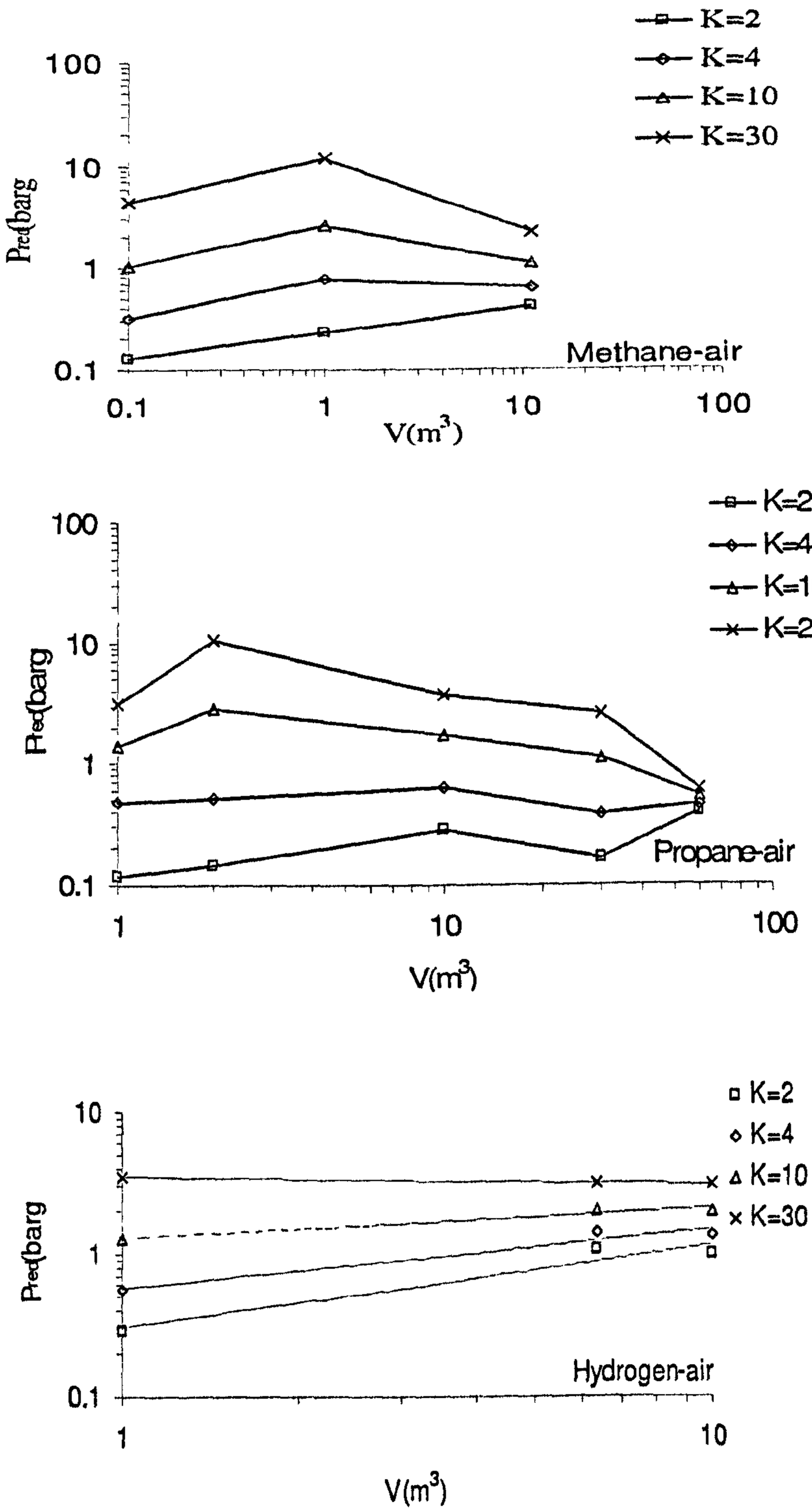

Figure 3.20 Effect of P_{red} on vessel volume at constant K

In practice the vast majority of accidental gas or vapour releases will involve a high molecular-weight compound which is then likely to lead to the formation of an inhomogeneous stratified mixture. There has been limited work in this area (Tamanini, 2000) and in many scenarios this is likely to result in reduced overpressures.

The effect implies flame deceleration effect at large volumes when the pressure is high at large K. This is not an effect that has been previously highlighted in the data. For sonic venting the pressures are higher and cellular flames occur earlier at high pressure and are there at the end of methane/air explosion in closed vessels even on a small scale. Andrews and Bradley (Andrews and Bradley, 1972) photographed cellular flames in a 300mm diameter closed cylindrical explosion vessel at the end of the flame propagation. Methane explosions at 1 bar need a greater distance than 150 mm to form cells and the pressure effect causes them to form at shorter distances. Thus at high K and P_{red} with sonic venting during venting explosion, the self acceleration is likely to have already occurred at the smaller volumes.

3.6 Concluding remarks

In this chapter, there is found that the correlation derived by Bartknecht (Bartknecht, 1993) have been shown to be under predicted most of the data presented. It can be said that the failure of the Bartknecht's correlation is due to the assumption of the same vent area is required irrespective of the volume. Further, most of the vessels involved in Bartknecht's correlation were large where there is suspected that self-acceleration may occur during the vented explosion and this parameter did not be taken into account in an appropriate manner. From this work, it is recommended that the validity and limitation of Swift's equation (Swift, 1983) can be extended to wider range for $P_{red} > 200$ mbar providing the parameter P_v is added into the equation.

A significant flame self acceleration effect for subsonic venting was shown for K<~5 and this effect is similar to vent induced turbulence and could be accounted by the β term in the burning velocity equation. The turbulence enhancement predicted based on Bartknecht's equation and proposed Method 2 were in a good agreement with β derived from tabulated experimental data based on Method 2 as seen in Table 3.5. It can be said that the β derived was perfectly reasonable value for β as used by other experimenters (Munday, 1963, Pasman, Groothuizen and Gooijer, 1974, Yao, 1974). The flame experiences deceleration effect in larger volumes when pressure is high in larger K and this effect has never been highlighted previously. It is postulated that at high K and P_{red}

with sonic venting during the explosions, the self-acceleration is likely to have already occurred at the smaller volumes.

It can be suggested that the use of K term is more suitable to be applied on cubic and spherical vessel for L/D = 2 but failed to give satisfactory results for non-cubic vessels. The A_s/A_v term is more favourable to correlate the influence of vessel's geometries for non-cubic vessels. The data and figures shown in this work also illustrated that P_{red} exponent of 0.5 in the subsonic flow regime and unity in sonic flow regime are supported by the experimental data. The main data scatter is due to the additional influence of volume. The use of P_{red} exponent of 0.582 in Bartknecht's equation compromises between subsonic and sonic flow regime which gave most of the data scattered outside the line.

It can be recommended that Method 2 gives reasonably good agreement with most of the experimental data and the use of S_g term to describe the unburnt gas displaced by the flame which gives approximately ~6 times the mass flow rate suggests it gives close estimation on P_{red} in relation with practical application in comparison by with S_u term used in Method 1. The net effect is as S_g is close to the flame speed, S_f in value, the approach is only slightly lower vent mass flow rate than that based on S_f.

CHAPTER 4

SIMPLY VENTED GAS EXPLOSIONS: THE PRACTICAL

4.0 Introduction

In order to further demonstrate the applicability of proposed equations (Method 1 and Method 2) to the present study, series of experimental works were carried out using Test vessel 1 and 2 as described in details in Chapter 2.Again, this is the purpose to study the impact of overpressure on venting at different vessel volume as Bartknecht's work indicated that the same vent area is required irrespective of the vessel's volume which is obviously incorrect. When the experimental data of Bartknecht is examined (Kasmani, Willacy, Phylaktou and Andrews, 2006, NFPA68, 2002), it is clear that the exponent of P_{red} is fitted to the data with $1/K > 0.2$ or $K < 5$ and the correlations should never be used for higher K. This is not recognized in NFPA 68 or in the draft European guidance on venting. The limitation on the correlation is stated as $P_{red} < 2$ bar and the experimental data shows that this is effectively a limit of K of 10. However, none of the experimental data for $P_{red} > 0.8$ bar fits the correlation and all is lower than the correlation. This effectively gives the validity of the correlation at $K < 5$ and $P_{red} < 0.8$ bar and this is the incompressible vent flow regime. Even the work in this area has been extensively investigated, yet there is still unclear explanation on the impact of the vent burst pressure on the overpressure (Bradley and Mitcheson, 1978a, Bradley and Mitcheson, 1978b, Chow, Cleaver, Fairweather and Walker, 2000, Cooper, Fairweather and Tite, 1986, Cubbage and Simmonds, 1955, Cubbage and Simmonds, 1957, Donat, 1977, Fairweather, Hargrave, Ibrahim and Walker, 1999, Harris and Briscoe, 1967, Kumar, Dewit and Greig, 1989, Pasman, Groothuizen and Gooijer, 1974, Thorne, Rogowski and Field, 1983).

From previous chapter, it is shown that the published guidelines, particularly with regard to the question of appropriate scaling of the correlation parameters are having their own limitations and validity to use in practise. It is crucial to note that there is another important factors i.e. turbulent, self-acceleration, volume and geometry effect influencing the mechanism in venting explosion which subsequently giving the published correlation a poor agreement with the experimental results. For the effect of bursting vent on maximum pressure in vented explosion, most of the work was limited to stoichiometric fuel concentrations (Bartknecht, 1993, Cooper, Fairweather and Tite, 1986, Cubbage and Marshall, 1974, Cubbage and Simmonds, 1955, Cubbage and

Simmonds, 1957, Donat, 1977, Pasman, Groothuizen and Gooijer, 1974, Runes, 1972, Zalosh, 1980, Thorne, Rogowski and Field, 1983). Changing the equivalence ratio changes the laminar burning velocity, S_u, of the flame and the mass burning rate of spherical flames scales as S_u^3. In this work, the effect of mixture reactivity from Φ =0.8 to 1.6 will be investigated in terms of P_{max}, P_v and flame speed, S_f for end and central ignition. In a vented explosion with a vent burst pressure the flame is larger when the vent bursts and the larger surface area give a greater burning rate. When the vent bursts, the outflow of unburnt gas is at a higher velocity and so the pressure losses in the vent are greater and the influence of the vent burst pressure is significant (Cooper, Fairweather and Tite, 1986).

4.1 General features of experimental tests

The geometries of Test vessel 1 and 2 used in the present study were cylindrical vessels which give the volume of 0.2 and 0.0065 m^3 respectively. The vessel was closed at the end and fitted at the other with a circular tube with diameter of 0.162 m, simulating the vent (either initially open or covered) to the 52 m^3 dump vessel, which effectively gave free vent discharge conditions (its volume was 260 times greater than the vented vessel) but enable the work to be carried out under laboratory conditions. The length of Test vessel 1 is 1 m while 0.315 m length is applied to Test vessel 2. For Test vessel 1, all experiments were ignited either at end wall ignition or at the centre of the vessel centreline but in a case of Test vessel 2, only end wall ignition was considered. Pressure development was monitored at various locations along the length of the test vessels (Refer to Fig.2.2). The distance, x from the spark divided by the test vessel diameter, D, x/D of the pressure transducers was kept approximately constant for all test vessels.

For Test vessel 1, the pressure was measured at three positions, P_0, P_1 and P_2 on the test vessel and at the dump vessel, pressure is measured by P_6. For Test vessel 2, two piezoresistive pressure transducers were mounted along the test vessel, namely P_0 and P_1 and P_6 situated at the dump vessel. For maximum reduced pressure, P_{max}, this was taken from P_1 pressure transducer as it located at the centre of the vessel for both test vessels. The flame front motion was determined using bare bead thermocouples arrayed along the vessel and the tube centreline (symbols as T_1-T_3 in Fig.2.2). The flame speed

data were generated from thermocouples for flame arrival times output and allocated to the position midway between the thermocouples or in the case of the first flame speed the time between the spark and arrival at the first thermocouple. There was no significant dead time in the thermocouple response but there was a large thermal lag due to the 0.5 mm diameter thermocouple bead that was used. This prevented its use for temperature measurement but was ideal for time of arrival measurement as the thermocouple survived the explosion. A further advantage of the thermocouple flame arrival detection technique is that it can be used with hydrogen. The alternative technique of ionisation probe flame detection does not work with hydrogen flames as they have no ionisation. As part of the experimental programme, three repeat tests were performed at each condition and these demonstrated good consistency and reproducibility, with peak pressures varying by less than ± 5 % in magnitude.

In Test vessel 2, vent covers from magazine paper, aluminium foil, Melinex membrane and 100g A4 paper were also used with four different bursting pressure (P_v) ranging from 98 to 424 mbar. The vent covers were located behind the gate valve and will be burst prior to the ignition for investigating the effect of initially closed venting on P_{max}. The reason to use the specific range of P_v is due to the P_v limitation imposed in Bartknecht's equation. These dynamic burst pressures, P_{dyn} were observed to be greater than P_v at all tests. The gate valve was closed during the explosion vessel mixture preparation by partial pressure. This method of mixture preparation could not be used without the exit gate valve as the vent would burst during the evacuation of the vessel. The gate valve was opening prior to ignition, when the pressure was 1 bar on both sides of the vent, exposing the vent cover to the explosion gases. The single-hole orifice plate was used to simulate the objective on varying the vent area which placed at the end of the vessel just before the gate valve as described in Chapter 2 (Refer to Fig. 2.2).

The present work is directed at providing further understanding in these two areas of gas explosion venting i.e. the impact of overpressure on vessel's volume and the influence of P_v on overpressure on vented gas explosion. Bartknecht (Bartknecht, 1993) presented a vent design correlation that is used in NFPA 68 (NFPA68, 2002) and the European vent design standard (2007). This static vent burst pressure, P_v was determined using the vent in the vessel and slowly (relative to the rate of pressure rise in an explosion) increasing the pressure of the vessel using compressed air until the vent

burst. However, the actual burst pressure in each explosion was easily determined from the drop in pressure P_1 when the vent burst.

The series of tests involved a range of experimental conditions in each test vessel. Different range of fuel/air concentration of premixed methane, propane, ethylene and hydrogen were prepared using the partial pressure method to an accuracy of 0.1 mbar (0.01 % of composition). The flammable mixture was initiated by an electrical spark which gives 16 J energies for the gas explosion tests. The summary of the tests are given below,

Table 4.1 Summary of the experimental tests

TEST VESSEL 1				
Fuel/air	**Φ**	**K**	**Vent type**	**Ignition**
Methane/air	0.84-1.43	16.4	Open	End/Centre
Propane/air	0.8 – 1.5	16.4	Open	End/Centre
Hydrogen/air	0.34 – 0.54	16.4	Open	End/Centre
Ethylene/air	0.6 – 1.6	16.4	Open	End/Centre

TEST VESSEL 2					
Fuel/air	**Φ**	**K**	**Vent type**	**Pv (mbar)**	**Ignition**
Methane/air	0.84-1.43	1.0,2.1, 3.3, 16.4	Magazine paper Aluminium foil Melinex membrane 100g A4 paper	98 178 209 424	End
Propane/air	0.8 – 1.5	16.4	Open	0	End
Hydrogen/air	0.34 – 0.54	16.4	Open	0	End
Ethylene/air	0.6 – 1.6	16.4	Open	0	End

4.2 General explosion development

In order to give a general overview of the typical explosion development of gas/air mixtures in both vessel tests, two representative pressure and flame position records for open venting are shown in Fig. 4.1 and 4.2 for $\Phi = 1.06$ for methane/air.

The vertical dashed line is the time at which the flame exited the test vessel marked as T_{out}. From Fig. 4.1, the flame initially propagated in a slow, laminar phase with low pressure and flame speed before the flame approaches the vent which took approximately 110 ms and 72 ms to travel from the ignition point of end and central respectively. The average flame speed is 22.8 m/s for end ignition and 16.5 for central ignition which was considerably greater than the laminar spherical flame speed of about 3.0 m/s. Based upon previous research on vented vessels (Chow, Cleaver, Fairweather and Walker, 2000, Cooper, Fairweather and Tite, 1986) and records of additional thermocouples positioned in the radial direction of the vessel, the flame initially developed hemispherically from the point of ignition at the end wall. Then as the vented flow field was set up, the flame began to elongate towards the vent and during this stage, unburnt gases were also being vented out to dump vessel. For centrally ignited, the flame is initially spherical flame, progressively stretched on one side towards the vent (flame accelerate towards the vent) and also at the opposite direction of vent. From this explanation, it suggests that end ignition had a much larger flame area than the central ignition and this reflects with end ignition gave higher overpressure that central ignition. For Fig.4.2, it has the same typical pressure-time profile for venting at initially open vent but the flame accelerates very rapidly towards the vent in respect with the one illustrated in Fig.4.1. It can be anticipated that suction effect is influencing the flame propagation for this vessel's explosion activity compared to self-acceleration mechanism. It should be noted that the vessel volume of Test vessel 2 is about 30 times smaller than Test vessel 1.This situation has been discussed in detail by McCann (McCann, Thomas and Edwards, 1985).

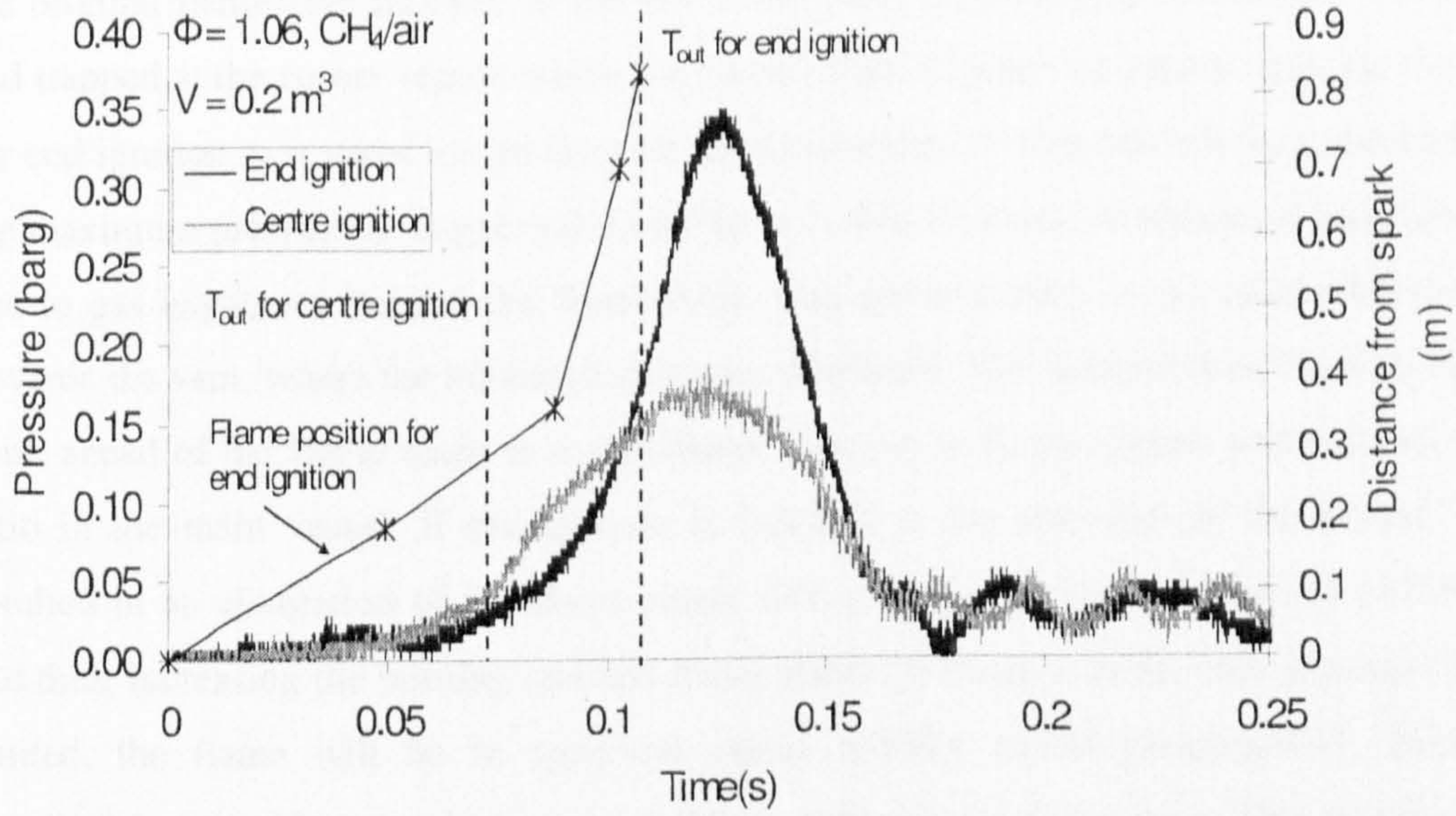

Figure 4.1 Typical pressure-time histories for centre and end ignition in Test vessel 1

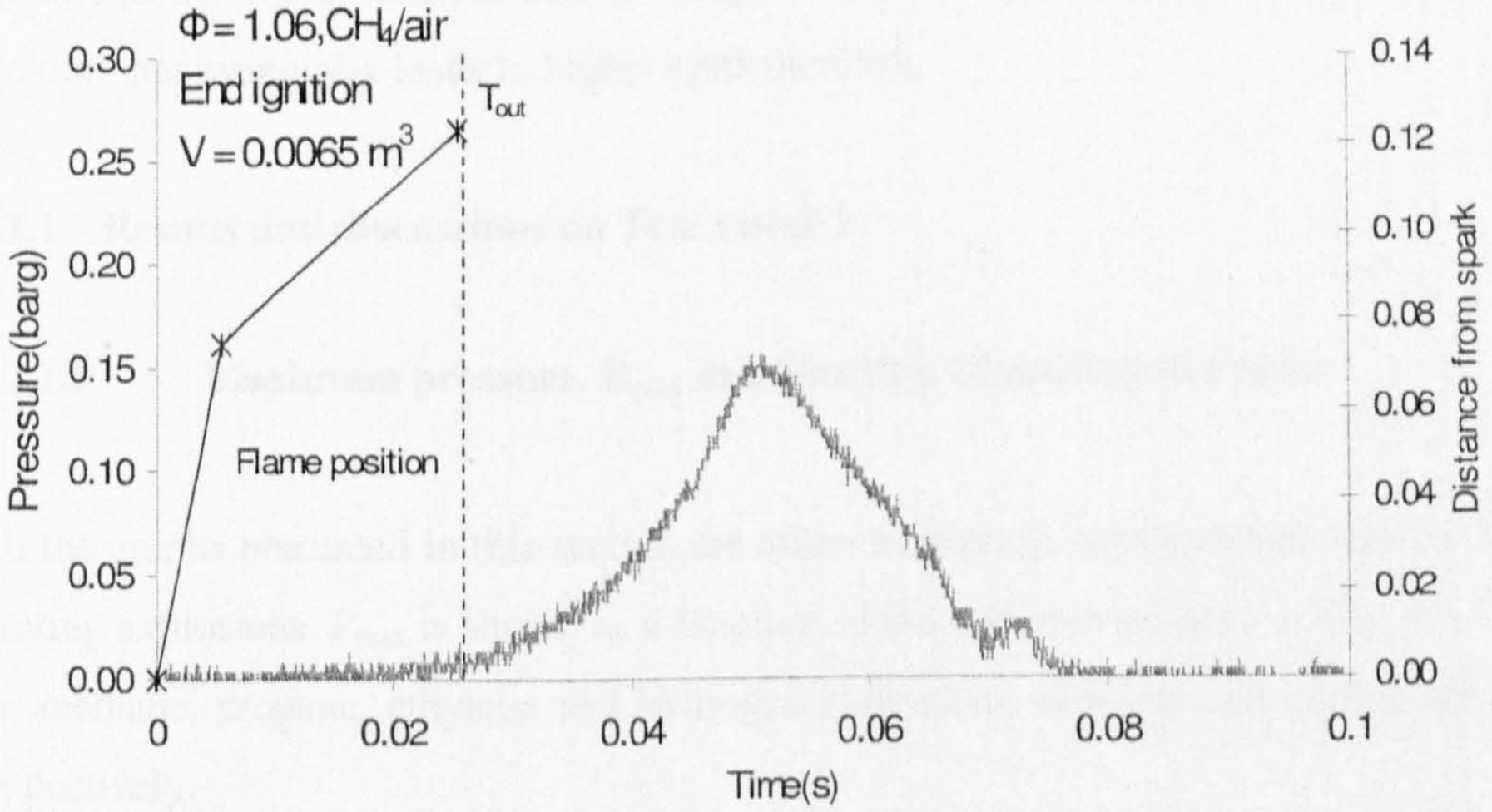

Figure 4.2 Typical pressure-time histories and flame position in Test vessel 2.

As can be seen in Fig. 4.1 and 4.2, the peak pressure occurred when the flame already exited from the vessel either when ignited at the end wall or central. It is considered that it is the variation of the mass burn rate and flame speed of the flame approaching the vent that has a strong influence on the vent flow and on the subsequent combustion behaviour. A major feature of the explosions is that there are substantial proportions of

the original flammable mixture in the test vessel after the flame has exited the vessel and trapped at the corner region inside the vessel. This is larger for central ignition than for end ignition as it takes longer time for the combustion to take place before reaching the maximum pressure as suggested from Fig. 4.1. The direction of unburned gas flow, due to gas expansion behind the flame front, was preferentially in the axial direction towards the vent, where the unburned gases are displaced. The induced flow through the vent, ahead of the flame leads to a significant increase in flame speeds and expansion ratio in the main vessel. If the ignition is initiated at the end wall of the vessel, it resulted in an elongation of the flame shape with a corresponding increase of its area and thus, increasing the burning rate and flame speed eventually. In the case of centrally ignited, the flame will be in spherical vessel initially before progressively being stretched on one side towards the vent and thus, reducing the flame area. This condition has been postulated by Ferrara et al (Ferrara, Benedetto, Salzano and Russo, 2006). In case of central ignition, there is an indication of higher quantity of residual unburned mixture in the vessel whereas almost complete combustion occurred in the case of end ignition that eventually leads to higher peak pressure.

4.2.1 Results and discussions on Test vessel 1

4.2.1.1 Maximum pressure, P_{max} as a function of equivalence ratio

All the graphs presented in this section are taken as average experimental data for open venting explosions. P_{max} is shown as a function of the equivalence ratio in Fig. 4.3 – 4.6 for methane, propane, ethylene and hydrogen explosions with end and central ignition respectively.

Figure 4.3 showed that P_{max} is higher at all equivalence ratios, Φ for end ignition corresponds to one for central ignition. The same trend showed that end ignition results higher P_{max} compared to central ignition for propane/air and ethylene/air explosion up to $\Phi = 1.13$ and 1.0 respectively. However, the univocal trend is not consistent where higher P_{max} seems to favour the central ignition for rich concentrations in propane/air and ethylene/air i.e. $\Phi > 1.3$. This inconsistent trend can be explained due to the mixture reactivity itself. Cooper at al (Cooper, Fairweather and Tite, 1986) reported that rich propane mixtures have much higher susceptibility than methane to develop surface

instabilities (flame cellularity) which would lead the flame to self-accelerate causing higher burning rates and hence rate of pressure rise and this could result in a more severe vented explosion as shown in Fig. 4.4.

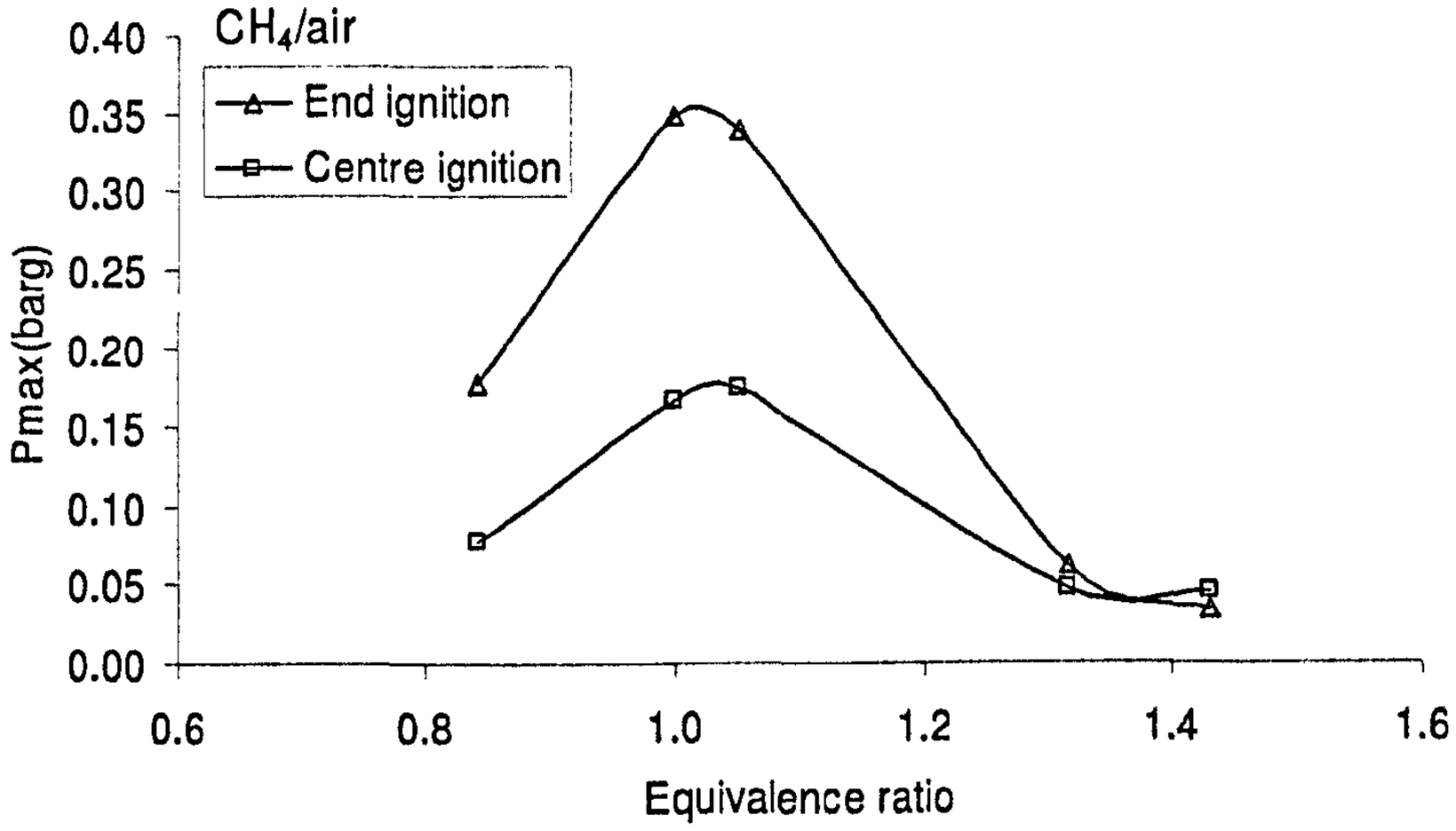

Figure 4.3 Methane/air at different equivalence ratio, Φ

Fundamentally, ethylene is more reactivity than propane and thus, it becomes more obvious on P_{max} for ethylene/air explosion for $\Phi = 1.4$ and 1.6 at centrally ignited (refer to Fig.4.5). The rate of pressure rise shows that at rich mixtures, the central ignition produced a more severe explosion and it is significant on propane/air where $dP/dt_{(max)}$ is 156.6 at $\Phi = 1.375$ than in ethylene/air with corresponding to end ignition on both cases as clearly pictured in Fig.4.6. The rate of pressure rise is a much more important yardstick of explosion severity as any explosion protection system (venting or suppression) has to cope with the maximum burning rate and maximum rate of pressure generation.

It is very interesting to investigate the more reactive gas mixtures than ethylene i.e. butane and pentene as this gas has been given little attention on its behaviour in vented gas explosion.

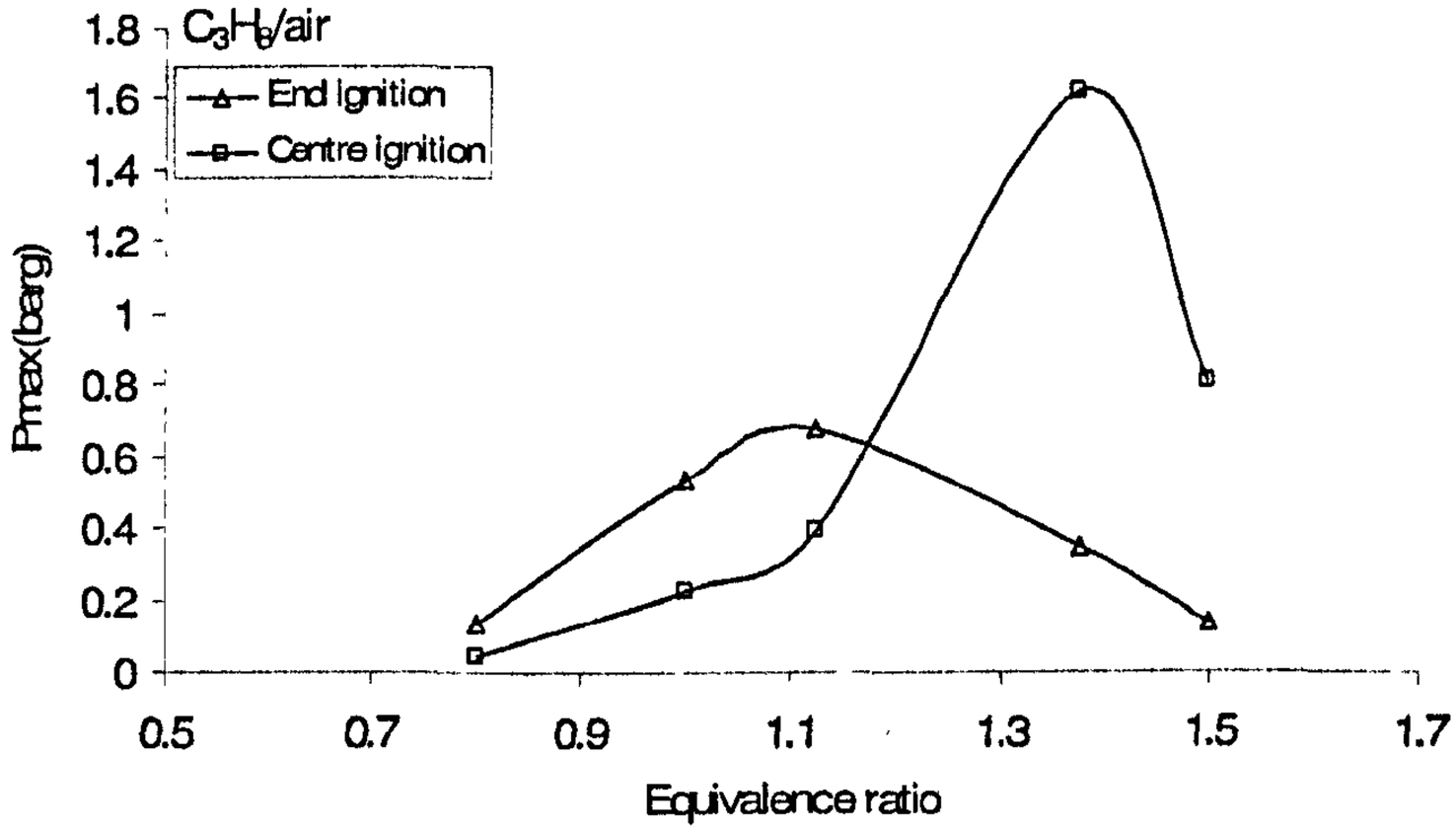

Figure 4.4 Propane/air at different equivalence ratio, Φ

In order to get insight about the reason of such behaviour, it should be based on the residual amount of unburned gases left inside the vessel that will be discussed in detail later and the ignition position effect. When mixtures are centrally ignited, the flame is stretched on both directions; substantially pushed out only small amount of burnt gases from the vessel. It can be postulated that combustion is still far form completion as there is larger amount of unburned gases left inside the vessel with respect to the almost complete combustion if mixtures ignited at the end wall ignition which leads to higher P_{max}.

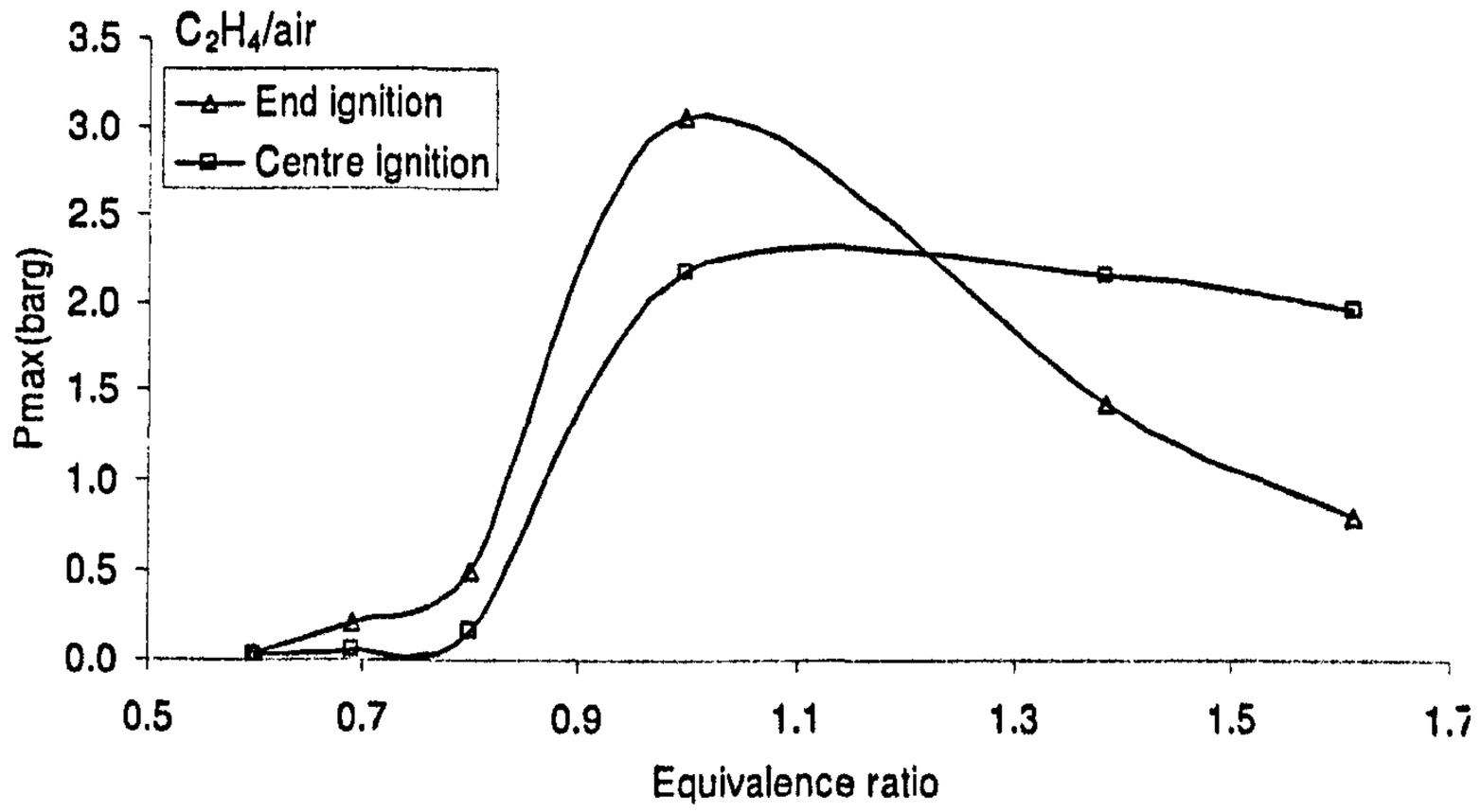

Figure 4.5 Ethylene/air at different equivalence ratio, Φ

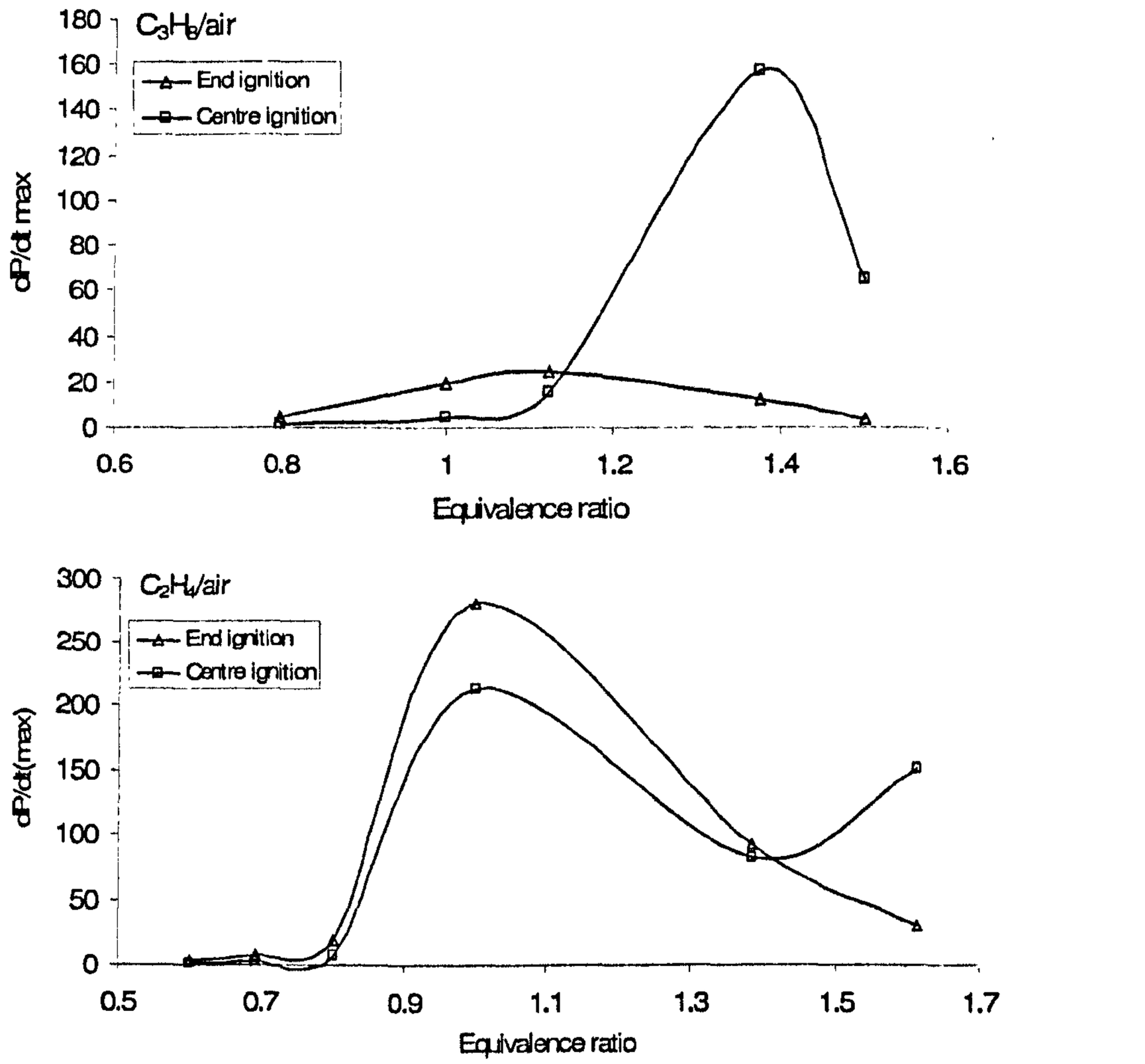

Figure 4.6 Maximum rate of pressure rise, dP/dt (max) at various equivalence ratio for propane/air (above) and ethylene/air (below).

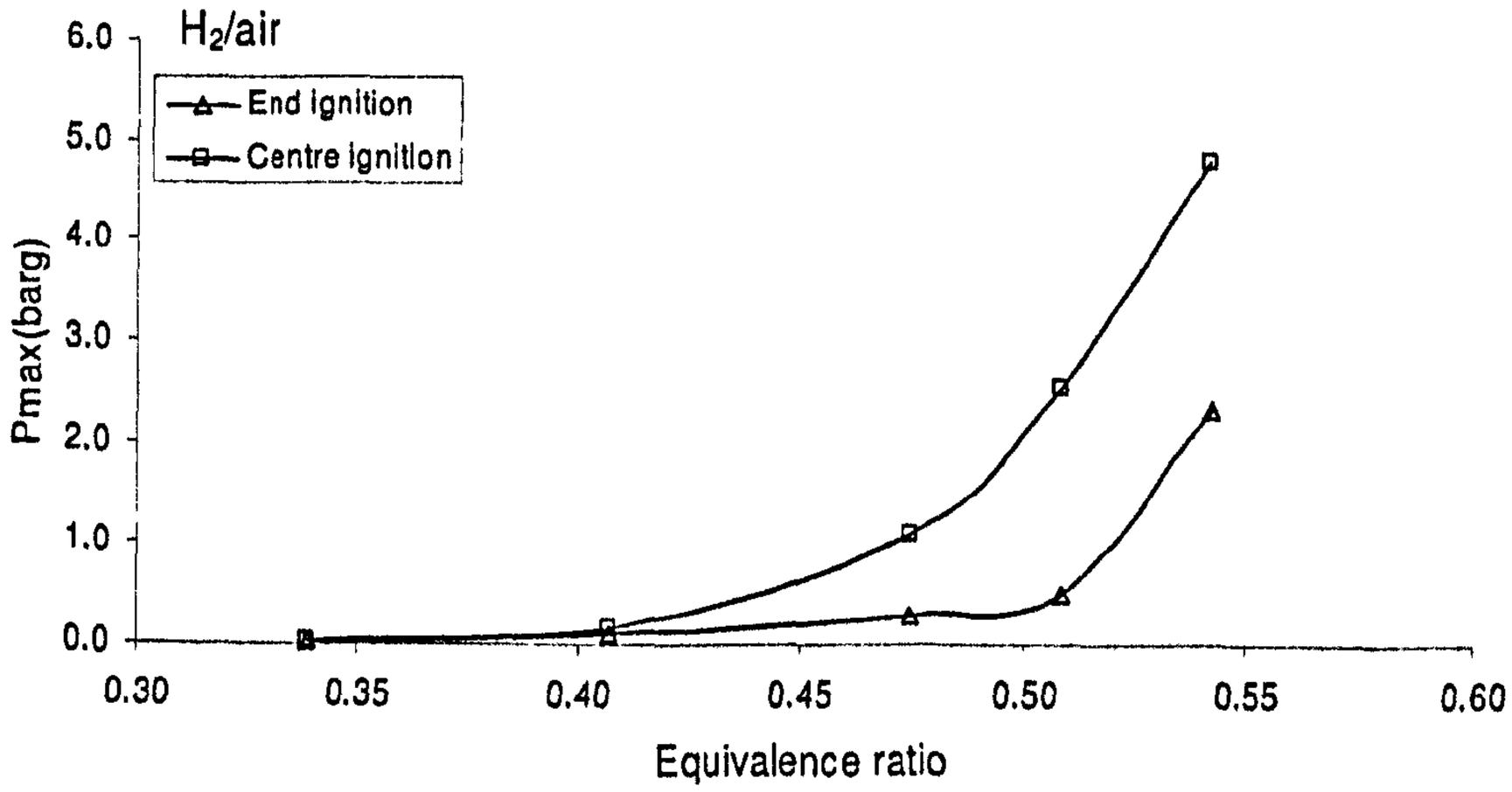

Figure 4.7 Hydrogen/air at different equivalence ratio, Φ

Meanwhile, Fig. 4.7 shows that central ignition produced more severe explosion at all equivalence ratios for hydrogen/air explosion. There is no significant in P_{max} on both ignition positions for Φ= 0.34 and 0.41 before it gave a rapid increase in P_{max} at centre ignition i.e. P_{max} = 2.7 barg at Φ = 0.54 compared to end ignition at higher equivalence ratio. Combustion times for central ignition are roughly half of the end ignition, therefore less time is available for gases in the vessel to flow out before combustion is completed, thereby reducing the effectiveness of venting (Kumar, Dewit and Greig, 1989). This observation implies that venting is effective at lower H_2 concentration (Φ < 0.41) but not in higher concentration in the case of smaller vent area i.e. high K.

It also can be concluded that end ignition gave higher P_{max} in lean to stoichiometric concentration in hydrocarbon/air mixtures and P_{max} in centrally ignited is highly dominant compared to P_{max} at end ignition in rich propane/air and ethylene/air mixtures (Φ = 1.1 to 1.6).

4.2.1.2 Flame speeds

Figure 4.8 – 4.11 reports the average flame speeds measured in second half of the main vessel (between T_2 and T_3 in Fig. 2.2) as a function of equivalent ratio and for the different ignition positions. It seems that end ignition gave higher flame speeds in the main vessel compared to centrally ignited explosion for methane/air mixtures regardless of its equivalence ratio. For central ignition, the flame speeds ranged from 2 to 10 m/s for lean and rich mixtures and up to15 m/s for the slightly rich mixtures i.e. Φ = 1.05. With end ignition, the maximum flame speed is 23 m/s, about 1.5 times higher than centrally ignition at the same concentration.

The faster flame speed with end ignition can be explained by the fact that the burnt gases are only allowed to expand in one direction which in turn will result in an elongated flame with increasing larger surface area (reaction front) and hence faster expansion than the centrally ignited flames. This acceleration of the flame towards the vent is also associated with self-acceleration of the hydrocarbon-air mixtures inside the vessel through the formation of cellular flames.

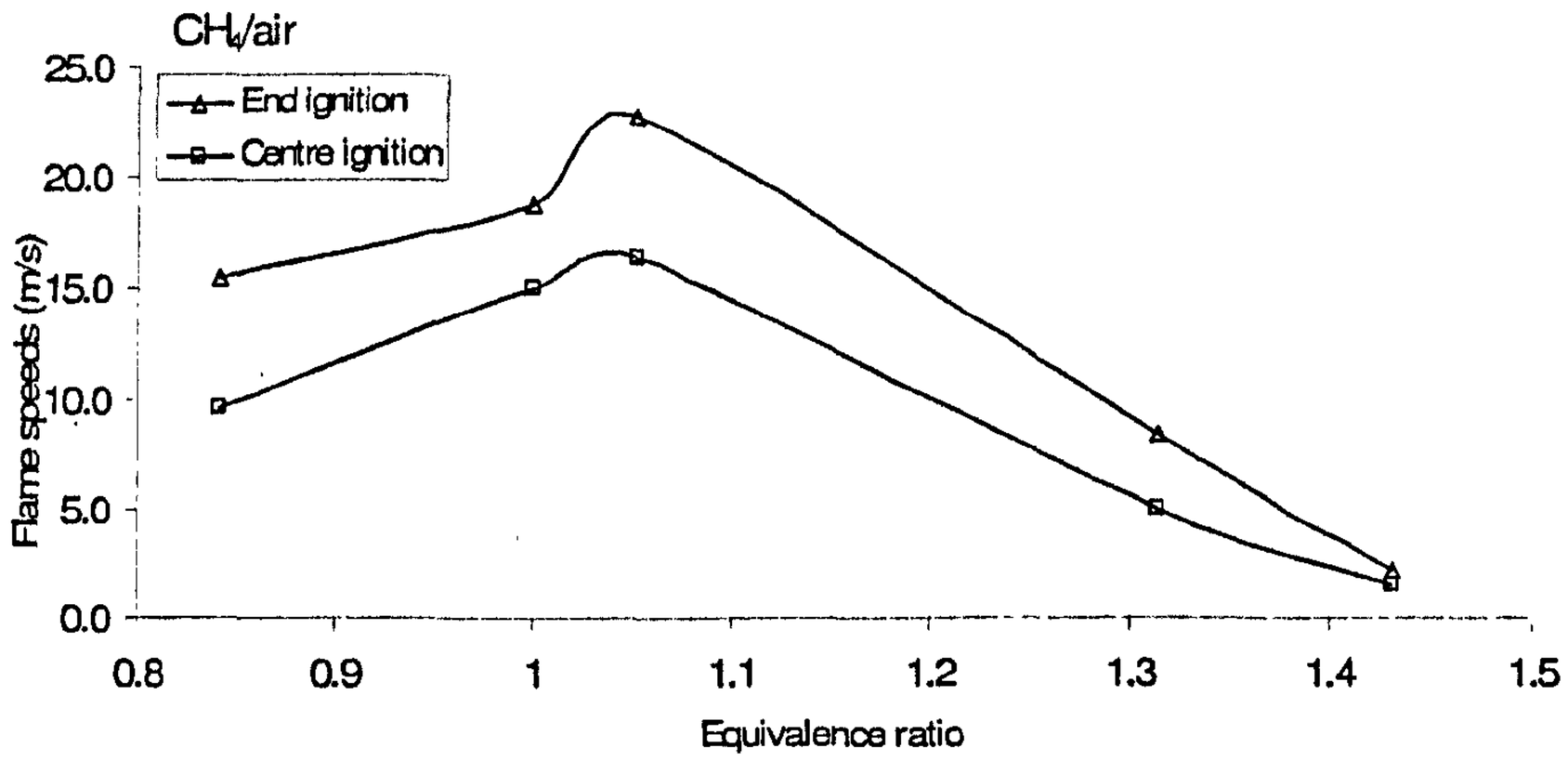

Figure 4.8 Flame speeds of methane/air at end and central ignition as a function of equivalence ratio.

The flame self acceleration occurs after a critical laminar flame propagation distance and the available distance with end ignition is twice that with central ignition and hence self acceleration is more likely. The net effect of the vent discharge and self acceleration are for the mass burning rate of the flame to increase due to faster flames, rather than due to the larger flame area of the spherical flame with central ignition. The measured flame speed is shown as a linear function of the flame distance from the spark towards the vent in Fig.4.9 for methane, propane and hydrogen/air mixtures which data were compared to NFPA 68 (NFPA68, 2002). Figure 4.9 shows the self acceleration of the flame, based on the K_{Gmax} v. closed vessel volume in NFPA 68 which shows that K_G increases with vessel volume. The data in NFPA 68 has been plotted as normalised K_G, based on K_G for the smallest volume (5 litres) being that for a laminar flame without cellularity and a flame speed of 3 m/s applied to these normalised results for methane, 3.5 m/s for propane and 20 m/s for hydrogen/air. This enables a prediction from the NFPA 68 data to be made of the self acceleration effect on flame speed and this is shown in Fig. 4.9. The first flame speed for the experimental data is based on the spark to first thermocouple time. The development of cellular flames in spherical explosions has been observed to occur at about 0.3m and the flame acceleration due to developing cellular flames continues until about 3m (Bradley, Cresswell and Puttock, 2001, McCann, Thomas and Edwards, 1985).

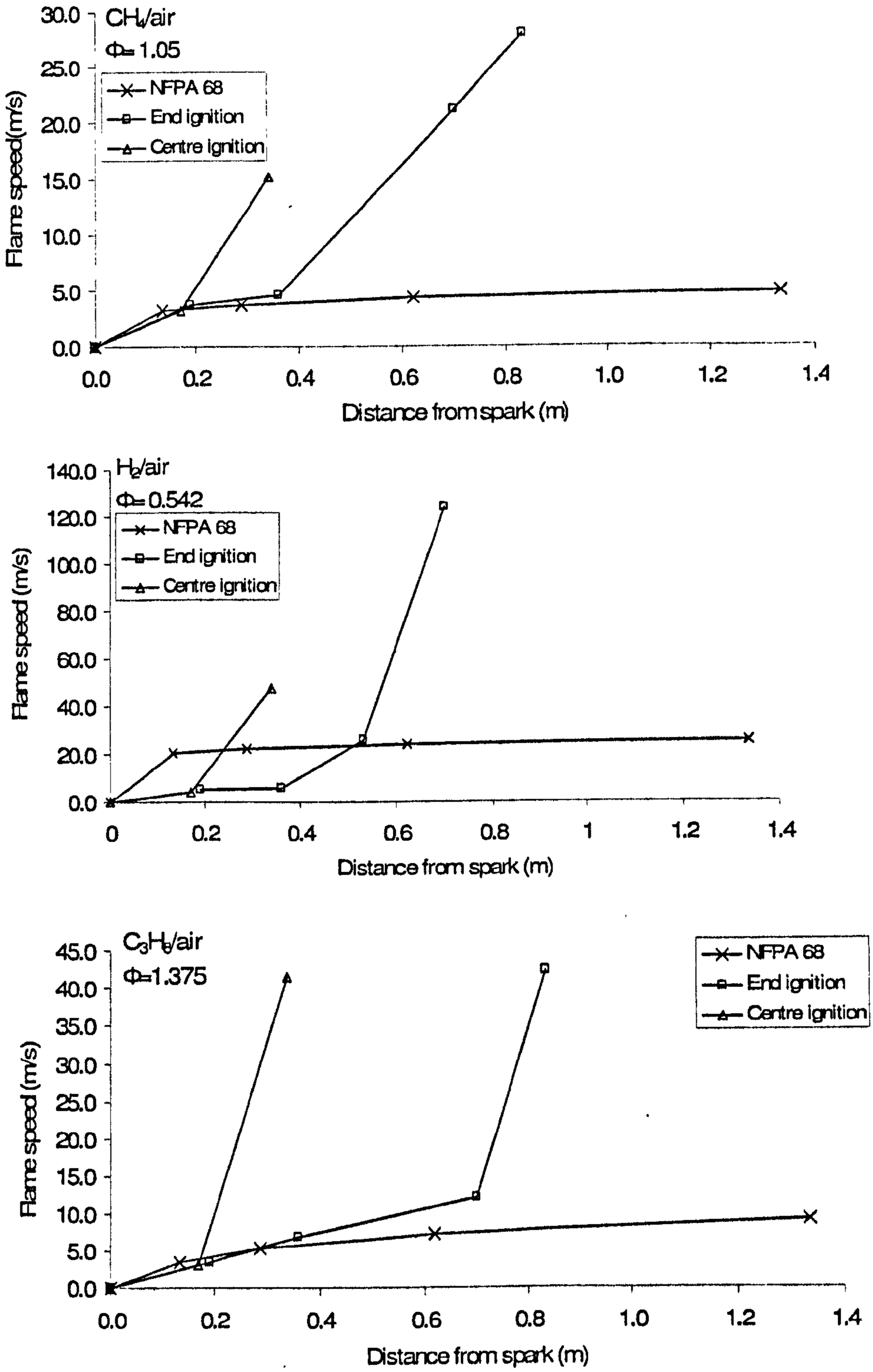

Figure 4.9 Flame speed as a function of flame distance from the spark for open venting.

Bradley et al (Bradley, Cresswell and Puttock, 2001) showed that the cell sizes changed in the flame propagation mechanism at an axial distance of about 3 m for a 550 m^3

rectangular vessel for hydrocarbon/air. The spherical laminar flame speed of methane-air explosions is about 3m/s for large radius flames, but below the onset of cellular flame development (Bradley, 1999, Gostintsev, Istratov and Shulenin, 1989, Groff, 1982).

From Fig.4.9, all graphs show a first flame speed measurement at 0.16m from the spark of around 3- 4 m/s and accelerating rapidly at 0.5 m from the spark to the flame speed of 28 m/s for methane/air, 42 m/s for propane/air and 124 m/s for hydrogen/air respectively. This is about 5 times higher than the spherical flame speed based on data excerpted from NFPA 68 for those gases. For central ignition, Fig. 4.9 shows that the flame accelerating is more significant after 0.17 m from the spark. It should be noted that suction effect is also played a significant role in stretching the flame towards the vent, resulting larger flame area and mass burning rate, thus high flame speed inside the vessel in respect to its own laminar burning velocity. The net effect is flame self-acceleration occurred at half diameter of the test vessel for hydrocarbon/air and hydrogen/air. It is also clear that for end ignition the distance to the vent is greater and hence the flame acceleration continuous over twice the distance as for the central ignition. Bradley et al (Bradley, Cresswell and Puttock, 2001) have shown that the effect of pressure is to increase flame cellularity or to reduce the distance for the first appearance of cellular flames.

However, the theory of end ignition gives higher flame speed is not supported by Fig. 4.10 and 4.13 for propane/air and ethylene/air mixtures respectively. At $\Phi = 0.8$ and 1.0, end ignition gave higher flame speeds of 11 and 20 m/s before the flame speeds of 27 m/s attained for central ignition compared to 24 m/s at end ignition at $\Phi = 1.12$. As been studied previously, propane exhibits spontaneous cell structure or flame cellularity in rich mixtures (Tseng, Ismail and Faeth, 1993, Wingerden and Zeeuwen, 1983a). In the case of central ignition where the flame travel is less compared to end ignition, very little unburnt gas mixture has been vented from the vessel; hence there is still substantial amount of unburnt gases trapped inside the vessel as illustrated in Fig. 4.11.

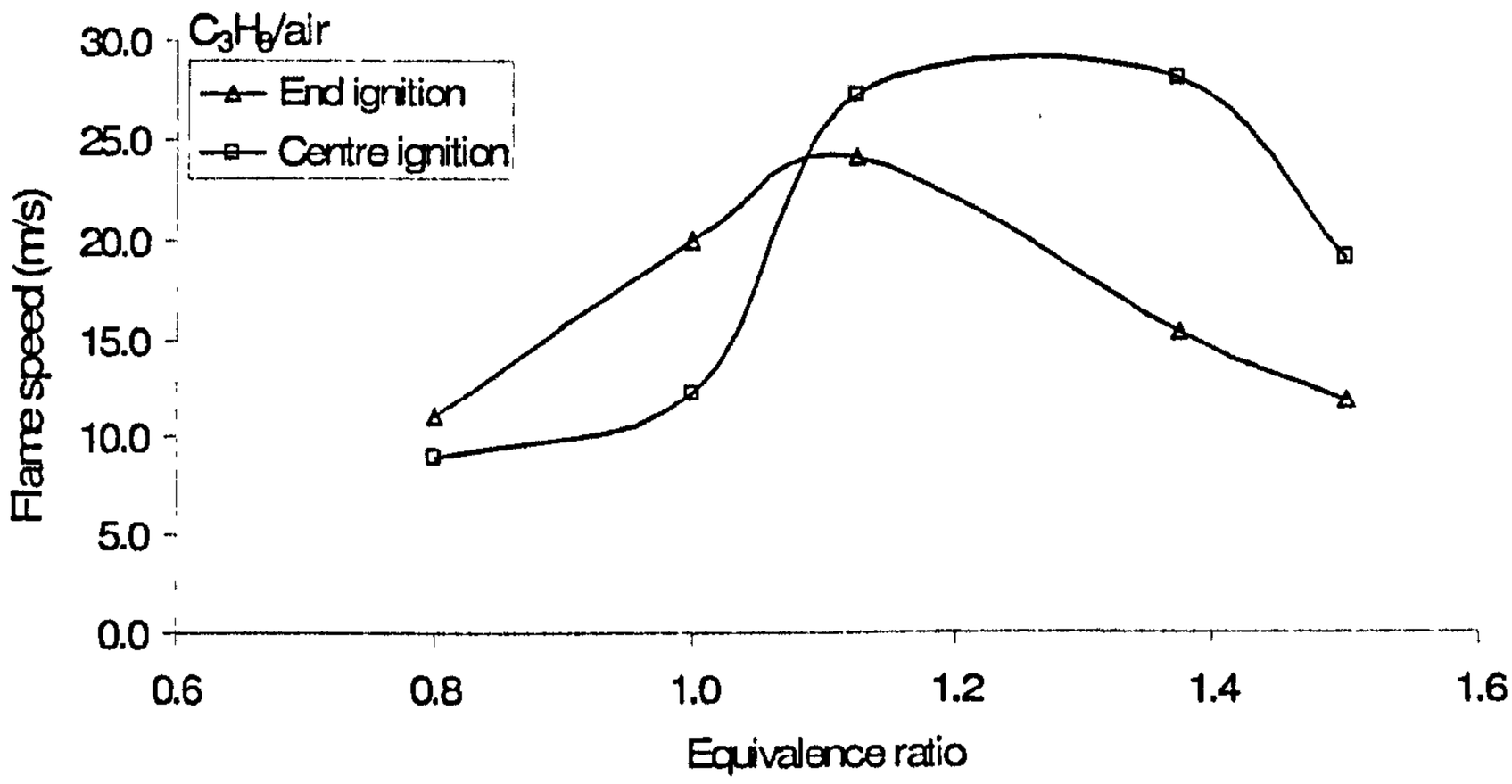

Figure 4.10 Flame speeds of propane/air at end and central ignition as a function of equivalence ratio.

Figure 4.11 demonstrated plots the time of flame arrival in the corner of the test vessel at the spark end, where a flame arrival thermocouple was located. It shown that the time flame leaving the vessel is about the same when flame reached the corner region in the case of end ignition, suggesting that there is little amount of flame trapped at the corner region of the vessel, and hence the increase in P_{max} will be associated with the flame self-acceleration and flame longer travel distance which causes the elongated flame area and thus, higher burning rate and flame speed. However, in the case of central ignition, it can be said that there is evident showing that considerable amount of unburnt gases left inside the vessel and propensity of the cell-cellularity in the case of rich propane concentration cause the rapid rise in the final pressure inside the vessel. The movement of the flame propagates towards the vent and at the same time left some amount of unburnt gases at corner region is best illustrated in Fig. 4.12. It can be said that the occurrence of external explosion resulting from the expelled combustible gases ignited by the emerging flame affects the internal pressure as reported by Harrison (Harrison and Eyre, 1987) is not valid in this case. The rapid rise of internal pressure is due to the rapid combustion of the substantial unburnt gases trapped inside the vessel.

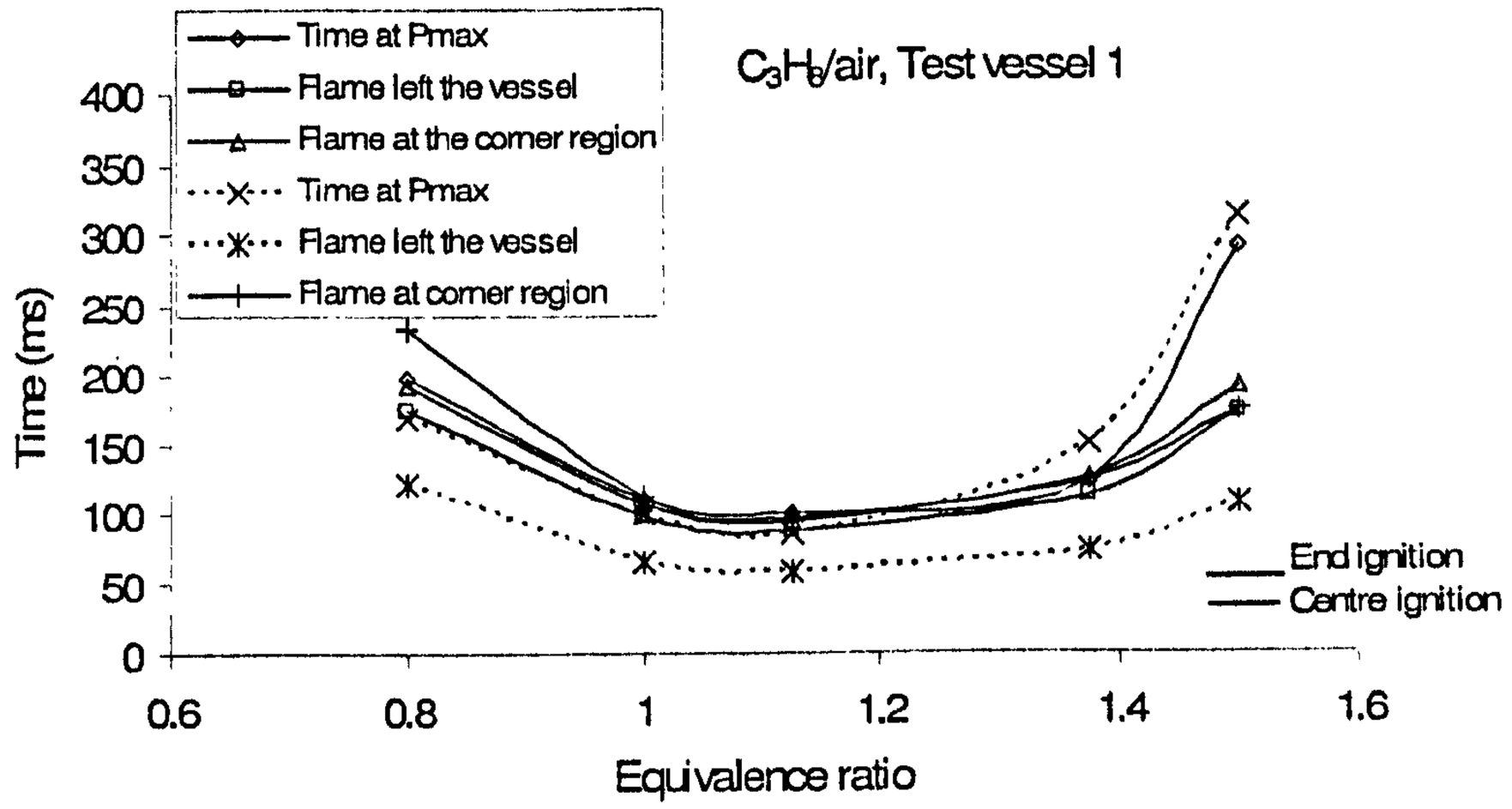

Figure 4.11 Time of flame arrival at maximum pressure, when leaving the vessel and at the corner region as a function of propane/air equivalence ratio.

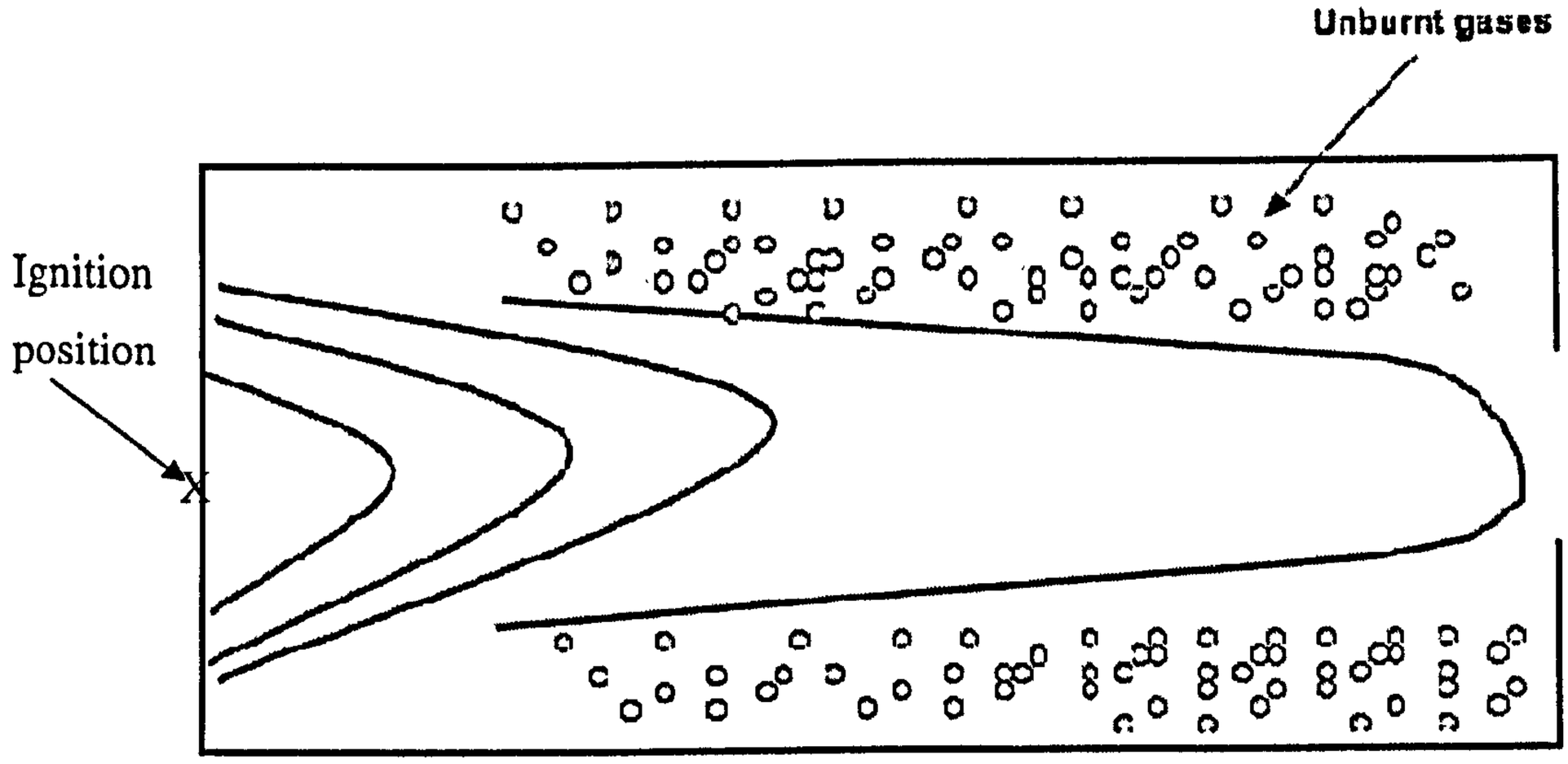

Figure 4.12 Diagram on the flame movement at end ignition and the unburnt gases left inside the vessel

The pressure-time profile of raw test of this concentration showed a significant pressure oscillation towards the end of the combustion process as been observed by previous investigator (Chow, Cleaver, Fairweather and Walker, 2000) although these do not give

rise to a distinct pressure peak. An acoustic wave generated during this period and propagating of flame front by induced turbulent due to a sudden venting enhances the unburnt gases left inside the vessel, resulting higher burning rate and thus, higher flame speeds. Markstein has shown that gas mixtures exhibiting spontaneous cell structures are very sensitive to pressure wave and therefore easily exhibit acoustically driven flame instability (Wingerden and Zeeuwen, 1983a).

For ethylene/air mixture, central ignition gave slightly higher flame speeds compared to end ignition for all equivalence ratio and reached maximum flame speed of 36 m/s at Φ = 1.38 as shown in Fig.4.13. Since ethylene/air is a faster burning velocity mixtures compared to propane/air, there would be strong and rapid turbulence induced by the flame flow towards the vent. Considering the valid assumption of the substantial amount of unburnt gases left inside the vessel in the case of central ignition, flame instabilities and acoustic wave pressure interaction incorporated with the effect of enhanced combustion will then result to higher burning rate and hence, the increase in flame speeds. In this case, flame propagation is suggested to be influenced by the onset of turbulent flow, with observed burning velocities of 3.18 to 4.48 m/s being greater than the laminar value of 0.68 m/s (Chow, Cleaver, Fairweather and Walker, 2000).

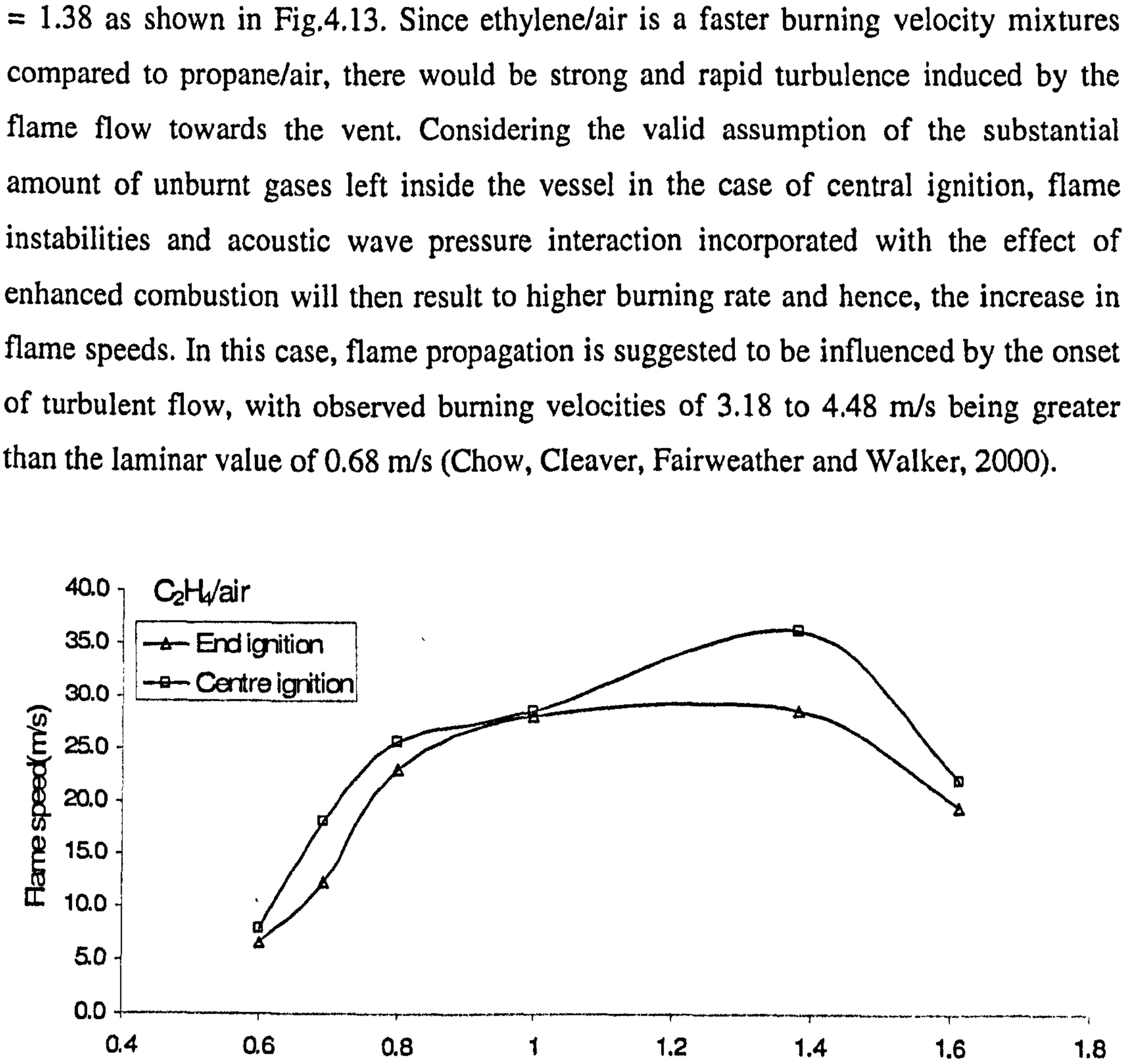

Figure 4.13 Flame speeds of ethylene/air at end and central ignition as a function of equivalence ratio

The flame speeds profile for hydrogen/air (Fig. 4.14) seems contradicted with the pressure results inside the vessel (refer to Fig.4.7). This unstable trend probably can be explained in terms of combustion time. For a given set of initial condition and vessel geometry, combustion times for central ignition are roughly half of end ignition. This means that less time is available for venting but not for end ignition. The flame travel time is longer and the burn rate enhancement is increased prior to venting which in turn increases the flame speeds inside the vessel as well as the self-acceleration. Meanwhile, for shorter time induced for venting in the case of central ignition encouraged more gas mixture combustion after the flame left the vessel since there is more restricted flow of flame to be expelled from the vessel. However, the gap between the time when flame leaving the vessel and reaches the corner region of the vessel is small as shown in Fig.4.15, not particularly similar trend in the case of propane/air in Fig.4.11. It can be postulated that acoustic oscillation (rapid venting can trigger the acoustic wave), flame self acceleration and amount of unburnt gases left inside the vessel are the significant factors of increase in magnitude of pressure peak for centrally ignition compared to end ignition even though the flame speeds showed opposite results. This brings out the important fact that high-burning velocity mixture such as hydrogen/air mixture behaves differently from those with low burning velocities.

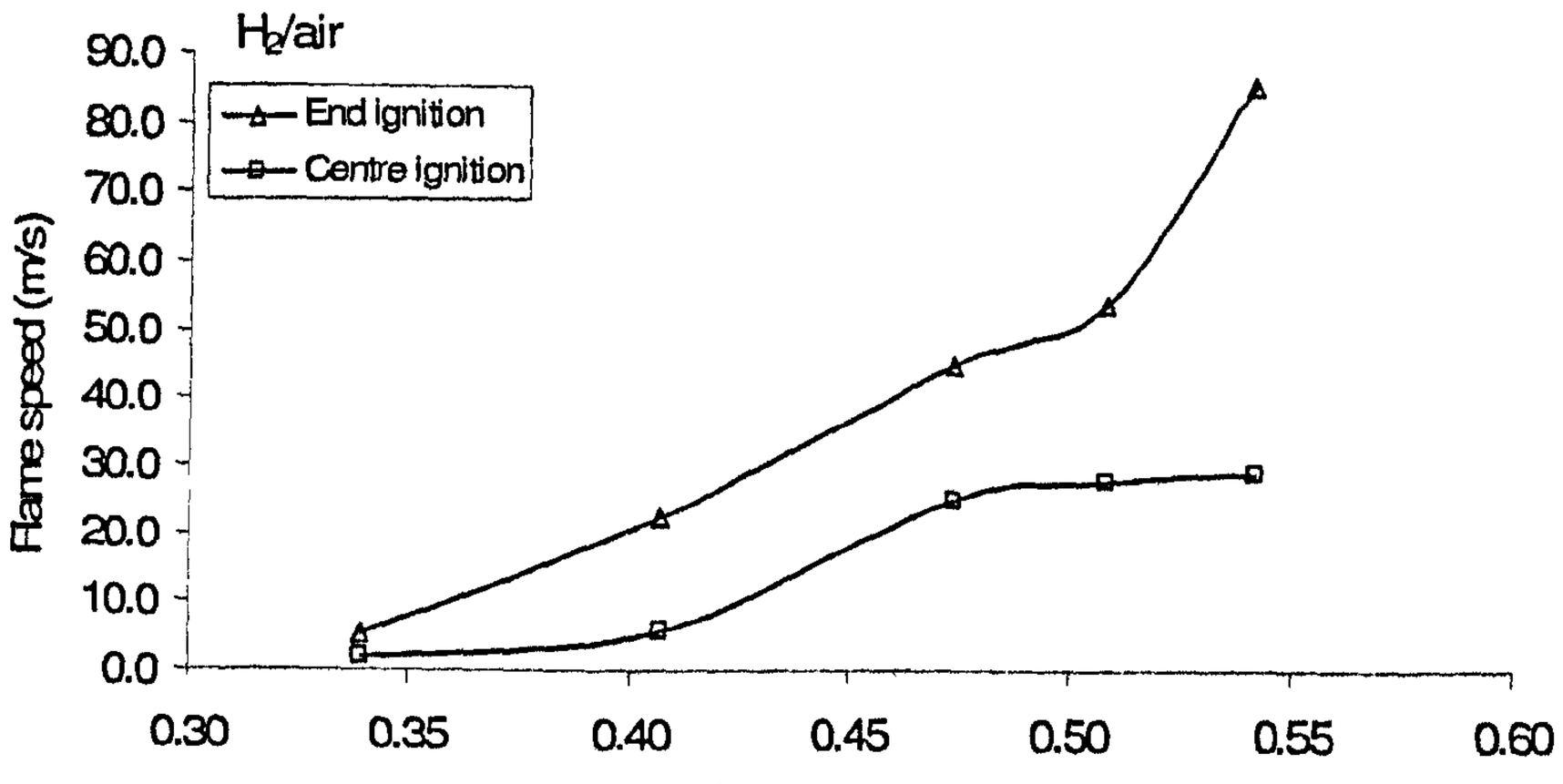

Figure 4.14 Flame speeds of hydrogen/air at end and central ignition as a function of equivalence ratio

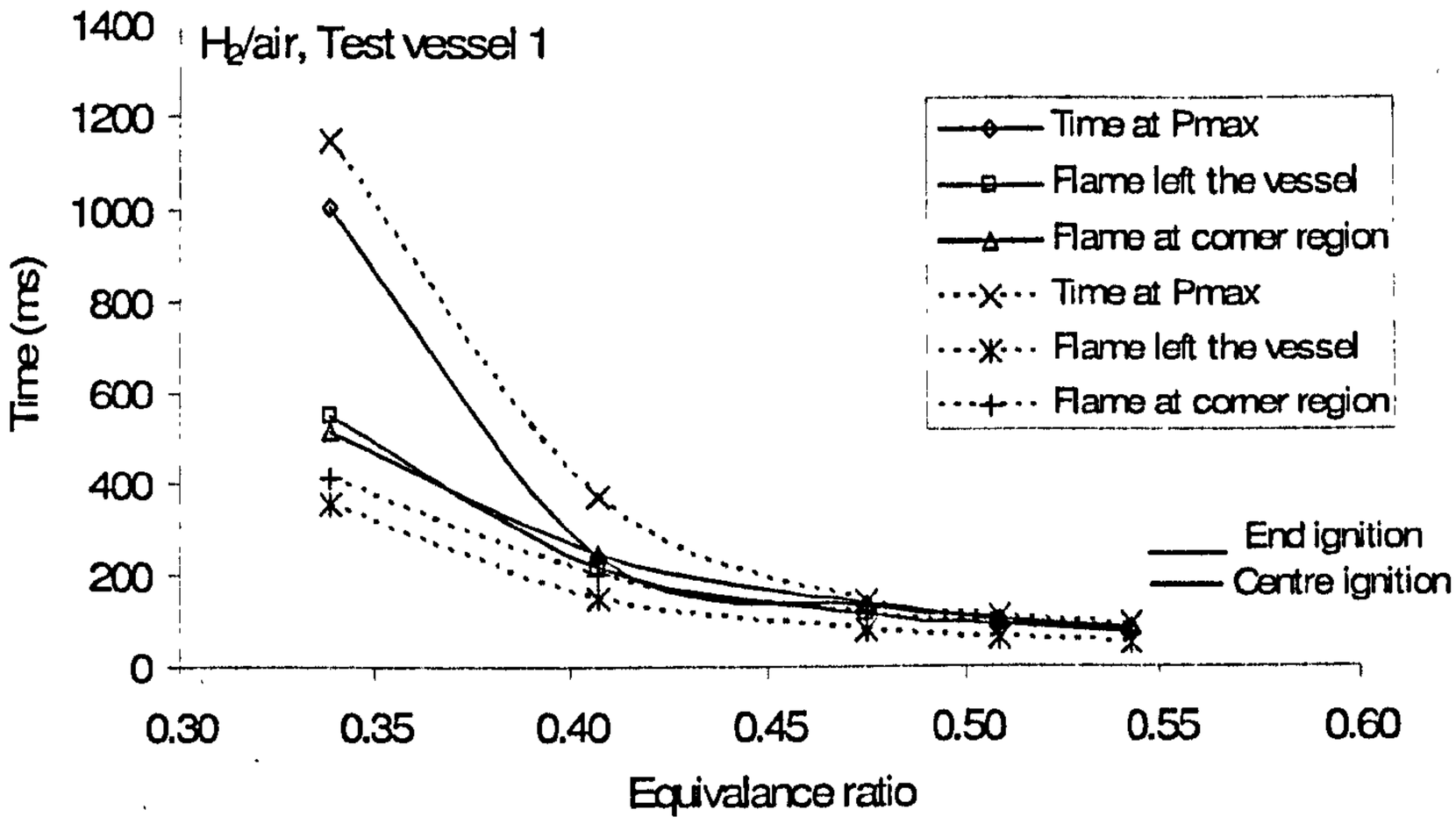

Figure 4.15 Time of flame arrival at maximum pressure, when leaving the vessel and at the corner region as a function of equivalence ratio.

4.2.2 Results and discussion on Test vessel 2

4.2.2.1 Maximum pressure, P_{max}

Test vessel 2 is a cylindrical vessel with internal diameter of 0.162 m and length of 0.315 m, closed at end and fitted at the other end with an orifice plate at different diameter simulating the vent (either covered or uncovered) before discharging to the dump vessel as shown in Fig.2.3. In the experiments for initially covered vent, four different vent materials were used as listed in Table 2.3 and placed after the gate valve. Only end wall ignition was used in this series of tests. The static bursting pressure was 98, 178, 209 and 424 mbarg for the vent cover used.

Figure 4.16 showed the pressure time history for different gas/air at stoichiometric concentration. It can be clearly seen that it takes shorter time for combustion to complete in hydrogen/air explosion ($t \approx 0.03s$) compared to methane/air explosion ($t \approx 0.07$ s). It can be expected that when the combustion time becomes shorter, it would be less time available for unburned gases in the vessel to flow out and hence reduces the effectiveness of venting. As might be anticipated, both the timing and magnitude of all maximum pressure peaks is explicable in terms of burning velocity of the mixtures

within the vessel; as the burning velocity increases, the magnitude of the maximum pressure peak increases, whilst the time of occurrence after ignition decreases. It also appeared that maximum peak pressure occurred after the flame exited the vessel which suggested that there is the variation of the mass burn rate and flame speed of the flame approaching the vent which has a strong influence on the vent flow and on the subsequent combustion behaviour.

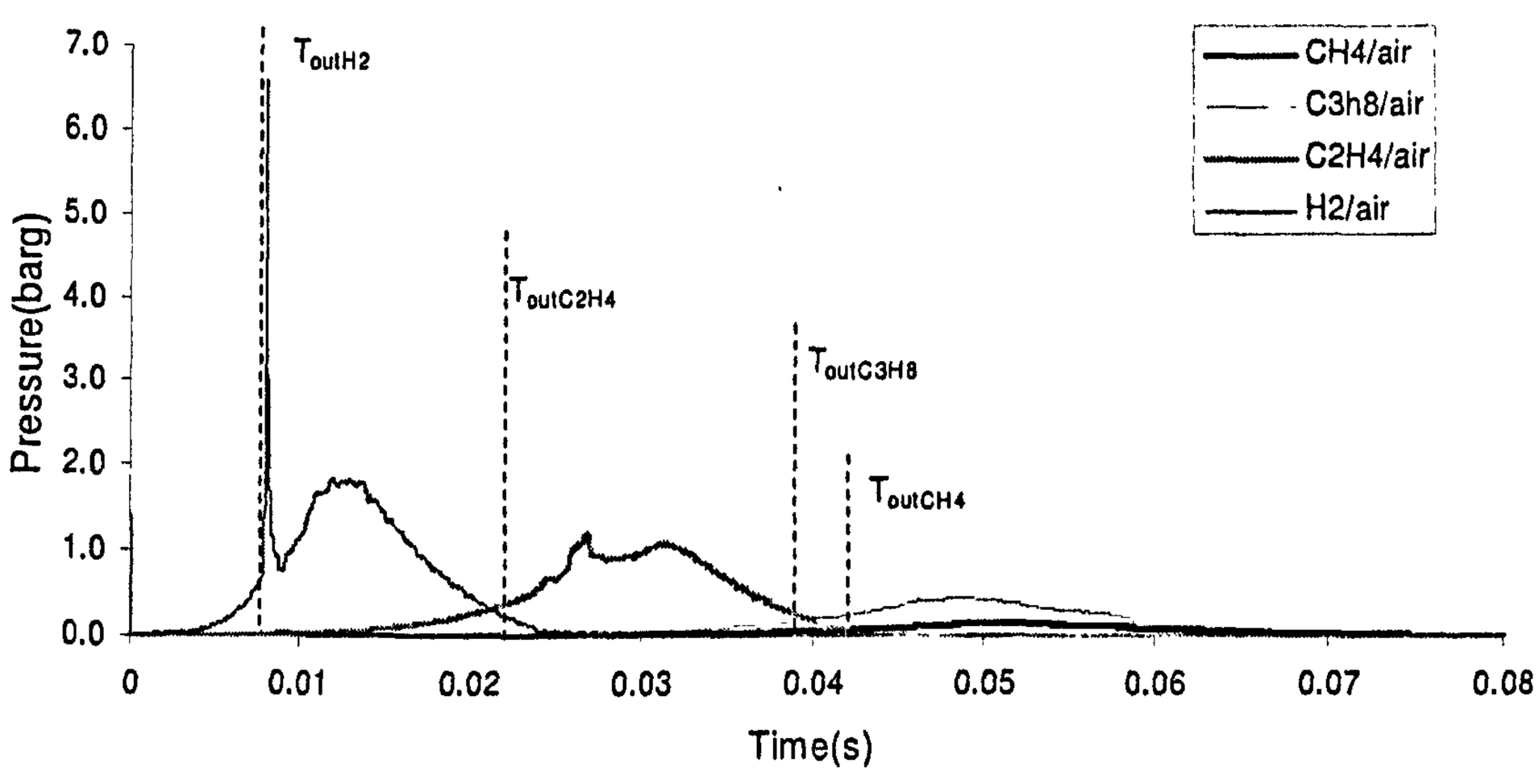

Figure 4.16 Pressure-time history for different fuels at $\Phi = 1.0$

It is very interesting to note that a sudden detonation spike appears in the pressure trace of H_2/air just after the flame left the vessel, posing a completely different trend with respect to other hydrocarbon/air mixtures investigated. Figure 4.17 shows that the spiky pressure occurs well after the flame has exited from the test vessel. The deflagration-to-detonation was not expected to 'appear' in this configuration. As mentioned above, the present study concerns vessel with small length to diameter ratios i.e. L/D= 2. Taking into account that the explosion initiated by a weak source (a standard automotive spark plug with a 16J), there is only a very low probability that a deflagration to detonation will occur in a manner similar to that observed in elongated tubes. It can be thought that the external explosion might cause this phenomena to happen. However, if this occurred then all the pressures in vessel test and the dump vessel would increase and eventually, Fig. 4.17 shows that this does not occur as there is no significant pressure difference between pressure inside the vessel and pressure inside the dump vessel.

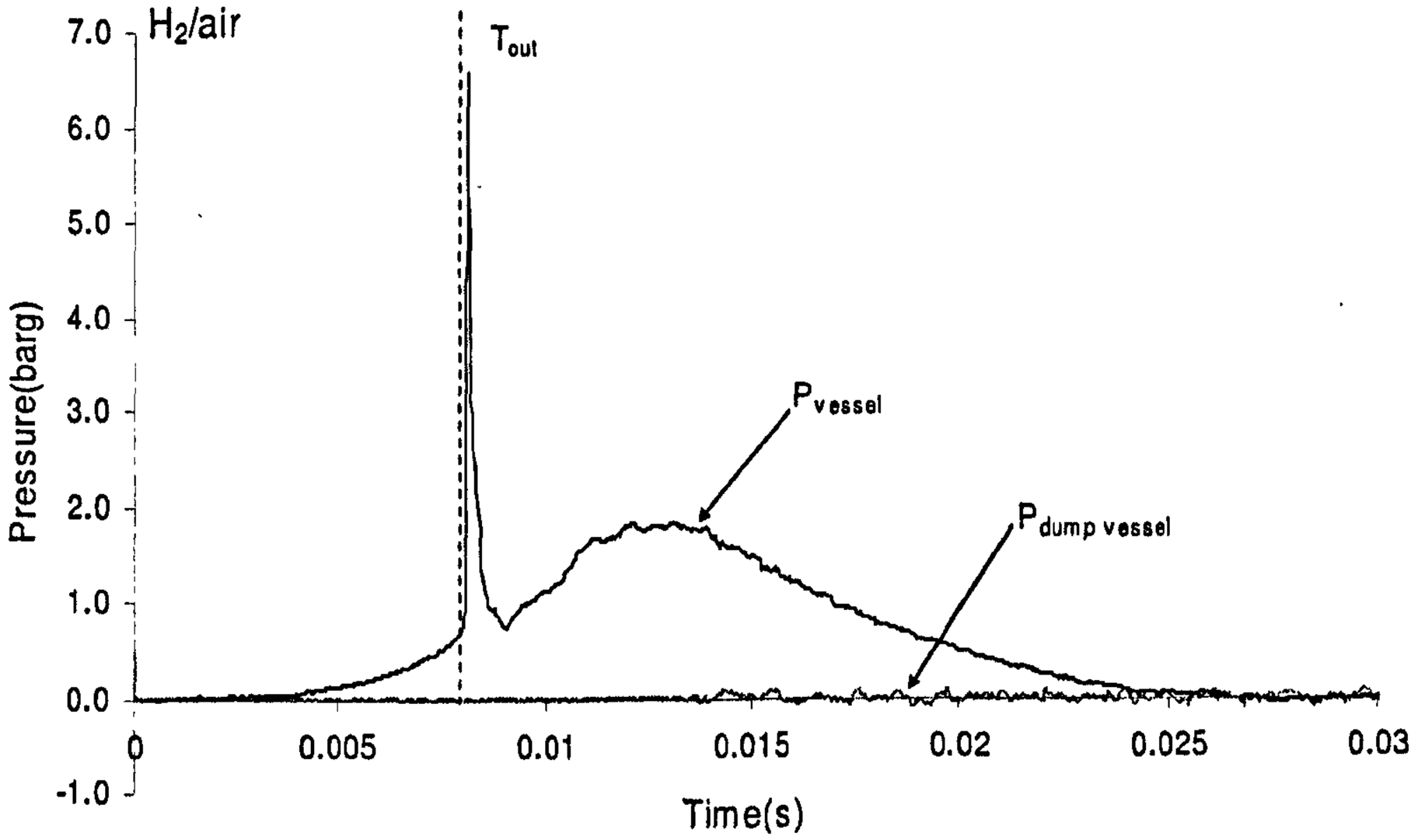

Figure 4.17 Pressure time history for maximum pressure inside the vessel (P_1) and pressure inside the dump vessel (P_6) at stoichiometric hydrogen/air

A major feature of the explosions is that there are substantial proportions of the original flammable mixture in the test vessel after the flame left the test vessel and eventually, these unburned gases trapped in the corner regions were auto-ignited, as will be shown later. This is larger for central ignition than for end ignition.

Figure 4.18 compares the maximum pressure, P_{max} of all fuel/air mixtures used in the tests as a function of equivalence ratio. It showed that the highest P_{max} was recorded and observed at $\Phi = 1.0$ for methane/air and propane/air and $\Phi = 1.18$ for ethylene/air and hydrogen/air. It can be said that the result has a good agreement to other investigations reported that at stoichiometric and slightly off-stoichiometric gas/air mixtures, maximum pressure inside the vessel exhibits higher pressure compared to the near and very rich concentration as at these concentrations, laminar burning velocity is at the highest values. It is interesting to note the highest P_{max} for hydrogen/air explosion recorded at 35 % concentration by volume ($\Phi = 1.18$), not at 40 % concentration (Φ= 1.36) that been reported to have highest maximum overpressure and laminar burning velocity (Andrews and Bradley, 1972, Andrews and Bradley, 1973, Kumar, Dewit and Greig, 1989). It should be noted that all maximum pressure obtained from hydrogen/air tests were recorded based on the peak pressures not the sudden pressure spike.

There is large increase in P_{max} for reactive mixtures i.e. ethylene/air and hydrogen/air compared to methane/air and propane/air and reached maximum overpressure at 1.25 and 2.28 barg for ethylene/air and hydrogen/air respectively. Higher P_{max} reflects to the higher flame speeds which in turns higher mass burning rate.

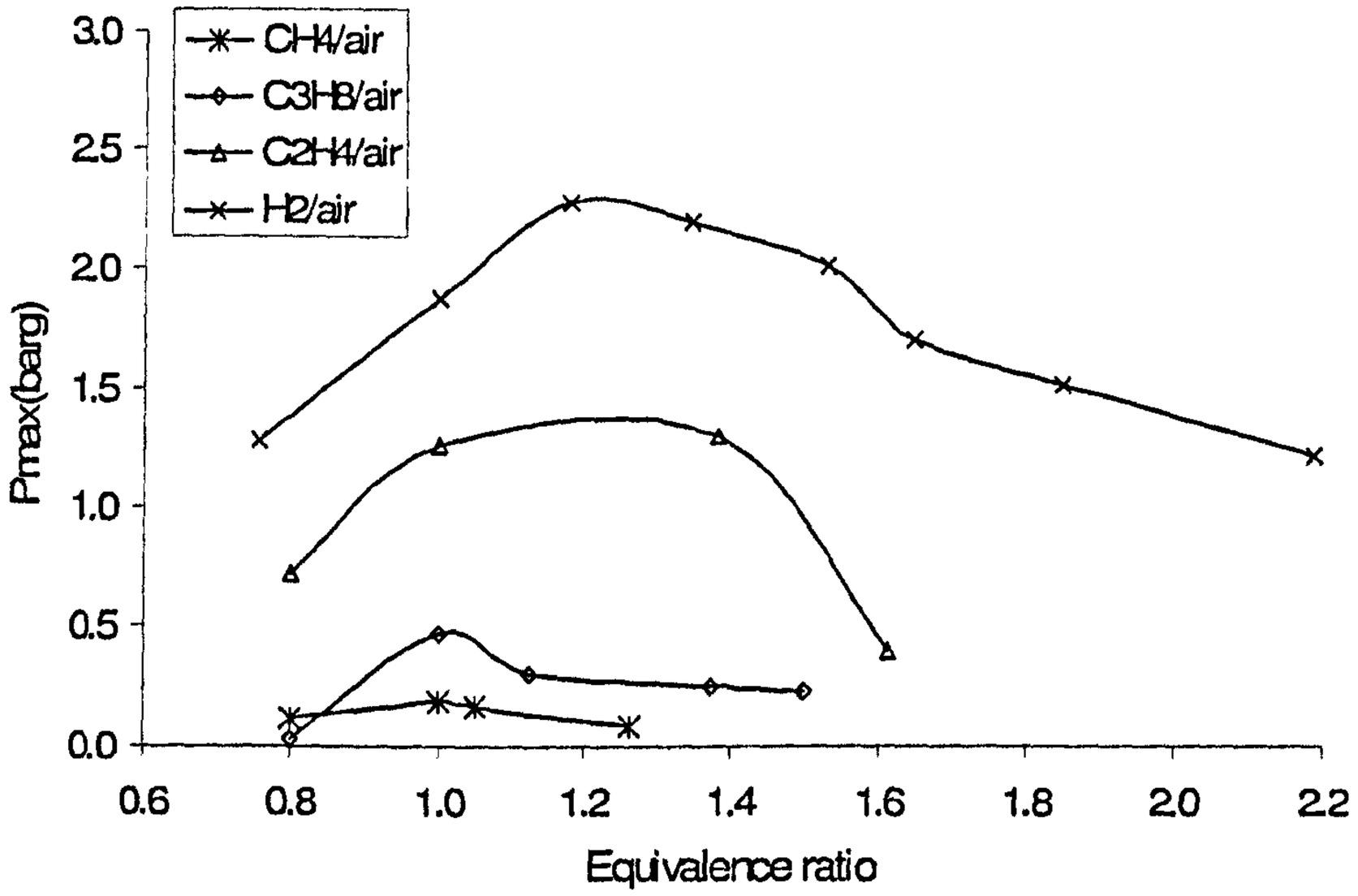

Figure 4.18 Maximum pressure P_{max} for different fuel/air mixtures as a function of equivalence ratio.

4.2.2.2 Flame speeds

The average flame speed measured between two thermocouples for different gases is shown, as a function of equivalence ratio in Fig. 4.19. The flame speed increased very rapidly in hydrogen/air up to $\Phi = 1.18$ before decreasing gradually at the very rich concentration. It showed that hydrogen/air exhibited higher flame speed of 53.8 m/s at $\Phi = 1.18$. This is about 28 times higher than 2.1 m/s at $\Phi = 0.34$. For ethylene/air, the peak flame speed of 13.6 m/s occurred at stoichiometric concentration ($\Phi = 1.0$); the same concentration at which methane/air and propane/air experienced the peak flame speed i.e. 8.2 m/s and 10.9 m/s respectively. The maximum flame speeds of these gases

were approximately 2 to 3 times higher than the corresponding laminar flame speed for the particular mixtures. These flame speeds which reflect the high overpressure inside the vessel as shown in Fig. 4.18 can be associated to these three factors; turbulence inside the vessel, acoustic resonance inside the vessel and combustion of gas outside the vessel (Harrison and Eyre, 1987). As stated earlier, external explosion is not the cause of the high pressure inside the vessel as shown in Fig. 4.17. The possible explanation for this condition is the induced turbulent and acoustic instabilities.

The faster flame speeds reflects higher velocity of unburned gases ahead of the flame that in turns causes higher turbulence field at the vent area as shown in Table 4.2. The vent can be simulated as a blockage or obstacle which can impede the flame propagation from laminar mode to turbulent flames. When the flame encountered this turbulence, it became turbulent itself and accelerated to a maximum speed of 58.3 m/s in a case of hydrogen/air at $\Phi = 1.18$. In particular, flame propagation through the vessel up until flame front venting is found to be substantially laminar with significant overpressure only being generated in the later stages of explosions due to rapid turbulent combustion in the shear layers and re-circulation zones induced by the obstacles (Fairweather, Hargrave, Ibrahim and Walker, 1999) but self-acceleration is not expected in this test vessel due to the length of the vessel is not on the onset of self-acceleration. This can be illustrated with simple calculation to measure how big is the flame area, A_f accordingly to vessel surface area, A_s. For Test vessel 2, A_s is 0.2 m^2 and A_v is 0.0021 m^2. Equation for Method 2 given in Chapter 3 is used for this calculation purpose. Rearranging the equation with density and compressibility factor to be taken into account gives;

$$A_s = \left[\frac{P_{red}.A_v^2}{C_1^2}\right]^{1/2} \tag{4.1}$$

$$\text{which } C_1 = \frac{S_u.\rho_u^{0.5}(E-1)}{C_d.\varepsilon.2^{0.5}} \tag{4.2}$$

From the calculation, it is found that the flame area is about 40 – 45 % of the vessel surface area for hydrocarbon/air when the pressure marked its P_{max} but only 10 % of A_s in the case of hydrogen/air. This is the valid explanation for the occurrence of detonation spike observed in the test vessel that will be discussed later.

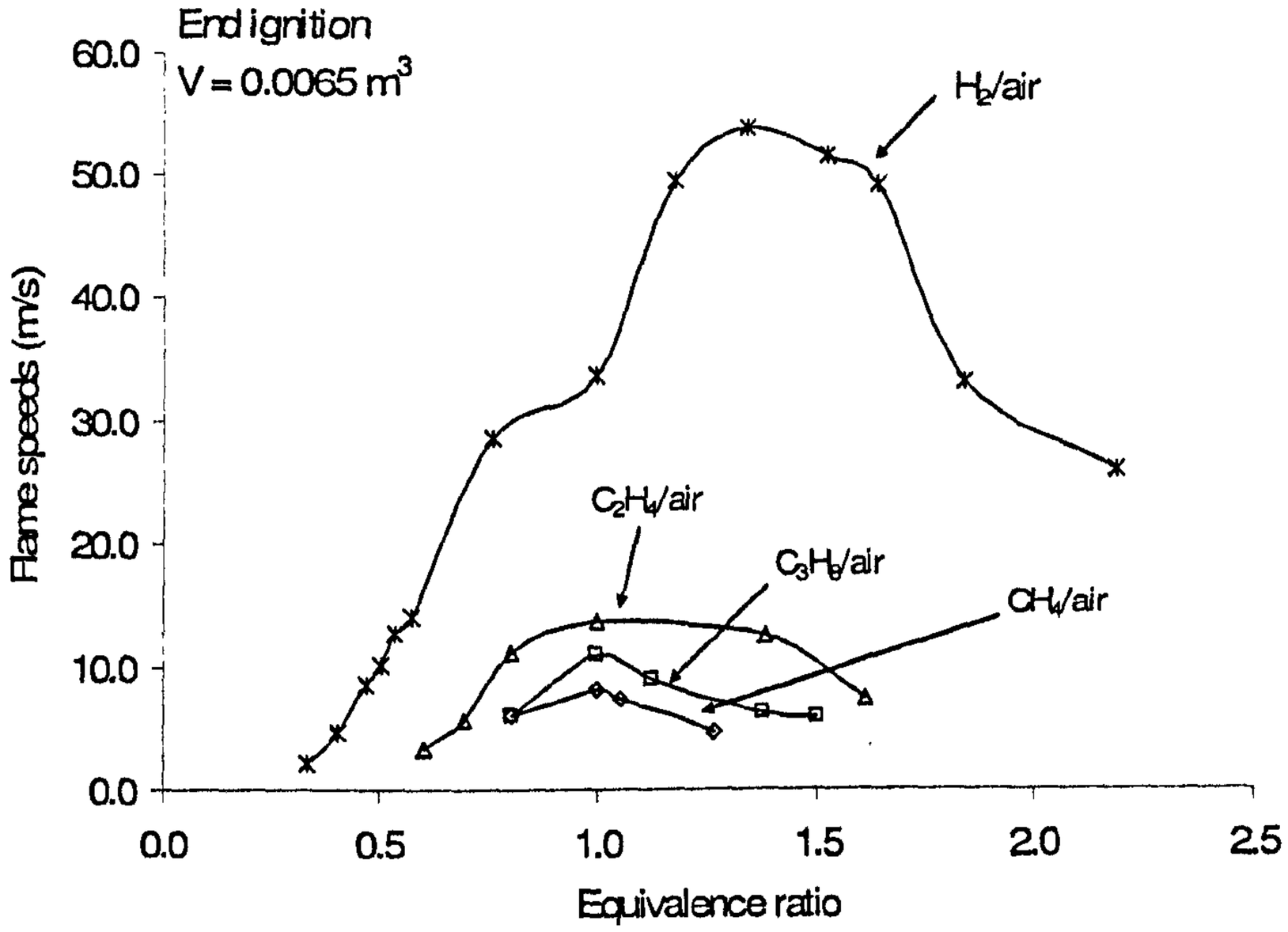

Figure 4.19 Flame speeds for the studied gas/air as a function of equivalence ratio.

The increase in burning velocity ahead of the flame due to turbulence might be attributed to the greater surface area of the outer boundary of the flame. As turbulence develops, the small scale turbulence begins to influence the mechanisms of flame propagation and further enhances the burning rate (Abdel Gayed and Bradley, 1981). Based upon the previous investigation on vented explosion (Cooper, Fairweather and Tite, 1986), the flame initially developed hemispherically from the point of ignition at the end wall. In the presence of the obstacle (in this case, the vent), the flow sets up a gradient filed leading to subsequent flame-area increase due to stretching. The interaction of the flame front and induced rapid turbulent generation associated with the instability mechanism. However, as been observed by McCann et al (McCann, Thomas and Edwards, 1985), cellular instabilities do not appear until the late stages of the flame development in smaller vessel and thus, they have no significant effect on the initial flame and pressure growth. The induced turbulent also triggers a rapid combustion of

the substantial amount of unburnt gases left inside the vessel to undergo bulk motion towards and away from the vent which results on increase in burning rate and higher flame speeds (Cooper, Fairweather and Tite, 1986, McCann, Thomas and Edwards, 1985).

Table 4.2 Summary of different gas/air properties at highest flame speeds. Values of Lewis no, Le and Markstein no, Ma taken from this sources (Clark and Smoot, 1985, Searby and Quinard, 1990, Tseng, Ismail and Faeth, 1993).

Gas/air	Φ	$Sf_{(measured)}$, m/s	S_g, m/s = 0.8 S_f	Le	Ma
CH_4/air	1.0	8.2	6.56	0.91	3.73
C_3H_8/air	1.0	10.9	8.72	1.7	3.69
C_2H_4/air	1.0	13.6	10.9	0.81	3.0
H_2/air	1.18	53.8	43.0	-	2.8

4.3 Deflagration to detonation in test vessel

As been mentioned earlier and demonstrated in Fig. 4.17, the significant pressure rise events or 'spikes' in the pressure traces were observed at a time when the leading flame front had already left the vessel. However, this deflagration to detonation situation was only occurred for hydrogen/air mixture in Test vessel 2 as clearly illustrated in Fig. 4.20. This phenomena is also observed in Test vessel 1 for both hydrogen/air ($\Phi > 0.51$) as shown in Fig.4.21 and ethylene/air at stoichiometric condition i.e. $\Phi = 1.0$. (Fig. 4.22)

From Fig. 4.20, the onset of the denotation spike occurred at $\Phi = 0.76$ with $S_f = 28.6$ m/s in hydrogen/air mixtures. Noting that it is a lean concentration with $S_f < 1970$ m/s (Chapman-Jouguet (CJ) flame speed) and the length of the vessel is shorter (L = 0.315 m), the onset of deflagration to detonation should not happened theoretically (Dorofeev, Bezmelnitsin and Sidorov, 1995, Moen, Bjerketvedt, Jenssen and Thibault, 1985) but Fig. 4.20 demonstrated the opposite results.

It clearly shown that there was a large difference and indicates a strong deflagration-to-detonation like event. As shown in Fig. 4.16, 4.21 and 4.22, the occurrence of the spike took few milliseconds ~ 3 ms. Both hydrogen and ethylene can produce fuel/air clouds which are more sensitive to detonation (Moen, Bjerketvedt, Jenssen and Thibault, 1985). Hydrogen/air mixtures have the smallest detonation cell sizes in comparison with the other common gases exceptionally to acetylene. Note that the smaller the cell size, the more sensitive is the mixture. This is based on the remark made by Ng and Lee (Ng and Lee, 2007). As been studied previously (Dorofeev, Bezmelnitsin and Sidorov, 1995, Moen, Bjerketvedt, Jenssen and Thibault, 1985, Ng and Lee, 2007), the deflagration to detonation mechanism can be instantaneously formed via direct initiation using powerful igniters or other means such as shock focusing. Alternatively, it can also occur from turbulent flame acceleration. Rapid turbulent flame acceleration can lead to deflagration to detonation transition when sufficiently intense turbulent mixing is achieved at the reaction zone. The strong mixing and hence, the turbulent combustion in the flame zone is often promoted by the interaction with obstacles (Ng and Lee, 2007).

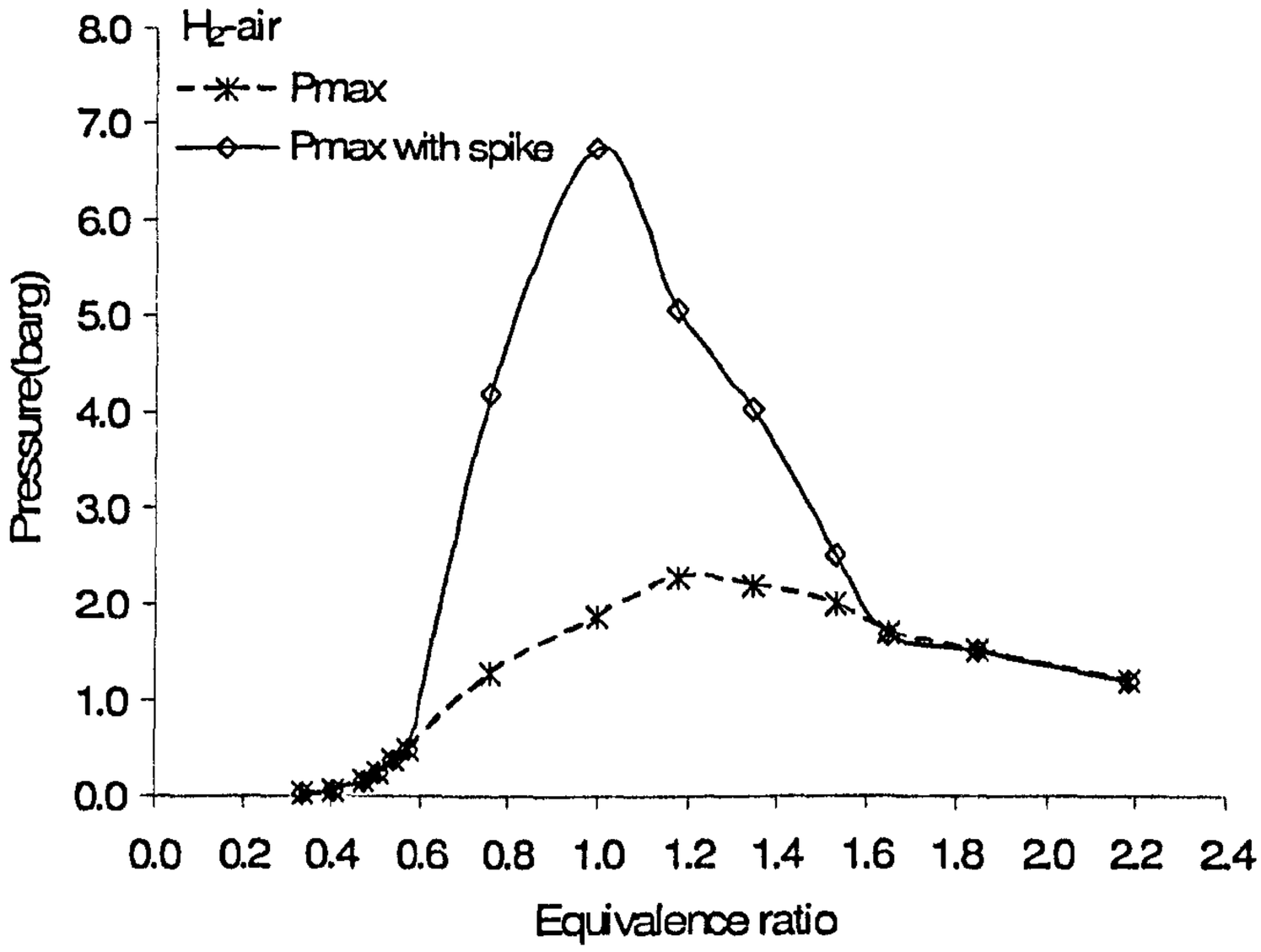

Figure 4.20 Maximum pressures with and without spike traces in hydrogen/air explosion in Test vessel 2.

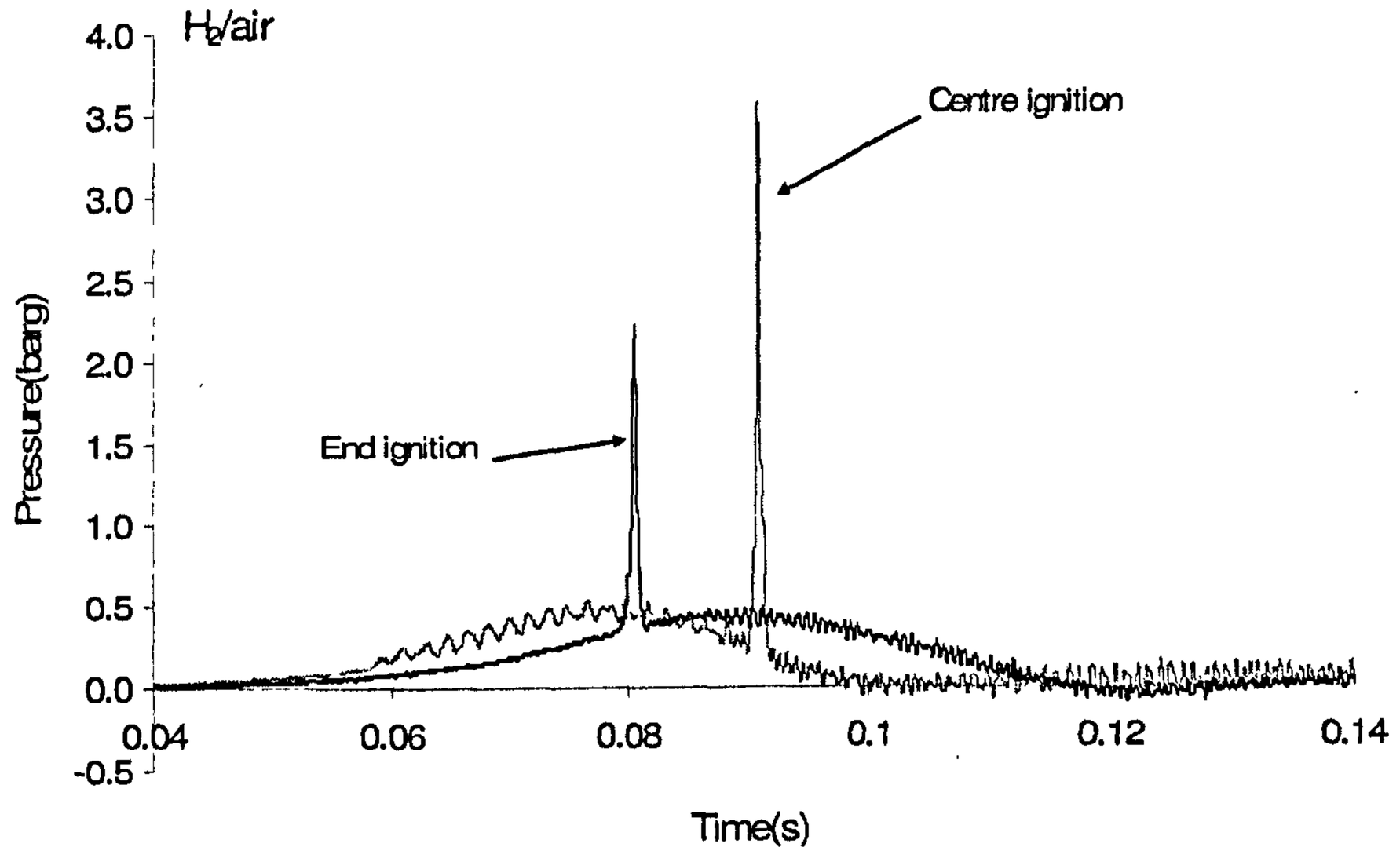

Figure 4.21 Hydrogen/air explosion at $\Phi = 0.54$ (16 % concentration) for Test vessel 1 at end and centre ignition.

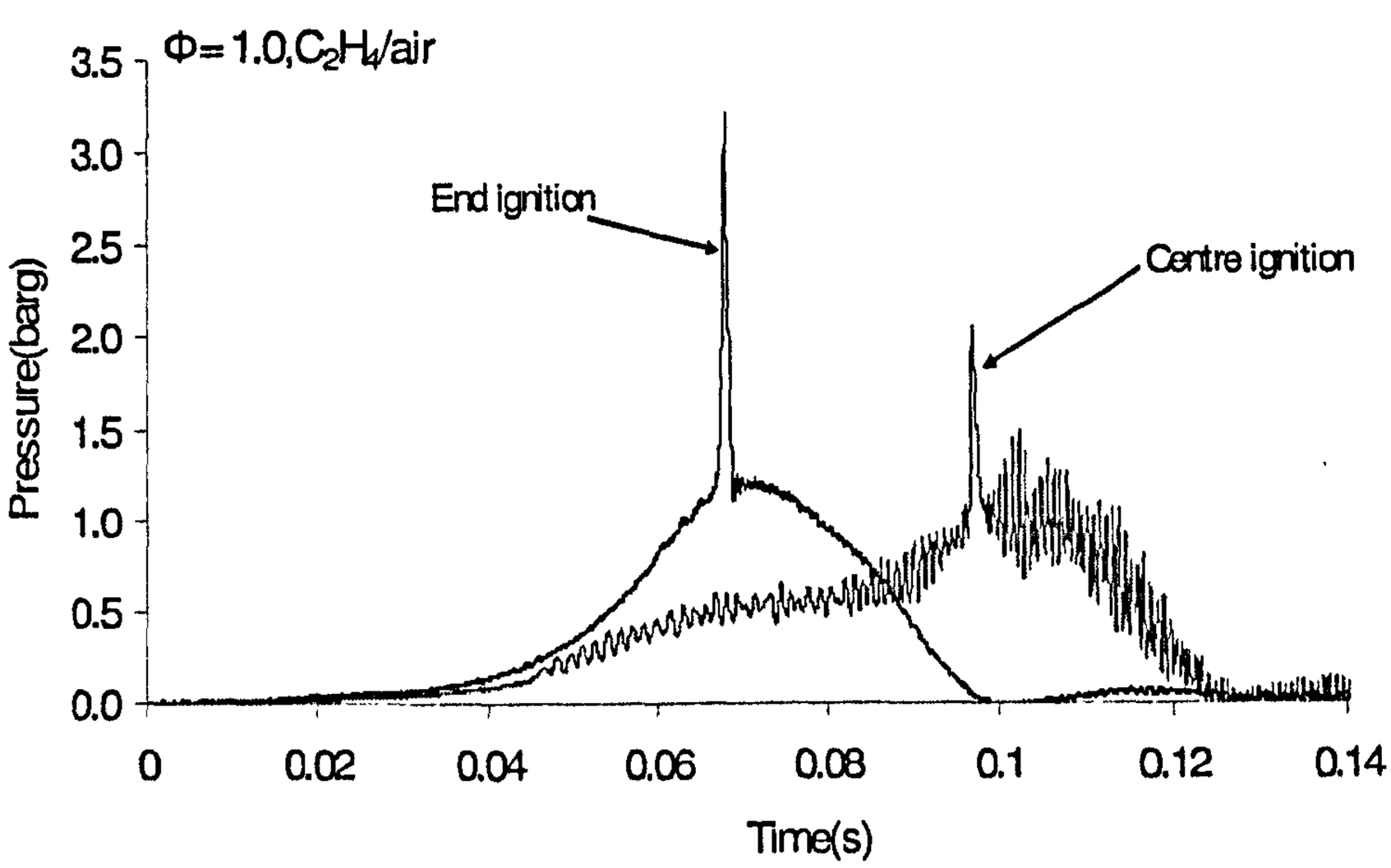

Figure 4.22 Ethylene/air explosion at $\Phi = 1.0$ (6.5 % concentration) for Test vessel 1 at end and centre ignition.

Fast flame acceleration towards the vent causes most of the unburnt gases trapped at the corner region of the vessel and both top and bottom of the vessel. As shown in section

4.1.3.2, estimated hydrogen flame area is 10 % of the vessel surface area which means there is more bulk flame area inside the vessel during the combustion. Since high value of K i.e. small vent area, flow restricted is experienced towards the venting of burnt gases which in turns promote the turbulent jet initiation prior to the vent. A sudden venting can give rise to flame instabilities and consequently to more intense mixing of combustion products and reactants (Dorofeev, Bezmelnitsin and Sidorov, 1995). The oscillatory peaks observed for central and end ignition in Fig 4.21 could be related to the interaction of the pressure/shock wave with the flame front. The effect of fast turbulent mixing of hot combustion products with reactant, flame shock interaction and flame instabilities causes the auto-ignition of the unburnt pockets of mixture inside the vessel or by specific, 'hot spots', leading to the explosion responsible for transition to a developing detonation. A hot spot or auto-ignition centre comprises a small kernel that is initially slightly more reactive than the surrounding mixtures (Gu, Emerson and Bradley, 2003). This argument is supported by the time of flame arrival in the corner region of the Test vessel 1 at the spark end, where a flame arrival thermocouple was located as shown in Table 4.3. The results showed that the time of the flame arrival in this corner region was very close to the time of the pressure spike's occurrence for end ignition but eventually not in the case of centrally ignited. It is considered that the corner region is not a high turbulence zone and hence, the auto ignition point or hot spot is the best described for the observation. Similar observation is reported for large scale test using 35 % H_2/air concentration where the localised explosion occurred inside the vessel after the outflow of flame in venting explosion (Dorofeev, Bezmelnitsin and Sidorov, 1995). However, this phenomena is not observed to propane/air and methane/air in both vessels.

Table 4.3 Time of flame arrival for Test vessel 1

Fuel/air	**Ignition position**	**Time of spike (s)**	**Time at the corner region (s)**	**Time the flame left the vessel (s)**
H_2/air	End	0.08 – 0.082	0.088	0.077
H_2/air	Centre	0.09-0.093	0.075	0.051
C_2H_4/air	End	0.067-0.07	0.062	0.054
C_2H_4/air	Centre	0.097-0.099	0.087	0.043

4.4 Influence of vent coefficient, K, volume and burst vent pressure, P_v on P_{max}

In Test vessel 2, vent area has been varied using orifice plate with blockage ratio ranged from 0 to 0.9, which represented a range of K of 1.0 to 16.4. The degree of vent coefficient, K can be expressed in term of blockage ratio as,

$$K = \frac{A}{A_v} = \frac{1}{1 - BR} \tag{4.3}$$

where A_v is the vent area and A is the area of the orifice plate. It is illustrated by Fig. 4.23 that the maximum overpressure will be reduced accordingly with the size of vent area i.e. lower K will give lower P_{max} which in this case, P_{max} = 0.0178 and 0.171 barg for K =1 and 16.4 respectively which about 10 times different in P_{max}. This is due to less flow restriction to spell out the unburned mixtures from the vessel. Since all test has done on the initially open venting, there is a large different on P_{max} between K = 1 and K = 16.4. The maximum pressure, P_{max} of 0.0178 achieved in the unrestricted venting case (K = 1) happened at t = 57 ms and interestingly, second peak pressure occurred later at t = 140 ms. This second peak exhibited sustained oscillatory pressure due to acoustic pressure disturbances generated by fluctuations in the rate of heat release and the interaction of the combustion of isolated pockets of unburned gas located in the corner of the vessel (Harris, 1983). The frequency of the acoustic wave is about ~ 20 Hz. Further, at K = 2.1, the same trend of this pressure-time profile has been observed but not obvious for K = 16.4. The influence of the acoustically driven flame instabilities appeared to play important role in K = 3.3 where two peaks pressure been observed which the second peak gave frequency of ~ 143 Hz. For initially open vented gas explosion, only single peak pressure should be appeared for typical idealised pressure-time histories (Harris, 1983). This effect has been investigated extensively in small and large vessels (Cooper, Fairweather and Tite, 1986, McCann, Thomas and Edwards, 1985, Solberg, Pappas and Skramstad, 1980, Wingerden and Zeeuwen, 1983a).

It suggests that at high K i.e. small vent area, the egress of combustion products were impeded. The occurrence of only one peak pressure in K = 16.4 corresponds to the

situation where the vent is relatively small and flame speed is higher in which dP/dt remains positive after the burnt gases been expelled from the vent (Harris, 1983).

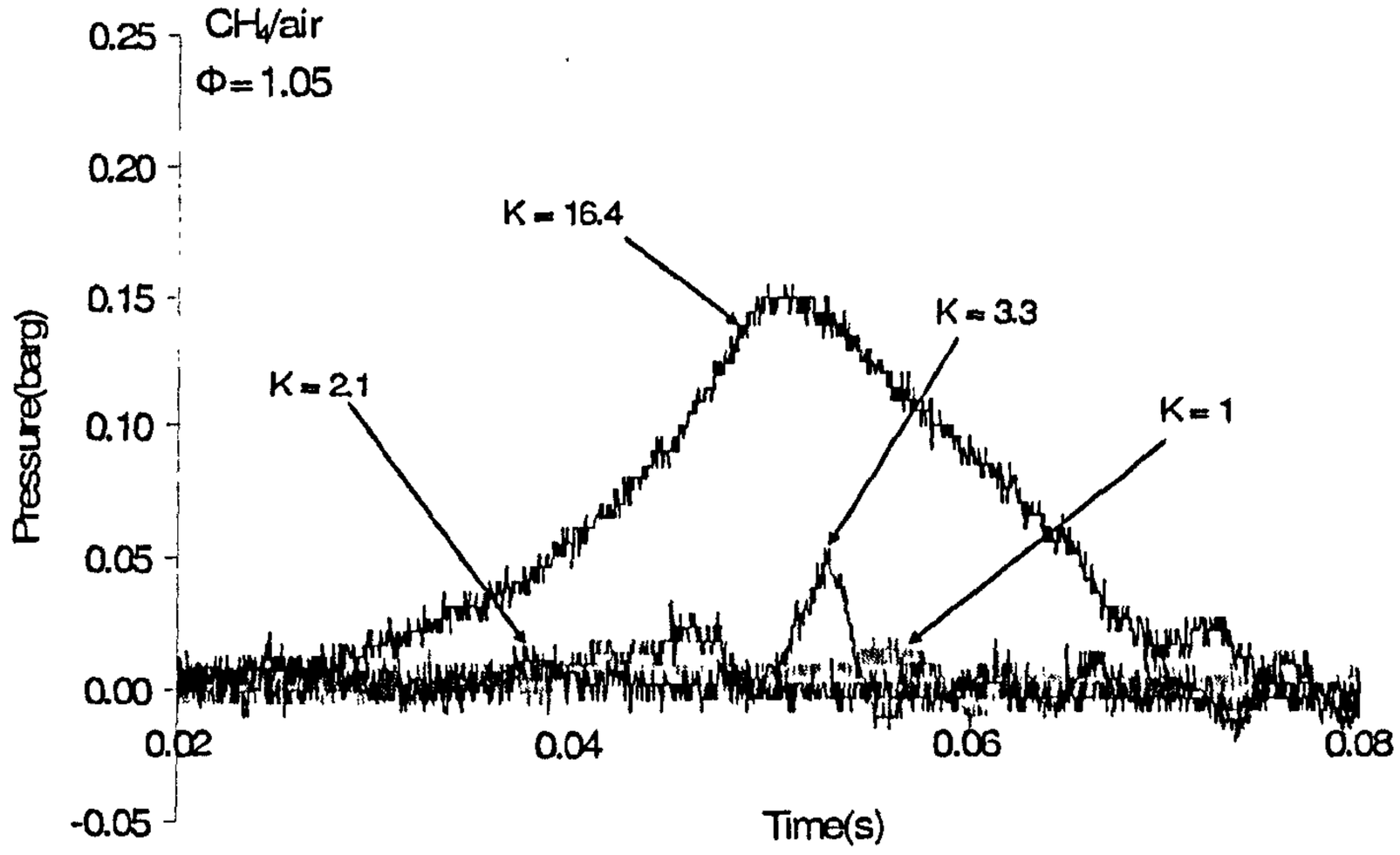

Figure 4.23 Methane/air at different K for $\Phi = 1.05$

As been mentioned earlier, self-cellularity is not the leading factor of the significant increase of P_{max} from K= 1 to K = 16.4 obtained in Test vessel 2. It is assumed that suction effect with the other instabilities mechanism triggering the high P_{max} in respect with the increase in K. To justify the hypothesis, prediction on flame area has been done using Method 2 approach as shown earlier in Section 4.1.3.2. It can be said that for lower K, the predicted flame area is bigger compared to high K, leading to the high burning mass and pressure rise, and thus resulting in bigger amount of burnt gases been expelled from the vessel due to the suction effect. It was shown earlier that the flame left the vessel before the peak P_{max} obtained, suggesting that combustion is still carried out inside the vessel. The net effect is lesser amount of unburnt gases is left inside the vessel and eventually will give lower P_{max} as shown in Fig. 4.24.

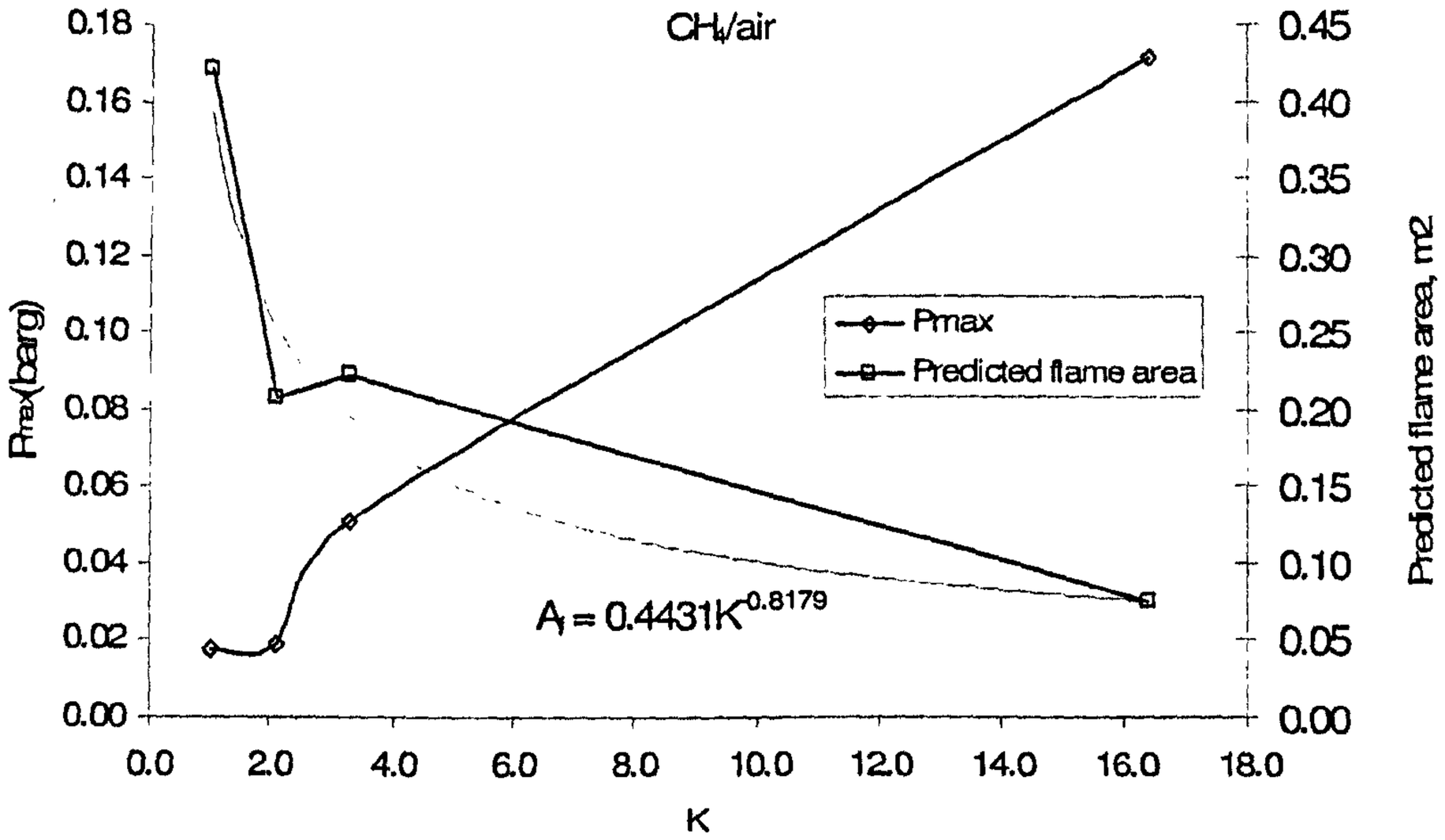

Figure 4.24 The influence of K on P_{max} and predicted flame area, A_f for methane/air mixture.

For hydrogen/air mixture, there is significant increase in magnitude of peak pressure for smaller vent area (K = 16.4) compared to larger vent area (K = 2.1). From Fig.4.25, it is clearly shown that at a very high K, deflagration-to-detonation transition occurred but not at larger vent area (small K). However, there is two peak pressure observed from the figure, suggesting that there is another mechanism occurred inside the vessel. At higher H_2 concentration, the initial turbulent induced by the gas flow, the longer flame travel time as been ignited at end vessel, the flame front instabilities due to the Taylor and acoustic instabilities affect the magnitude of the pressure peaks. Further, there is a sharp negative flow from the pressure traces suggesting that turbulent from the outflow flowing back inside the vessel which then encouraging the rate of burning of unburnt gases trapped in the corner region of the vessel and hence, increase the rate of pressure rise and sharp increase in second peak of maximum pressure as similar as the trend observed for methane/air at K = 3.3

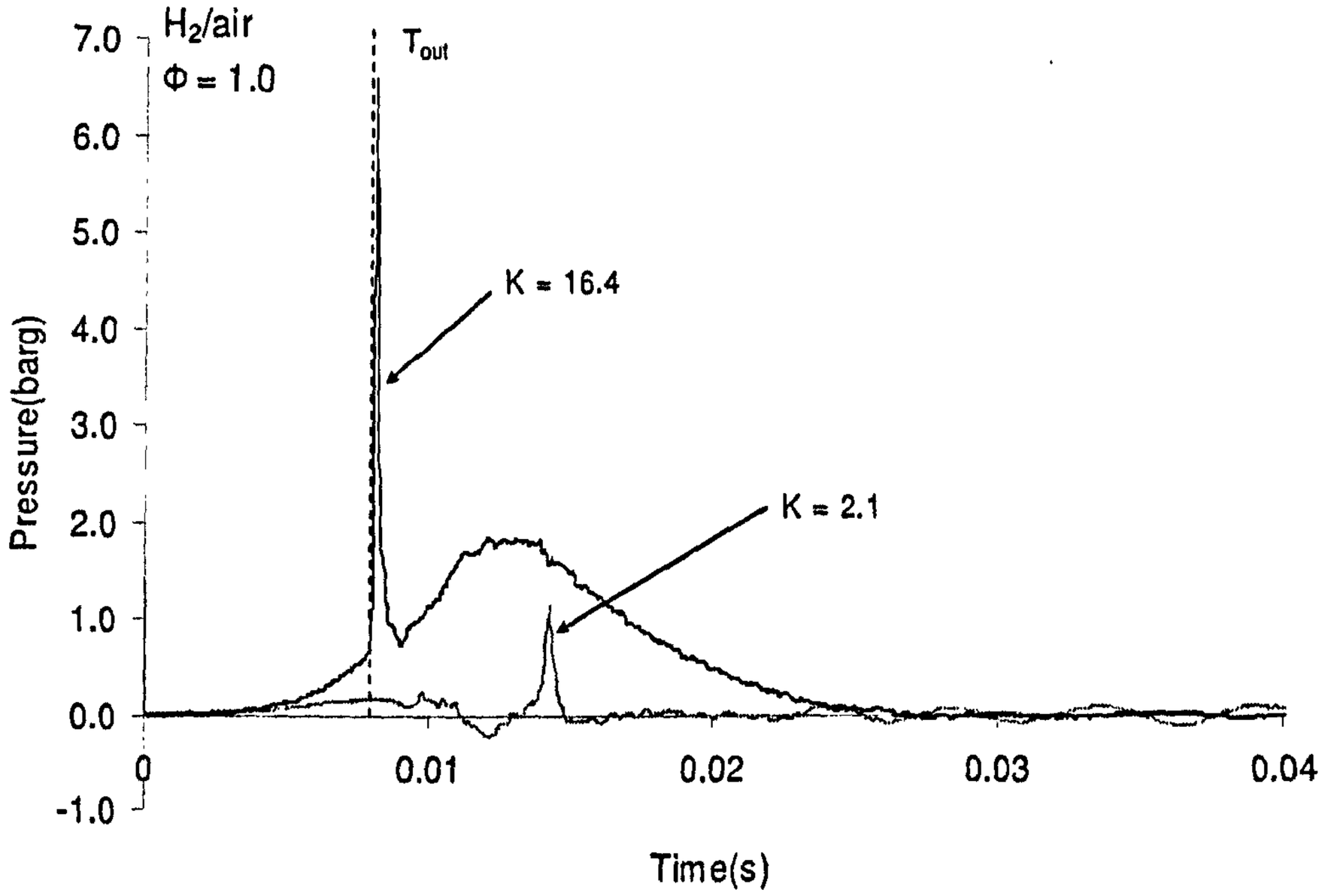

Figure 4.25 Hydrogen/air at stoichiometric concentration for different K.

The $V^{2/3}$ dependence of overpressure on the test vessel volume is a characteristic of spherical or compact vessel explosions, where the flame remains mostly in spherical shape during venting process. If the spherical flame propagates at a constant rate irrespective of the vessel volume, there should be no other dependence of P_{red} on V other than K. However, there is not what the experiment show in the case of the same K for different volumes as shown in Table 4.4.

From the listed data in Table 4.4, it can be said that in larger volume, 0.2 m^3 in the present study, it is obvious that self-acceleration is the important feature in increasing the P_{max} in Test vessel 1. Comparing the ratio of P_{max1}/P_{max2} in Table 4.4 with the turbulent values calculated from the original Bartknecht's work to the predicted P_{red} from Method 1 and 2 given in Table 3.2, it can be considered that those values gave a good agreement. This implies that the turbulent factor, β can be regarded as flame self-acceleration factor occurred during venting. It can be postulated that the ratio of P_{max1}/P_{max2} can be considered on how fast the flame accelerates inside bigger vessel, and self-acceleration is the main factor of the fast flame propagation and the high pressure.

Table 4.4 Summary of experimental P_{max} for Test vessel 1 and 2 for K = 16.4. The ignition position is end ignition.

Gas/air	Φ	Test vessel 1 P_{max1} (barg)	Test vessel 2 P_{max2}(barg)	Ratio $=P_{max1}/P_{max2}$
CH_4/air	0.80	0.18	0.12	1.50
	1.00	0.35	0.19	1.84
	1.05	0.34	0.17	2.00
	1.26	0.06	0.08	0.75
C_3H_8/air	0.8	0.14	0.03	4.67
	1.0	0.54	0.47	1.15
	1.13	0.68	0.30	2.27
	1.38	0.35	0.25	1.40
	1.5	0.14	0.23	0.61
C_2H_4/air	0.6	0.04	0.078	0.51
	0.7	0.21	0.23	0.91
	0.8	0.50	0.72	0.69
	1.0	3.06	1.25	2.45
	1.4	1.42	1.30	1.09
	1.6	0.79	0.40	1.98
H_2/air	0.34	0.015	0.027	0.56
	0.41	0.11	0.057	1.93
	0.48	0.28	0.17	1.65
	0.51	0.52	0.25	2.08
	0.54	2.3	0.37	6.21

To further justify that self-acceleration plays important factor in determining the final P_{max}, ratio of average flame speed, S_{favg} of Test vessel 1 and Test vessel 2 was calculated and shown in Table 4.5. The flame speed at which the flame front propagates through gas/air mixtures during an explosion determines the rate at which burnt gases are generated (Harris, 1983). The differences in the flame speeds shown are due to the bulk flame area distortion effects. If Table 4.4 and 4.5 were compared, the ratio value

between P_{max} and S_{favg} in Test vessel 1 and 2 were about the same but significantly higher for S_{favg} ratio for hydrogen/air.

As shown earlier by using reverse calculation on Method 2, the flame area corresponding to the P_{max} is given about 40 to 45 % of total surface area of the Test vessel 2 for hydrocarbon/air. As predicted, for hydrocarbon/air mixtures, it is about 84 - 99 % of flame area occupying the vessel, meaning that there is a big cloud of flame during the explosion development if the same calculation is made. The flame is about 33 to 42 % of total surface area in hydrogen/air for Test vessel 1 while the flame area was just 10 to 27 % of total surface area when the flame left the vessel in Test vessel 2. However, in lean concentration range, the flame susceptibility to cell cellularity is not significant (Kumar, Skraba and Greig, 1987) and the result in Table 4.5 for hydrogen/air is not supported the argument made. It shown the high ratio of S_{favg1}/ S_{favg2} in which can be explained with the mass burning rate of the flame to increase due to faster flames, rather than due to the larger flame area and also due to the larger bulk flame left trapped inside the vessel that triggering subsequent combustion inside the vessel and hence, increase the overpressure attained.

This finding confirmed the observation reported by McCann et al (McCann, Thomas and Edwards, 1985) that flame cellularity is appeared in the early stage of the explosion in larger volume compared to the smaller volume and hence, influence the mass burning rate and P_{max} inside the vessel. Further, the ratio of S_{favg1}/S_{favg2} is about 2 to 3 for slightly off-stoichiometric hydrocarbon/air mixtures which suggests that rich mixtures are known to be more susceptible to develop surface instabilities (flame cellularity) which would lead to higher burning rates and hence higher flame speeds attained in Test vessel 1 as shown in Table 4.5 in respect to Test vessel 2. This in turn could result in a more sever vented explosion than might be expected (on the basis of its laminar burning velocity). This also confirms that vessel volume is the major factor in determining the final overpressure in vented gas explosion.

Table 4.5 Summary of experimental average flame speed, S_{favg} for Test vessel 1 and 2 for K = 16.4. The ignition position is end ignition.

Gas/air	Φ	Test vessel 1 S_{favg} (m/s)	Test vessel 2 S_{favg} (m/s)	Ratio $= S_{favg1}/A_{favg2}$
CH_4/air	0.80	15.51	6.15	2.5
	1.00	18.83	8.21	2.3
	1.05	22.78	7.51	**3.0**
	1.26	8.35	4.60	1.8
C_3H_8/air	0.8	11.04	6.15	1.8
	1.0	20.01	10.91	1.8
	1.13	24.05	8.90	**2.7**
	1.38	15.37	6.32	2.4
	1.5	11.89	5.90	2.0
C_2H_4/air	0.6	6.57	3.41	1.9
	0.7	12.25	5.70	2.1
	0.8	23.06	11.23	2.1
	1.0	28.11	13.61	2.1
	1.4	28.61	12.49	2.3
	1.6	19.31	7.40	2.6
H_2/air	0.34	5.31	2.11	2.5
	0.41	22.47	4.78	4.7
	0.48	44.69	8.66	5.2
	0.51	53.62	10.11	5.3
	0.54	85.10	12.68	**6.7**

As discussed in Chapter 3, the pressure at which the vent relief cover, P_v begins to fail has a more significant effect on the magnitude of the P_1 and P_2 (Figure 3.2). The opening/breaking of the vent would delay or hinder the venting process, causing the maximum burning rate increasing due to the bulk flame area compressed towards the vent and hence, the rates of pressure rise increases as well as the pressure inside the vessel in comparison to the open vent mechanism. At low opening vent pressure P_v, the resistance to flow expansion out of the chamber to the duct is less than at higher P_v. At

higher P_v, since the vent opened at a relatively late stage, when the total flame area had increased significantly compared to the lower P_v case, the rate of burned gas production exceeded the rate of unburned gas venting which in turn caused a continuation in pressure rise within the vessel (Chow, Cleaver, Fairweather and Walker, 2000).

The effect of vent burst pressure, P_v has been studied extensively (Cooper, Fairweather and Tite, 1986, Cubbage and Marshall, 1974, Cubbage and Simmonds, 1955, Cubbage and Simmonds, 1957, DeGood and Chartrathi, 1991, Donat, 1977, Rasbash, Drysdale and Kemp, 1976, Runes, 1972, Zalosh, 1980, Thorne, Rogowski and Field, 1983) in order to know at what extent this parameter will influence the magnitude of P_{max} and the associated mechanism. From the investigation, it is found that P_{max} increases with the increase of P_v due to the reason above as illustrated in Fig. 4.26.

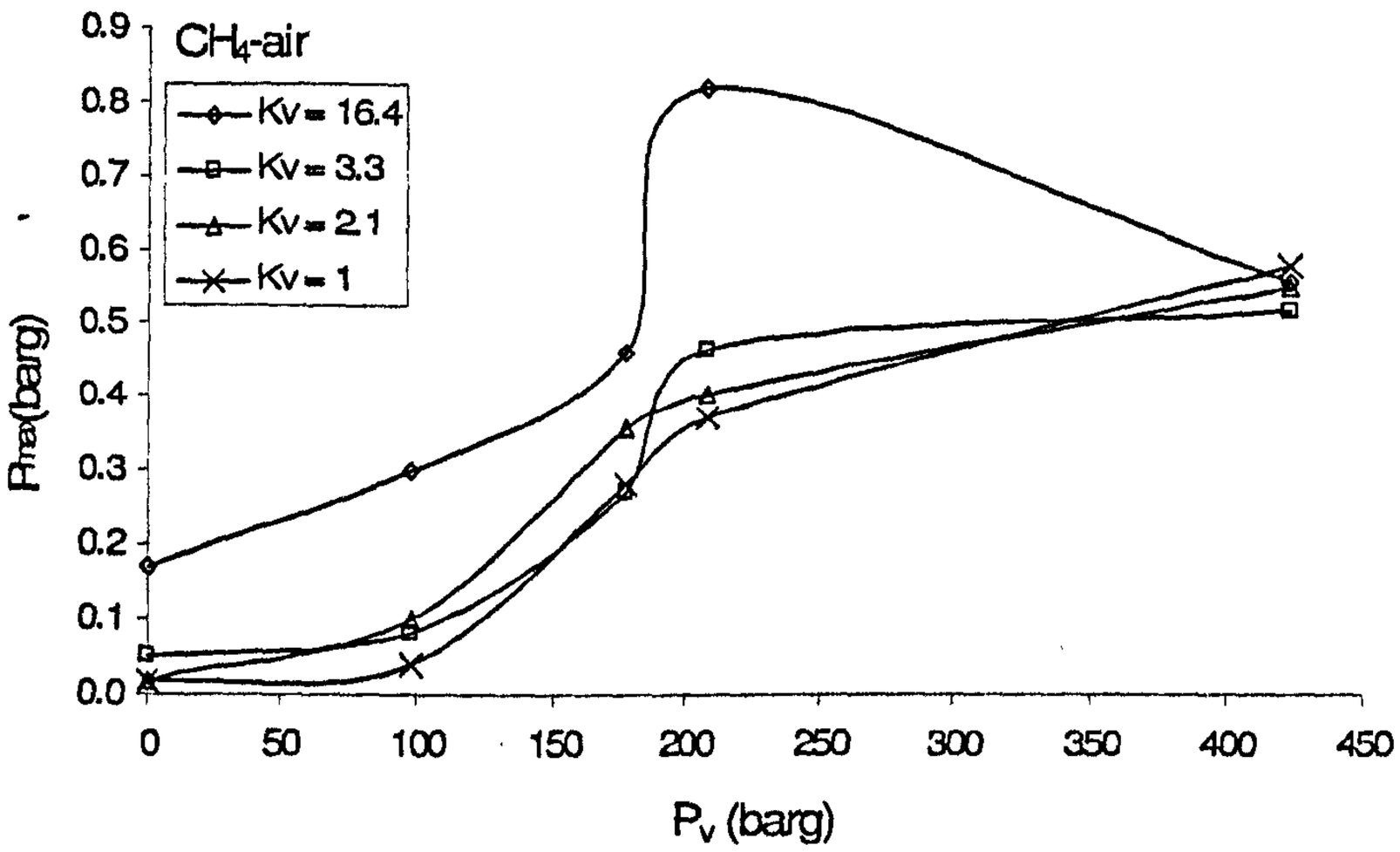

Figure 4.26 Influence of P_v on P_{max} for Test vessel 2

However, this condition is only satisfied the previous works for low K i.e. K =1 and 2.1 but not with larger K in this test configuration. It is apparent that a decrease in P_{max} occurred at K = 16.4 from P_v = 209 mbar to P_v = 424 mbar, about 1.5 times different and there was no significant increase in P_{max} for P_v = 209 and 424 mbar respectively at K = 3.3. It should be noted that the concentration used (10 % methane/air) was the slightly off stoichiometric which showed the higher P_{max} in the tests conducted at varying equivalence ratio. This similar phenomena has been observed in Bartknecht's

work (Bartknecht, 1993) and Harris and Briscoe (Harris and Briscoe, 1967). The occurrence of this peculiar behaviour is due to two opposing effects. At higher P_v, even if the flow acceleration is stronger, the explosion is vented at a later stage when the flame is closer to the walls. Thus, there can only be small increase in flame area and almost immediately followed by gas cooling and flame quenching at the nearby wall. This results a small increase in burning rate and hence, the overpressure inside the vessel (Ponizy and Leyer, 1999a, Ponizy and Leyer, 1999b). Similar result has shown in Leeds work for larger cylinder. Heat losses after the flame has touched the wall make the peak pressure decreases (Phylaktou and Andrews, 1991, Phylaktou, Andrews and Herath, 1990). Experiments with turbulent gas mixtures at large vent showed that the maximum pressure increased rapidly with high pressure of the bursting disc compared to smaller vent (Harris and Briscoe, 1967). Turbulent could increase the burning velocity and cause the increase in maximum overpressure. Hence, an explosion vented in its early stages will give a higher pressure than one vented at a later stage.

4.5 Comparison between theory and experimental data

Experimental P_{max} at the stoichiometric concentration for Test vessel 1 and 2 was compared with the proposed venting equations (Method 1 and 2) as well as other correlations, in order for validation as shown in Table 4.6. All calculations used parameters listed in Table 3.2 when appropriate. From the table, it shows that Bartknecht's (Bartknecht, 1993) and Swift's equation (Swift, 1983) offered by NFPA 68 gave gross estimation on maximum pressure and this corresponds with the percent error deviation between the experimental data and calculated results as illustrated in Table 4.7. In comparison with the experimental data, it is found that prediction given by Method 2 and Bradley and Mitcheson have a good agreement to each other. It is due to the S_g value used on both equations, suggesting that it best describes the pressure development in vented explosions. For Bradley and Mitcheson's equation, it gave 9.5 to 232 % deviation between the experimental and calculated data for Test vessel 1 but the error (168 – 1774 %) is huge for smaller vessel i.e. $0.0065m^3$ for Test vessel 2. Meanwhile, Molkov's equation over predicted the maximum overpressure compared to experimental data which gave about 189 to 505 % deviation for methane and propane/air mixture on both test vessels. However, the equation gave better agreement

with experimental result on reactive mixtures i.e. ethylene and hydrogen. This is shown on lower percent error deviation of 0.3 to 95 % for both mixtures on test vessels.

As seen on Table 4.6 and 4.7, Method 1 gave under prediction results compared to the experimental data but not for Method 2. Method 2 seems to have closer results with experimental data where it gave about 134 to 220 % deviation for Test vessel 1 and about 127 to 489 % deviation for Test vessel 2 (refer to Table 4.7). Yet, Method 2 does not give satisfied result when applying on hydrogen/air mixture where the percent error is significantly large i.e. 1879 %. From this result, it shows that Method 2 gave consistent agreement with the experimental result for calculating the maximum overpressure. Among all the published correlations, Bradley and Mitcheson's equation fitted well to the experimental data for all hydrocarbon/air mixtures but Molkov's equation gave better agreement with experimental data on hydrogen/air. The term S_u (E-1) used in Method 2 which regards the mass burning rate to be ~7 times higher than the mass burning rate based on S_u as the flame front rate of consumption of unburnt gases seems to agree with the experimental profile for predicting the overpressure which also been used by Bradley and Mitcheson (Bradley and Mitcheson, 1978a, Bradley and Mitcheson, 1978b) as well as Runes (Runes, 1972). The results shown in Table 4.6 for Method 1 and 2 were calculated without the turbulent enhancement factor, β. The key point is that the constant derived from Method 2 do not need any β factor at this stage (initially open venting) but may have to be included for P_v influences. The discrepancy of adding the turbulent enhancement factor, β from previous investigators (Bradley and Mitcheson, 1978b, Chippett, 1984, Pasman, Groothuizen and Gooijer, 1974, Runes, 1972, Swift, 1984) to agree with the experimental data should not be the major problem in regards to take other parameters into consideration i.e. the density dependence on the pressure, the compressibility factor, ε and the orifice discharge coefficient, C_d.

Again, the same K results the same P_{max} for different volume as shown in Table 4.6 for experimental results from Test vessel 1 and Test vessel 2. It is recommended to use the A_s term to replace K in order to provide precise estimation on venting area and thus, P_{max} for given vessel volumes.

Table 4.6 Experimental data and calculated equations for test vessels at $\Phi = 1.0$

Test vessel 1							
Gas/air	Experimental data (bar)	Method 1 (bar)	Method 2 (bar)	Bartknecht Eq (bar)	Swift Eq (bar)	Bradley and Mitcheson Eq (bar)	Molkov Eq (bar)
CH_4/air	0.35	0.035	1.12	5.44	12.43	1.163	2.09
C_3H_8/air	0.53	0.04	1.24	7.45	20.92	1.46	2.26
C_2H_4/air	3.06	0.095	2.84	10.92	20.92	3.35	3.07
H_2/air	-	1.44	45.13	14.57	-	42.72	4.16
Test vessel 2							
CH_4/air	0.19	0.035	1.12	5.44	12.43	1.163	1.15
C_3H_8/air	0.47	0.04	1.24	7.45	20.92	1.46	1.36
C_2H_4/air	1.25	0.095	2.84	10.92	20.92	3.35	2.32
H_2/air	2.28	1.44	45.13	14.57	-	42.72	4.44

Table 4.7 Percent error deviation for experimental and calculation result

Test vessel 1						
Gas/air	Method 1	Method 2	Bartknecht Eq	Swift Eq	Bradley and Mitcheson Eq	Molkov Eq
CH_4/air	-90.0	220.0	1454.3	3451.4	232.3	497.1
C_3H_8/air	-92.5	134.0	1305.7	3847.2	175.5	326.4
C_2H_4/air	-96.9	-7.2	256.9	583.7	9.5	0.3
H_2/air	-	-	-	-	-	-
Test vessel 2						
CH_4/air	-81.6	489.5	2763.2	6442.1	512.1	505.3
C_3H_8/air	-91.5	163.8	1485.1	4351.1	210.6	189.4
C_2H_4/air	-92.4	127.2	773.6	1573.6	168.0	85.6
H_2/air	-36.8	1879.4	539.0	-	1773.7	94.7

Table 4.8 illustrated the experimental results of initially closed venting in comparison with the calculated equations. It should be noted that since vent cover was in place, the effect of bursting vent pressure, P_v should be taken into consideration in predicting P_{max}, hence the turbulence enhancement factor, β is included. For Method 1 equation, β is 20 and 4 for Method 2 equation for all K except for K = 16.4. From the list, Bradley and Mitcheson's equation gave a very satisfied result in comparison with the experimental values. Method 2 seems to agree with experimental data for small K but it gave under prediction result for K = 2.1 and 1.0. Molkov's equation gave bit peculiar results in order to calculate the overpressure for P_v at different K. The result show a decrease P_{max} at increase P_v which really contradicted with the experimental data obtained.

In summary, it can be concluded that the experimental data obtained for simply vented explosions are in between the assumptions of the vent unburnt gas maximum mass flow rate based on S_u and S_u (E-1).

Table 4.8 Comparison of methane/air mixture with different P_v for Test vessel 2

P_v (bar)	Exp P_{max} (bar)	P_{max} (M1) bar	P_{max} (M2) bar	P_{max} (Bartknecht Eq) bar	P_{max} (Swift Eq) bar	P_{max} (Bradley and Mitcheson Eq) bar	P_{max} (Molkov Eq) bar
K = 16.4							
0.098	0.30	0.59	1.12	5.42	12.43	3.84	0.56
0.178	0.46	0.59	1.12	6.2	12.43	3.84	0.54
0.209	0.82	0.59	1.12	6.5	12.43	3.84	0.53
0.424	0.56	0.59	1.12	9.2	12.43	3.84	0.48
K = 3.3							
0.098	0.083	0.38	0.73	0.34	0.5	1.81	0.20
0.178	0.27	0.38	0.73	0.40	0.5	1.81	0.19
0.209	0.47	0.38	0.73	0.43	0.5	1.81	0.19
0.424	0.52	0.38	0.73	0.58	0.5	1.81	0.17
K = 2.1							
0.098	0.10	0.15	0.29	0.16	0.2	1.33	0.079
0.178	0.36	0.15	0.29	0.18	0.2	1.33	0.076
0.209	0.41	0.15	0.29	0.19	0.2	1.33	0.075

0.424	0.55	0.15	0.29	0.27	0.2	1.33	0.70
K = 1							
0.098	0.041	0.035	0.067	0.04	0.046	1.07	0.0018
0.178	0.28	0.035	0.067	0.048	0.046	1.07	0.017
0.209	0.37	0.035	0.067	0.05	0.046	1.07	0.17
0.424	0.58	0.035	0.067	0.07	0.046	1.07	0.16

Table 4.8 cont

4.6 Concluding remarks

Experiments performed in two different cylindrical vessel volumes in this present study have been used to identify the physics and dynamics mechanisms responsible for the generation of the pressure peaks, in particular on the occurrence of the deflagration-to-detonation in simply vented explosions. In general, end ignition gives higher P_{max} compared to central ignition in hydrocarbon/air mixtures. The flame is allowed to propagate in one direction, leading to more elongated flame towards the vent and hence, increase in mass burning rate and high flame speed. Self-acceleration is expected to be one of the important features for the increase in P_{max} magnitude which occurred in Test vessel 1 in comparison with P_{max} in Test vessel 2 at the same equivalence ratio. This is justified by the reversed calculation done using Method 2 equation. It shown that about 80-90 % of flame area has been occupying the vessel total surface area. It is confirmed the observation reported by McCann et al (McCann, Thomas and Edwards, 1985). In their work, they said that the flame cellularity (self-acceleration) appeared in earlier stage in larger volume and this give significant effect on the overpressure inside the vessel. For smaller vessel i.e. 0.0065 m^3, experiments have shown that the presence of pressure oscillation and this coupling with the induced turbulence by the vent flow increased the P_{max}. For centrally ignited explosion, the increase intensity of the flame cellularity during flame propagation produces accelerating flame front which later interact with the vessel wall. Due to the rapid deceleration of the flame front as it approach the vessel wall, it results on the strong rare fraction waves which triggering further combustion of a large amount of unburnt gases left inside the vessel and lead to a significant P_{max} inside the vessel for reactive gas/air mixtures as shown on ethylene/air and hydrogen/air mixtures. The ratio of P_{max1}/P_{max2} also illustrated that there was about

2-7 times increases in overpressure in Test vessel 1 compared to Test vessel 2 at the same equivalence ratio and K, suggesting that flame is self-accelerated in bigger vessel and propensity of cell cellularity is susceptible in rich mixtures of hydrocarbon/air.

Auto-ignition is the main factor of the appearance of spiky pressure traces on hydrogen/air and ethylene/air in the test vessels. It can be said that fast turbulent mixing of the combustion products and reactants initiates the 'hot spot' or auto-ignition centre to lead to the explosion responsible for transition to a developing detonation.

CHAPTER 5

VENTED DUCT GAS EXPLOSIONS

5.0 Introduction

In this chapter, the discussion on venting explosion is explored to the other applications i.e. venting with the relief duct for gas explosion. In many practical situations, vented equipment is located inside a building or near personnel work areas. For this reason, a vent should be connected to the piping duct in order to discharge the hot gases to a 'safe area'. However, care must be taken in the design of discharge ducts to ensure that they do not compromise the effectiveness of explosion relief. Studies (Ponizy and Leyer, 1999a, Kordylewski and Wach, 1988, Ponizy and Leyer, 1999b) have shown that discharging explosion products into a duct will always increase the pressure developed in the vessel which is being protected- in comparison to the pressure generated with no discharge duct present. NFPA 68 recommends the results of Bartknecht (Bartknecht, 1993) where P_{max} with a discharge ducts is presented for two duct lengths of less than or equal to 3m and greater than 3m. It showed that about 2 to 12 fold increase in reduced pressure, regardless of the reactivity of the explosive mixtures in comparison to the pressure generated with free venting.

Works by DeGood et al (DeGood and Chartrathi, 1991) and McCann et al (McCann, Thomas and Edwards, 1985) on varying the duct length in vented gas deflagration supported this observations. It found that the P_{max} increased to more than two fold if the duct length is increased. The surprising feature from this results showed that the length of the duct is not a major parameter and yet, Bartknecht gave results based on his work for short and long ducts (Bartknecht, 1993). This is because the increase in the overpressure is dominated by duct entry and exit pressure losses; on which a duct would have to be about 100 pipe diameters long before the flow friction losses were equal to the combined inlet and exit pressure losses. The present work used a relatively short duct of 1m long with 162mm-internal-diameter which gives L/D of 6.2 (refer to Fig. 2.3), but it exhibited all the features of explosion venting with a vent duct attached. In Bartknecht's work (Bartknecht, 1993) the 3 m long pipe was 0.5m diameter and hence the L/D was 6, close to that used in the present work. As pipe friction losses are a function of pipe L/D a dependence of the vent overpressure on the L/D would be expected rather than simply on the length of the duct, irrespective of its diameter.

This is a consequence of the need to overcome the inertia of the air within the duct, before an outward flow of gases from the vessel can be established and pressure relief commence. In practice therefore, a discharge duct should be as short as possible and have a cross-sectional area at least as large as the area of the relief vent. It should be also preferably be the same shape. Since even short ducts can lead to doubling of the overpressure generated in the vessel being protected, it is suggested that whenever a discharge duct is used in conjunction with the relief vent, the effective strength of the plant should be taken to be half of the value originally assumed. The strength of the discharge duct itself should be sufficient to withstand the anticipated explosion pressure and the pressure associated with any explosions that occur within the duct itself.

Sudden pressure peak occurrence in the duct is also mentioned by Kordylewski and co-worker (Kordylewski and Wach, 1988) and maximum pressure effect in the vessel is found to occur with a particular duct length, equal to about 12 diameters. It is known now that the intensification of the combustion in the vessel is driven by an impulse generated during the burn-up or secondary explosion in the initial part of the duct, shortly after the flame penetrates into it (Ponizy and Leyer, 1999a, Ponizy and Leyer, 1999b). Iida et al (Iida, Kawaguchi and Sato, 1985) found that in some cases the flame was found to extinguish or hesitate in the channel before passing through, depending on the equivalence ratio of the mixture, the channel width and the flame inflow velocity. Other studies supported the above hypotheses by using relatively narrow ducts with a sharp vessel-duct area (Iida, Kawaguchi and Sato, 1985, Ponizy and Leyer, 1999a, Ponizy and Leyer, 1999b). When relatively narrow ducts are used with a sharp vessel-duct area change, the flame front entering the duct can be temporarily extinguished due to stretch (caused by the inlet vena contraction effect, which locally increases centreline velocities by 64 %) and cooling through turbulent mixing with unburned gas which brings about stronger burn-up (i.e. with higher pressure amplitudes) during re-ignition (Ponizy and Veyssiere, 2000).

The presence of the duct has been addressed in terms of the increased pressure drop due to the gas flow through the vessel-duct assembly. However, the same argument on the increased of the pressure inside the vessel is affected by the violent explosion occurred at the initial section of the duct rather than the additional pressure losses. The flow restriction in correspondence of the duct entrance is responsible for a strong flow

acceleration that produces high level of turbulence (Iida, Kawaguchi and Sato, 1985, Kasmani, Andrews, Phylaktou and Willacy, 2007a, Kasmani, Andrews, Phylaktou and Willacy, 2007b, Ponizy and Leyer, 1999a). When the flame enters the duct due to the high turbulence levels, hot and fresh gases undergo an effective mixing that promotes a violent burning in the initial section of the duct. This related pressure impulse in the duct has been suggested to temporarily induce a flow reversal across the vent (usually referred to the back-flow).

The only guidelines for the design of ducted vents for gas explosions are those proposed by Bartknecht (Bartknecht, 1993) which also reported in NFPA 68. The guideline gives barely an empirical correlation based on simply vented vessels indications presented in the same reference. The correlation based on the assumption that the peak pressure in the presence of duct is a function of the peak pressure attained inside the vessel without the presence of the duct and the duct length. The equations are:

$$P_{red \text{ with the duct}} = 0.779\,(P_{\text{red without the duct}} - 1.013)^{1.161} + 1.013 \quad Lt < 3m \tag{5.1}$$

$$P_{\text{red with the duct}} = 0.172\,(P_{\text{red without the duct}} - 1.013)^{1.936} + 1.013 \quad 3m \le Lt \ge 6m \tag{5.2}$$

Equation 5.1 and 5.2 are the replacement of the previous equations applied in previous version NFPA 68 (NFPA68, 2002), the only difference was the value of the constant used. The previous equations given for different duct length were provided by Bartknecht (Bartknecht, 1993, Bartknecth, 1981) as the correlations of his experimental results carried out in a 1m3 explosion vessel with a vent burst pressure of 150 mbar and a vent diameter of 0.2 m or K = 33.3. The equations are,

$$P_{red \text{ with the duct}} = 1.24\,P_{\text{red without the duct}}^{0.8614} \quad Lt < 3m \tag{5.3}$$

$$P_{\text{red with the duct}} = 2.48\,P_{\text{red without the duct}}^{0.5165} \quad 3m \le Lt \ge 6m \tag{5.4}$$

Applying all equations above, it shown that the results would give overly conservative prediction by comparing with the experimental data obtained by Cubbage and Marshall (Cubbage and Marshall, 1972), McCann et al (McCann, Thomas and Edwards, 1985) and DeGood and Chartrathi (DeGood and Chartrathi, 1991). For example if P_{red} was 0.4

barg, Eq. 5.1 predicts that the addition of a vent pipe of the same size as the vent would increase the pressure to 1.27 bar and to 1.04 bar for Eq. 5.2. This is about 0.56 bar for Eq. 5.3 and 1.54 given by Eq. 5.4. The present work investigates a K of 16.4 and 0.162 m diameter and 1.0 m long vent pipe (L/D of 6.2) for a 0.2 m^3 cylindrical vessel. However, the results that will be shown later give over conservative agreement with Eq. 5.2 and no agreement with Eq. 5.3 but better agreement with Eq. 5.4. There has been no validation of Eq. 5.1 and 5.2 for different K or vessel volumes even though they are the basis of the US and European Standards for the use of duct pipes.

The increase in P_{max} with the addition of a vent duct is so large that vent ducts cannot be used without increasing the vent area and duct size to achieve a reduction in the overpressure. However, there is insufficient design data for gases to enable this to be done effectively and the physics of the process for gas explosion venting is not well understood. This contrasts with the situation for dust explosions, where a substantial experimental data base exists (Lunn, Crowhurst and Hey, 1988). Recently, Tamanini and Fisher (Tamanini and Fisher, 2003) derived a correlation to take into effect of the duct when the duct explosion is occurring. All of these correlations explicitly take into account the dependence on the duct length, duct diameter and the vessel volume.

5.1 Phenomenology of vessel vented through the duct

Several studies have been undertaken since the beginning of the 1980s, proving that the presence of the duct to discharge the explosions products generally increases the severity of the explosion compared to the situation encountered with a vessel vented directly to the atmosphere. It has been demonstrated that the deflagration pressure can exceed by a factor of 10 or more than obtained in experiments with venting directly to atmosphere (Bartknecth, 1981, Molkov and Nekrasov, 1981). This is mainly due to the complex interaction of the combustion inside the duct pipe and vessel. Despite of the numerous experimental studies and their findings (Bartknecht, 1993, DeGood and Chartrathi, 1991, Ferrara, Willacy, Phylaktou, Andrews, Benedetto, Salzano, 2005, Kasmani, Andrews, Phylaktou, Willacy, 2007, Kordylewski and Wach, 1988, McCann, Thomas, Edwards, 1985, Molkov and Nekrasov, 1981, Ponizy and Leyer, 1999a, 1999b,), the whole picture of the interaction between the gas dynamics inside the duct

and the vessel as well as the geometry and operating conditions on the maximum pressure remains unclear.

Some investigators proposed that violent secondary explosion occurred inside the duct is the important factor leading to an increase in overpressure inside the vessel (Kordylewski and Wach, 1988, Molkov and Nekrasov, 1981, Ponizy and Leyer, 1999a, 1999b) while some proposed that the pressure rise in the vessel is related to the reduced effectiveness of venting process caused by the pressure rise in the duct (Ferrara, Benedetto, Salzano and Russo, 2006). Two different mechanisms for the enhanced burning rate have been discussed. The interaction of the flame front with the turbulence promoted by the violent flow reversal from the occurrence of the secondary explosion inside the duct is one of those severity observed in venting duct explosions (Molkov, Baratov and Korolchenko, 1993, Ponizy and Leyer, 1999a). The other mechanism proposed is due to the growth of flame instabilities (Taylor-Rayleigh instability and acoustic instability) triggered by the interaction of the residual combustion in the vessel with the strong pressure wave produced inside the duct (Kordylewski and Wach, 1988, McCann, Thomas and Edwards, 1985).

The additional frictional loss due to the presence of the duct and the duct gas column inertia are also considered in reducing the venting flow rate, depending on the duct diameter and length (Ferrara, Benedetto, Salzano and Russo, 2006). Bartknecht (Bartknecth.W, 1981) pointed out that the increase of the explosion violence and the peak pressure in the vessel are strongly affected by the hydromechanical drag and gas column inertia of the duct. The same observation has been described by Ponizy and Leyer (Ponizy and Leyer, 1999a) that the frictional losses and inertia are the key factors in influencing the evolution of the explosion inside the vessel. This finding has been confirmed by Ural (Ural, 1993) using mathematical model.

In this present work, it is aimed to investigate the physic of the venting process with the duct attached to understand why the increase in the overpressure was so large with no vent bursting pressure and the effect of vent burst pressure which in some cases, reducing the overpressure compared to simply vented explosion. There have been few investigations on the effect of the mixture stoichiometry in venting for the open vent gas explosion and none for venting with a vent duct. Changing the equivalence ratio

changes the laminar burning velocity, S_u, of the flame and the mass burning rate of spherical flames scales as S_u^3. This directly influences the velocities in the vent pipe and hence on the influence of the vent pipe in the explosion. Thus a study of venting with reduced burning velocities will help to understand and model the influence of the vent pipe in faster explosions (Kasmani, Willacy, Phylaktou and Andrews, 2007). In this present work, the effect of mixture reactivity from $\Phi = 0.54$ to 1.6 will be investigated in terms of P_{max}, flame speeds and unburnt gas velocity ahead of the flame.

5.1.1 Effect of the relief duct fitted to the test vessel

In the previous chapter, the details explanation for the physics and dynamics of the simply vented gas explosion were given to get better understanding on the venting mechanism. Figure 5.1 showed the pressure traces for simply vented and duct vented explosion for methane/air at $\Phi = 1.06$ for end ignition. It illustrated that P_{max} for vented explosion with the duct fitted is about 4 times higher than for the corresponding P_{max} in simply vented explosion. A similar trend is also showed for the maximum rate of pressure rise, dP/dt. It is interesting to note that there are two peaks for $dP/dt_{(duct\ vented)}$ traces. It shows that the maximum burning rate reaching the first peak after the flame exited the duct pipe and it suggests that the combustion is still taking place after a rapid decrease in dP/dt to give the second peak before dropping to -80 barg s^{-1} and finally deceasing to atmospheric condition inside the vessel. The maximum peak pressure for both cases occurred at the same time but at different magnitude. This can be proposed that they have the same mechanism but the presence of the duct has triggering the pressure rise inside the vessel.

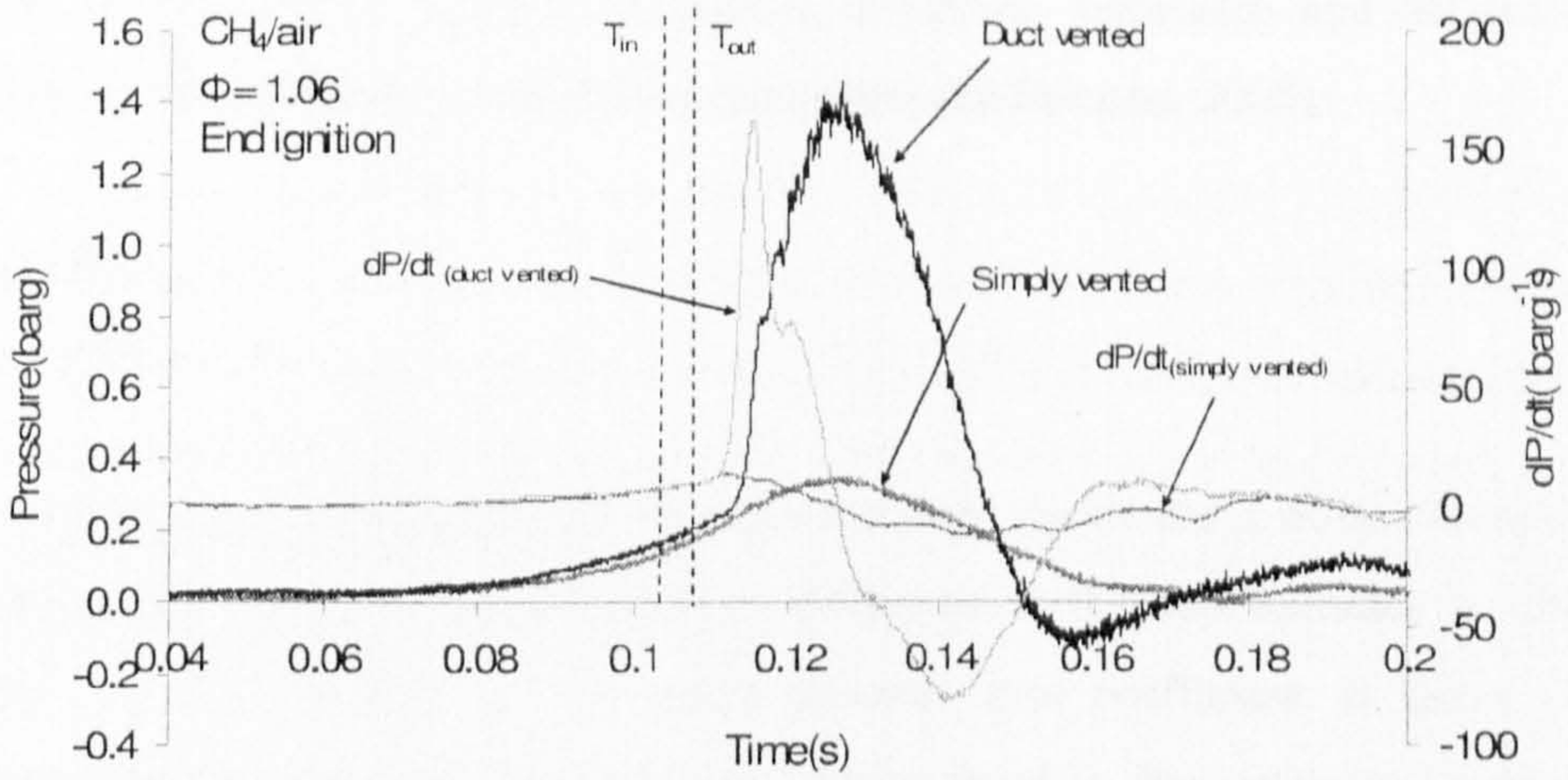

Figure 5.1 Pressure-time histories for simply vented and duct vented explosion for methane/air at $\Phi = 1.06$ for end ignition (initially open venting). dP/dt traces were given for both cases.

In order to get insight about the mechanism of vented duct explosion, the flow and combustion dynamic is presented in Fig. 5.2. Again, the peak overpressure, P_{max} at P_{vessel} occurs after the flame has exited the vent pipe, and it happened to all explosions with or without the vent bursting pressure, P_v observed from the experiments. The peak pressure does not occur when the flame is in the duct as postulated by Lunn et al (Lunn, Crowhurst and Hey, 1988). After the slow, laminar phase of flame propagation in the vessel, the flame enters the duct ($t = t_{in}$) which was followed by a sudden increase in pressure at the duct inlet caused by a very fast propagating flame in the duct (S_{flame}= 350 m/s). This fast flame and associated sonic flow condition encounters the strong turbulence field a few diameter of the vena contracta which leads to a subsequent violent combustion or known as burn-up. The burn-up phenomena or known as secondary explosion has been investigated by Bartknecht (Bartknecth.W, 1981), Ponizy and Leyer (Ponizy and Leyer, 1999a, 1999b) and Molkov et al (Molkov, Dobashi, Suzuki and Hirano, 1999). They identified the burn-up phenomena and deduced that the flow reversal resulting from the action is the main mechanism responsible for the increased reaction rate in the vessel.

This strong combustion inside the duct causes the massive reversal of the pressure (negative pressure drop) towards the test vessel and this marked as $\Delta P_{2\text{-}3}$. This flow pattern is associated with flow pressure (energy) losses which are characteristic of the geometry and expressed in terms of the pressure loss coefficient, K as been shown by

Ferrara et al (Ferrara, Willacy, Phylaktou, Andrews, Benedetto and Mkpadi, 2005, Ferrara, Willacy, Phylaktou, Andrews, Benedetto and Salzano, 2005)

$$K = \frac{\Delta P}{\frac{1}{2}\rho S g^2} \tag{5.5}$$

The pressure loss, ΔP is measured between the main vessel and a point downstream of the disturbance. In this case, the pressure difference at the duct entrance is 150 mbar, marked as $\Delta P_{2\text{-}3}$ in Fig.5.2. The entry pressure loss coefficient is fairly constant (characteristic for the geometry) and for a large vessel to duct ratio (as in the present study), it is of the order of 0.5 (Franzini and Finnemore, 1994). The maximum value of this pressure difference relating to the induced unburned gas flow was measured just prior to the flame entry into the duct pipe, i.e. to the left of the 'T_{in}' dashed line in Fig. 5.2. Substituting 150 mbar into Eq. 5.5 using density of ρ = 1.2 kg/m^3 (ignoring any small pressure rise and any compressibility effects), the calculated unburnt gas flow velocity is around 230 m/s. If this calculation is compared to the flame speed inside the duct of 350 m/s, the calculated S_g is 280m/s ($S_g = 0.8\ S_{flame}$). This means that there is a very large flow velocity into the duct pipe and thus will generate a very turbulent flow field within the duct.

This abrupt negative pressure occurred in a short duration about t ~ 6 ms but have a dramatic effect on the combustion taking place inside the vessel. It prevents further outflow of gases from the explosion and at the same time it increase the combustion rate (indicated by high dP/dt as shown in Fig.5.1) by promoting increased turbulence (by the intense backflow into the vessel) and by the interaction of the shock/pressure waves with the flame front as the flame exits the duct. Consequently, these situation gave a rapid pressure rise inside the test vessel as shown by P_{vessel} traces in Fig. 5.2 and similar effect have also been described by others (Ferrara, Willacy, Phylaktou, Andrews, Benedetto and Mkpadi, 2005, Ferrara, Willacy, Phylaktou, Andrews, Benedetto and Salzano, 2005, Molkov and Nekrasov, 1981, Ponizy and Leyer, 1999a, 1999b)

Positive pressure drops were then restored and venting of the explosion gases continued. A pressure difference of >1 bar was established between the vessel and the receiver (i.e. the dump vessel) and this generated sonic venting conditions in the vent. After this the

duct flow can only increase its mass flow by increasing the vessel pressure, as the mass flow rate in sonic venting is a linear function of the upstream vessel pressure. The action of the vent burst pressure is to stop any flow in the duct prior to the vent bursting. The flame propagation inside the vessel will be longer and the time between the vent bursting and a flame entering the duct will be shorter. The effect of this is investigated in the present work, as it is not clear whether this will be beneficial or lead to further increases in the overpressure. For very large vent burst pressures it is anticipated that the higher jet velocities and their sudden generation when the vent cover bursts will generate more turbulence in the duct and higher duct velocities will result with consequently higher overpressures.

The ignition position clearly has not fundamental influence on the physics of the duct vented explosion, not does the static vent burst pressure, and although both do in general increase the peak overpressure with end ignition having higher overpressures than central and increasing the vent burst pressure usually increases the peak overpressure. However, in some cases this does not occur. It is considered that it is the variation of the mass burn rate and flame speed of the flame approaching the vent that has a strong influence on the vent flow and on the subsequent combustion behaviour. A major feature of the explosions is that there are substantial proportions of the original flammable mixture in the test vessel after the flame has exited the vent duct. This is larger for central ignition than for end ignition. It will be shown that the initial vent flow reaches sonic conditions and hence the vent pipe is choked. Principally, the vent flow is a linear function of the internal vessel pressure and from the relationship, the internal vessel pressure increases until the mass of vented gases reduced the vent flow to subsonic and lower pressure loss occur.

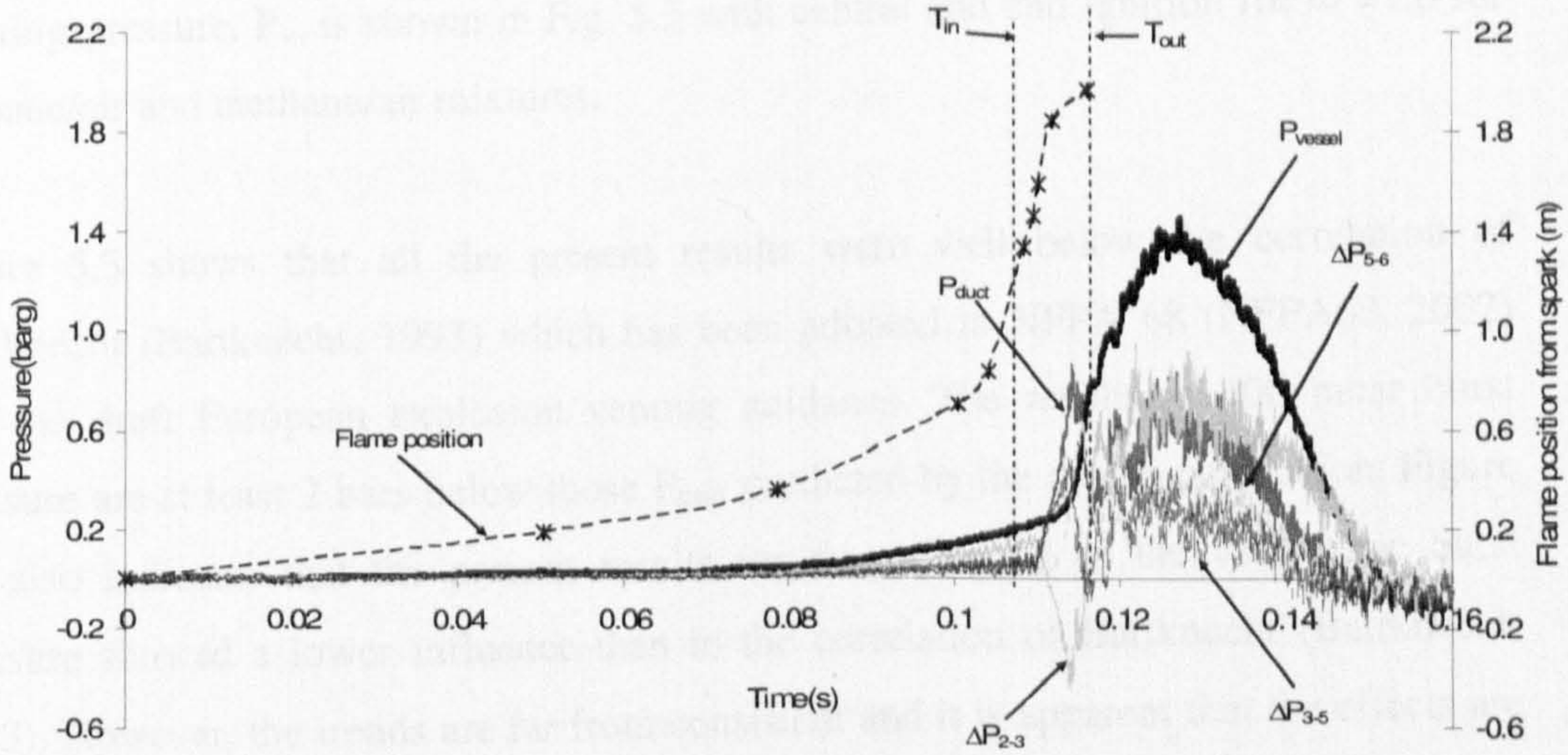

Figure 5.2 Pressure records at selected positions along the test vessel for methane/air at $\Phi = 1.06$ for end ignition. $\Delta P_{2\text{-}3}$ is the pressure difference at the vent entrance, $\Delta P_{3\text{-}5}$ is pressure difference inside the pipe and $\Delta P_{5\text{-}6}$ is the duct exit pressure loss. T_{in} and T_{out} indicate the time flame enters and leaves the duct respectively

5.1.2 The influence of static bursting pressure, P_v on maximum pressure, P_{max}

As been discussed in detail in Chapter 4 previously, the presence of vent generates a pressure wave which interacts with the flame front to distort it and hence increase its surface area and mass burning rate. In this manner, the initial flow of gases into the duct will be larger than for an initially open vent. These combined effects of turbulence and pressure waves created by the vent bursting result in acceleration of the flame prior to the vent duct and also increase the flow velocity, turbulence and flame speed in the vent duct. Tests with ducted explosion vents generally display Helmholtz oscillations, that is the pocket of burned gas within the vessel undergoes bulk motion towards and away from the vent opening, due to the mass of the duct contents and the compressibility of the gas in the primary enclosure that acts as a spring (McCann, Thomas and Edwards, 1985).

In order to investigate the influence of the P_v on P_{max}, four different vent covers which P_v ranged between 0 to 500 mbar were used. Comparison results between open venting and closed venting was also studied to understand the physics of vented explosion mechanism on each cases. The variation of the maximum over pressure, P_{max}, with static

bursting pressure, P_v, is shown in Fig. 5.3 with central and end ignition for Φ =1.0 for propane/air and methane/air mixtures.

Figure 5.3 shows that all the present results were well below the correlation of Bartknecht (Bartknecht, 1993) which has been adopted in NFPA 68 (NFPA68, 2002) and the draft European explosion venting guidance. The results at 100 mbar burst pressure are at least 2 bars below those P_{max} predicted by the design correlation. Figure 5.3 also indicates that the present results for the influence of the vent static burst pressure showed a lower influence than in the correlation of Bartknecht (Bartknecht, 1993). However, the trends are far from consistent and it is apparent that the effects are different for propane and methane as well as for end and central ignition.

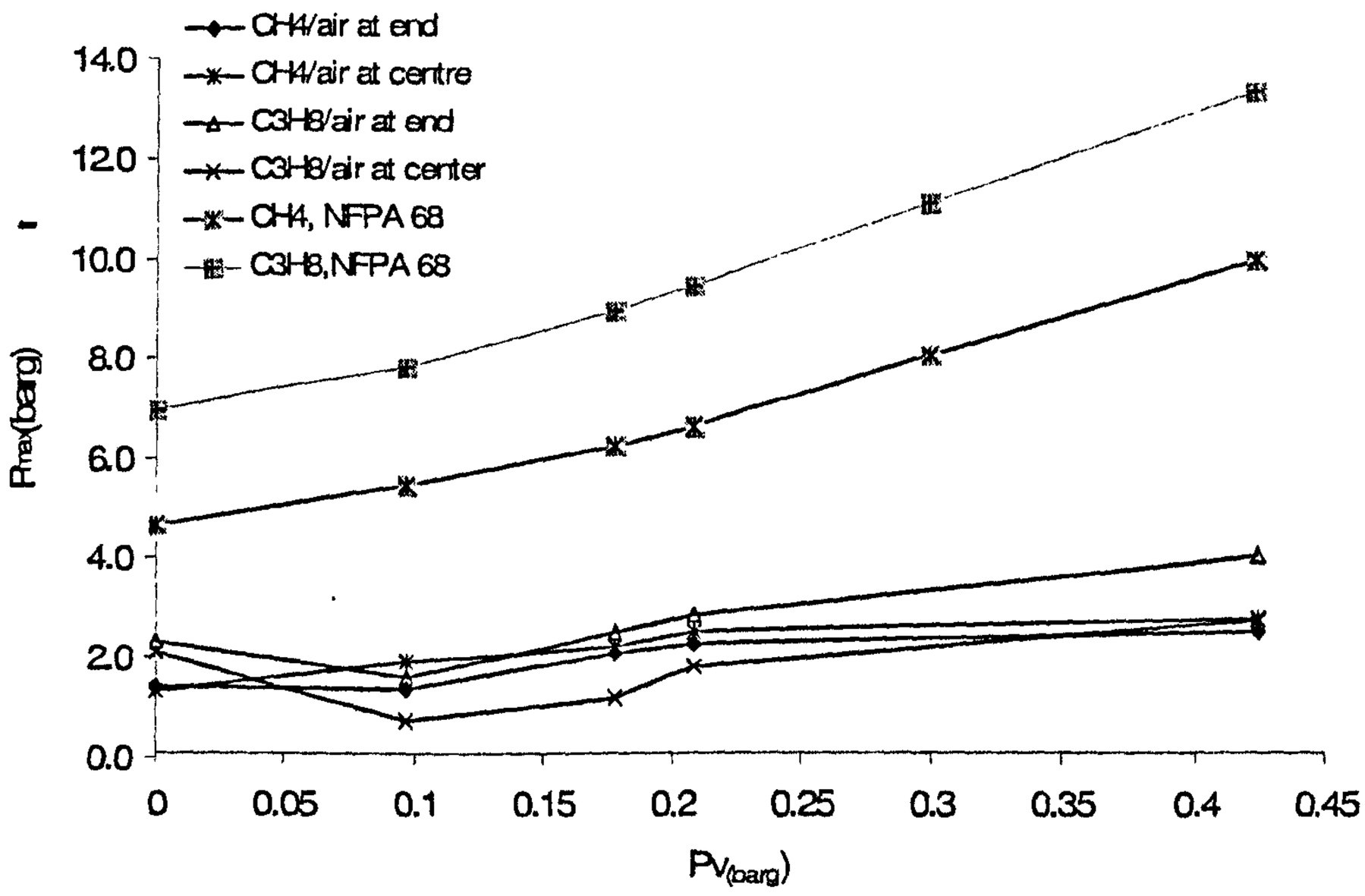

Figure 5.3 P_{max} v P_v on stoichiometric propane/air and methane/air for 1 m length duct.

There are several unusual features in the results. There was a decrease in P_{max} with P_v for propane up to a P_v of 180 mbar. Completely different trends for methane than for propane were found with central ignition worse for methane than for propane. The results with no static vent burst pressure and an initially open vent (Ferrara, Willacy, Phylaktou, Andrews, Benedetto and Mkpadi, 2005, Ferrara, Willacy, Phylaktou, Andrews, Benedetto and Salzano, 2005) showed different trends to those with 100 mbar vent burst pressure in relation to the sensitivity of P_{max} to the ignition position. This was

much larger with a static vent burst pressure for propane and the effect is reversed for methane once a vent is in position. None of these effects are reflected in any vent guidance (NFPA68, 2002) or have been reported by others.

Figure 5.3 also shows that the influence of P_v on P_{max} for methane/air explosion was small for end and central ignition and this behaviour was similar to initially open vent ignition (Ferrara, Willacy, Phylaktou, Andrews, Benedetto and Mkpadi, 2005, Ferrara, Willacy, Phylaktou, Andrews, Benedetto and Salzano, 2005). This trend was also apparent for stoichiometric propane/air with central ignition. However, propane/air with end ignition showed a much larger influence of P_v and for all cases the effect of P_v on P_{max} below 220 mbar was much more complex than a linear constant dependence on P_v.

For hydrogen/air and ethylene/air test, the comparison with the NFPA 68 (NFPA68, 2002) was not possible to perform at equivalence ratio of 1.0 as they showed a deflagration-like-detonation behaviour at $\Phi = 0.57$ for hydrogen/air and $\Phi = 0.8$ for ethylene/air and no tests are allowed to perform if P_{max} exceeded 10 bars. Since K_G values provided by NFPA 68 are given at $\Phi = 1$, calculated K_G at different concentrations is derived using the relation between K_{st} or K_G as a function of burning velocity, S_u (Kumar, Bowles and Mintz, 1992),

$$K_G = 4.84 S_u (P_m / P_i)^{1/\gamma} (P_m - P_i) \qquad (5.6)$$

From Fig. 5.4, it is found that P_{max} on ethylene/air and hydrogen/air are higher at central ignition at all P_v values compared to end ignition which totally disagreed with the discussion on stoichiometric methane/air and propane/air above. At end ignition, it seems that the experimental results were underestimated compared to NFPA 68 but inconsistent trend illustrated for ethylene/air at central ignition. The trend followed the propane/air result for $P_v = 0$ and 98 mbar but P_{max} drastically increased for $P_v = 178$ and at the highest for $P_v = 209$ mbar before decreasing at $P_v = 424$ mbar. This observation is the same for hydrogen/air where central ignition also exhibited higher P_{max} compared to end ignition. There is no significant different of P_{max} observed at $P_v = 98$, 178 and 209 mbar for centrally ignited and only slightly increased of P_{max} at the same P_v for end ignition. Interestingly, P_{max} is almost the same at $P_v = 424$ mbar either for centrally or end ignition.

The possible explanation is since the P_v is high, so that the time the vent cover is removed, the pressure differential across the vent opening is larger and subsequently, the pressure inside the vessel will fall rapidly. In fact, the momentum of the gases being vented may be sufficient to cause the pressure inside the vessel to fall temporarily below atmospheric pressure (Harris, 1983). Molkov (Molkov, 1994) also observed the same trend in his work. At low P_v values (P_v < 0.2 MPa), the peak pressure increases with increasing P_v but not at high P_v (P_v > 0.2 MPa). He explained that at high P_v, the combustion inside the vessel is almost completed and as a consequence, when the vent opens, the turbulent 'micro explosion' in the duct does not have any effect on the turbulence inside the vessel due to lack of 'power'.

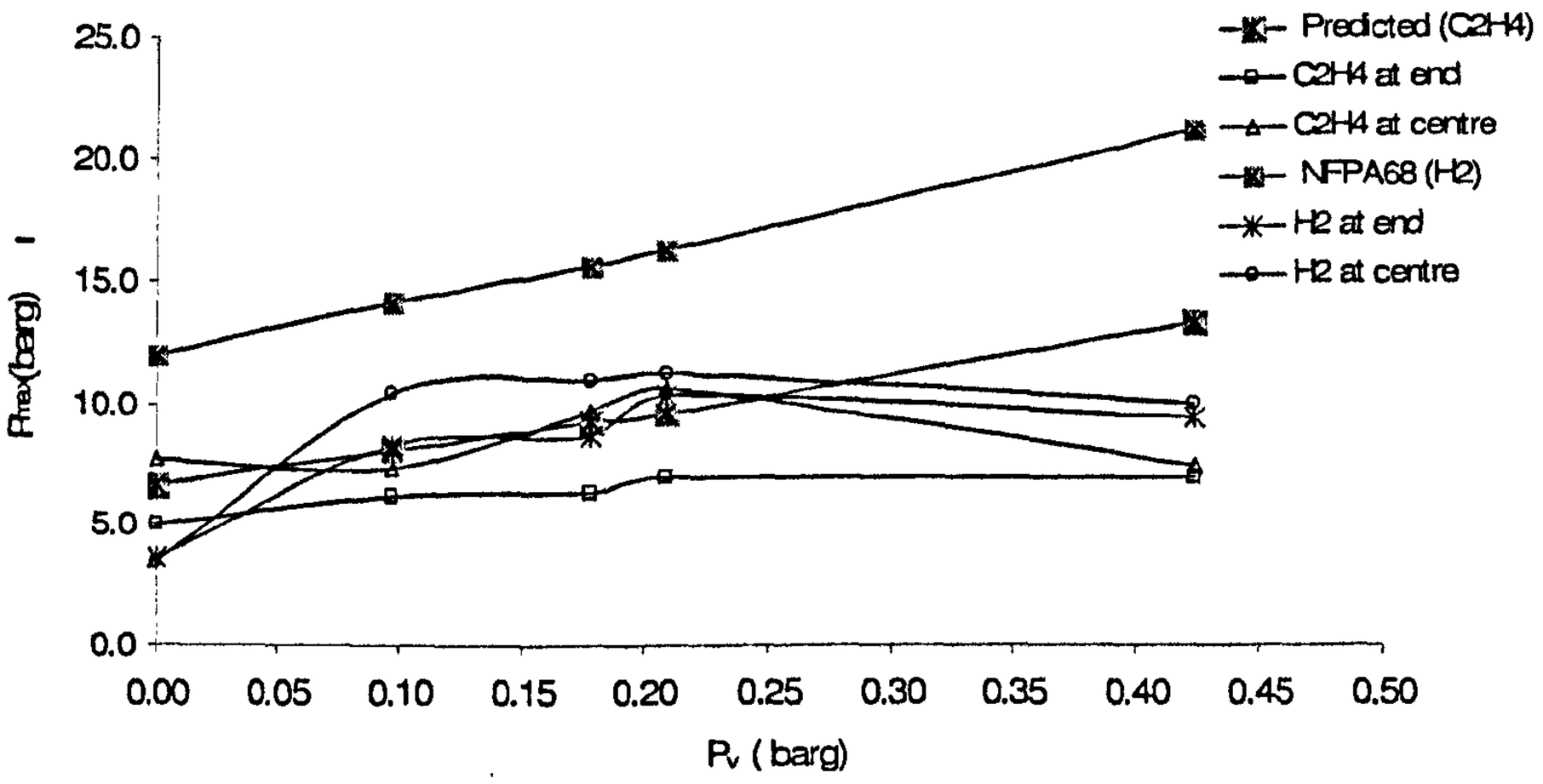

Figure 5.4 P_{max} v P_v for ethylene/air at $\Phi = 0.8$ and hydrogen/air at $\Phi = 0.54$

Whilst at lower P_v, the mixture in the vessel is still not completely burned when the vent opens and this eventually leading a very strong turbulence in the vessel and combustion intensity increased due to the back flow propagation when significant and fast energy release during the explosion in the duct. Bartknecht (Bartknecht, 1993) also reported the same finding on his work where P_{max} was increasing with P_v up to P_v = 500 mbar and decreasing P_{max} observed afterwards before it was increasing again. This peculiar trend was observed at smaller vent area i.e. 0.04 m^2 for 1 m^3 cubic methane/air explosion.

5.1.3 The influence of ignition position

In the previous chapter, the influence of the ignition position has been discussed in details for simply vented explosion which end ignition gave higher P_{max} for lean to stoichiometric hydrocarbon/air mixtures but not in the case of most reactive gas/mixtures. However, there is no existence of external pressure which could give a rise to the internal pressure inside the vessel. In the vented explosion with the relief duct, the interaction of the vessel and the duct pipe is more complex and crucial due to the confined nature of the external explosion (duct). Ferrara et al (Ferrara, Willacy, Phylaktou, Andrews, Benedetto and Mkpadi, 2005, Ferrara, Willacy, Phylaktou, Andrews, Benedetto and Salzano, 2005) investigated the venting in the present vessel with no vent burst pressure. They found that end and centrally ignited propane and methane/air mixtures resulted in approximately the same maximum pressure reached in the main vessel, but with substantially different rates of pressure rise with the end ignited presenting higher rates. This was attributed to more violent secondary explosions in the duct in the end case due to higher terminal flame speeds in the vessel. A simple duct flow pressure loss analysis was used to explain the results, with the critical event being the entry of the flame into the duct, which caused a dramatic increase in the overpressure due to the sudden increases in the unburnt gas velocity ahead of the flame.

From Fig. 5.4 and 5.5, it is obvious that end ignition gave higher P_{max} in methane/air and propane/air at slightly off-stoichiometric mixtures at the presence of vent cover compared to the central ignition. It can be elucidated that the different flame propagation patterns characterizing end and centrally ignited mixtures are responsible for different residual amounts of unburnt gases left inside the vessel at the time the flame reaches the vent and ignites fresh mixtures in the duct. As mentioned in previous chapter, end ignition gives the maximum distance between the flame and the vent. The action of the vent is to distort the flame shape from hemispherical as the flame develops preferentially in the direction of the vent, where the unburnt gases are displaced. The induced flow through the vent duct, ahead of the flame leads to a significant increase in flame speeds and expansion ratio in the main vessel, known as 'suction effect' in previous chapter.

In the previous study (Bradley, Hicks, Haq, Lawes, Sheppard and Woolley, 2003), the influence of flame stretch will also increase the turbulent velocity with a lower value of Lewis, Le and Markstein no, Ma inside the vessel. Explosion flames, particularly in rich hydrocarbon mixtures are conducive to the development of hydrodynamic and thermo diffusive effects. At sufficiently small Markstein number, and particularly when they are negative, the thermo diffusive effects (smaller Lewis no) are no longer stabilizing. Thermo-diffusive instabilities arising from the preferential diffusion of reactants with respect to thermal transport can lead to cellular flame structures that augment flame propagation through an increase in flame surface area (Bradley, Sheppard, Woolley, Greenhalgh and Lockett, 2000). The flame self acceleration occurs after a critical laminar flame propagation distance and the available distance with end ignition is twice `that with central ignition and hence self acceleration is more likely. The net effect of the vent discharge and self acceleration are for the mass burning rate of the flame to rapidly increase due to faster flames in end ignition, rather than due to the larger flame area of the spherical flame with central ignition. Further, from Fig. 5.4 and 5.5, it is worth noting that both figures suggest that the enhanced combustion phase in the end ignition is of very short duration while it stands for a quite longer time in centrally ignited case. The latter case confirmed the hypothesis stated by Ferrara et al (Ferrara, Benedetto, Salzano and Russo, 2006). They said that in case of central ignition, there is an indication of higher quantity of residual unburned mixture in the vessel whereas almost complete combustion occurred in the case of end ignition that eventually leads to higher peak pressure.

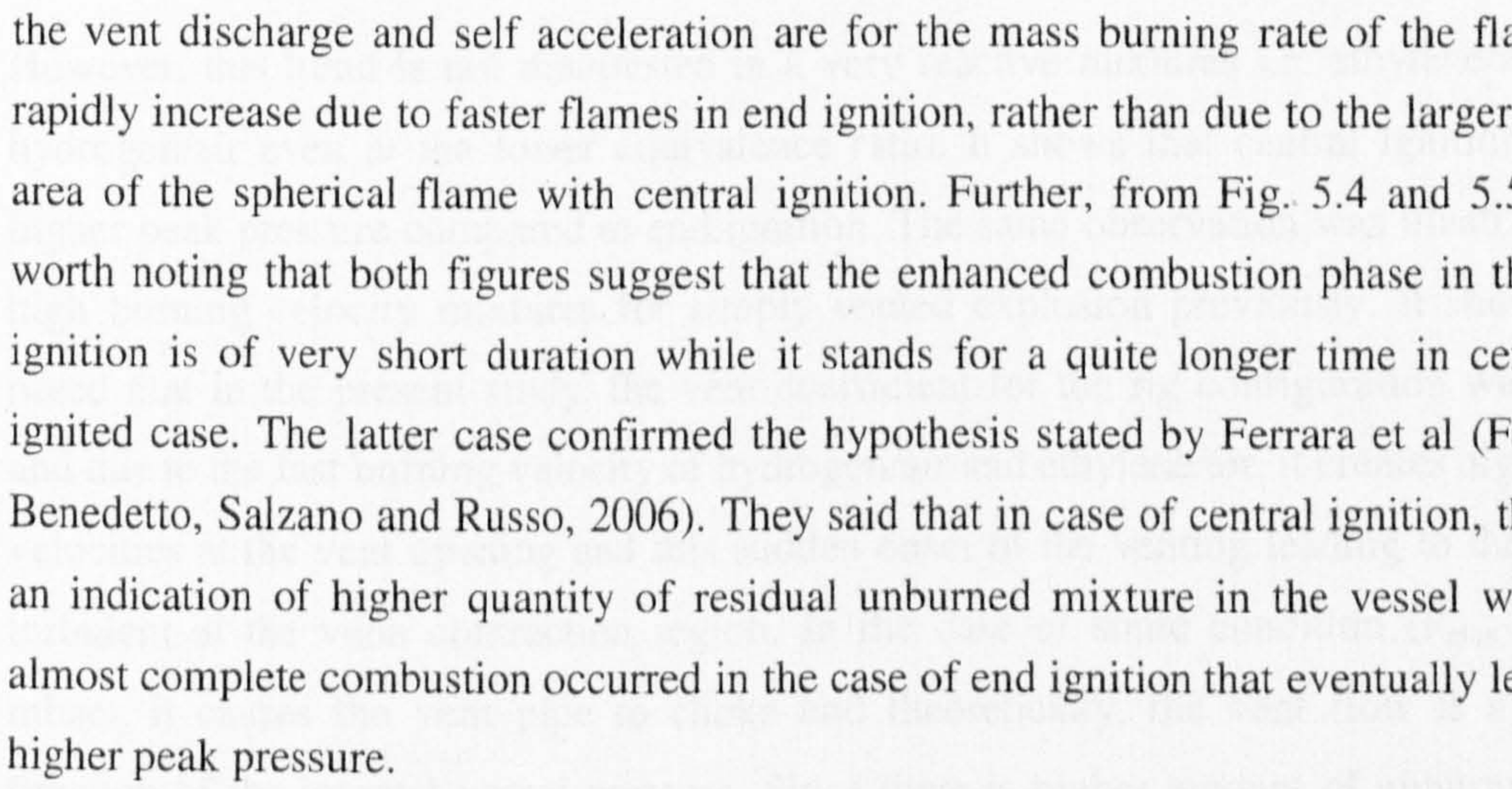

Figure 5.4 Methane/air at P_v = 178 mbar

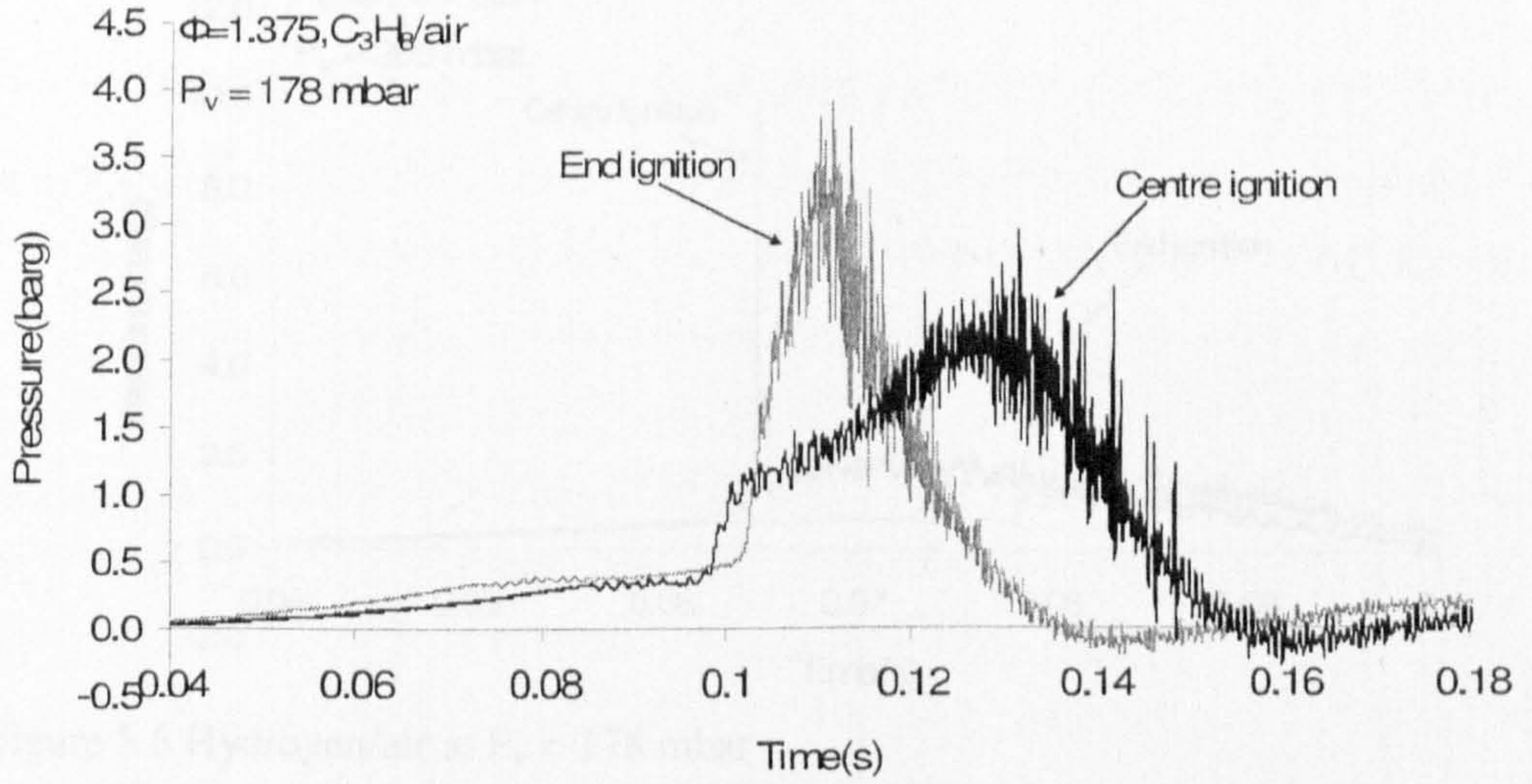

Figure 5.5 Propane/air at P_v = 178 mbar

However, this trend is not manifested in a very reactive mixtures i.e. ethylene/air and hydrogen/air even at the lower equivalence ratio. It shows that central ignition gave higher peak pressure compared to end ignition. The same observation was illustrated at high burning velocity mixtures for simply vented explosion previously. It should be noted that in the present study, the vent coefficient for the rig configuration was 16.4 and due to the fast burning velocity of hydrogen/air and ethylene/air, it creates higher jet velocities at the vent opening and this sudden onset of the venting leading to the rapid turbulent at the vena contraction region. In the case of sonic condition (P_{max} > 900 mbar), it causes the vent pipe to choke and theoretically, the vent flow is a linear function of the internal vessel pressure. Since there is higher amount of unburnt gases left in the vessel for the central ignition in respect of end ignition, it increases the combustion rate due to the subsequent turbulisation (by the physical back-flow into the vessel) and by the interaction of the shock pressure waves with the flame frame. Indeed, the entrainment of fresh gas pockets operated at high velocity hot gases is well known to originate a violent ignition (Bradley, Emerson and Gu, 2003, Lee and Guirao, 1982) and under certain conditions, leading to detonation as observed in Fig. 5.6 and 5.7.

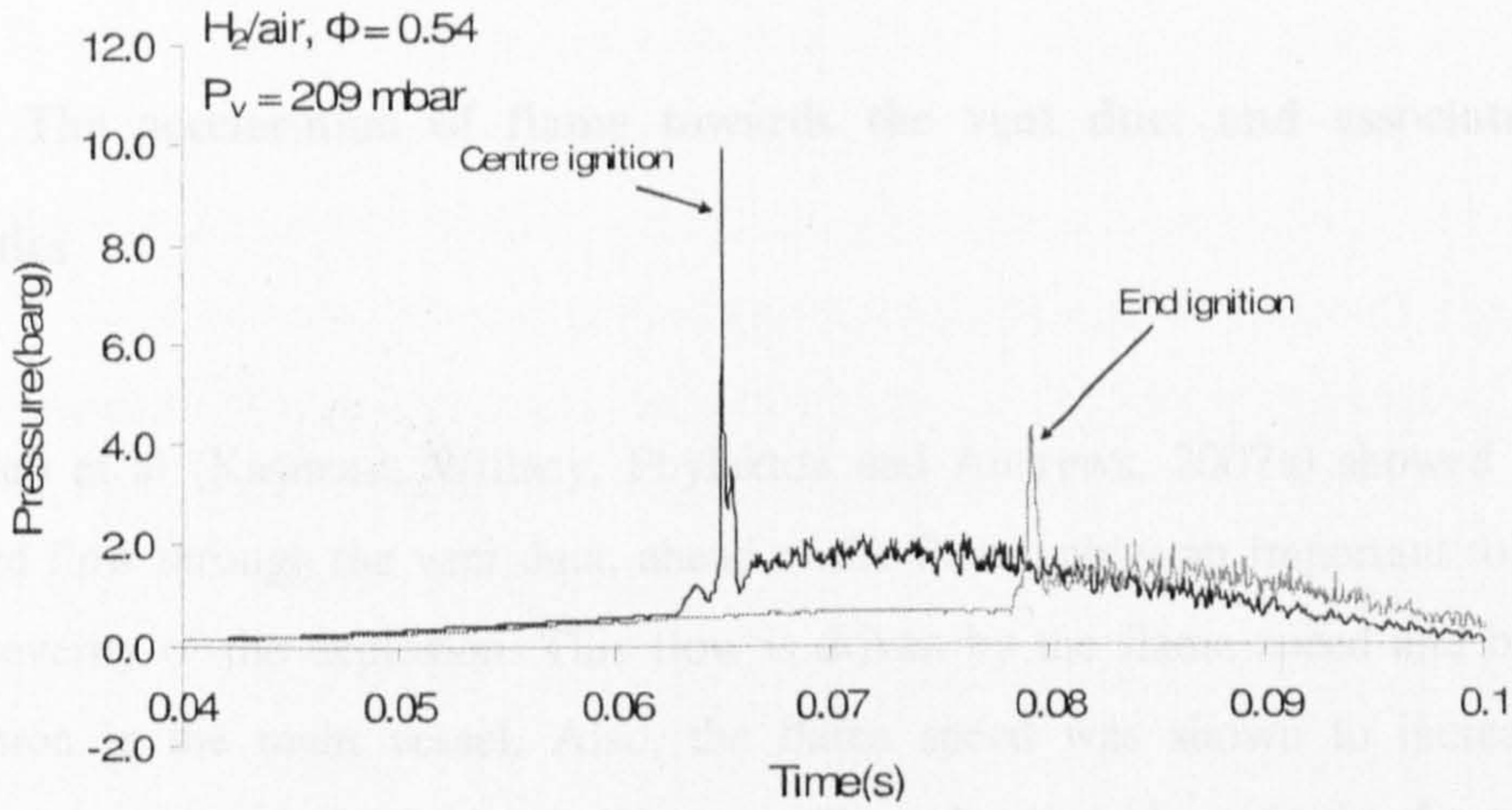

Figure 5.6 Hydrogen/air at P_v = 178 mbar

It can be concluded that for high burning velocity mixtures i.e. ethylene and hydrogen, central ignition showed much larger influence of P_v on P_{max}, contradicting with the results obtained for hydrocarbon/air. As the reactive mixtures concentration increases, the combustion time become shorter and less time is available for gases inside the vessel to flow out before the combustion is completed, thereby reducing the effectiveness of venting (Kumar, Dewit and Greig, 1989). The combustion times for central ignition are roughly half of the end ignition and this explained the obtained results.

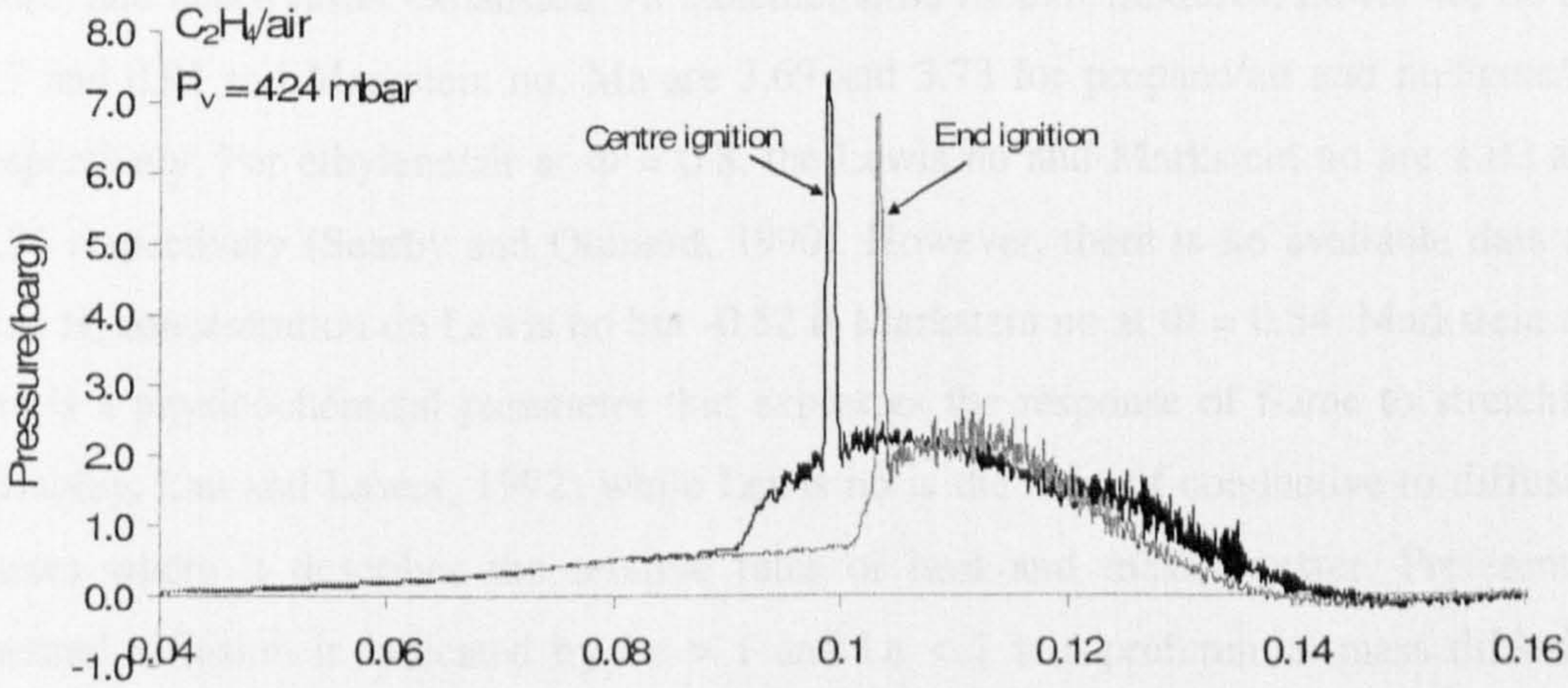

Figure 5.7 Ethylene/air at P_v = 424 mbar

5.1.4 The acceleration of flame towards the vent duct and associated vent velocities

Kasmani et al (Kasmani, Willacy, Phylaktou and Andrews, 2007a) showed that the induced flow through the vent duct, ahead of the flame, plays an important role in the final severity of the explosion. This flow is driven by the flame speed and burnt gas expansion in the main vessel. Also, the flame speed was shown to increase with distance from the ignition spark due to self-acceleration through the formation of cellular flame. The self-accelerating mechanism has been detailed in Chapter 4.

In a compact vessel with L/D = 2 (the limit of application of the Bartknecht venting data (Bartknecht, 1993, Bartknecth.W, 1981)), end ignition gives the maximum distance between the flame and the vent. The action of the vent is to distort the flame shape from hemispherical as the flame develops preferentially in the direction of the vent (a suction effect as shown in Fig. 5.8 by Cooper at al (Cooper, Fairweather and Tite, 1986)), where the unburnt gases are displaced. The flame progressively stretches towards the vent and this will result in a long cylindrical flame. The data listed in Table 5.1 (refer to S_f inside the vessel) suggested that a much longer flame area (reaction front) and hence faster expansion. At stoichiometric fuel/air mixtures, Lewis no, Le are 1.7 and 0.91 and Markstein no, Ma are 3.69 and 3.73 for propane/air and methane/air respectively. For ethylene/air at $\Phi = 0.8$, the Lewis no and Markstein no are 1.02 and 4.34 respectively (Searby and Quinard, 1990). However, there is no available data for lean H_2 concentration on Lewis no but -0.82 is Markstein no at $\Phi = 0.54$. Markstein no, Ma is a physicochemical parameter that expresses the response of flame to stretching (Bradley, Lau and Lawes, 1992) while Lewis no is the ratio of conductive to diffusive fluxes where it describes the relative rates of heat and mass transfer. Preferential thermal diffusion is indicated by Le > 1 and Le < 1 is a preferential mass diffusion (Clarke, 2002). Lower value of Markstein no with Le < 1 indicates the propensity of the flame become unstable and prone to cellular instability and self-fragmentation (Bradley, Hicks,Haq, Lawes, Sheppard and Woolley, 2003). The net effect of the self-acceleration and vent discharge 'suction' effect is for the mass burning rate of the flame to increase due to faster flames. This shows greater for end ignition as the flame travel distance to

the vent is twice that for central ignition. The increase in flame surface area due to the 'suction' effect and longer flame travel distance are to compensate for the lower initial mass burning rate of end ignition with its 50 % reduced flame surface area and heat losses to the end flange. The net effect from this behaviour is higher overpressure with end ignition for methane/air and propane/air mixtures but not in the case of reactive mixtures i.e. ethylene and hydrogen as shown in Table 5.1.

In Table 5.1, simple momentum conservation and mass continuity were used to calculate the downstream duct pipe velocity, S_g prior to the flame entry to the pipe. Assuming ideal incompressible flow within a duct with no wall friction, mass continuity gives,

$$\dot{m} = \rho U_1 A_1 = \rho U_2 A_2 \tag{5.7}$$

where $\dot{m}$ is the mass flow rate, A is the duct cross-sectional area and U is the flow velocity. Subscripts 1 and 2 refer to the duct measurement at two different point positions. The gas velocity is then given by,

$$S_g = \frac{\dot{m}}{\rho A} \tag{5.8}$$

As the area of the circular pipe is a function of the diameter, we can reduce the calculation further by,

$$S_g = S_{gvessel}\left(\frac{A_1}{A_2}\right) \tag{5.9}$$

However, Eq 5.9 assumed that the flame behaves as a piston, which is not the reality as the flame is 'pear shaped and not flat' (Ellis, 1928). When compared to the prediction using the loss pressure calculation using Eq. 5.5 previously, the resulted gas velocities from Eq. 5.9 are very high and greater than sonic (in some cases for propane/air and methane/air at high P_v but most cases for ethylene/air and hydrogen/air mixtures).

The use of adiabatic expansion, E assumes that the reaction was instantaneous; with no heat loss to the vessel walls and that the flame front that delineated the unburnt reactants from the products of combustion was of negligible thickness.

Mach number, Mach can be used to stipulate the flame propagation inside the vessel which correspondent to the maximum generated overpressures. The equation given as,

$$Mach = \frac{S_f}{c_u} \tag{5.10}$$

where c_u is the speed of sound (m/s) which calculated using,

$$c_u = \sqrt{\frac{\gamma RT}{M}} \tag{5.11}$$

where γ is the ratio of the specific heat at constant pressure and volume and taken as 1.4 for air, R is the molar gas constant, T is the temperature (K) and M is the molecular mass of the substance. The Mach no resulted from Eq. 5.10 is 0.5 to 2.0 which suggests that the sonic flow been experienced inside the vessel towards the vent and this condition agreed with the high flame propagation velocities. This high flame propagation velocities correspond with the lower flame residence time which illustrates the cooling of burnt gases products immediately behind the flame front was limited.

Table 5.1 also indicates the little change in the peak final flame speed with P_v but it should be remembered that the mass burning rate will increase with P_v due to the flame density term. For the highest vent burst pressure, this gives close to a 30 % increase in the mass burning rate when the vent bursts according to the K_{Gvent} values. This does not change the velocity of sound in the vent duct and hence the Mach number is not affected. A method of taking into account the bulk shape of the flame is to look at the rate of change of P_1 with time just prior to the flame entering the duct. This is shown in Table 5.1 with K_{Gvent}. This shows low values for central ignition at low P_v, which increase with P_v to be nearly 16 times that for an open vent for methane/air and 10 times for propane/air. For ethylene/air and hydrogen/air, it is about 2 times and 1.4 times that for an open vent respectively. With end ignition the effect is much lower apart from propane at the highest P_v. This may be due to the greater influence of the increasing

pressure at high P_v for spherical central flame propagation, due to its larger surface area in spite of the lower flame acceleration.

The faster mass burn rate approaching the vent as P_v increases causes sonic flow in the vent and hence choked flow is experienced. This prevents there being any outflow from the duct until the pressure has risen in the vessel to drive the burnt gases out. There then follows a period of mixed burnt gas and unburnt gas venting with micro explosions and detonations (propane/air rear ignition at P_v = 427 mbar and most cases in ethylene/air and hydrogen/air) in the vent duct. This has been detailed in section 4.2.

Figure 5.9 - 5.10 show the present flame speed measurements were considerably higher than the values expected on the basis of the development of cellular flames, for all studied fuel/mixtures in this present work. As been discussed in previous chapter to confirm the occurrence of self-acceleration of the flame, the same method was applied based on the K_{Gmax} adopted from NFPA 68. This enables a prediction from the NFPA 68 data to be made of the self-acceleration effect on flame speed and this is shown in Fig. 5.9 and 5.10.

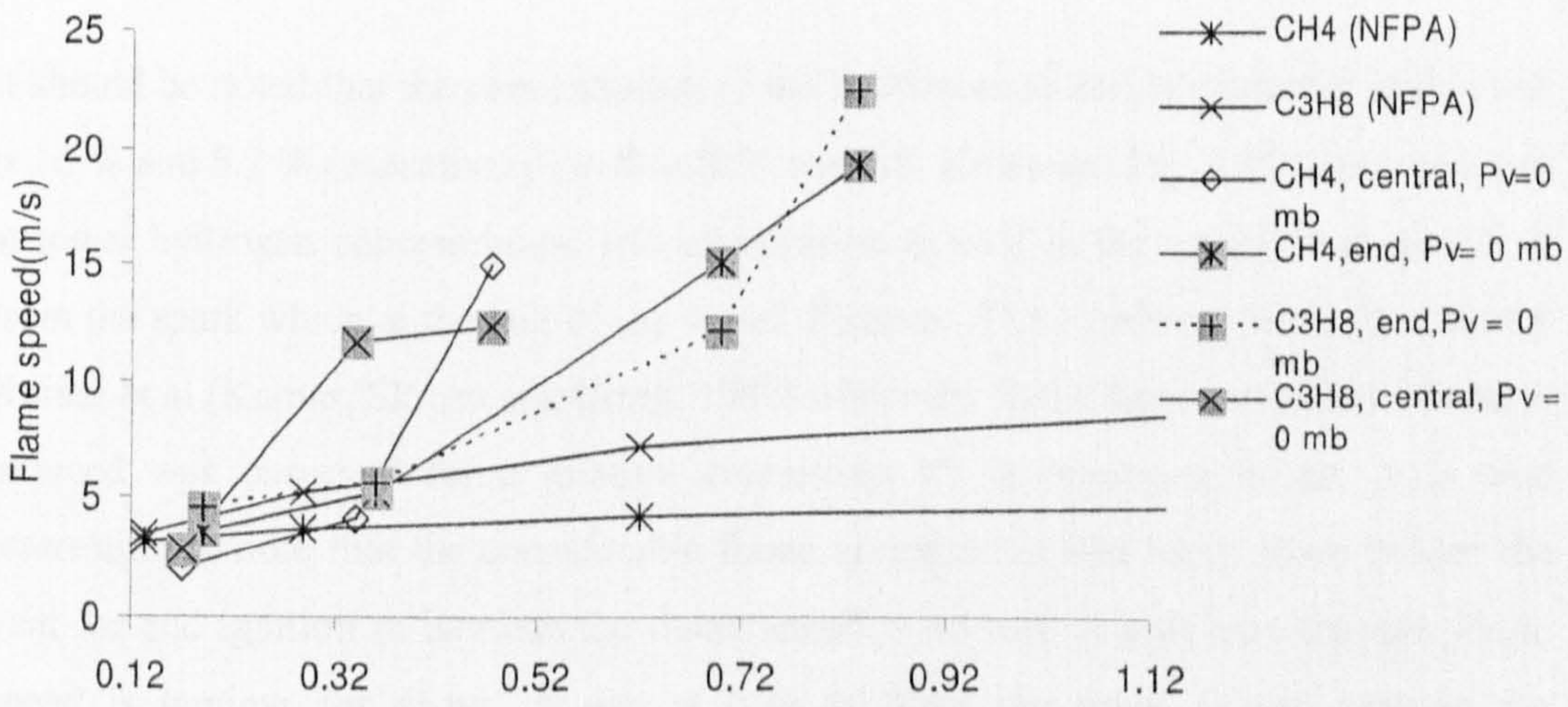

Figure 5.9 Flame speed a function of the flame distance from the spark for $P_v = 0$ for methane/air and propane/air. $\Phi = 1.0$ for both gas/mixtures.

Figure 5.9 showed that the present flame speed measurements were considerably higher then the values expected on the basis of the development of cellular flames, for both

methane and propane. However, up to a flame distance from the spark of 0.35m, Fig. 5.9 shows that the flame speed increase with distance was roughly that expected from the development of cellular flames with flame speeds of 4 and 5 m/s for methane/air and propane/air respectively. For central ignition, the flame speed increases to about 12 m/s for methane and propane at close to 0.5m from the spark. For end ignition the large flame propagation distance gave a flame speed increase to about 20 m/s. This is twice the 10 m/s maximum flame speed recorded by Bradley et al (Bradley, Cresswell and Puttock, 2001) for self acceleration of flames at a flame radius of 4 m. The increase in flame speed was due to the 'suction' action of the vent outflow, as there was no vent cover bursting effect to create pressure waves or turbulence.

At the K of 16.4, there was a high velocity created in the unburnt gas flow through the vent and this induces movement in the unburnt gas upstream of the vent, leading to flame acceleration towards the vent. The effect is to distort the flame into a pear shape, with the apex of the pear passing through the vent first. This effect is similar for methane and propane and the difference in the peak flame speeds were not large, whereas they should have been large if flame instabilities were the cause of the acceleration.

It should be noted that the concentration of the hydrogen/air and ethylene/air in this test is 16 % and 5.2 % respectively i.e. $\Phi = 0.54$ and 0.8. However, Fig. 5.10 illustrated that at lower hydrogen concentration, self-acceleration existed in the vessel at about 0.5 m from the spark which at the half of the vessel diameter. This confirms the work done by Kumar et al (Kumar, Skraba and Greig, 1987) where the flame front instability was self-induced was observed for a mixture containing 15 % hydrogen in air. It is also interesting to note that the considerable flame acceleration had taken place before the vent for end ignition to increase the flame speed to 43 m/s. It also seen that the flame speed is laminar for about 6 m/s at 0.36 m from the spark at end ignition for ethylene/air and hydrogen/air and this trend of the laminar flame speed at this point also been observed in methane/air and propane/air mixtures in Fig.5.9. Again, there is about 1.5 to 2 times increase in flame speed of hydrogen/air compared to ethylene/air, propane/air and methane/air for both ignitions. For central ignition, the maximum flame speed is about 25 m/s for hydrogen/air and 17 m/s for ethylene/air.

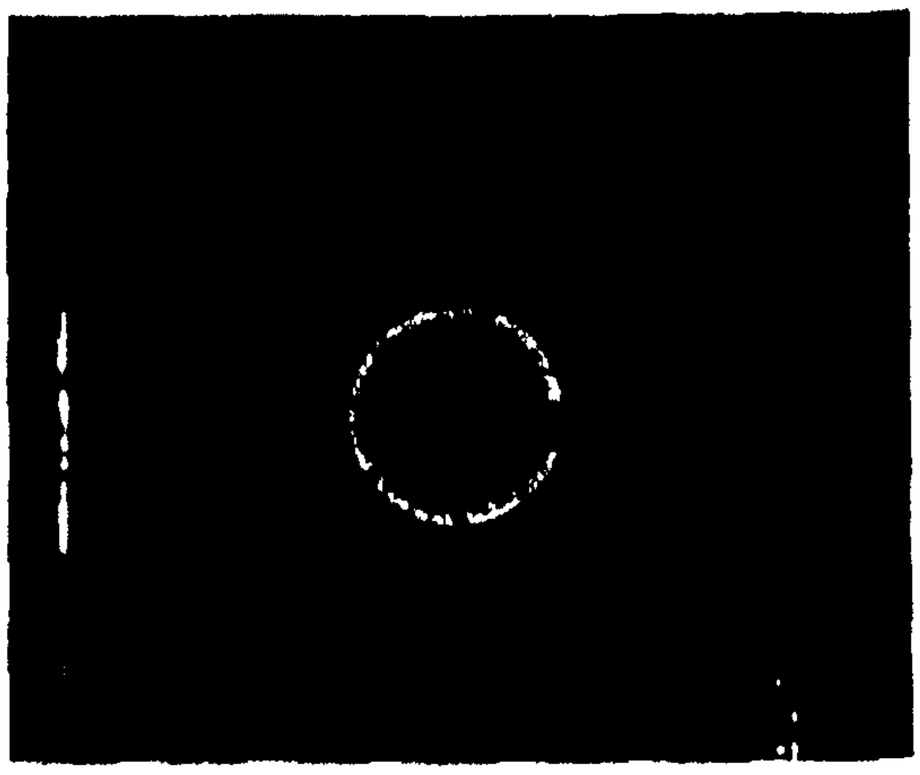

Fig. 2a.

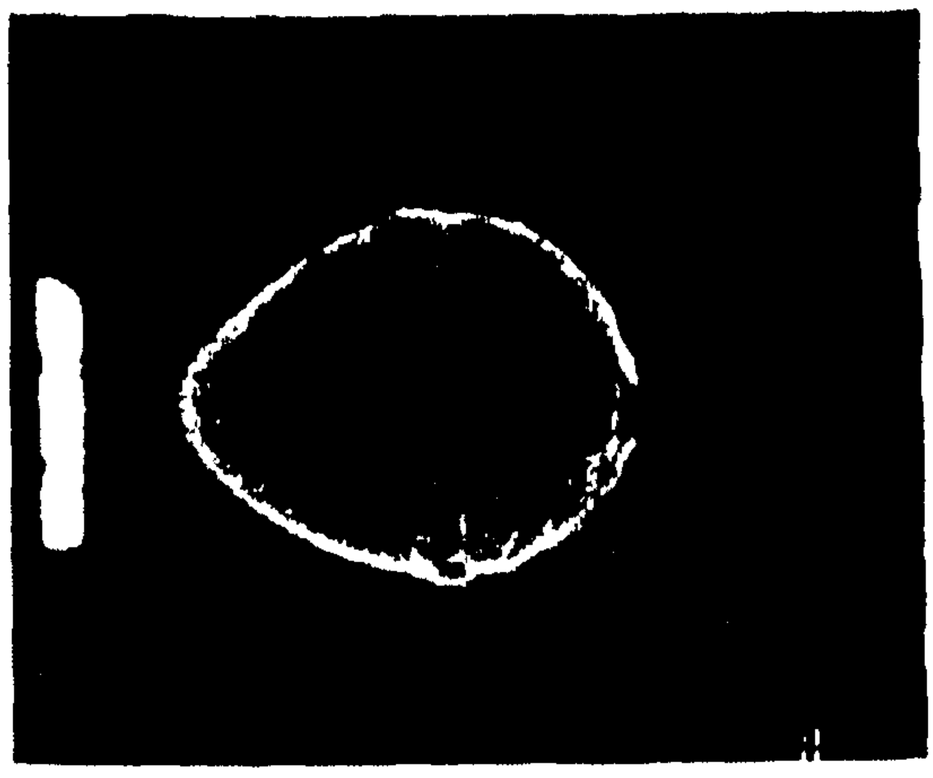

Fig. 2b.

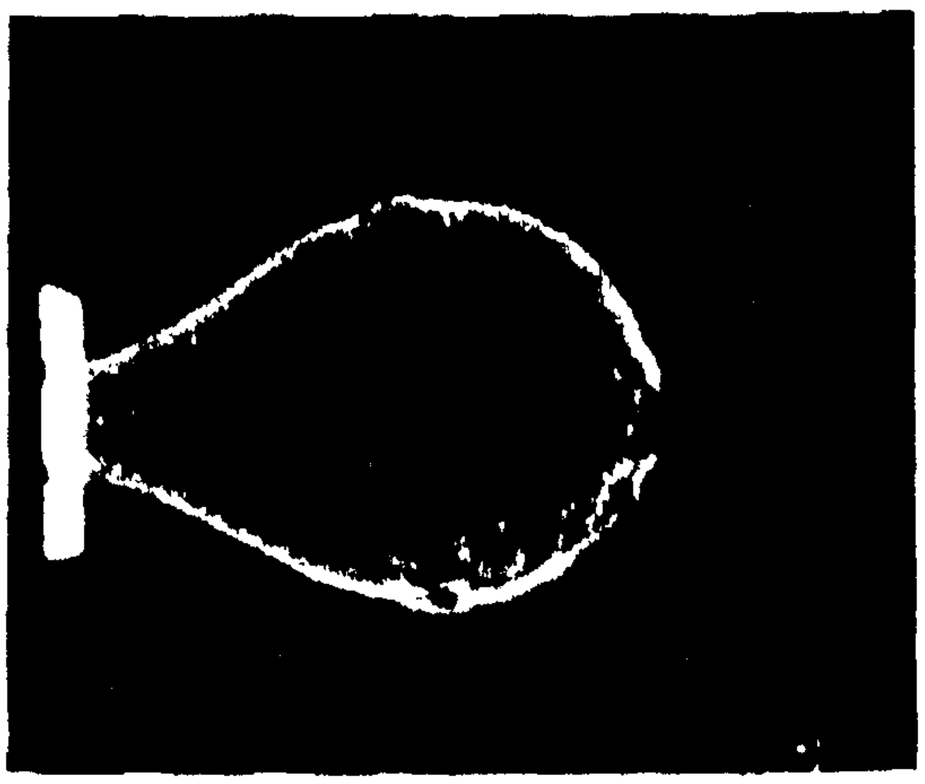

Fig. 2c.

Fig. 2d.

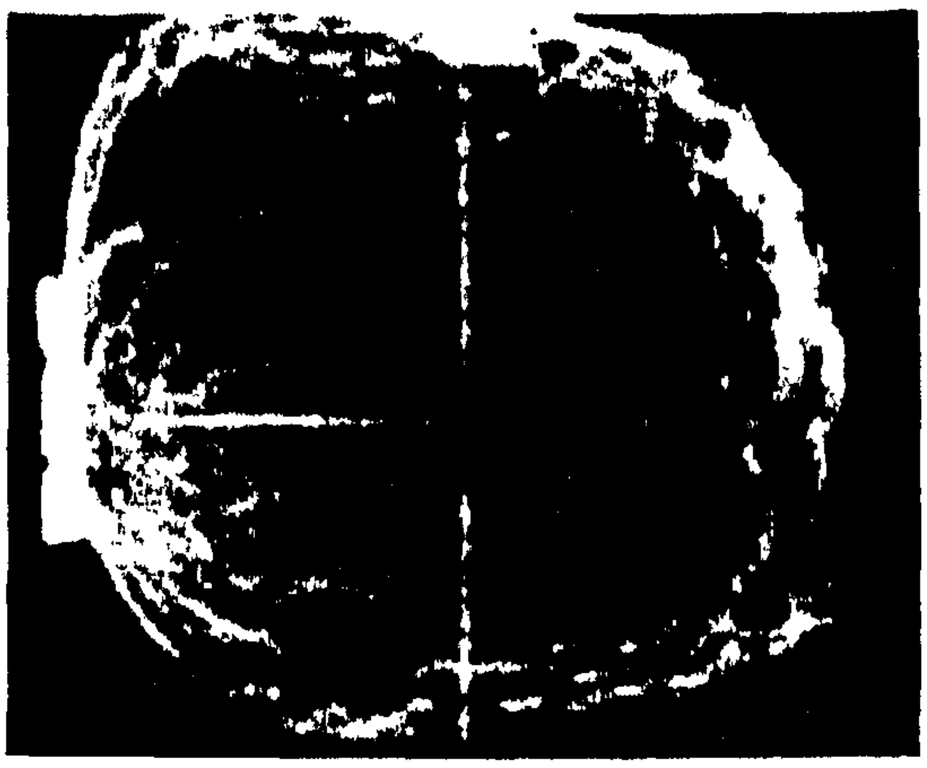

Fig. 2e.

Fig. 2f.

Figure 5.8 Reproduced from Cooper et al (Cooper, Fairweather and Tite, 1986). Flame propagation mechanism at the various phases of a vented explosion.

Table 5.1 Explosion data for 4.0% propane/air, 9.5% methane/air, 5.2% ethylene/air and 16% hydrogen/air mixtures. Flame speed, S_f in the vessel refers to the speed from the spark towards the vent (Tv_4-Tv_2) while flame in the duct is the average value obtained along the duct (T_{out}-T_o).S_t is the turbulent burning velocity as S_f/E where E is the adiabatic expansion ratio. K_G is (dP/dt) $V^{1/3}$ and K_{Gmax} is based on the maximum dP/dt from pressure transducer P_1, which occurs after the flame has exited the duct. K_{Gvent} is based on the rate of pressure rise just prior to the flame entering the duct pipe and is proportional to the mass burning rate upstream of the vent.* Spiking pressure trace

Data for 4.0% propane/air and 9.5% methane/air mixtures

Fuel	Ignition	P_v (barg)	P_{max} (barg)	K_{Gmax}	$K_{G\ vent}$	$S_{f\ vessel}$, m/s	St $_{vessel}$, $=S_f/E$ m/s	S_g $=S_f$ (E-1)/E S_{vessel} m/s	$S_{g.duct}$ = Sg (0.5/0.162)^2 = 9.52 Sg m/s	$S_{f\ duct}$, m/s	Unburnt gas velocity prior to duct entrance Sg_{duct} m/s
C_3H_8	Central	0	2.1	67.3	0.5	10	2.0	8.0	76	171	137
C_3H_8	End	0	2.3	137.4	5.9	37	7.4	29.6	282	227	182
CH_4	Central	0	1.3	63.7	0.3	11	2.2	8.8	84	140	112
CH_4	End	0	1.4	97.1	4.3	19	3.8	15.2	145	159	127
C_3H_8	Central	0.098	0.7	57.9	0.5	20	3.6	14.2	135	61	49
C_3H_8	End	0.098	1.6	105.3	5.1	27	4.9	19.6	187	134	108
CH_4	Central	0.098	1.9	88.3	1.5	16	7.6	30.4	289	156	124
CH_4	End	0.098	1.3	95.9	3.5	24	3.8	15.2	145	105	84
C_3H_8	Central	0.178	1.2	91.8	4.8	24	4.0	16.0	152	225	180
C_3H_8	End	0.178	2.5	150.3	5.5	29	5.7	22.9	218	323	259
CH_4	Central	0.178	2.2	94.7	5.0	25	8.0	31.8	303	250	200
CH_4	End	0.178	2.1	138.0	3.8	27	5.0	19.9	189	179	143
C_3H_8	Central	0.209	1.8	89.5	5.3	20	5.5	21.9	208	237	189
C_3H_8	End	0.209	2.8	201.2	5.5	35	12.4	49.6	472	431	345
CH_4	Central	0.209	2.5	141.5	5.5	22	6.7	26.8	255	257	205
CH_4	End	0.209	2.2	142.7	4.5	24	4.7	18.6	177	135	108
C_3H_8	Central	0.424	2.9 4.0 *6.5	117.0	5.5	30	5.2	20.8	198	216	173
C_3H_8	End	0.424		296.5	5.5	55	20.2	81.0	771	666	533
CH_4	Central	0.424	2.7	109.4	5.5	26	7.9	31.7	302	313	250
CH_4	End	0.424	2.5	190.1	5.5	34	5.5	21.8	208	290	232

Data for 5.2% ethylene/air and 16% hydrogen/air mixtures

Fuel	Ignition	P_v (barg)	P_{max} (barg)	K_G (max)	K_G (vent)	S_f (vessel) m/s	$S_t = S_f/E$ m/s	Sg $=S_f$ (E-1)/E $_{(vessel)}$ m/s	Sg (duct) m/s = Sg (0.5/0.162)^2 = 9.52 Sg	S_f (duct), m/s	Unburnt gas velocity prior to duct entrance $Sg_{(duct)}$, m/s
C_2H_4	Central	0	*7.7	469	2.7	17.1	3.4	13.6	130	181	187
C_2H_4	End	0	*5.0	323	7.9	16.8	3.4	13.5	128	272	331
H_2	Central	0	*3.4	190	11.6	25.2	5.0	20.2	192	227	330
H_2	End	0	*3.5	142	7.9	21.4	4.3	17.1	163	227	208
C_2H_4	Central	0.098	*7.3	502	0.3	11.7	2.3	9.4	89	211	272
C_2H_4	End	0.098	*6.1	364	8.2	17.2	3.4	13.7	131	156	296
H_2	Central	0.098	*9.9	323	6.4	25.9	5.2	20.7	197	453	306
H_2	End	0.098	*4.2	232	4.4	28.5	5.7	22.8	217	243	404
C_2H_4	Central	0.178	*9.7	580	1.8	15.2	3.0	12.1	116	234	385
C_2H_4	End	0.178	*6.2	416	7.3	19.8	4.0	15.8	150	190	404
H_2	Central	0.178	*8.8	354	12.4	27.4	5.5	21.9	209	509	410
H_2	End	0.178	2.8	133	2.0	28.3	5.7	22.7	216	298	435
C_2H_4	Central	0.209	*10.7	650	3.8	15.7	3.1	12.5	119	247	408
C_2H_4	End	0.209	*6.9	480	7.4	22.8	4.6	18.3	174	235	459
H_2	Central	0.209	*9.1	312	13.6	31.5	6.3	25.2	240	544	420
H_2	End	0.209	3.2	181	10.5	30.5	6.1	24.4	232	338	439
C_2H_4	Central	0.424	*7.4	461	5.1	10.0	2.0	8.0	76	252	467
C_2H_4	End	0.424	*6.9	519	7.7	24.2	4.8	19.4	184	243	499
H_2	Central	0.424	*8.9	331	16.5	17.3	3.5	13.8	132	319	453
H_2	End	0.424	2.0	104	5.7	37.2	7.4	29.8	284	341	499

Table 5.1 cont

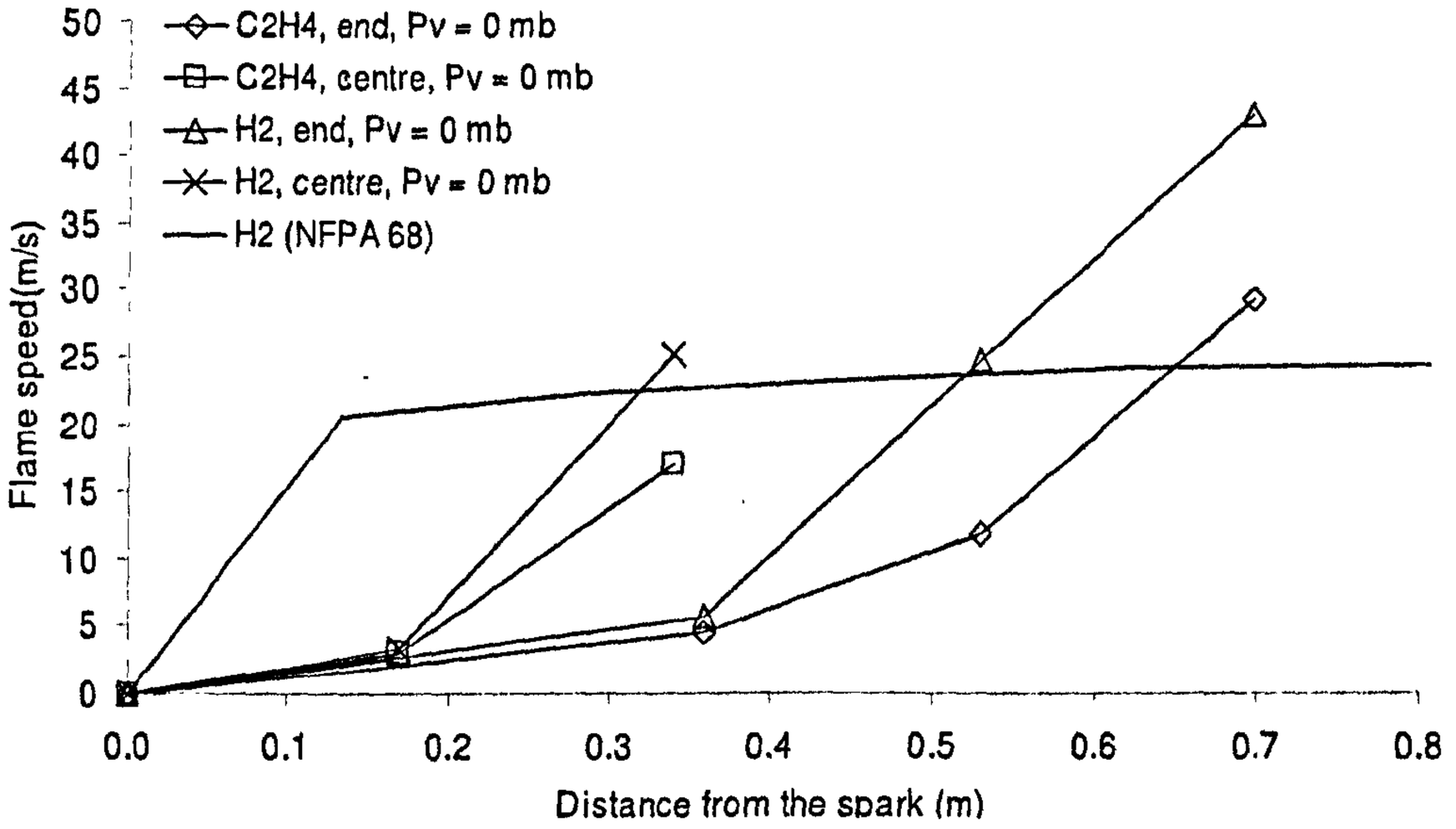

Figure 5.10 Flame speed as a function of distance from the spark for P_v = 0 for ethylene/air (Φ = 0.8) and hydrogen/air (Φ = 0.54). Noted that only hydrogen line for NFPA 68 was drawn as there is no available data for ethylene in the guidance.

To justify the influence of vent cover been placed during the present work, Fig. 5.11 and 5.12 shown the upstream flame speed results from the experimental tests. The mass of the burnt mass at the time of the vent bursting may be calculated from the assumption that the pressure rise at the time of the vent bursting occurs when the burnt mass of gas is $P_v/P_{initial}$, where $P_{initial}$ is the initial pressure of 1 bar atmospheric pressure. If the flame shape is assumed to be a sphere for central ignition and a hemisphere for end ignition and the volume of burnt gas is assumed to be the mass burnt times the unburnt to burnt gas density ratio for constant pressure combustion (7.6 for propane and 7.5 for methane), then the flame radius may be calculated with the further assumption that the flange and spark plug heat losses may be ignored. These predicted flame radius at the point of the vent bursting are shown in Table 5.2.

Table 5.2 Predicted flame radius when the vent burst for gas/air.

Vent burst pressure (mbar)	**98**	**178**	**209**	**424**
Methane/air (Central ignition)	0.16 m	0.20 m	0.21 m	0.27 m
Methane/air (End ignition)	0.21 m	0.25 m	0.27 m	0.34 m
Propane/air (Central ignition)	0.16 m	0.20 m	0.21 m	0.26 m
Propane/air (End ignition)	0.20 m	0.24 m	0.26 m	0.33 m
Hydrogen/air (Central ignition)	0.15 m	0.18 m	0.19 m	0.24 m
Hydrogen/air (End ignition)	0.19 m	0.23 m	0.24 m	0.30 m
Ethylene/air (Central ignition)	0.14 m	0.17 m	0.18 m	0.23 m
Ethylene/air (End ignition)	0.18 m	0.22 m	0.23 m	0.29 m

The reliability of these predictions may be judged by comparison with the position of the flame determined from the flame position as a function of time in Fig. 5.11- 5.14. Hydrogen/air at end ignition, predicted 0.3 m flame radius gave good agreement to the measured flame position when the vent burst was 0.34 m. For methane/air with central ignition at P_v = 424 mbar, the measured flame position when the vent bursts was 0.3 m, very close to that predicted (refer to Fig. 5.14). For end ignition with propane/air, the measured flame positions in Fig. 5.12 and 5.13 were 0.3 and 0.4m for 178 and 424 mbar respectively and these were roughly 20% greater than that predicted.

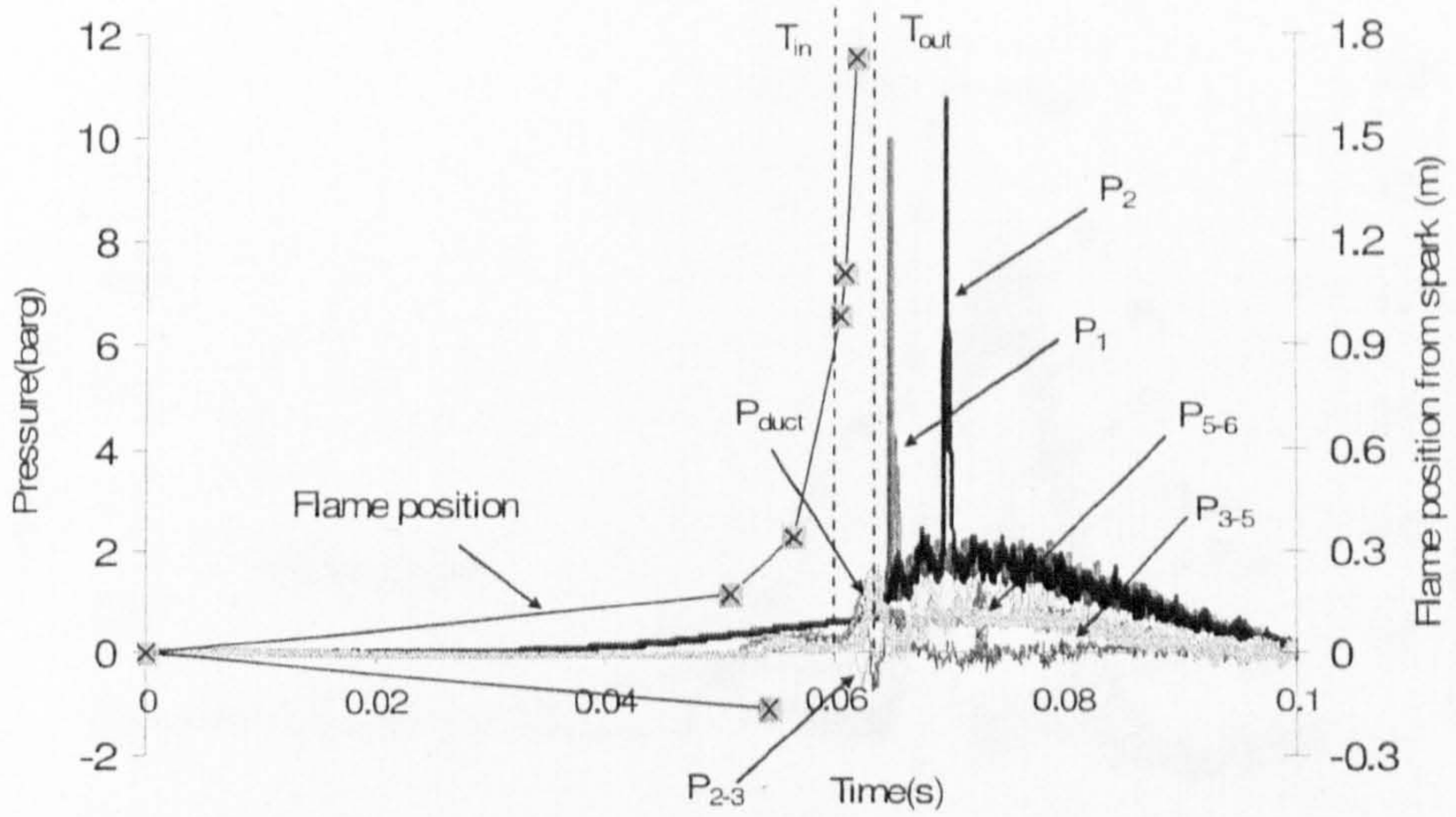

Figure 5.11 Hydrogen/air at $\Phi = 0.54$ for end ignition. $P_v = 209$ mbar

The reason for the greater flame movement than expected with end ignition was due to the greater expansion of the flame on the centreline compared with the edges, which were subject to more cooling. This is a well known effect for large L/D vessel and for very large L/D vessels results in an elongated U flame, with very fast centreline flame speeds (Phylaktou and Andrews, 1991). If the distances in Table 5.2 are compared with the flame speed results in Fig. 5.15 it can be seen that as soon as the vent burst there was an increase in the flame speed. This occurs at a shorter flame radius for central ignition, as predicted in Table 5.2. Also Fig. 5.9 and 5.10 shows that without a vent cover, flame acceleration above that due to cellular flames, started at distances similar to those in Table 5.2 for $P_v = 98$mbar.

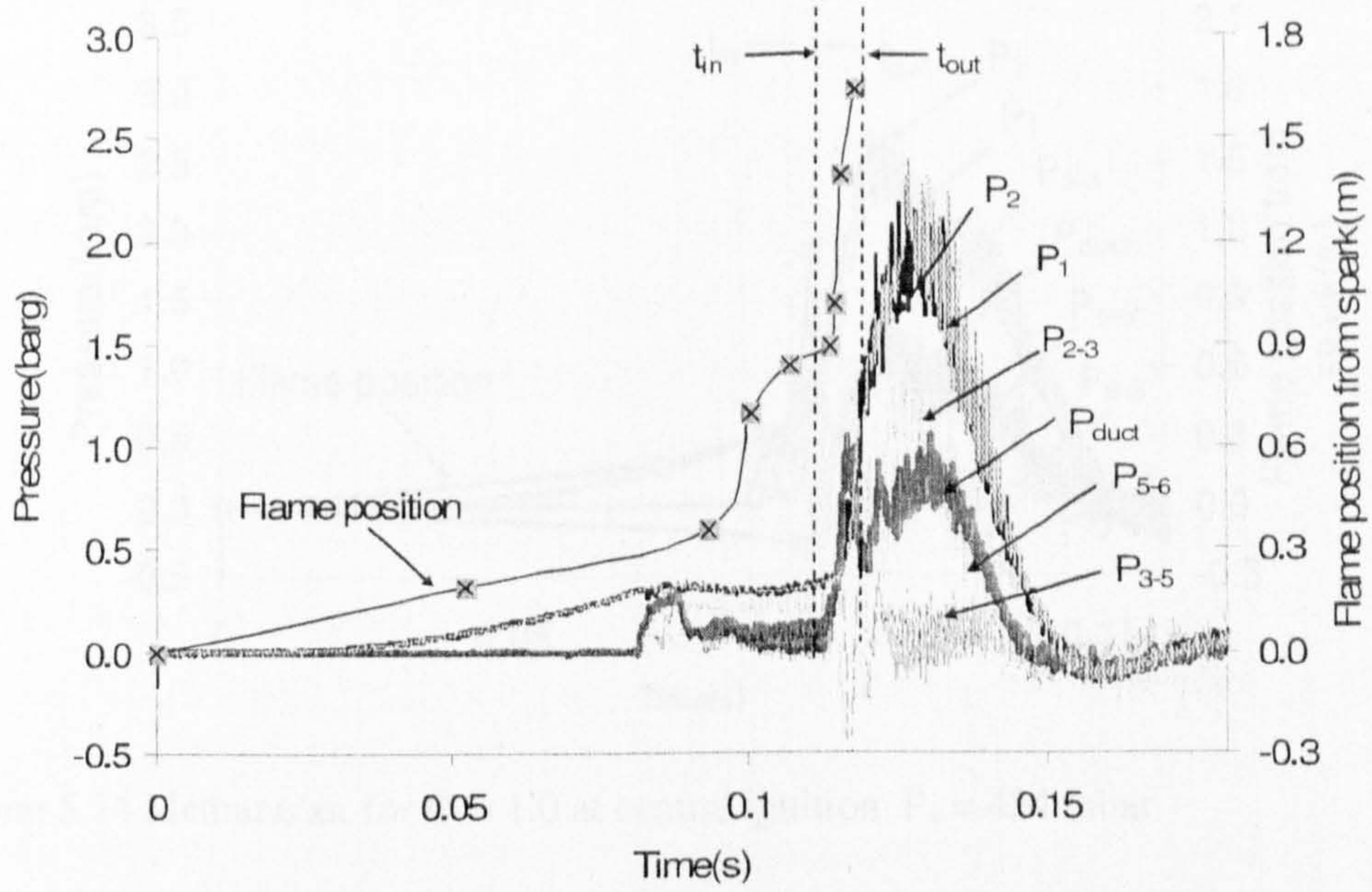

Figure 5.12 Propane/air at $\Phi = 1.0$ for end ignition. $P_v = 178$ mbar

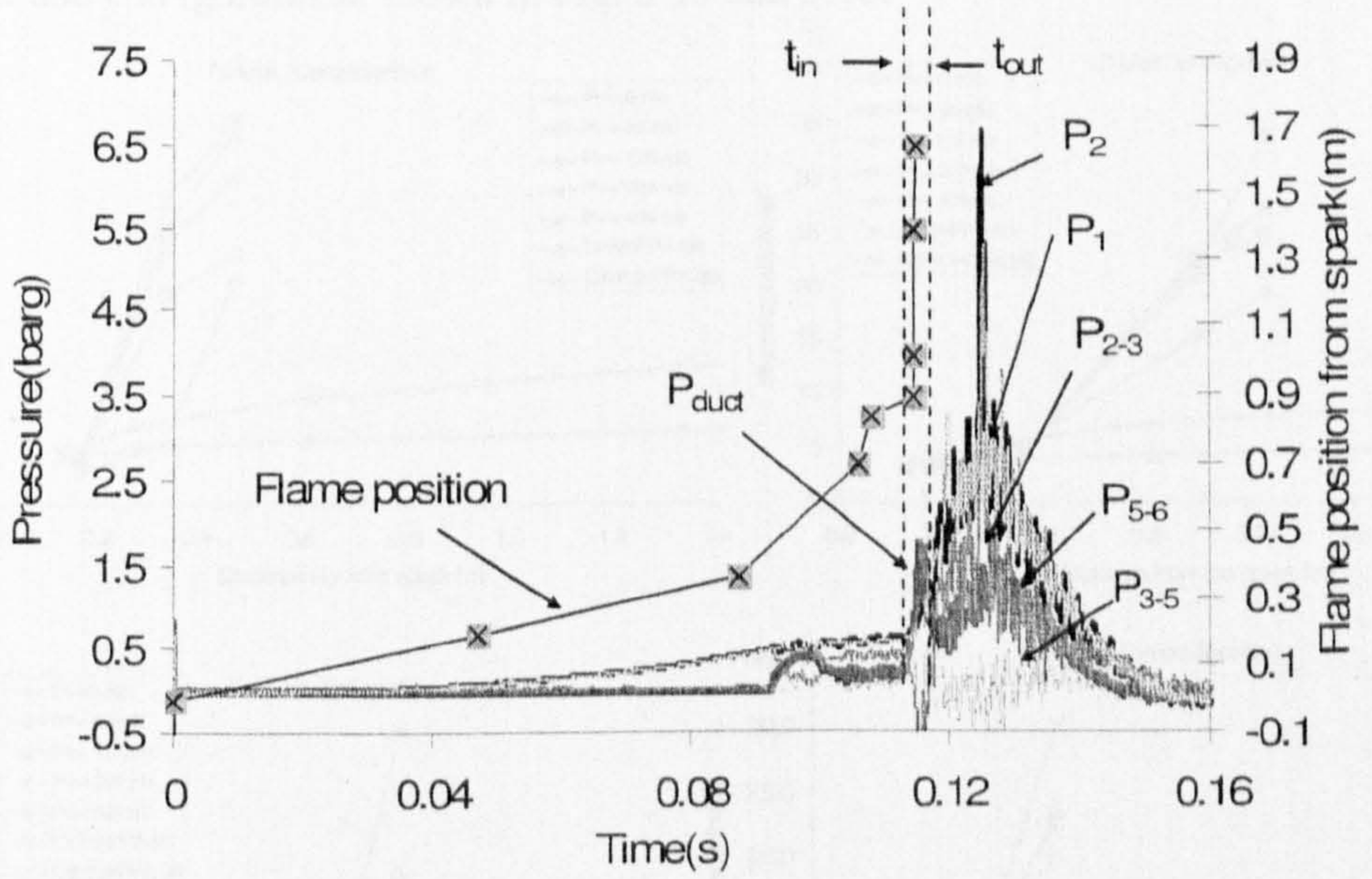

Figure 5.13 Propane/air at $\Phi = 1.0$ for end ignition. $P_v = 424$ mbar. Spiky pressure peak is observed in this test.

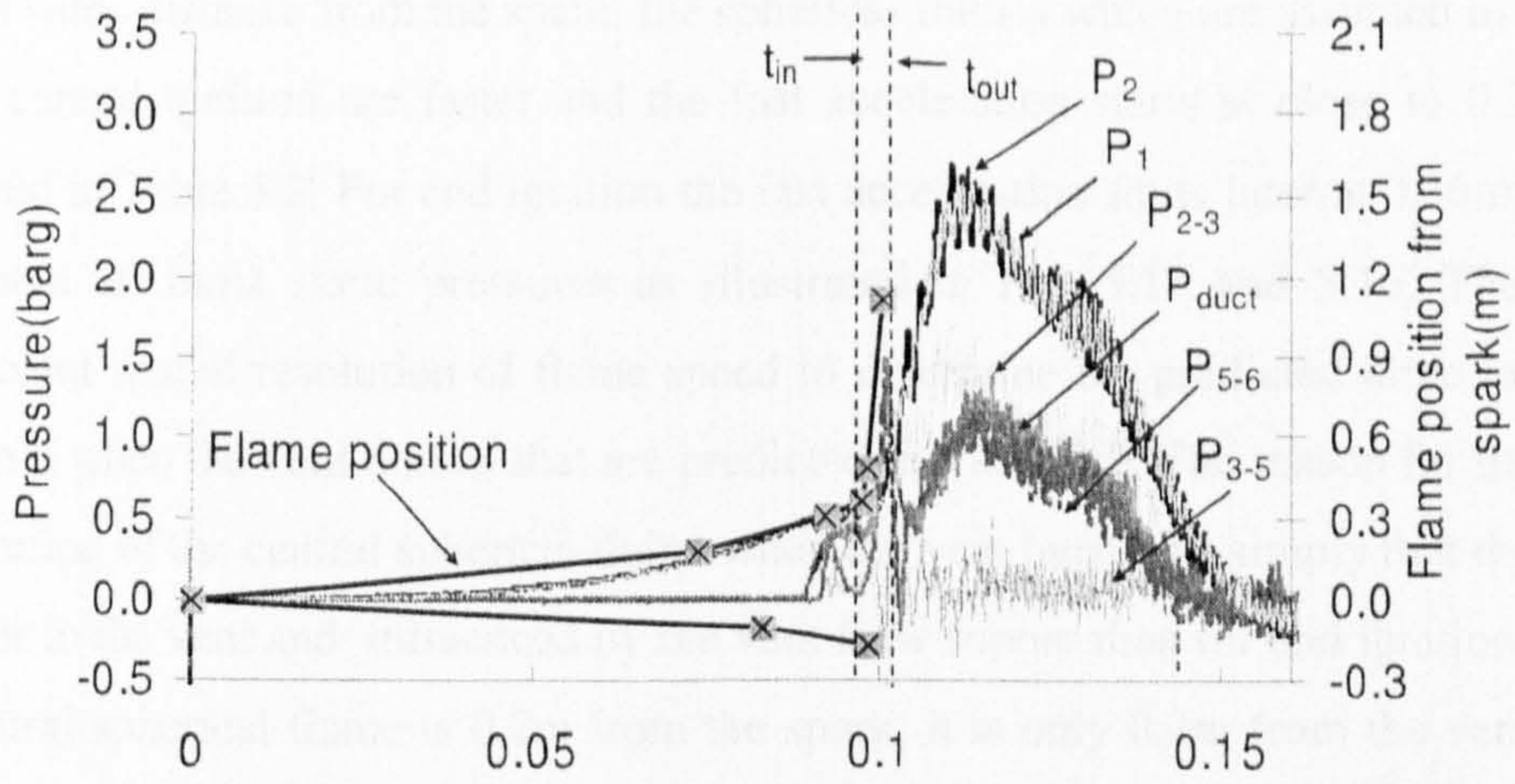

Figure 5.14 Methane/air for $\Phi = 1.0$ at central ignition. $P_v = 424$ mbar

As mentioned earlier, the flame speed after the vent burst increases rapidly for both central and end ignition as shown in Fig. 5.15 and 5.16.

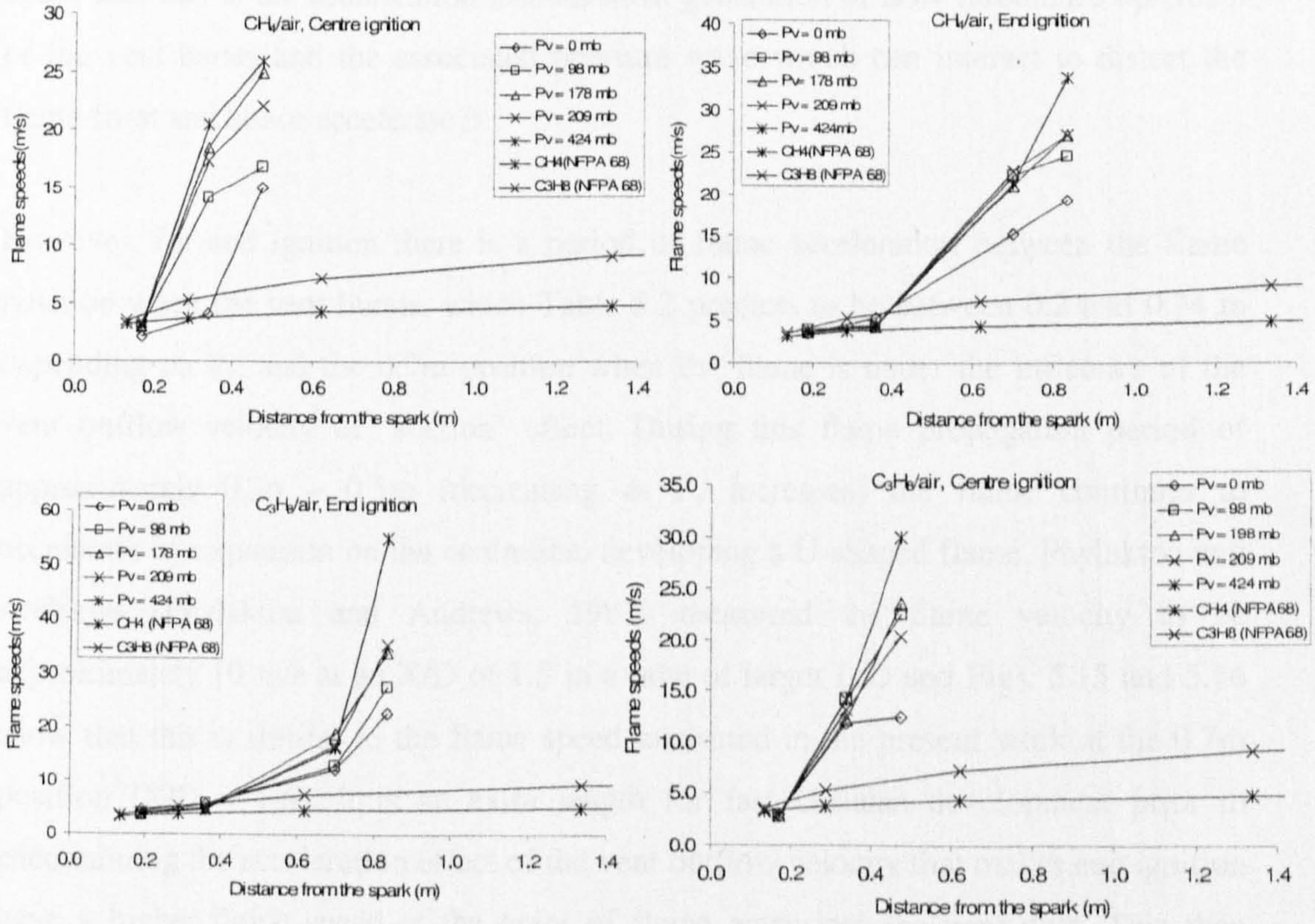

Figure 5.15 Influence of Pv on flame speed upstream of the vent for methane/air (Φ = 1.0) and propane/air (Φ=1.0) with end and central ignition.

For the same distance from the spark, the spherical flames which are assumed to behave in the central ignition are faster and the fast acceleration starts at close to 0.2 m, as predicted in Table 5.2. For end ignition the fast acceleration starts later at 0.36 m for all gases and all burst static pressures as illustrated in Fig. 5.15 and 5.16. There was insufficient spatial resolution of flame speed to determine the predicted large radius of the flame when the vent bursts, that are predicted in Table 5.2. The reason for the faster acceleration of the central spherical flame when the vent burst was simply that the flame is closer to the vent and influenced by the vent flow sooner than for end ignition. When the central spherical flame is 0.2m from the spark, it is only 0.3m from the vent. With end ignition, the flame would have to be 0.7m from the spark to be 0.3m from the vent. Both Fig. 5.15 and 5.16 showed that at this distance from the vent P_v starts to have a significant influence on the flame speed and this increases with P_v. This is a very similar effect for central and end ignition. The influence of P_v amplifies the flame speeds more than ten times compared to laminar flame speeds. Further, the increase of flame speeds could also due to the acceleration mechanisms: generation of flow turbulence upstream of the vent bursts and the associated pressure wave which can interact to distort the flame front and hence accelerate it.

However, for end ignition there is a period of flame acceleration between the flame position when the vent bursts, which Table 5.2 predicts to be between 0.2 and 0.34 m depending on P_v, and the 0.7m position when the flame is under the influence of the vent outflow velocity or 'suction' effect. During this flame propagation period of approximately 0.36 – 0.5m (decreasing as P_v increases) the flame continues to accelerate by expansion on the centreline, developing a U-shaped flame. Phylaktou and Andrews (Phylaktou and Andrews, 1991) measured the flame velocity to be approximately 10 m/s at an X/D of 1.5 in a tube of larger L/D and Figs. 5.15 and 5.16 show that this is similar to the flame speed measured in the present work at the 0.7m position (X/D = 1.6). It is an extra length for fast U-flame development prior to encountering the acceleration effect of the vent outflow velocity that makes end ignition have a higher flame speed at the point of flame entry into the vent duct. This then produces the higher overpressures shown in Table 5.1. There is no need to invoke turbulence effects of the vent flow or pressure waves from the vent bursting to explain the flame acceleration upstream of the vent. There is no mechanism by which turbulence created by flow through the vent can be convected upstream and hence this

mechanism of flame acceleration in vented explosions has always been a dubious explanation of why the laminar burning velocity has to be increased by a turbulence factor of the order of 4 or 5 to give agreement between theory and measurements (Bradley and Mitcheson, 1978b).

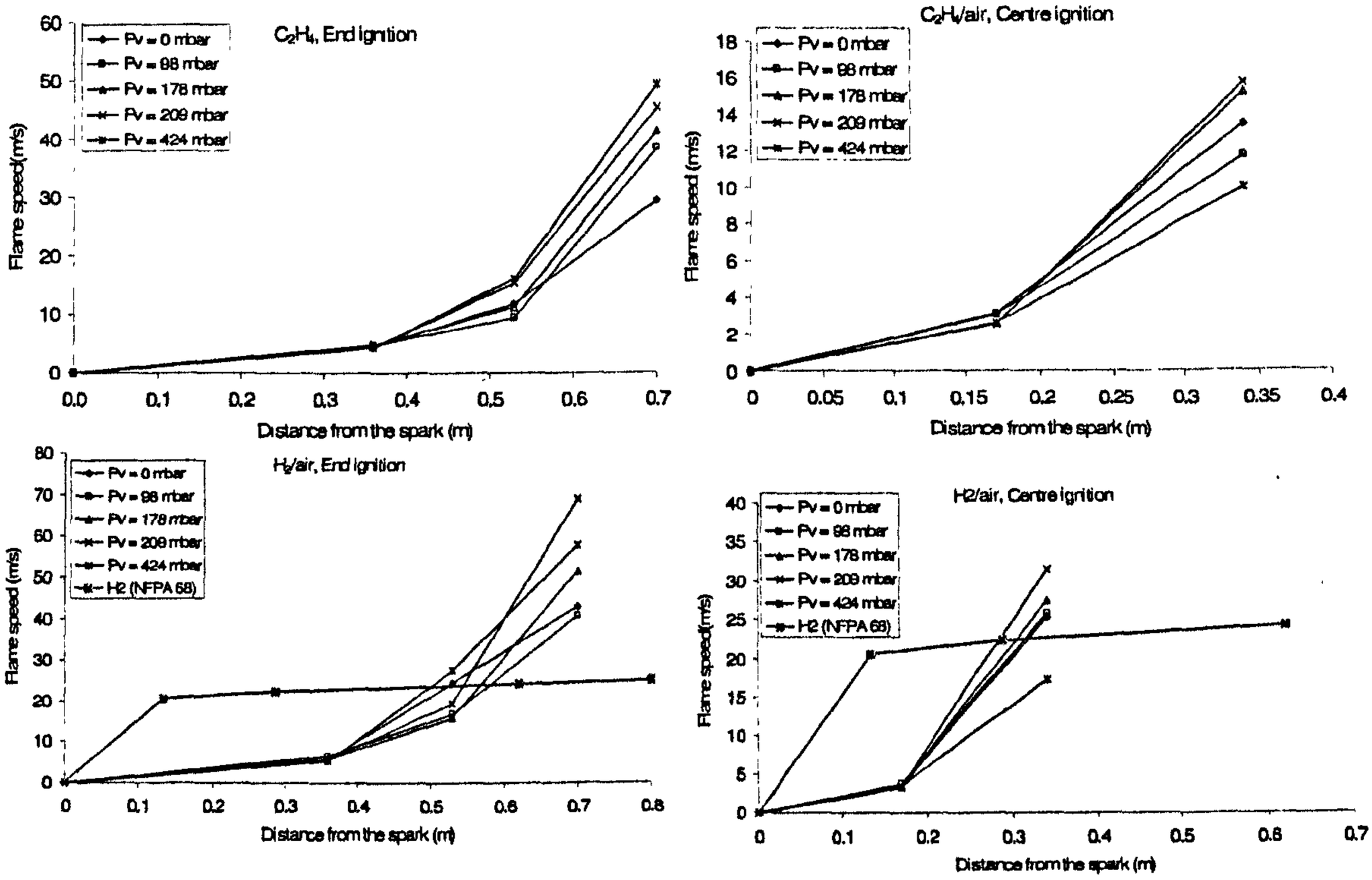

Figure 5.16 Influence of P_v on flame speed upstream of the vent for ethylene/air (Φ = 0.8) and hydrogen/air (Φ = 0.54) with end and central ignition.

The results of the maximum flame speeds in the vessel are shown as a function of equivalence ratio in Fig. 5.17 – 5.20 for methane, propane, ethylene and hydrogen/air with end and central ignition. These figures report the average flame speeds measured in the second half of the main vessel (between Tv_2 and Tv_4 in Fig.2.3). These flame speeds are considerably greater than that for the laminar spherical flame which 3m/s for methane, 3.6 m/s for propane, 5.5 m/s for ethylene and 19.7 m/s for hydrogen/air.

For methane/air profile, the flame speed increases with respect with the increase in P_v but the case where flame speed with open vent always gives lower flame speed is not featured in propane/air and those reactive mixtures i.e. ethylene/air and hydrogen/air. For propane/air with end ignition, Fig. 5.18 shows that flame speed, just upstream of

entry into the vent duct, was 19 m/s for $\Phi = 0.8$ with no vent cover and increased to 50 m/s for $P_v = 424$ mbar. The laminar burning velocity at $\Phi = 0.8$ is approximately 0.35 m/s and the adiabatic spherical flame speed approximately 3 m/s. The measured flame speeds are much higher than this and the increase is considered to be due to flame self-acceleration resulted from the formation of cellular flames (Kasmani, Willacy, Phylaktou and Andrews, 2007). The maximum reactivity of propane/air mixtures is at $\Phi = 1.1$, as the peak flame temperature occurs here.

Figure 5.17 Methane/air for end and central ignition as a function of equivalence ratio

The results in Fig. 5.18 show that the maximum flame speed with no vent cover was 52 m/s, considerably higher than the 3.6 m/s for a spherical adiabatic laminar flame speed. This increased to 120 m/s with the 424 mbar vent burst pressure. However, for richer

mixtures with $\Phi = 1.35$ the flame speed increased to 234 m/s for the highest vent burst pressure of 424 mbar. For no vent burst pressure this mixture had a lower flame speed than for $\Phi = 1.1$, as expected on the basis of laminar flame speeds. For very rich mixtures of $\Phi = 1.65$, which is close to the rich flammability limit, the flame speeds reduce sharply to values close to those at $\Phi = 0.8$. These flames speeds were 20 - 40 m/s and are very fast for such a near limit mixtures.

For the conditions with no vent burst pressure the results are reasonably explained by self acceleration of the flame as been discussed earlier, which are a function of Lewis number and Markstein no. Literature shows that for these are < 1 for rich propane mixture, which gives high flame acceleration (Bradley, 1999, Clarke, 2002, Markstein, 1964). However, the effect of the vent burst pressure on the flame speed is difficult to explain. It is known that increasing the pressure, which occurs when P_v is increased, accelerates the cellular flame effect and makes it occur at shorter distances (Bradley, 1999). This combined with the Lewis number effect, which increases the flame acceleration for rich mixtures (Clarke, 2002, Markstein, 1964), are the most likely causes the flame speed variations with equivalence ratio. It is shown below that these effects directly cause the peak overpressure to be greatest for the $\Phi = 1.35$ rich mixture. Similar results were found for central ignition of propane/air mixture (Fig. 5.18), but the flame speeds were lower at all P_v due to the shorter distance for flame self acceleration (Kasmani, Willacy, Phylaktou and Andrews, 2007). The maximum flame speed still occurred at $\Phi = 1.34$ with 145 m/s compared with 234 m/s for end ignition. For methane/air mixtures the results were also similar, but the peak flame speeds were lower and the maximum flame speed was in the near stoichiometric region and not for very rich mixtures, as found for propane. The reason for these differences with methane was the much lower tendency for self acceleration via the cellular flame mechanism (Bradley, 1999, Clarke, 2002, Markstein, 1964).

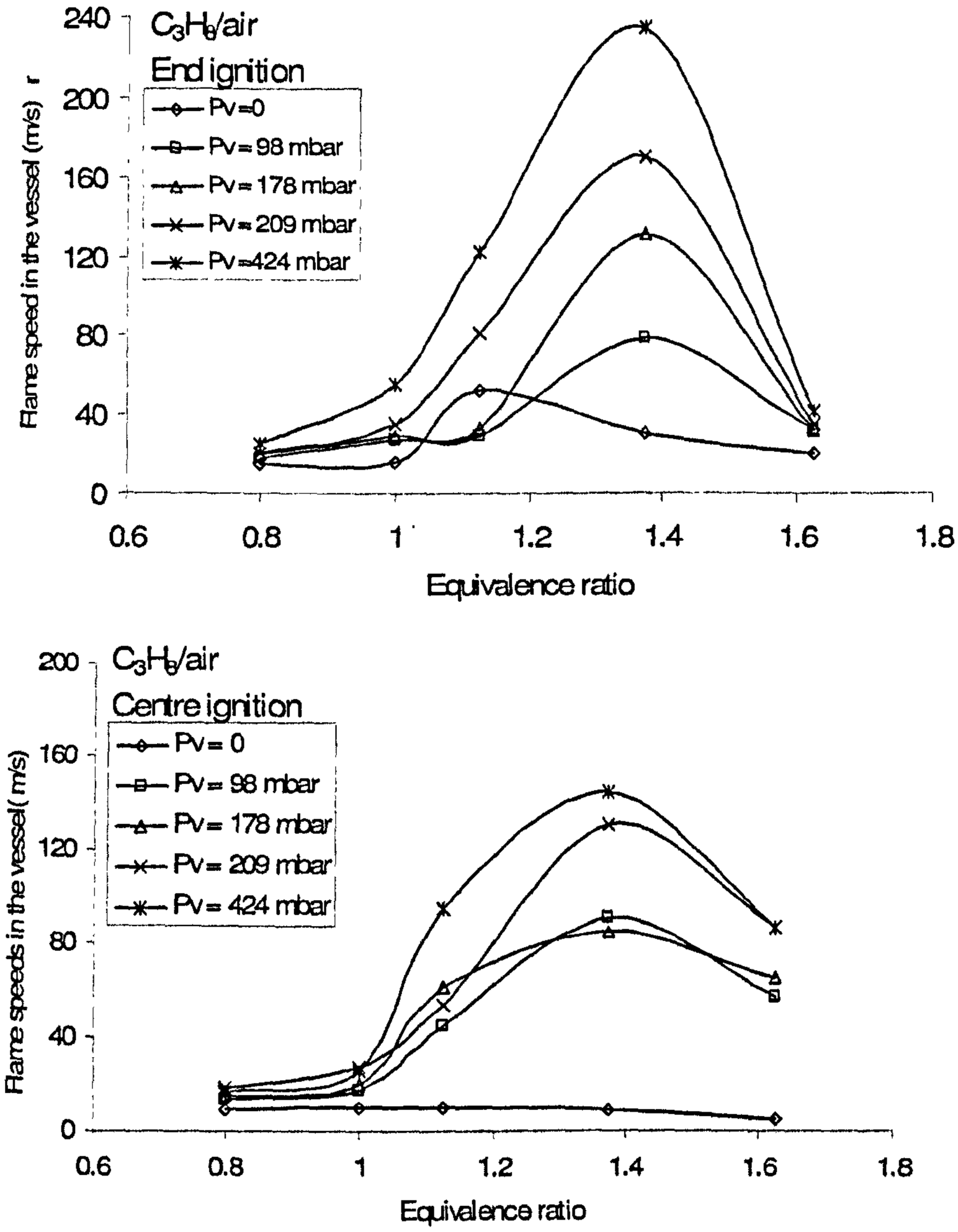

Figure 5.18 Propane/air for end and central ignition as a function of equivalence ratio

However, since only lean limit can be done on ethylene/air and hydrogen/air mixtures in this work due to the safety procedure, it can be said that ethylene/air has the same features as what been illustrated in propane/air explosion at lean limit mixtures. With no vent cover, the maximum flame speed was 17 m/s and this increased to 24 m/s with the 424 mbar vent burst pressure as pictured in Fig. 5.19. There is not that much significant increase in flame speed in various P_v for end and central ignition as the occurrence of flame cellularity is not great at this lean concentration stage but the turbulence generated by the backflow and flame front interaction with pressure wave substantially increase the P_{max} as shown in Fig. 5.23 later.

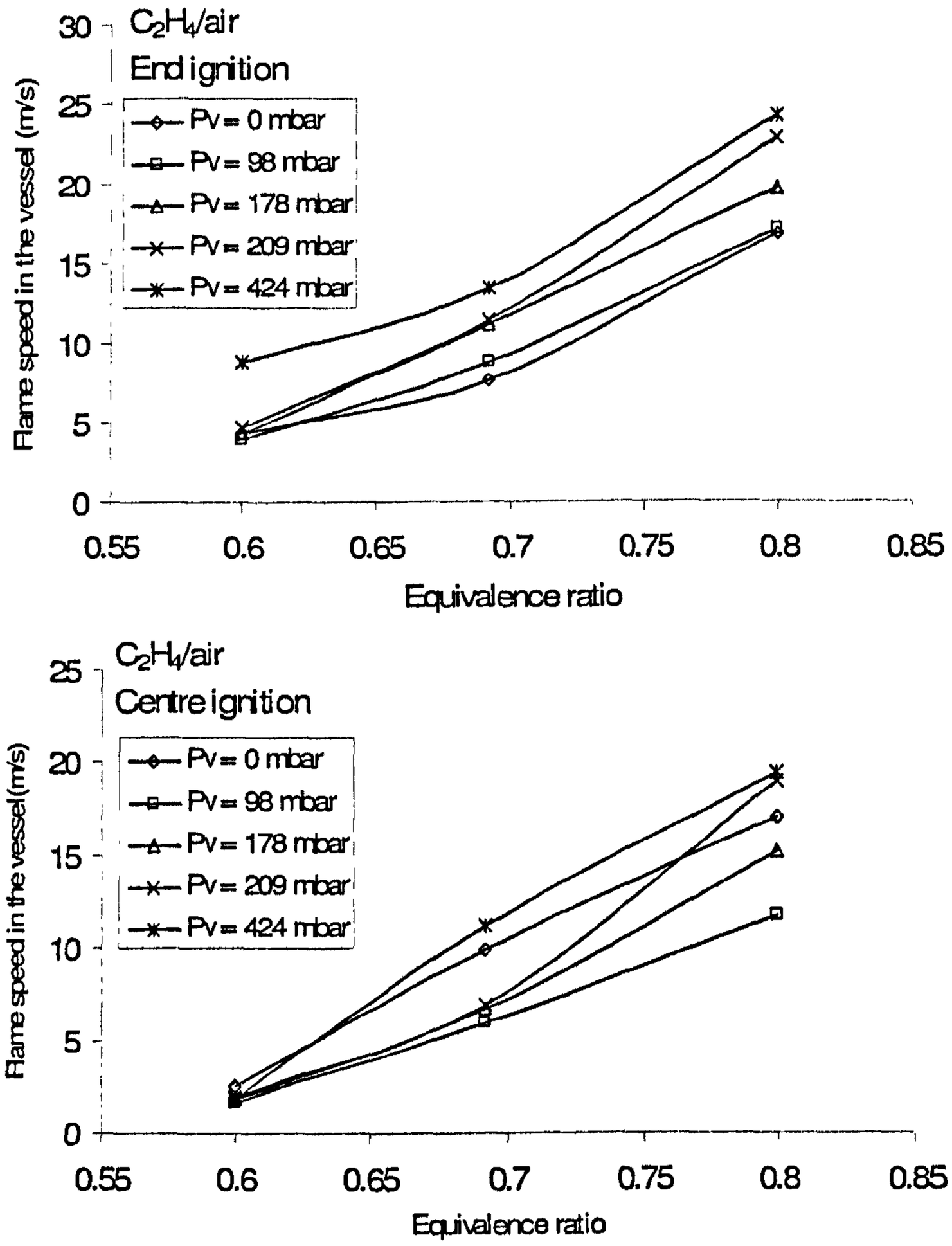

Figure 5.19 Ethylene/air for end and centre ignition as a function of equivalence ratio

For hydrogen/air explosion, end ignition shows that there was not much difference on flame speed at equivalence ratio for various P_v except for P_v of 98 mbar. Open vent gave same effect on flame speed propagation as highest P_v i.e. 424 mbar. The results can be then suggested that cellular instabilities developing on the flame surface (due to Taylor type, auto turbulence as observed in Kumar et al (Kumar, Dewit and Greig, 1989)) and longer distance for flame travel are the important factors causing the high flame speed inside the vessel regardless of the P_v effect for end ignition. Meanwhile, this trend is not featured in central ignition where the flame speed was 39 m/s at P_v = 424 mbar and 23 m/s at initially open venting. This is about 2 times higher in flame speed for high P_v in respect to open vent. Here, it can be postulated that self-induced flame is the

responsible mechanism that triggering the high flame speed inside the vessel as there is considerable flame acceleration had taken place before the vent bursts.

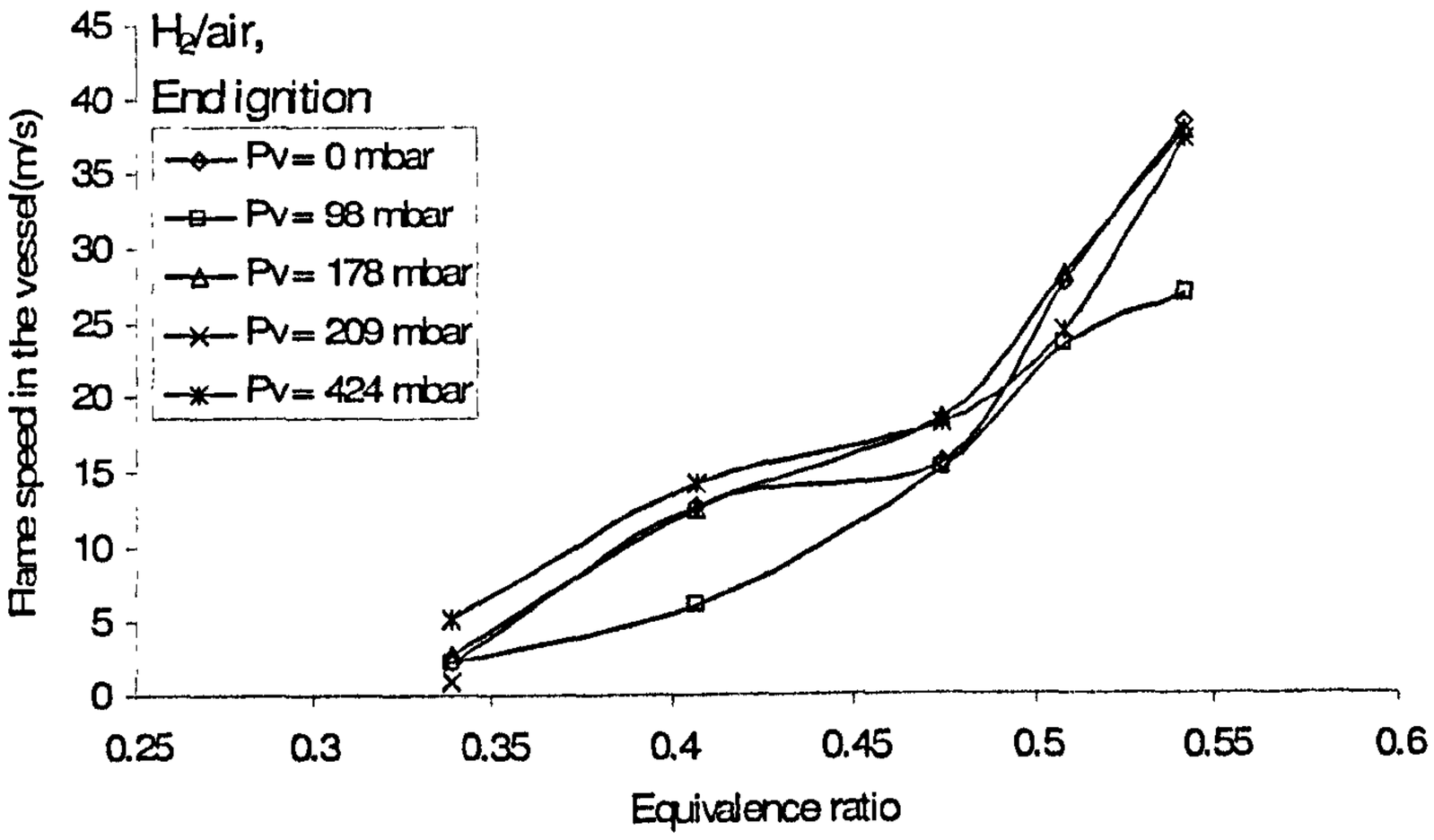

Figure 5.20 Hydrogen/air for end and centre ignition as a function of equivalence ratio.

5.1.5 The duct flame speeds and gas velocities

The peak measured flame speeds prior to the flame entering the duct pipe are shown in Fig. 5.9, 5.10, 5.15-5.16, 5.17-5.20 as well as in Table 5.1. The associated unburnt gas velocity and the turbulent burning velocity upstream of the vent, based on this flame speed and adiabatic burnt gas expansion are also shown in Table 5.1. The turbulence burning velocities measured with central ignition give a S_T/S_L burning velocity ratio of

approximately 5, similar to that used by Bradley and Mitcheson (Bradley and Mitcheson, 1978b). However, as shown above, the mechanism of the flame acceleration is not due to flow turbulence. Simple momentum conservation allows the unburnt gas velocity in the duct just prior to the flame entry to be predicted and these are also shown in Table 5.1. This calculation assumes that the flame behaves as a piston, which is not the reality as the flame is 'pear 'shaped and not flat. However, the resultant gas velocities are very high and greater than sonic in a few cases (incompressible flow was assumed in the momentum equation). This indicates that near sonic flow is likely in the vent and the absolute pressure ratio, P_2/P_6, across the vent duct in Fig. 5.11 to 5.14 confirmed this observation. It is important to realise that this duct flow is driven by the fast flames upstream of the vent, shown in Fig. 5.9, 5.10, 5.15 -5.16 and 5.17-5.20.

The flame speeds in the vent duct were measured and tabulated in Table 5.1. These were very fast flames even for an open vent. They were consistently higher for end ignition due to the faster flames and the predicted faster unburnt gas velocities in the duct. The flame speeds are reasonably close to the predicted unburnt gas velocities computed from the upstream flame speeds. There are generally higher due to the influence of the turbulent burning velocity. However, it is clear that the dominant cause of the fast flames in the vent duct is the fast upstream flames detailed above. The unburnt gas velocity ahead of the flame in the duct has been estimated as 80 % of the flame speed in Table 5.1. For an adiabatic explosion the gas velocity ahead of the flame is (E-1)/E times the flame speeds and this is 87 % of the flame speed for stoichiometric hydrocarbons. The lower value has been used to account for duct wall heat losses (Phylaktou, Foley and Andrews, 1993).

In the case of equivalence effect, the high flame speed upstream of the vent induces higher unburnt gas velocities ahead of the flame. These high vent pipe unburnt velocities results in a very high pipe turbulence level and consequently very high flame speed in the duct pipe as shown of the worst case of propane/air in Fig. 5.21 and hydrogen/air in Fig. 5.22. This shows a very large increase in flame speed inside the vent duct with P_v from 200 m/s to 700 m/s as the P_v increases from zero to 424 mbar in the case of propane/air at end ignition for $\Phi = 1.0$. In the case of hydrogen/air, the flame speed inside the vent duct was 300 m/s for $P_v = 0$ and increases sharply to 550 m/s for $P_v = 424$ mbar for $\Phi = 0.54$. The cause of this is the large increase in flame speed

upstream of the vent in Fig. 5.20 from 23 to 40 m/s corresponding to the increase in P_v. This high flame speed inside the duct pipe at lean concentration in hydrogen is responsible to induce high turbulent flow leading to an intense mixing of cold and hot gases which brings to a subsequent violent combustion (burn-up) inside the duct during re-ignition (Ponizy and Leyer, 1999a, Ponizy and Leyer, 1999b). Burn-up in the duct has then to be considered a crucial phenomena affecting the final overpressure of the vessel and in this case, to lead to a detonation.

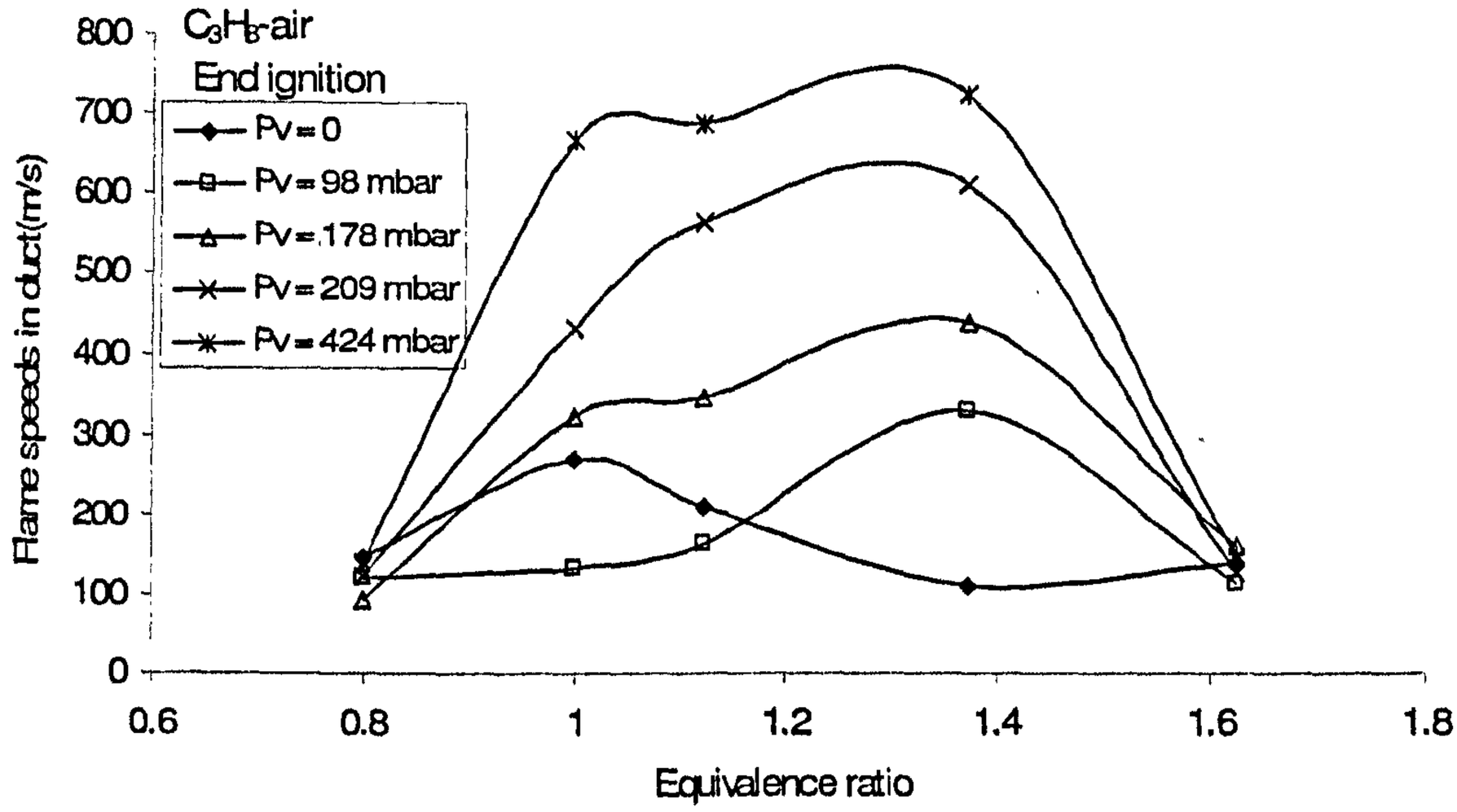

Figure 5.21 Flame speed in the duct pipe for propane/air as a function of equivalence ratio at end ignition.

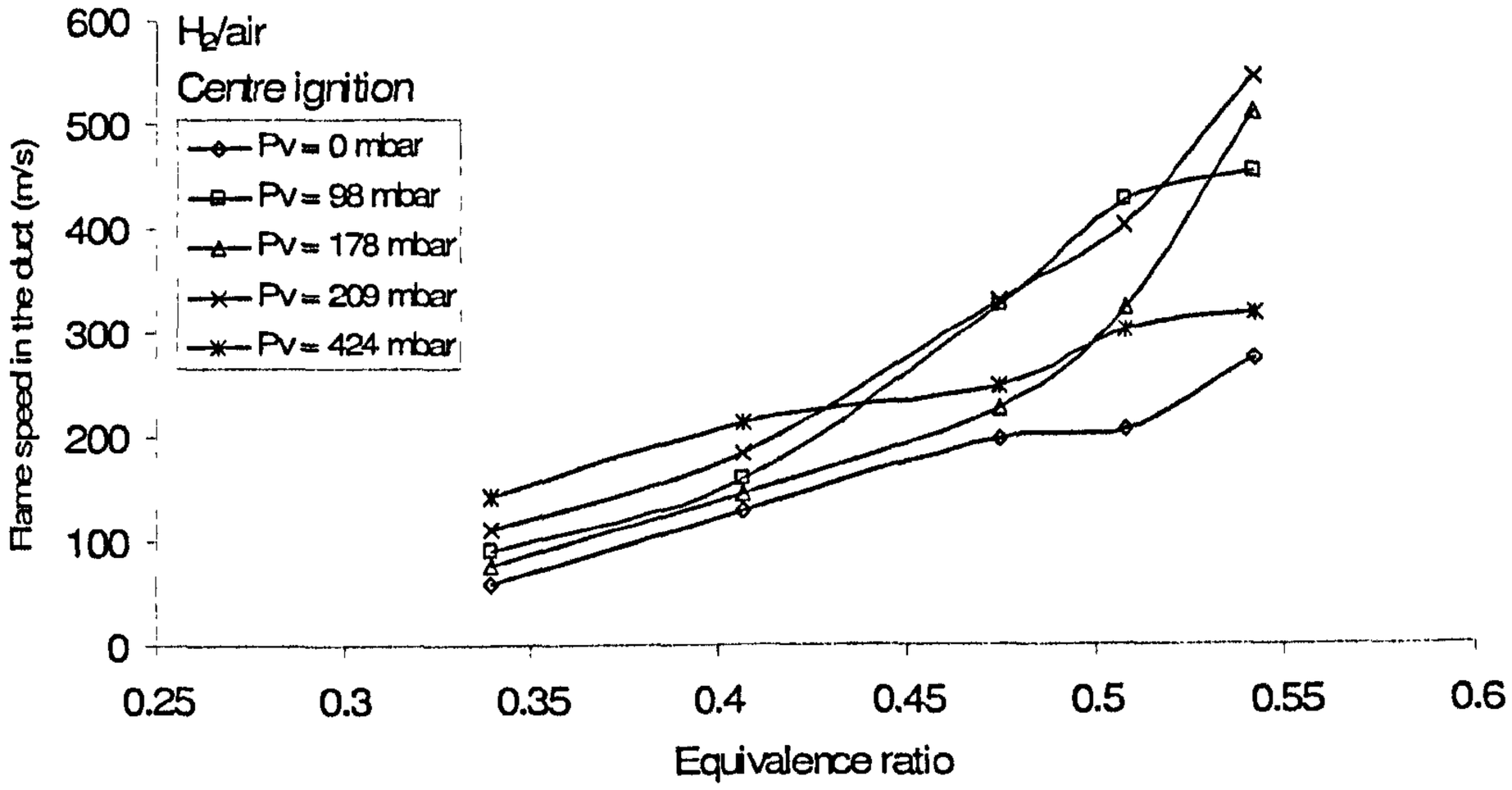

Figure 5.22 Flame speed in the duct pipe for hydrogen/air as a function of equivalence ratio at end ignition.

5.2 The influence of equivalence ratio on P_{max}

P_{max} is shown as a function of the equivalence ratio in Fig. 5.23-5.26 for methane, propane, ethylene and hydrogen explosions with end and central ignition. For an open vent, Fig. 5.24 shows that P_{max} was higher than with P_v = 98 mbar for propane/air with end ignition from Φ = 0.8 to 1.12. The same figure also shows that for central ignition the open vent had much higher overpressures for P_v = 98 mbar and 178 mbar from Φ = 0.8-1.15. This did not occur in the methane/air explosions in Fig. 5.23, where the open vent was always the lowest P_{max} for all equivalence ratios. These lower overpressures for 98 mbar and 178 mbar vent burst pressures compared with open vents for the propane explosions are difficult to explain. The upstream flame speeds result in Table 5.1 does showing a higher flame speed for the open vent for Φ = 1.0 and at Φ = 1.37 as shown in Fig. 5.18. Propane is propensity for cellularity at rich concentration (Tseng, Ismail and Faeth, 1993) and this would explain the higher P_{max} in comparison of methane/air. For propane, the onset of cellular flames occurs over a shorter distance and the self acceleration of the flame is greater, which is a function of the distance from the spark. The significant effect from this is to accelerate the flame towards the vent more quickly than for methane/air explosions, as shown in Fig. 5.15. The effect is to stretch the propane flame so that it is more elongated than a methane/air flame. The action of

the static burst pressure of the vent is, for low burst pressures, to delay the acceleration of the flame to the vent. The flame does not know that the vessel is vented until the vent bursts and was propagating as in a closed vessel. For low vent burst pressure this gives a smaller flame area when the vent bursts and it is the effect of the vent burst pressure on the flame bulk shape and not on its centre line velocity that causes the pressure to be reduced. It is considered that this effect has a greater relative influence on the propane flames due to their greater acceleration to the vent and this is why propane and methane flames behaved differently for low vent opening pressures. A higher initial flame speed would indicate a higher mass burn rate and hence a higher mass flow rate in the vent pipe and this would create more turbulence and hence higher overpressures due to the faster flame speeds in the vent pipe.

Unfortunately, this was the only result that gave a higher flame speed prior to the vent and hence this mechanism cannot explain all the results. Further, it is very significant that only the propane explosions demonstrated this effect. This is also indicated that the quicker onset of cellular flames and the greater self acceleration of propane flames may be the cause of this difference. It is conjectured that P_{max} was generated by the rapid turbulent combustion of the unburnt gases left upstream of the vent in the main vessel. The flame preferentially accelerates in the direction of the vent once this is open, leaving a large proportion of the unburnt mixture in the vented explosion vessel. The gases in the outer part of the vessel are unburnt when the flame enters the vent. A high flow back pressure is generated by the high velocity unburnt gas flow in the vent and the subsequent high flame speeds in the vent pipe, as shown in Fig. 5.21. This forces the upstream flow to reverse and ignite the outer unburnt gas flow in a fast burning turbulent flame. This then accelerates the burnt gas flow out the vent pipe, which increasing the pressure rise.

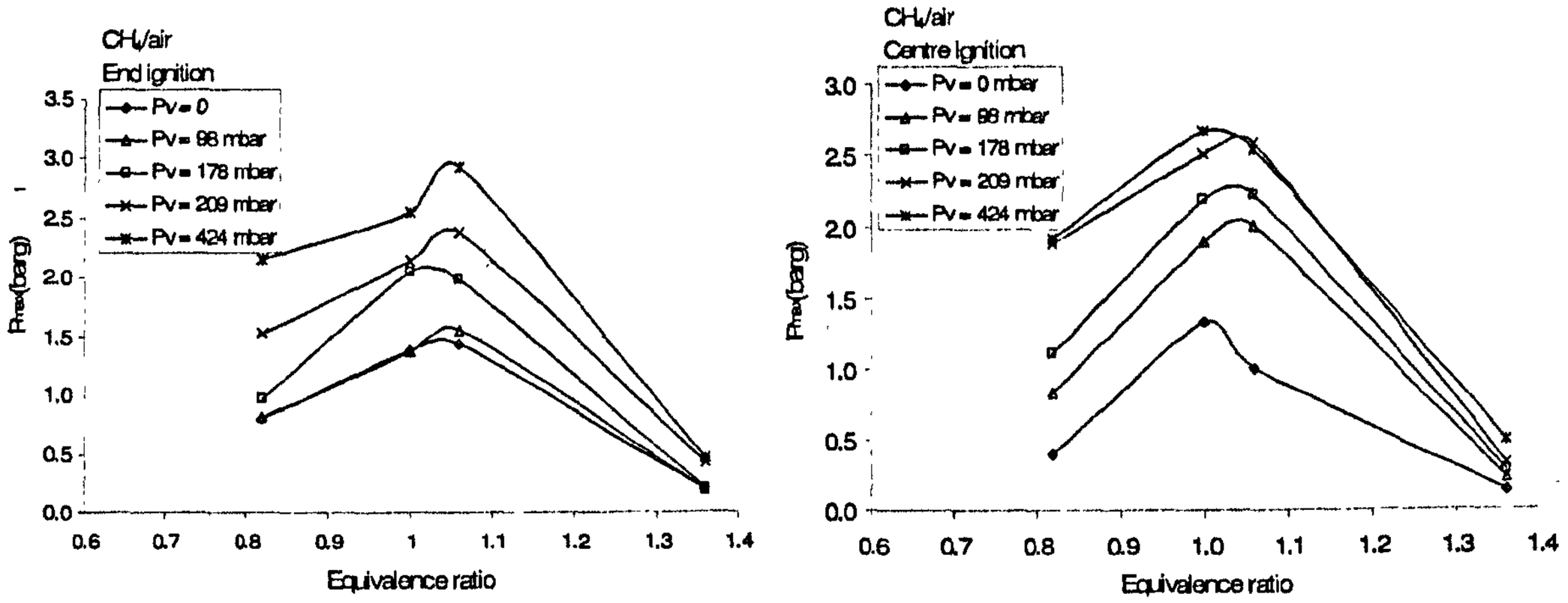

Figure 5.23 Methane/air at end (left) and centre (right) ignition at various P_v

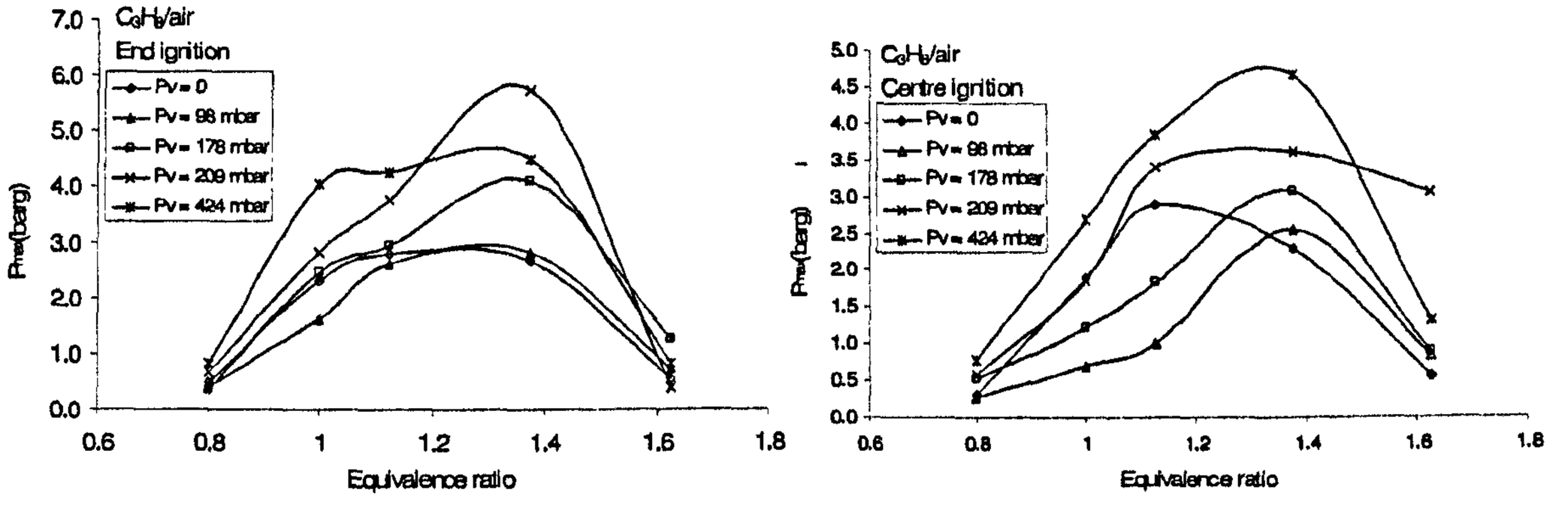

Figure 5.24 Propane/air for end (left) and centre (right) ignition at various P_v.

However, for higher vent burst pressures > 200mbar, P_{max} always increased relative to the open vent case for both methane/air and propane/air. This was due to the greater flame area and mass burning rate when the vent opened, together with the sudden acceleration of the gases in the vent pipe when the vent burst due to the imposed pressure difference. This produced a large increase in the mass flow through the vent and hence in the overpressure. It is considered that this significant influence of cellular flames with propane explosions will be greater for ethylene and hydrogen explosions and this is shown in Fig. 5.25 and 5.26 for ethylene/air and hydrogen/air respectively.

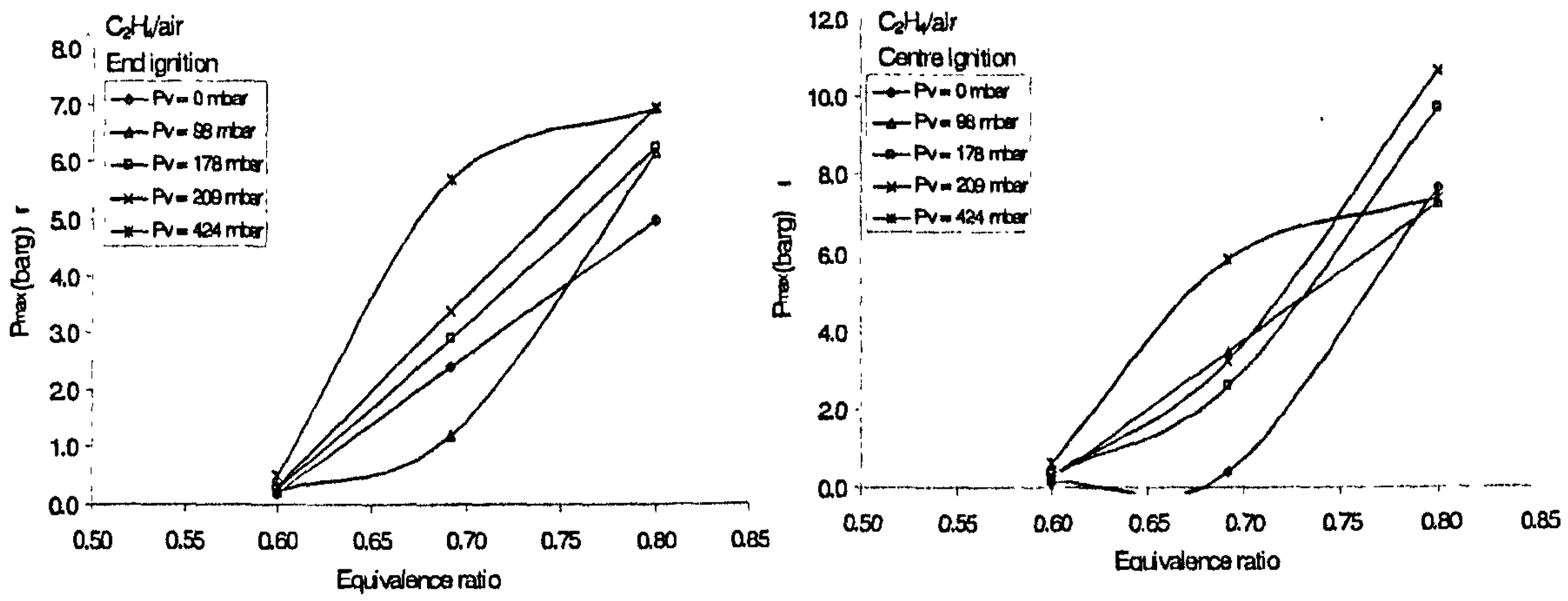

Figure 5.25 Ethylene/air for end (left) and centre (right) ignition at various P_v

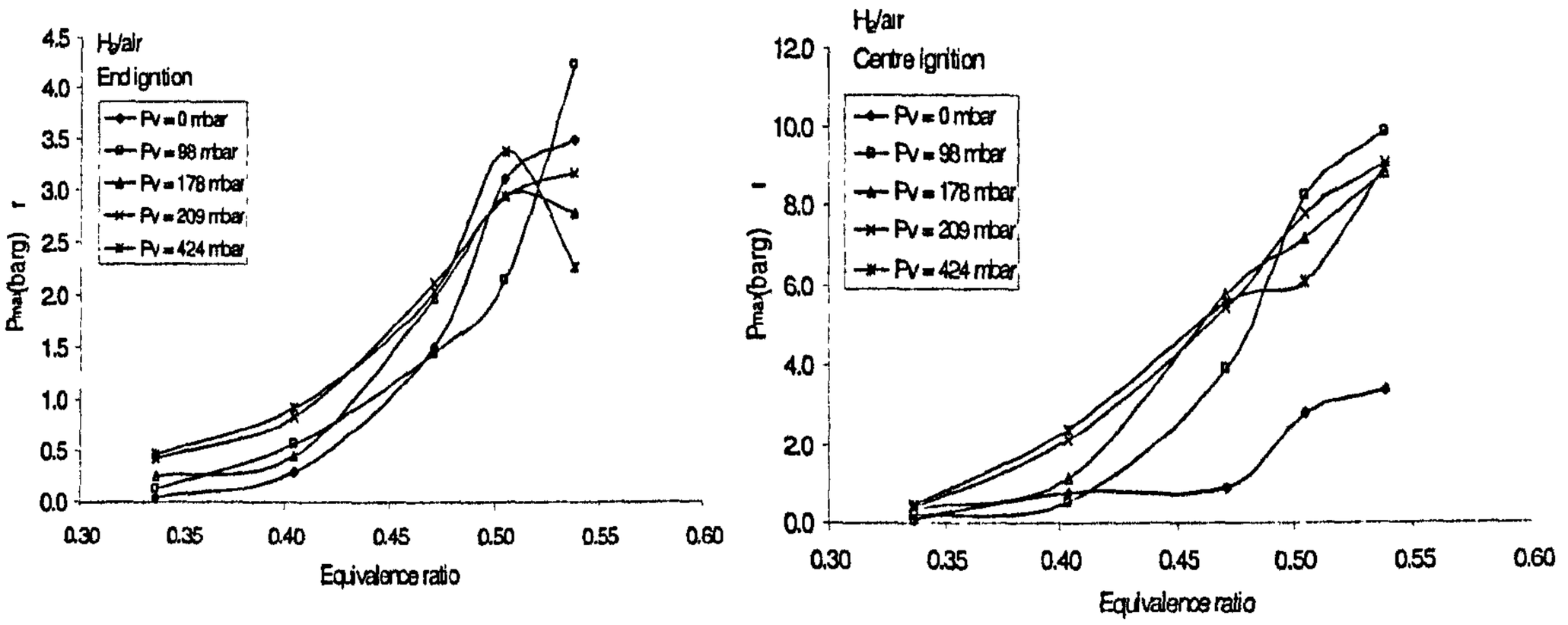

Figure 5.26 Hydrogen/air at end (left) and centre (right) ignition at various P_v.

For both gas/mixtures, central ignition gave higher P_{max} as a function of equivalence ratio compared to the two hydrocarbon/air mixtures investigated. As tabulated in Table 5.1, the peak P_{max} is the resultant of detonation spike occurred in the pressure traces for both mixtures and it was above the maximum adiabatic pressure inside the closed vessel of 8 bars at $\Phi = 0.8$ for ethylene/air and $\Phi = 0.54$ for hydrogen at centrally ignited. This observation brings out an important fact that high burning velocity mixtures such as hydrogen/air and ethylene/air mixtures behave differently from those with low burning velocities. The self acceleration and formation of flame cellularity is another factor that enhances the mass burning rate inside the vessel but the considerable amount of unburnt gases left trapped inside the vessel (mixture reactivity) is the important factor that leads to the increase the P_{max} with detonation spike observed.

5.3 Comparison with other experimental data

In order to develop understanding on the phenomenology of duct vented explosion, the current work results were compared to other published experimental data (Russo and Benedetto, 2007, McCann, Thomas and Edwards, 1985, Molkov, Baratov and Korolchenko, 1993, Ponizy and Leyer, 1999a, Ponizy and Leyer, 1999b). Later, all the experimental works including the current project will be compared with the correlation offered by NFPA 68 to investigate the discrepancy between theoretical approach and experiments.

Figure 5.27 showed the P_{red} with duct as a function of the reduced pressure obtained in the same tests without the presence of duct. On the same figure, all experimental data were compared to the correlation given in NFPA 68 for duct pipe length in between 0 to 3 m. As expected, the correlation given by NFPA 68 is under predicted the experimental data results, suggesting that there is more complex interaction between the vessels with the presence of duct with respect to the ductless vessel explosion i.e. simply vented. It is also interesting to note that even though the same reduced pressure obtained in vented explosion without the duct pipe attached, there was a variance of P_{red} in the presence of duct pipe. This situation implied the correlation associated P_{red} with the duct pipe and without the duct pipe should not be taken as simple as given in NFPA 68 but other parameters should be taken into account to accommodate the increase of P_{red} when the duct pipe is attached with respect to simply vented explosion. As previously discussed, ignition position, vessel volume, self-acceleration, induced turbulent, pressure loss as well as secondary explosion should be included in the correlation in order to fit with the results obtained experimentally. All published experimental data are listed in Appendix A (Table A.2).

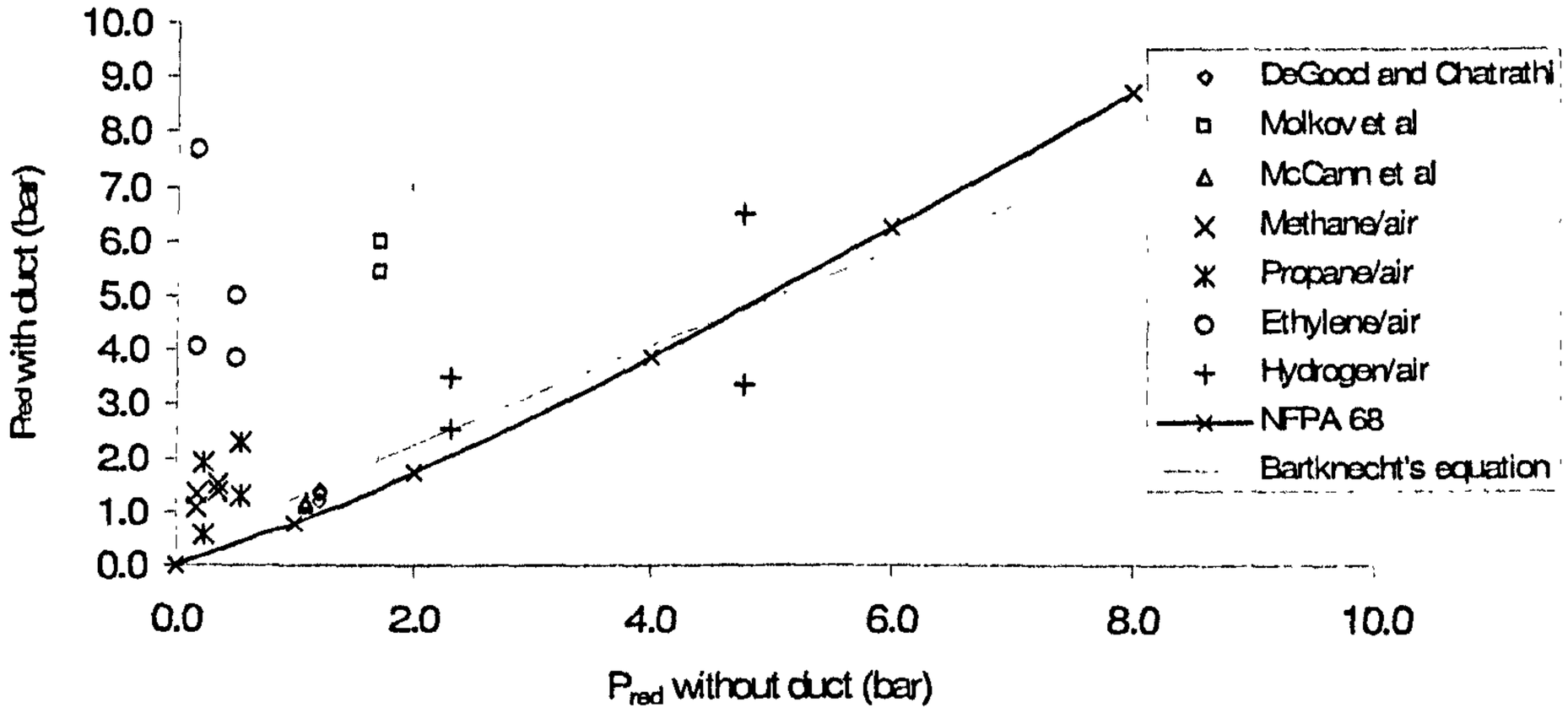

Figure 5.27 Comparison between other published experimental data and current project. The data reported were 10 % methane/air, 4.5% propane/air, 5.2% ethylene/air and 16 % hydrogen/air and 5 % acetone/air. NFPA 68 correlation (NFPA68, 2002) and Bartknecht's equation (Bartknecht, 1993) are used for $0 < L_d > 3$ m.

Another interesting point to highlight is the influence of L/D to P_{red}. It is clearly shown that L/D is not main factor influencing the increase in P_{red} on the presence of the duct pipe. As shown in Fig.5.28, P_{red} was almost insignificant at the different L/D obtained in Ponizy and Leyer's work (Ponizy and Leyer, 1999a, Ponizy and Leyer, 1999b) at end ignition. The same L/D gave insignificant P_{red} at the different mixture reactivity (propane/air and methane/air mixtures) illustrated by DeGood and Chartrathi (DeGood and Chartrathi, 1991), McCann et al (McCann, Thomas and Edwards, 1985) and results from this works either end or central ignition. This condition can be suggested that L/D is not significant in influencing P_{red} when the duct pipe attached in low burning velocity mixtures but not in high burning velocity mixtures i.e. hydrogen.

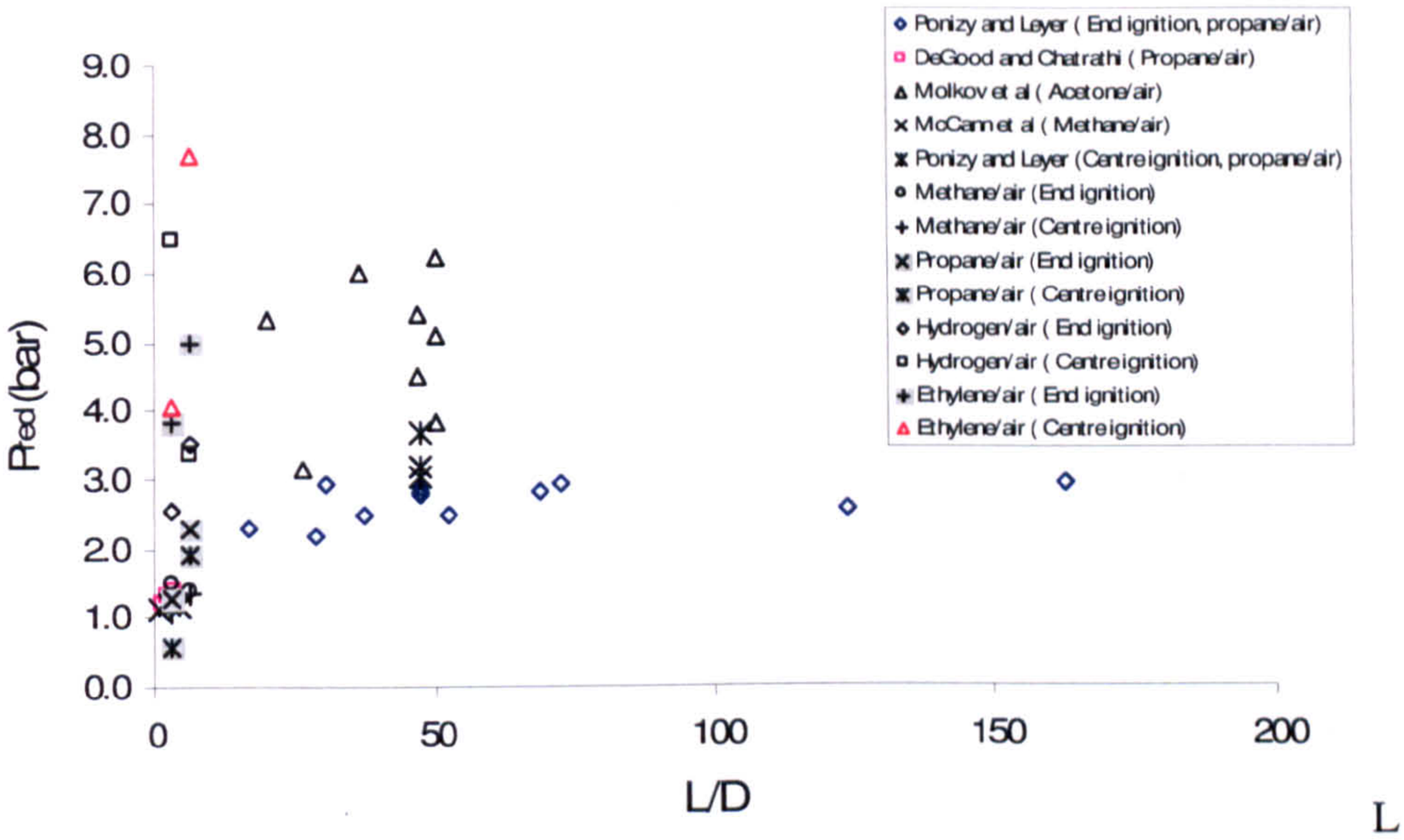

Figure 5.28 P_{red} as a function of L/D

5.4 Concluding remarks

The high overpressure due to the addition of a vent duct, to a 0.2 m^3 closed vessel with an L/D of 2 and K of 16.4, occurs after the flame has exited the vent duct, but is not due to an external explosion. The main effect of the ignition position is to give a greater distance from the spark to the vent and greater flame acceleration. End ignition gave higher P_{max} for low burning velocities mixtures but central ignition is the worst case scenario in P_{max} for hydrogen/air and ethylene/air. It was found that substantial amount of unburnt gases left inside the vessel after the vent burst is the leading factor in increase of P_{max} for high burning velocity mixtures for centrally ignited. The associate gas velocities ahead of the flame create high unburnt gas flows conditions at entry to the vent and this give rise to high back pressures.

As P_v increases, the distance of normal spherical flame propagation increases and there is a further reduction in acceleration distance. This initially reduces the overpressure at low P_v. The effect of the vent burst pressure is to increase the flow velocity in the duct when the vent burst, as the flame has had more time to grow upstream of the vent and this gives a higher vent duct flow velocity once the vent cover bursts. The effect of the vent burst pressure is complex and non-linear and is not represented by the linear effect in the correlation of Bartknecht (Bartknecht, 1993) used in NFPA 68 (NFPA68, 2002).

The greater self acceleration of flames due to cellular flame development for propane relative to methane is shown in the results. Propane has a very strong influence of equivalence ratio on the flame speeds and overpressures, especially for rich mixtures where the highest flame speeds and overpressures are exhibited for $\Phi = 1.35$. It cannot be assumed that the mixture with the highest laminar burning velocity, measured on small diameter flames with no cellular flames, is the mixture with the worst case explosion hazards. For gases such as propane that have a strong cellular flame development the worst case explosion hazard will be for rich mixtures, where this effect is maximized. In the present work this was $\Phi = 1.35$ for propane. For methane the vented overpressure occurred at the same mixture strength as that for the maximum laminar burning velocity, but the cellular flames did contribute to the higher flame speeds and overpressures. This is because for methane rich mixtures do not have greater cellularity. At lean concentration (low equivalence ratio), high burning velocities mixtures exhibit a detonation spike in the pressure traces inside the vessel even though the behaviour of secondary explosion (burn-up) and pressure drops at the duct entrance reproduce what have been observed in methane/air and propane/air mixtures well after the flame has left the vessel-duct assembly.

The correlation offered in NFPA 68 (NFPA68, 2002) and from Bartknecht's work (Bartknecht, 1993) for the calculation of Pred with the duct was shown not to be conservative in comparison with the experimental data reported. It also highlighted that L/D is not the important factor in increase of P_{red} with the duct pipe in propane/air and methane/air but not for high burning velocity mixtures.

CHAPTER 6

VENTED DUCT GAS EXPLOSIONS WITH BIGGER DIAMETER PIPE ATTACHED

6.0 Introduction

The influence of duct attached to the main vessel on P_{max} has been investigated in earlier chapter. The investigation confirms the findings of the previous works and highlights some conclusive factors that lead to the severity of vented gas explosions with the duct pipe attached. From the work, major influences on the behaviour of vented explosions with attached duct pipe which leads to a severe P_{max} are;

- Increasing the aerodynamic resistance to flow as high unburnt gas velocity ahead of the vent is experienced in most of the cases, causing it choked and reducing the flow of unburnt gases out of the vessel ahead of the flame front. It then increasing the amount of trapped unburnt gases inside the vessel and hence the P_{max} also increases. The burn-up mechanism or secondary explosion inside the duct pipe causes the back flow towards the vessel and the interaction with the flame front will generate turbulent pressure wave and thus, enhancing the pressure inside the vessel and at some cases in high burning mixtures, it will lead to detonation.

- The acoustic oscillation induced in the duct that generate pressure in the vessel and thus modify the flame propagation inside the vessel and been studied extensively by Kordylewski and Wach (Kordylewski and Wach, 1988). The coupling of the flame with acoustics, flame turbulence interaction and sonic blockage in the duct were the possible explanation of the high pressure generated inside the vessel for venting gas explosion with the duct attached.

In order to reduce the peak over pressure in an explosion with a vent duct to that of a simply vented explosion (venting without the duct pipe attached), the vent area and vent pipe diameter needs to be increased (2002), but there has been no specific experimental validation of this procedure as this topic has been sparsely researched. In the presence of a vent duct, an increase of venting area and duct diameter has been found to not always result in a decrease in the peak over pressure (Ponizy and Leyer, 1999a). This returns the focus to the more realistic scenario of whether the similar behaviour would

be observed when the bigger duct pipe is attached in comparison to the duct area is the same as the vent.

The main reason for the increase in the overpressure when long vent ducts are attached to vents is due to the phase in the explosion when the flame is in the vent pipe with unburnt gas mixture ahead of it. The expansion of the burnt gases in the vent pipe greatly accelerates the unburnt gas flow and this increases the vent pipe friction, inlet and exit pressure losses (Lunn, Crowhurst and Hey, 1988). These effects are a function of the dynamic pressure in the vent pipe. In principle, the dynamic pressures in the vent pipe can be reduced by simply using a larger vent diameter than that for the vent, rather than increasing both the vent and vent pipe size. For example, if the vent pipe was twice the diameter of the vent then the vent pipe dynamic pressure would be reduced by a factor of 16, if the vent mass flow rate is remained constant. Some evidence that a larger vent pipe diameter would reduce the overpressure with no change in the vent size was provided by Nagy (Nagy and Verakis), which is quoted in NFPA 68 (2002). Nagy investigated the influence of a 35 % increase in the vent duct diameter (83 % increase in area) for the same vent diameter and compared this with an explosion with a 35 % increase in vent diameter and pipe diameter. Vent pipe lengths up to 5 m were investigated and showed that the overpressure where the vent pipe alone was increased in diameter was only 7 % higher than that when the vent and pipe diameter were increased. From the experiments performed on dust explosions with vent pipes (Lunn, Crowhurst and Hey, 1988), Hey (Hey, 1991) has suggested that the technique of using a larger vent duct diameter than the vent diameter is effective if the duct area/vent area is about ~ 2-2.5 and when P_{max} is less than 0.5 barg. It is considered that this approach would be a simpler method of designing for safe vent pipes and the present work investigated for gas explosions a vent pipe that was close to twice the vent diameter, as recommended by Hey (Hey, 1991).

To achieve equivalent venting with a larger vent pipe, a 0.5 m flange opening in the dump vessel was attached to a 0.315 m diameter vent pipe which was 1m long (L/D = 3.2) and 1.94 times the diameter of the 0.162 m diameter vent as mentioned in previous chapter (Test vessel 3). The same 0.162 m diameter gate valve was attached to the vent and discharged into the large vent duct. All the ducts were pressure rated at 25 bar, as detonation in the vent pipe was known to be a possibility with overpressure in the 15

bar range possible (Iida, Kawaguchi and Sato, 1985, Kordylewski and Wach, 1988, Lee and Guirao, 1982, Ponizy and Leyer, 1999a, Ponizy and Leyer, 1999b, Russo and Benedetto, 2007). If the 1 m long vent pipe was removed than the vent pipe was reduced to the 0.3m of the gate valve and dump vessel connecting flange (L/D 1.85). This was effectively a free vented explosion discharge and this configuration was used as the baseline free venting condition. The vented gases discharged into a 50 m^3 dump vessel, as shown in Fig. 2.3b. The vented gases 50 m^3 containment dump vessel was pressure rated at 11 bars as a detonation in here could not occur.

In this present work, only uncovered vent case was carried out with four different gases (methane, propane, ethylene and hydrogen) at different equivalence ratios. All mixtures were ignited at the end wall and/or at the centre of the vessel centreline by an electrical spark which gives 16 J energies for the gas explosion tests.

6.1 Effect of duct diameter on P_{max}

Figure 6.1 shows, for the most reactive methane/air mixture, the pressure-time profile inside the vessel at P_1 for the short 0.162m diameter pipe, which is effectively a free discharge, and for the two 1m long vent ducts of 0.162 and 0.315m diameter respectively. The results show that the larger pipe diameter (duct area / vent area, A_p/A_v = 3.78) has little effect on the overpressure compared to that with the vent duct the same diameter as that of the vent. This was not the expected result and did not agree with the results of Nagy (2002, Nagy and Verakis) or Hey (Hey, 1991). However, this situation is not been observed in hydrogen/air explosion as illustrated in Fig. 6.2 where vented explosion with bigger pipe attached (D_p = 0.315m) shown the pressure peak is about 2 times higher than vented explosion with duct diameter of 0.162m. Interestingly, the peak pressure for vented explosion with 0.162 m diameter pipe attached gave the same peak pressure as the baseline case i.e. simply vented. Interestingly, this trend is not observed for end ignition where maximum pressure is lower for baseline case in respect with duct vented explosion as shown in Fig. 6.3. Again, for centre ignition, the pressure rise inside the vessel is directly influenced by the mixture reactivity left inside the vessel after the flame exited the vessel and the presence of the duct gave little effect to the final value of pressure in this case. This observation contradicts with the other works

where the presence of the duct pipe attached with the vessel gave higher P_{max} compared to simply vented explosion.

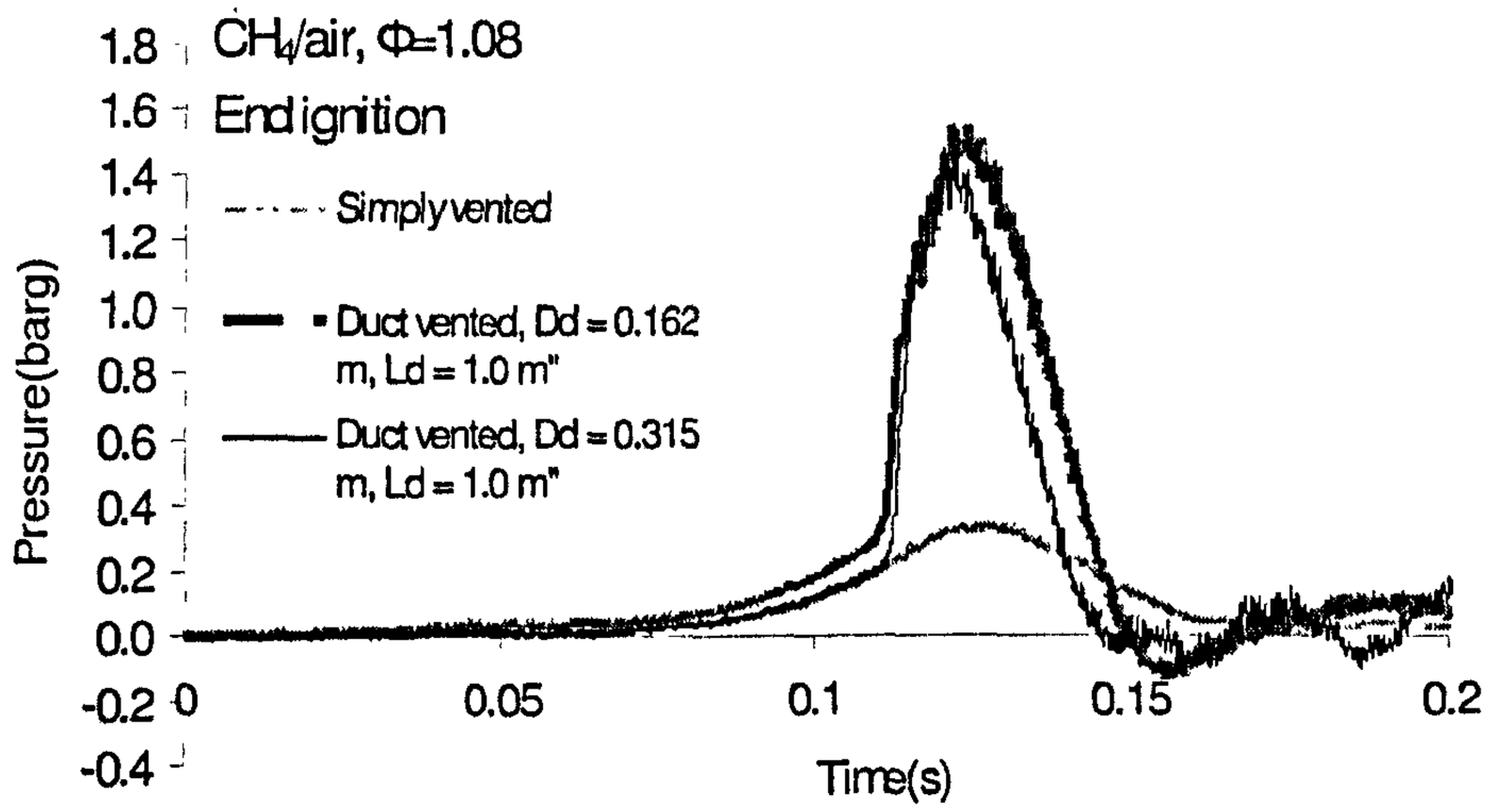

Figure 6.1 Pressure time profile for methane/air at $\Phi = 1.08$

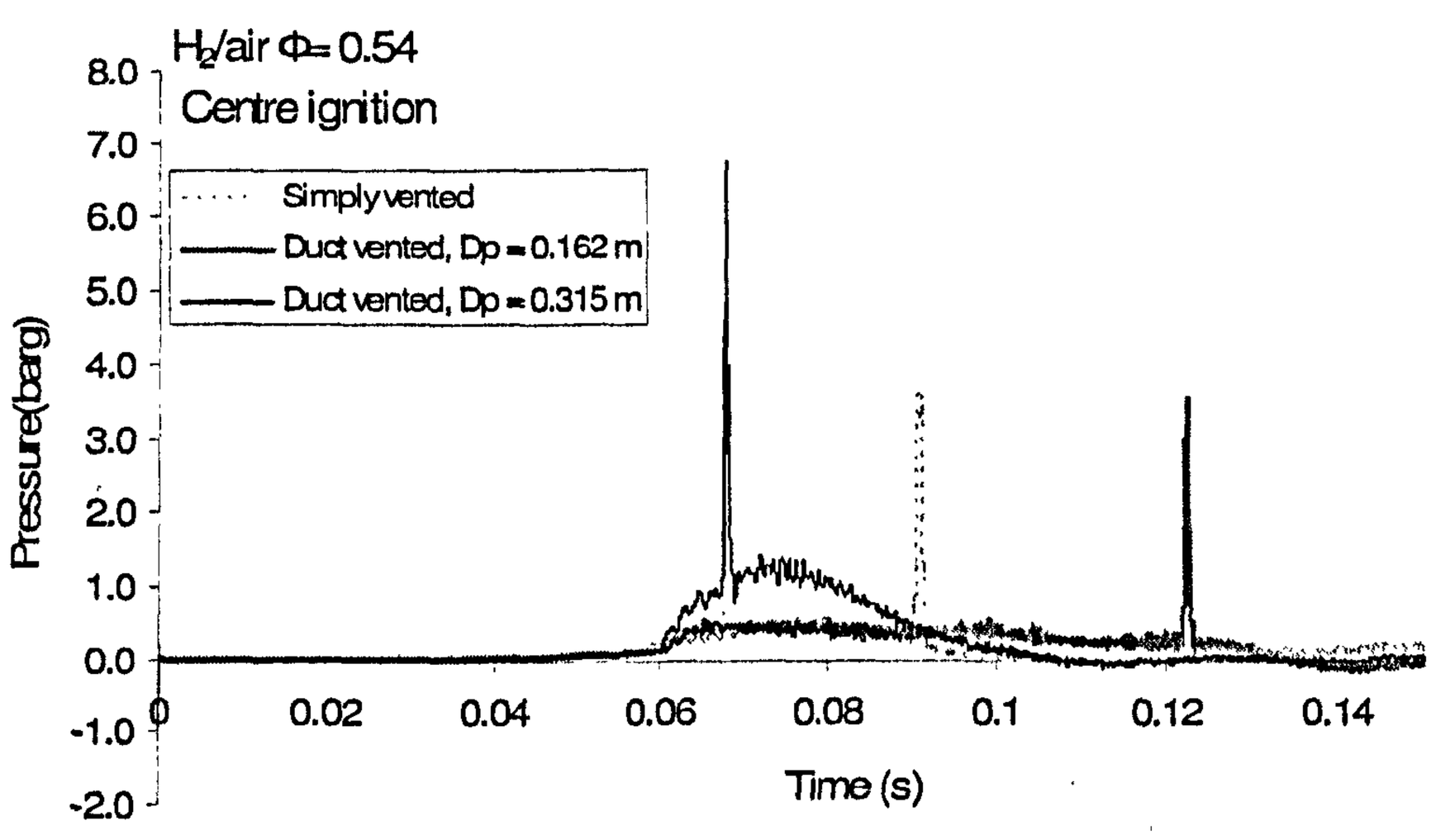

Figure 6.2 Pressure time profile for hydrogen/air at $\Phi = 0.54$

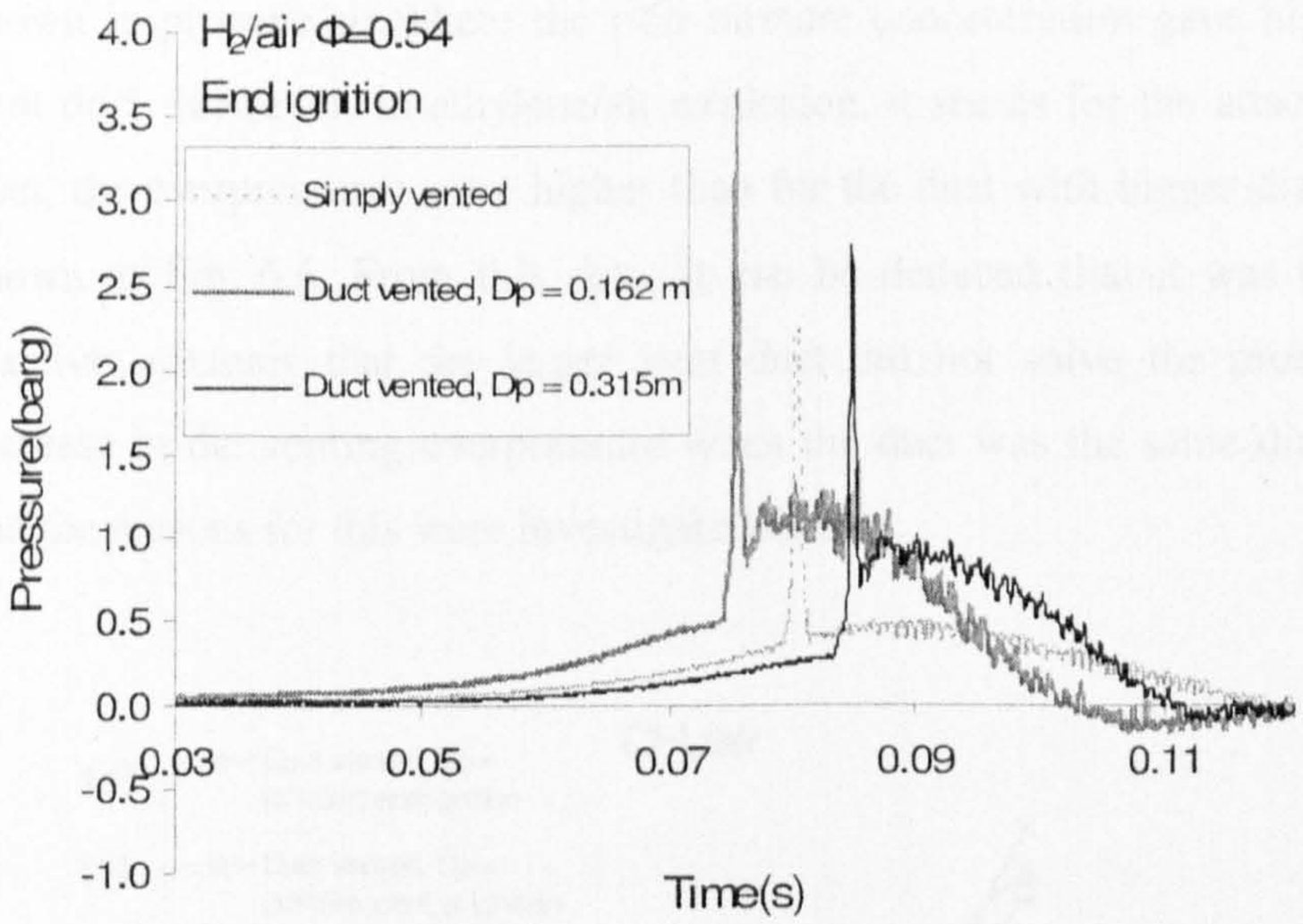

Figure 6.3 Pressure time profile for hydrogen/air at end ignition. $\Phi = 0.54$

From Fig. 6.2 and 6.3, it can be deduced that ignition position gives important influence on the final pressure inside the vessel. As discussed in previous chapters, the combustion inside the vessel is almost completed when the flame exited into the duct pipe, leaving only small amount of unburnt gases inside the vessel which results in high flame speeds and hence high unburnt burning velocity prior to duct entrance. The final pressure inside the vessel is directly due to the high turbulent reversal flow from the duct pipe to the vessel from a violent burn-up or secondary explosion and the flame front interaction with the pressure/shock waves. In other words, there is a mutual interaction between the vessel and duct during the explosion development marking to the final pressure inside the vessel. For central ignition, the interaction between vessel and the duct seems not playing an important role in order to determine the final pressure but due to the substantial amount of unburnt gases left inside the vessel.

To further investigate the overall trend of vented gas explosion with bigger diameter pipe attached, P_{max} as a function of equivalence ratio for all studied gases were presented in Fig 6.4 – 6.7. For methane, at $\Phi = 0.84$, the larger vent duct had only a slightly larger overpressure than for the near free vent condition and at $\Phi = 0.68$, the overpressures were the same. However, for the 0.162 m vent duct the overpressures were always much higher than for the free vent at all equivalence ratios but slightly lower in respect with larger vent pipe at $\Phi = 1.05$ for end ignition. The same trend is

shown in propane/air where the rich mixture concentration gave high P_{max} for larger vent duct. However, in ethylene/air explosion, it seems for the attached 0.162 m vent duct, the overpressures were higher than for the duct with bigger diameter attached as shown in Fig. 6.6. From this data, it can be deduced that it was only for the most reactive mixtures that the larger vent duct did not solve the problem of the large increase in the venting overpressure when the duct was the same diameter as the vent and the reasons for this were investigated further.

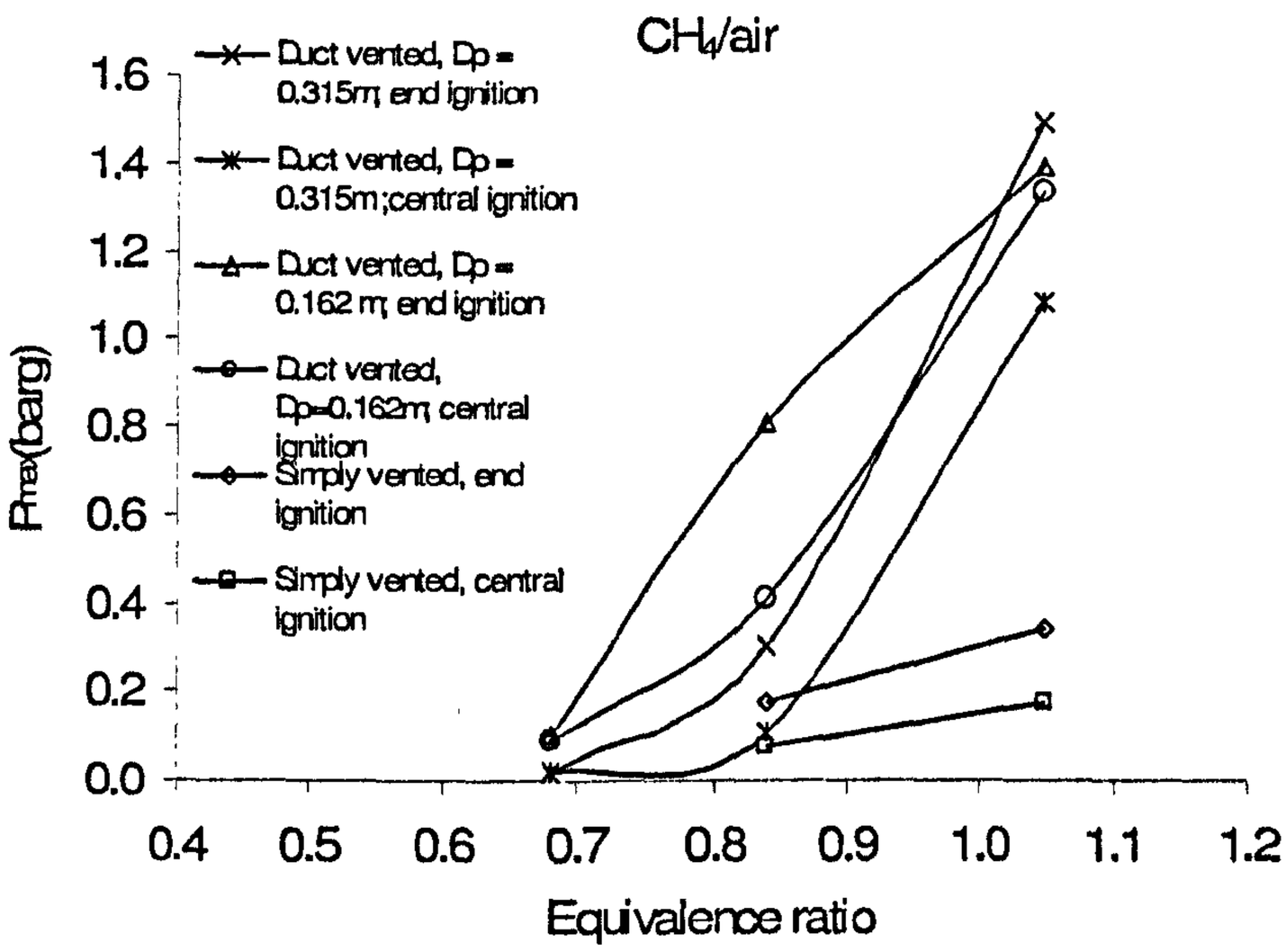

Figure 6.4 P_{max} of methane/air as a function of equivalence ratio

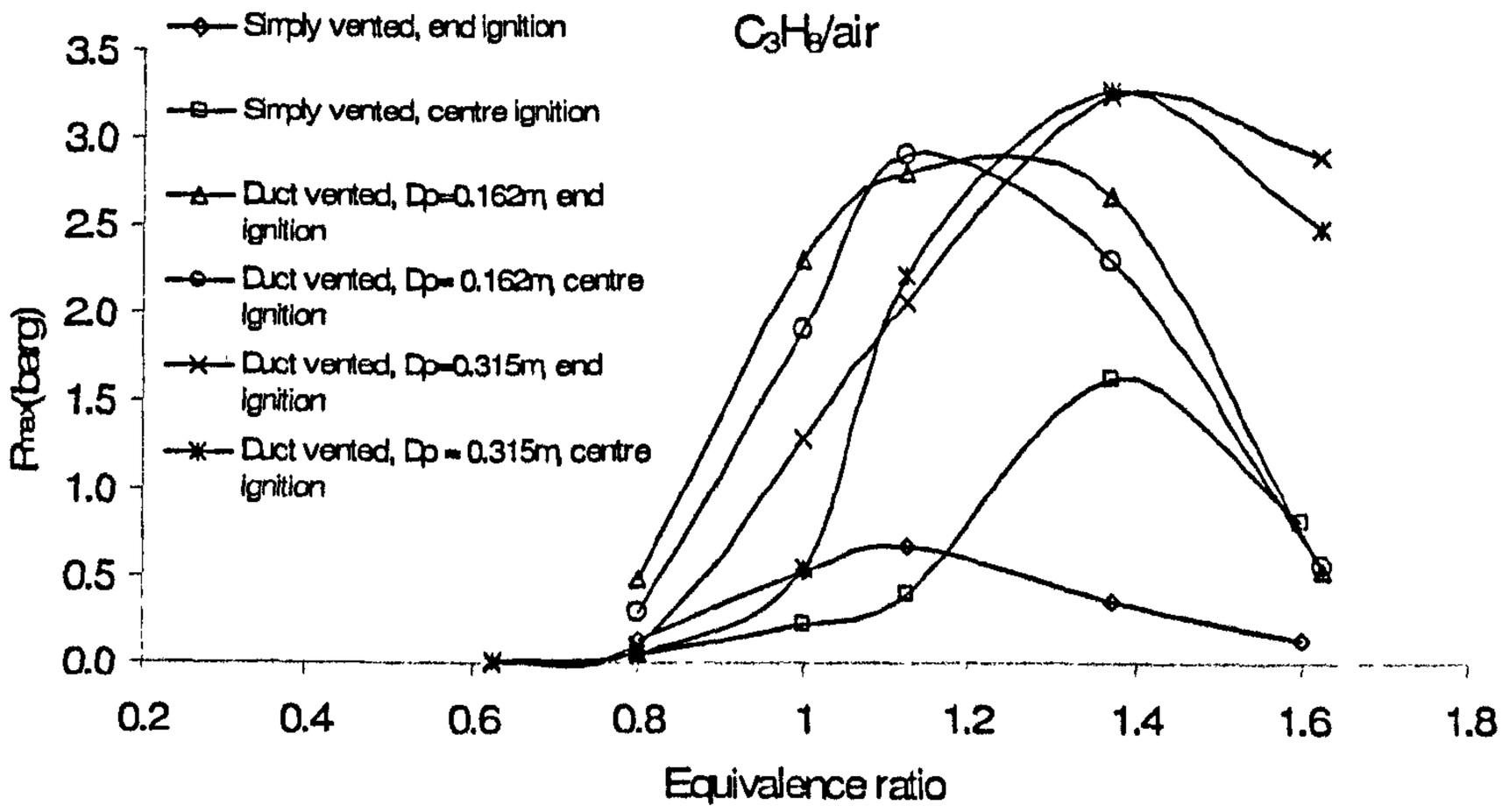

Figure 6.5 P_{max} of propane/air as a function of equivalence ratio

The overpressures in Fig. 6.4 and 6.5 for the most reactive mixture (P_{max} = 1.49 bar for Φ = 1.08 for methane/air at end ignition and P_{max} = 3.26 bar for Φ = 1.375 at centre ignition for propane/air) cannot be predicted from recommended correlations by Bartknecht (Bartknecht, 1993) as written in Eq. 5.3 and 5.4. As mentioned in Chapter 3 for simply vented explosion, Bartknecht (Bartknecht, 1993) gave the correlation for 100 mbar static vent burst pressure as;

$$\frac{1}{K} = \frac{0.1265 \log K_G - 0.0567}{P_{red}^{\ 0.5817}} \tag{6.1}$$

The free vent overpressure is predicted by Eq. 6.1 to be 5.45 bar for methane/air compared with the measured value of 0.35 bar. It is 7.46 bar for propane/air from Eq. 6.1 and 1.62 bar experimentally. It is clear that Eq. 6.1 cannot be applied to smaller vessel volumes. Examination of the venting data of Bartknecht (2002) shows that all of his vessel volumes had lower overpressures than for Eq. 6.1 and that this was the correlation for his data for a 10 m^3 vessel. If the measured free vent overpressure of 0.35 bar for methane is taken then the effect of a vent duct < 3m long is predicted by Eq. 5.1 and 5.3 to be an increase in the overpressure to 1.23 bar and only 0.5 bar respectively, well below that measured experimentally. However, if the correlation in Eq. 5.4 for duct length > 3m is used then the predicted increase in the measured overpressure is 1.44 bar for methane and 3.18 bar for propane, which is closer to the measured results in Fig. 6.4 and 6.5 for methane/air and propane/air respectively. Yet, Eq. 5.2 given for duct length in between 3 m and 6 m seems to give under predicted value of 1.03 bar for methane and 1.44 bar for propane if compared to Eq. 5.4. Summary of the predicted values based on Eq. 5.1-5.4 and experimental results is shown in Table 6.1.

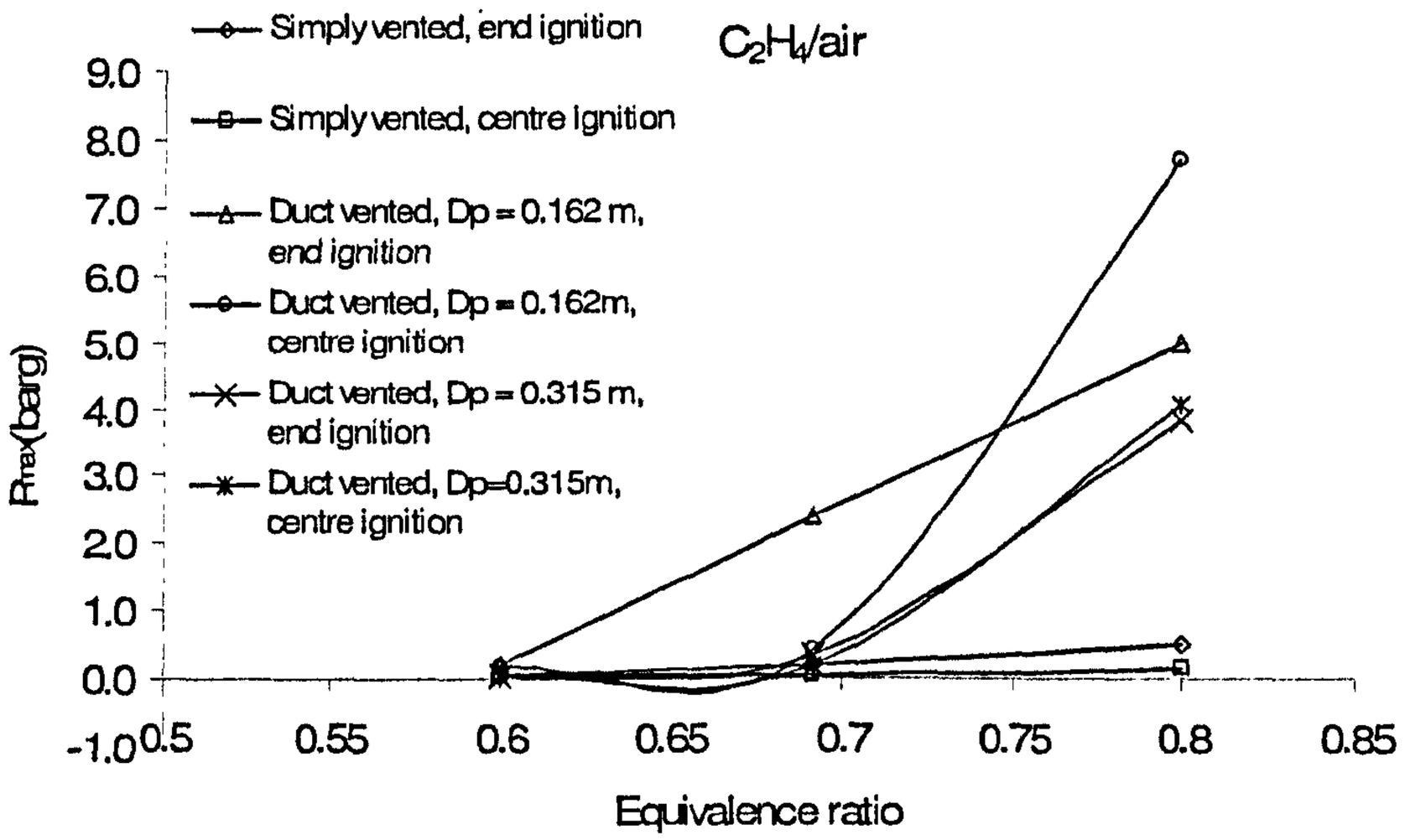

Figure 6.6 P_{max} of ethylene/air as a function of equivalence ratio

Table 6.1 Summary of experimental results (highest P_{max} either end or central ignition) with predicted values from Eq.5.1, 5.2, 5.3 and 5.4 where P_{red} without duct obtained from the simply vented experimental data.

Gas/air	Expt data with 0.315 m dia. duct	Expt data for simply vented	Eq.6.1	Eq.5.1	Eq.5.2	Eq.5.3	Eq.5.4
Methane/air (Φ= 1.08)	1.49	0.34	5.44	1.23	1.03	0.49	1.42
Propane/air (Φ = 1.37)	3.26	1.62	7.46	2.37	1.45	1.87	3.18
Ethylene/air (Φ = 0.8)	3.82	0.50	10.93	1.36	1.06	0.68	1.73
Hydrogen/air (Φ = 0.54)	6.50	4.78	14.59	5.80	4.57	4.77	5.56

From Table 6.1, it can be recommended that Eq.5.4 for duct length in between 3 and 6 m derived by Bartknecht (Bartknecht, 1993) gave reasonable value compared to experimental data. As discussed previously, Eq.5.4 applies for sonic venting conditions as well as long vent pipes and it will be shown below that the venting conditions are close to sonic with a vent pipe attached. It can be postulated that the present results are quite at variance with the correlations for vent design and vent ducts in Eq. 6.1 and 5.4 respectively and further work is recommended in the reliability of these correlations, especially for smaller volumes and high K. It is possible that for smaller K the lower vent flow velocities would create less turbulence in the vent ducts and the present large back pressures would be eliminated. The effect is essentially the same as using leaner mixtures with the present case. At lower K the velocities in the vent pipe would not be as high for the most reactive mixture and the back pressure increase with the vent would be lower.

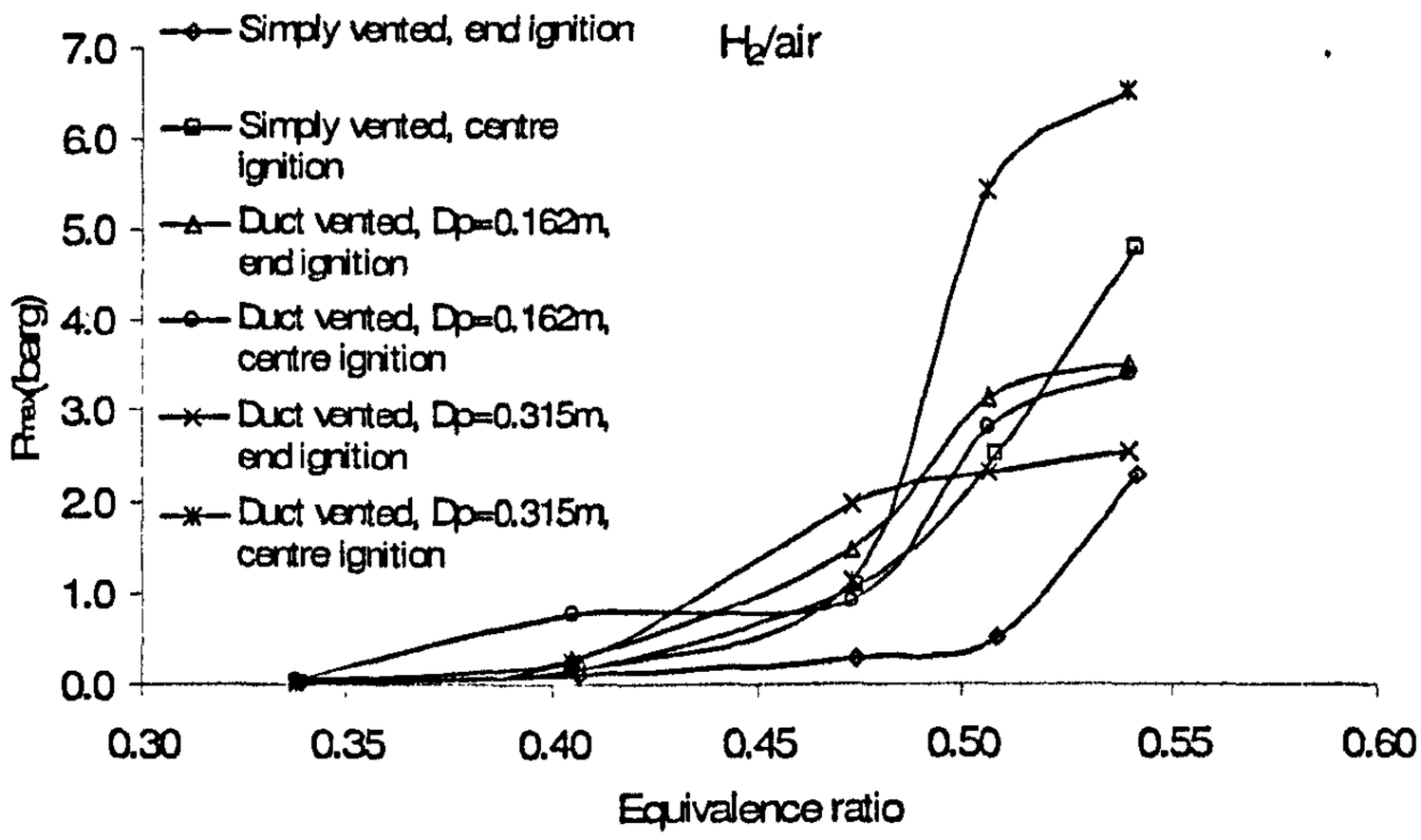

Figure 6.7 P_{max} of hydrogen/air as a function of equivalence ratio.

However, the trend showed an impingement in the case of H_2/air from previous experimental results obtained in hydrocarbon/air. At lower concentrations magnitude of P_{max} is higher with larger duct pipe compared to 0.162 m diameter duct pipe with respect to hydrocarbon/air's profile as shown in Fig. 6.7. Surprisingly, higher overpressure is observed for simply vented result at Φ = 0.54 for central ignition in comparison with vented explosion with 0.162 m diameter duct pipe attached. As illustrated in Fig. 6.3, a sudden detonation spike appeared in all cases, venting with the duct pipe attached and simply vented. This peculiar result envisages that the violent of

burn-up mechanism inside the duct can be ruled out to be the important role for the final overpressure inside the vessel in the case of centre ignition. Conclusion can be drawn based on this observation; the significant rapid rise of final pressure inside the vessel or 'detonation spike' depends on the flame instabilities (sudden venting can give rise to flame instabilities and rarefaction wave (Dorofeev, Bezmelnitsin and Sidorov, 1995)), auto-ignition/auto turbulence of the unburned pockets of mixtures inside the vessel which increase the burning rate due to faster flame and the scale of flow distortion. The plots of flame time arrival at the corner of the vessel at the spark end where a flame arrival thermocouple was located would be best illustrated for auto-ignition condition observed in the present case (refer to Fig. 6.8). If the plot is also valid for central ignition, then it is confirmed that auto-ignition is the significant role for the high pressure rise or 'spike detonation' observed in the hydrogen/air tests. The details of deflagration-to-detonation mechanism are also discussed in Chapter 4.2 for simply vented case. It then can be postulated that with central ignition, the bigger quantity of fresh mixtures left for the residual combustion in the vessel is the main contribution of the high magnitude of 'spike detonation' pressure in comparison with the pressure peak attained at end ignition inside the vessel. However, as observed before, 'detonation spiky pressure' is not exhibited in methane/air as methane does not auto-ignite easily but it can undergo highly turbulence combustion.

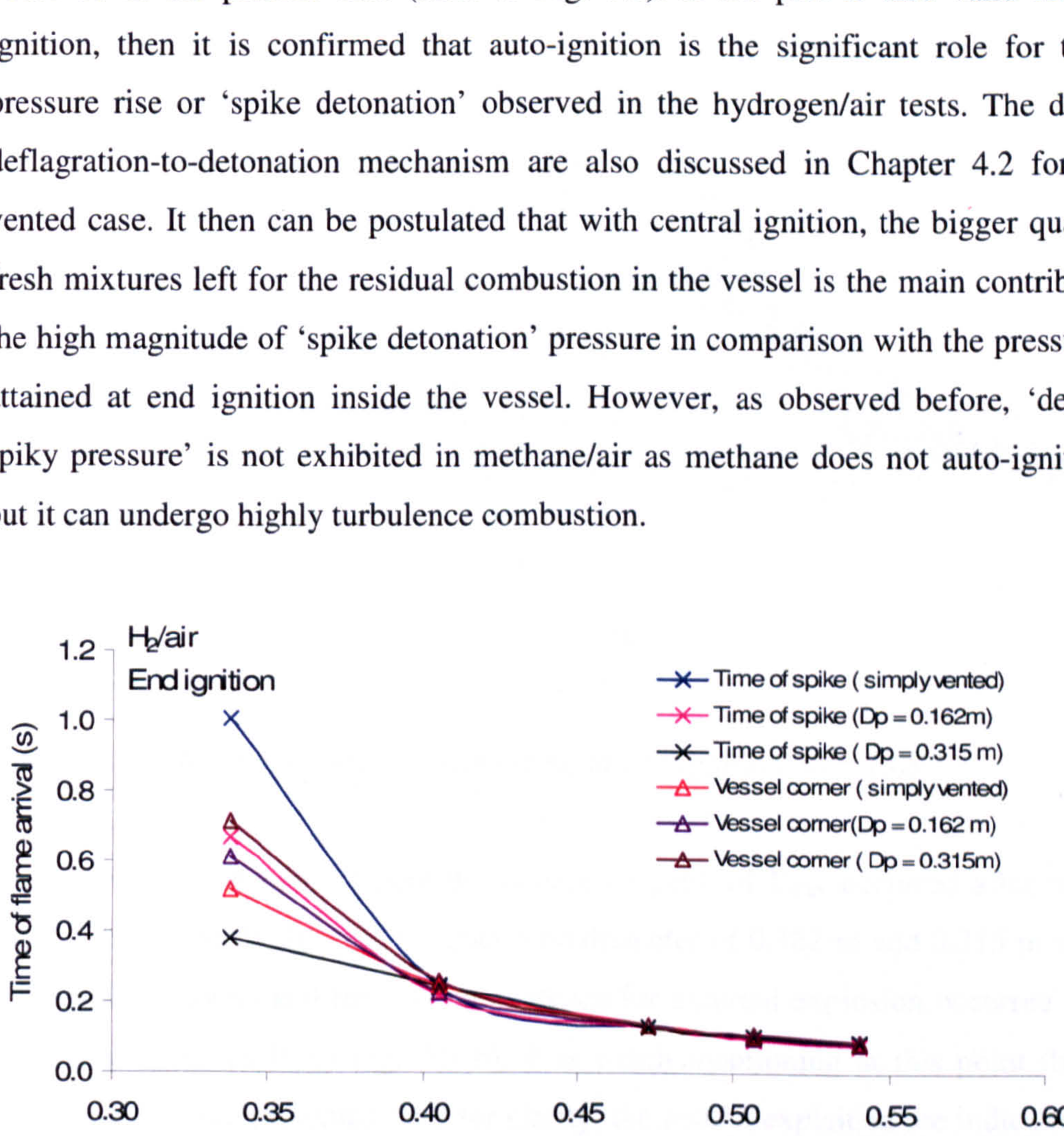

Figure 6.8 Time of flame arrival as a function of equivalence ratio.

The implication from this foregoing is that, if the flammable mixture is initially rich in the case of hydrocarbon/air then the combustion-like-explosion (burn-up) inside the duct may be much severe than expected on consideration of the magnitude of simply vented case, due to the high flame speeds and hence the high unburnt gas velocity ahead of flame prior to duct entrance in the case of hydrocarbon/air. To get more insight to this phenomena, the flow interaction between the main vessel and the duct were illustrated in Fig. 6.9.

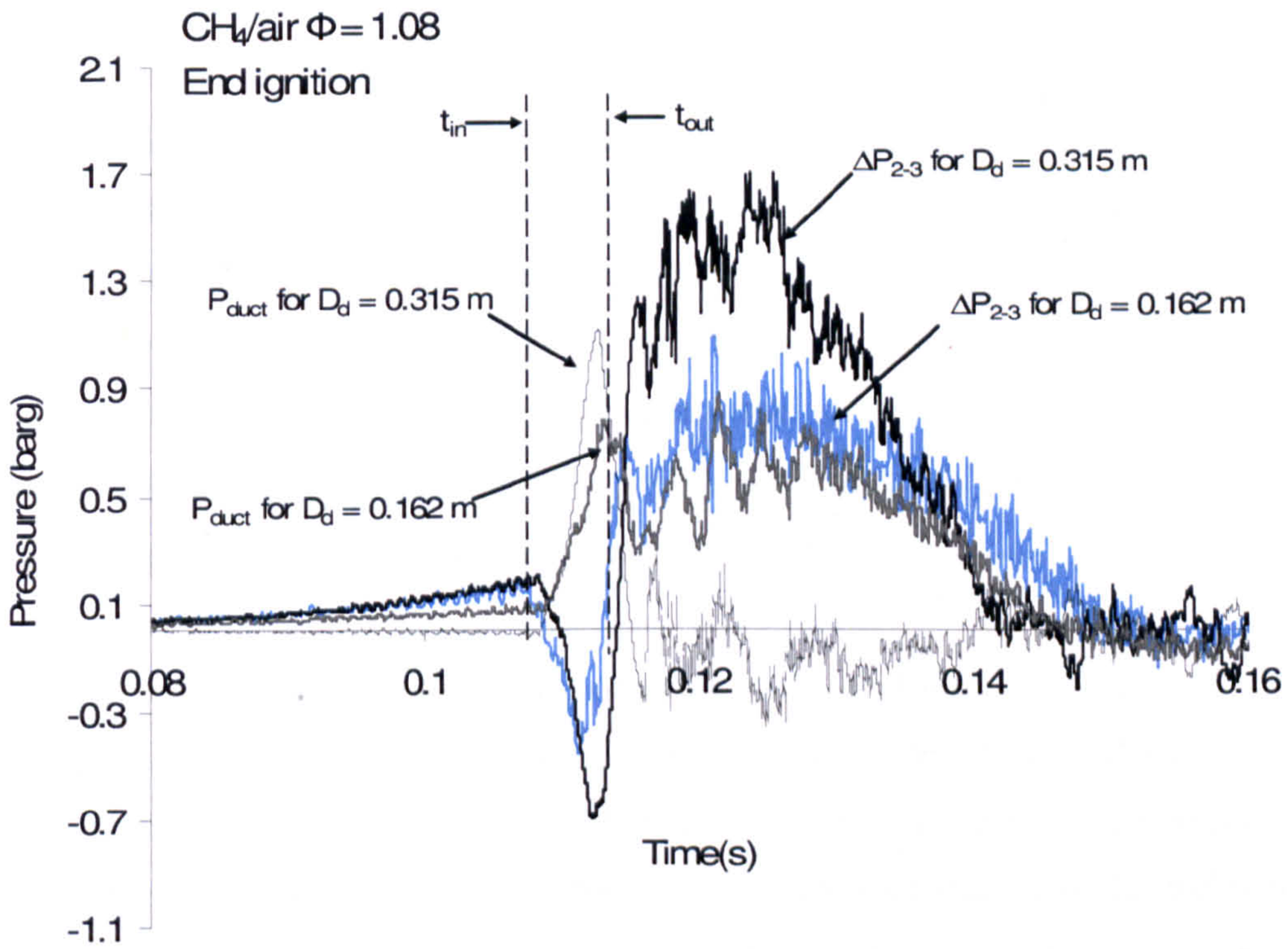

Figure 6.9 Flow interactions for methane/air at end ignition. Φ = 1.08

The same trend observed where the maximum peak of P_{max} occurred after the flame exited the duct for both cases i.e. duct pipe diameter of 0.162 m and 0.315 m as shown in previous chapters and there is no evidence for external explosion occurred in dump vessel (indicated as P_6 in Fig. 2.3 b). It is worth mentioning at this point that while individual test was presented here for clarity, the results explained are indicative of the trends displayed for this test vessel for all studied gas/air. At this point, methane/air at Φ = 1.08 would be the best representative to describe and explain the phenomena occurred during the explosion development in comparison with the smaller duct pipe diameter i.e. 0.162 m. The pressure difference between the explosion vessel and the vent pipe is shown in Fig. 6.9 as a function of time, together with the vent duct explosion pressure.

This shows that when the flame was in the duct, there was a negative pressure difference, which was higher for the large vent duct attached. The pressure difference between the explosion vessel and the duct in the initial stage of the explosion can be used to compute the mean velocity of unburnt gas into the duct, during the period before the flame entered the vent duct. The dynamic head pressure loss for a pipe inlet for incompressible flow is 0.5. The pressure difference reaches a maximum of 0.2 bar, just prior to the flame entry in the vent duct, as shown in Fig. 6.9. This corresponds to a mean unburnt gas velocity in the vent of 258 m/s. However, the sharp edge to the vent will produce a vena contraction and the velocity at the vena contraction, using a contraction coefficient of 0.61, would be 423 m/s. This is close to the speed of sound (360 m/s) and the compressible form of Bernoulli's equation should be used. However, this shows that very high unburnt gas velocities close to sonic conditions were generated at the vent and these create high turbulence conditions in the vent pipe which the shock waves will be generated and this creates a high back pressure and the observed reverse flow back into the explosion vessel (Kasmani, Andrews, Phylaktou, Willacy, 2007, Ponizy and Leyer, 1999a, 1999b). The details of the pressure loss and unburnt gas velocity will be discussed later in Section 6.3.

The bigger negative pressure difference occurred at the duct pipe region (illustrated as t_{in} and t_{out}) indicates the strong outflows from the pipe to the vessel and then creates high turbulence in the explosion vessel. Much of the unburnt gas mixture remains in the explosion vessel at the time that the flame enters the vent duct and the turbulence created by the reverse flame flow from the vent duct in the explosion vessel causes a sudden increase in the turbulent burning rate in the explosion vessel, marking the rate of pressure rise to 220 bar/s and creating a high rate of vent discharge and thus, the large increase in the overpressure. The higher overpressure with the large vent was due to the larger negative pressure between the vessel and the vent duct the large induced reverse flow.

The implication of this action is reverse flow caused by the larger duct diameter would result in larger scale mixing into the vessel as shown in Fig. 6.10. This phenomena has also been found by other workers (Kasmani, Andrews, Phylaktou, Willacy, 2007, Ponizy and Leyer, 1999a, 1999b). When the pressure difference between the vent duct and the vessel was high, the vent duct pressure became low and this was the greatest

difference for the large vent duct. For the small vent duct the static pressure in the duct was similar magnitude to the pressure difference between the vessel and the duct.

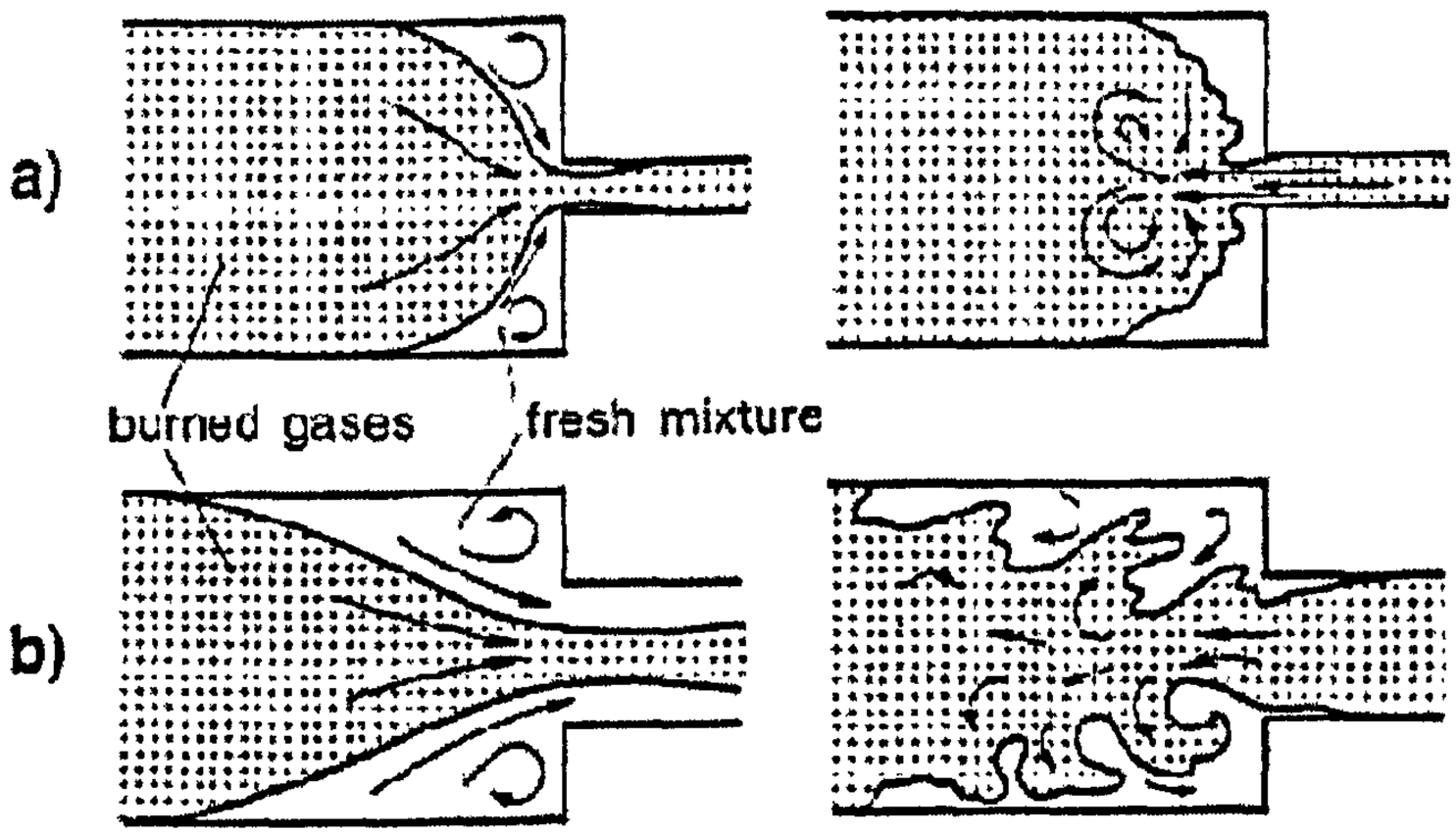

Figure 6.10 Flow regimes in vessel before and after explosion-like combustion in duct, effect of the flame front distortion; a) narrow ducts b) large duct. Reproduced from (Ponizy and Leyer, 1999b)

Ponizy and Leyer (Ponizy and Leyer, 1999a) demonstrated that a significant increase of overpressure occurred in relatively large vent ducts. This was shown to be due to the compression wave propagating towards the vessel, which was generated at the flame front in the duct created by the highly turbulent vent discharge flame. A model of the turbulent acceleration of dust in ducts have been performed by Clark and Smoot (Clark and Smoot, 1985). The model showed that the flame accelerates more rapidly and propagates at higher velocities in larger ducts. Increasing the diameter will increase the turbulent Reynolds number and since the turbulent Reynolds number is the only way in which turbulence is incorporated into the model, a very high pipe turbulence level leads to very high flame speeds in the vent pipe. It is considered that this phenomena was occurring in the present work with the large diameter vent pipe and much smaller vent.

However, using the bigger duct pipe diameter seems to agree with the theory stated above for lean mixtures concentration where the overpressure inside the vessel is lower, compared to the pipe having the same diameter as the vent as shown in ethylene/air at Φ

= 0.8 for end ignition (Fig. 6.11). Apparently, the peak pressure for duct pipe of 0.162 m diameter reached its peak earlier after the flame exited the duct in comparison with explosion with larger vent and simply vented. A possible explanation for this lies to the different sequence of events inside the vessel and the duct.

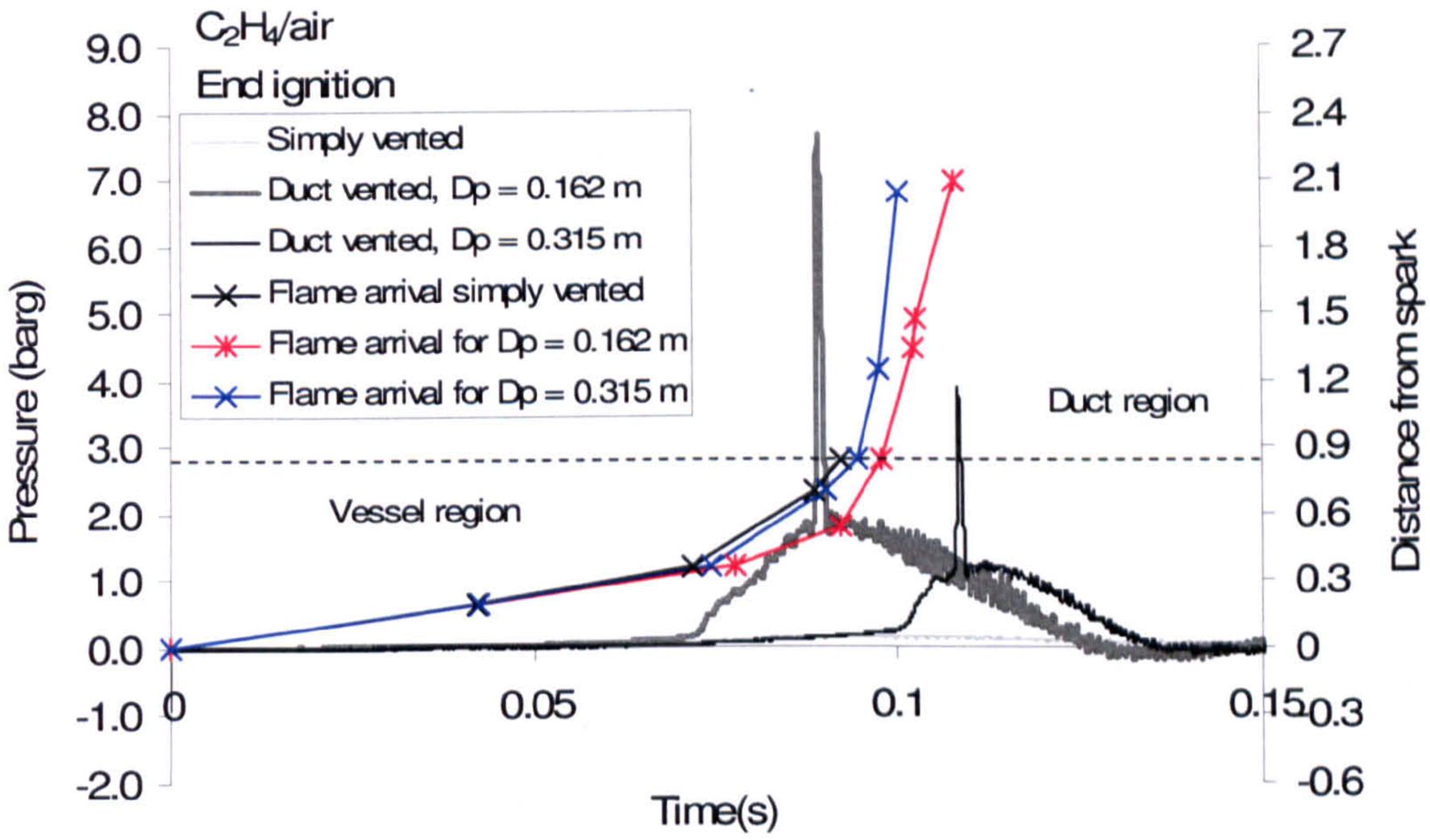

Figure 6.11 Pressure time histories and flame arrival for ethylene/air at $\Phi = 0.8$.

For leaner combustion at relatively small vent area, the outflow of unburnt gases into the larger vent duct is less turbulent and hence, the combustion-like-explosion event inside the duct is less severe. Hence, the final explosion inside the vessel is reduced as expected. Lower value of P_{duct} in larger duct diameter is due to faster discharge of fresh from the vessel but also to earlier arrival of the flame front at the duct entrance (refer to Fig. 6.11 and 6.13). However, it is apparent that the combustion is still occurred inside the 0.162 m duct pipe when the peak pressure inside the vessel marked its peak, suggesting that there is still strong interaction between the vessel and the duct before the flame exited the duct pipe and hence, producing a greatly increased pressure rise in respect to the simply vented explosion.

The study by Iida et al (Iida, Kawaguchi and Sato, 1985) mentioned that flame was found to extinguish or hesitate in the channel before passing through in some cases, depending on the equivalence ratio of the mixture, the channel with and the flame inflow velocity. Other studies supported the above hypotheses by using relatively

narrow ducts with a sharp vessel-duct area (Iida, Kawaguchi and Sato, 1985, Ponizy and Leyer, 1999a,1999b). It showed that the flame front entering the duct can be temporarily extinguished due to stretch and cooling through turbulent mixing with unburned gas which brings about stronger burn-up (i.e. with higher pressure amplitudes) during re-ignition (Ponizy and Veyssiere, 2000). At this point, generally an oscillating flow is profoundly established as shown in Fig. 6.11. It seems that at lower equivalence ratio, inertia of the gas column plays a more conspicuous part in pressure variations inside the vessel for the vented explosion with narrow duct pipe, i.e. 0.162 m diameter pipe in this present case. The same result was also observed with propane/air explosion at $\Phi = 0.8$ as shown in Fig. 6.13. Even though there is no 'spiky' pressure traces, the pressure generated with duct vented at larger duct diameter is lower compared to simply vented explosion. This complex situation is difficult to explain. The possible explanation is due to the reverse flow penetrates essentially into the region where there is very little unburned gas mixture left inside the vessel. Further, the short time for the flame front reaches the vessel walls will reduce its surface area rapidly and cause less burning rate inside the vessel and hence producing lower pressure.

The current results generally showed that the use of enlarged duct diameter can reduce the P_{max} below the value generated when using the narrow duct when applied to leaner concentration but P_{max} profoundly higher or about the same when applied to rich/reactive concentrations. From these results, it can be deduced that the flame self-acceleration is the important role in effecting the P_{max} inside the vessel with the duct pipe attached which is not be accounted in the venting guidelines i.e. NFPA 68 and European Gas Explosion Venting Guidance 2007. Further, these results are strictly applicable for open venting even though it is unlikely that the P_{max} of the vessel will be affected if P_v does not exceeded 100 mbar.

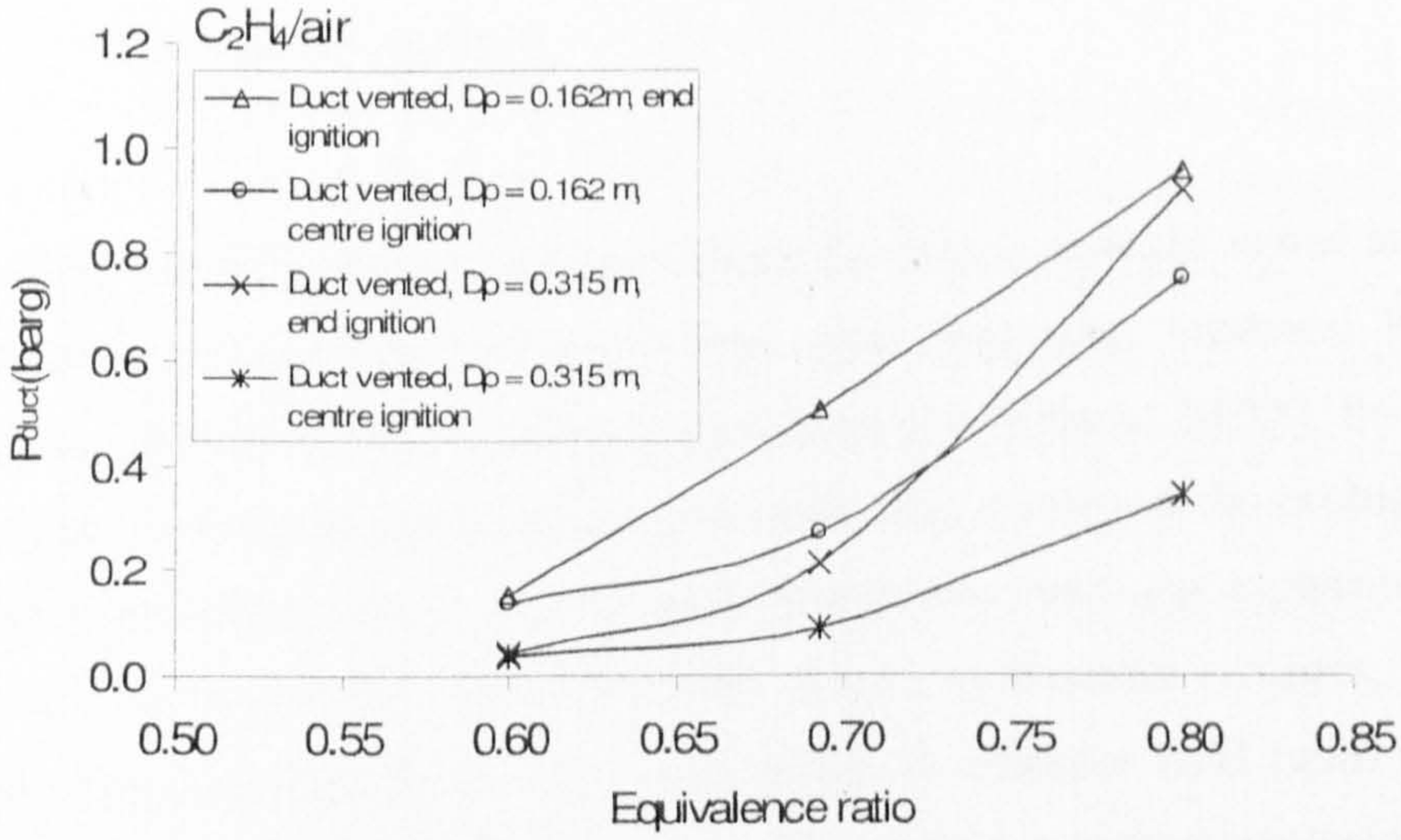

Figure 6.12 Pressure inside the duct for ethylene/air as a function of equivalence ratio.

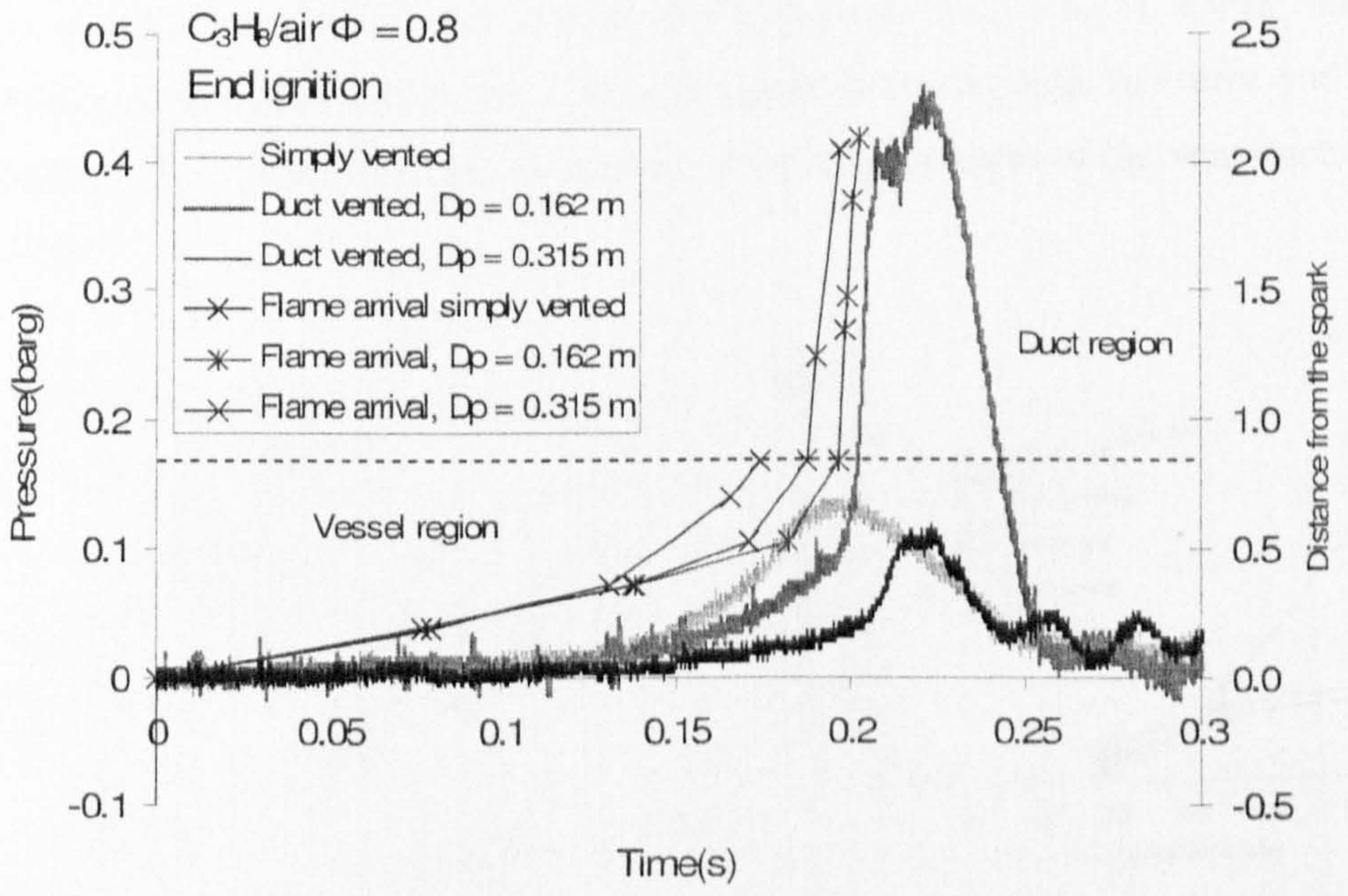

Figure 6.13 Pressure time histories and flame arrival for propane/air at Φ = 0.8 for end ignition.

6.2 Flame speeds analysis

Figure 6.14 shows the average flame speeds measured inside the vessel and the duct for methane/air. As reported from previous work (Kasmani, Andrews, Phylaktou and Willacy, 2007a, Kasmani, Andrews, Phylaktou and Willacy, 2007b), the induced flow through the duct plays an important role in the final severity of the explosion. This flow in the vent pipe is driven by the flame speeds and burnt gas expansion in the main vessel. The same figure also shows that at lean methane/air mixtures, i.e. $\Phi = 0.68$, there was negligible effect of the duct length or diameter (L/D ratio) on both flame speeds inside the vessel and the duct. At $\Phi = 1.08$, the highest explosion vessel flame speed of 22.8 m/s occurred for the short vent duct, which was close to a free discharge. For the large vent duct ($D_p = 0.315$ m or $L/D = 3.17$) the peak upstream flame speed was 19 m/s and for the vent duct the same size as the vent ($L/D = 6.17$), it was 16.8 m/s. The flame speeds approaching the vent were much lower for lean mixtures and hence the induced flow was lower and the impact on the overpressures of the vent ducts were then lower.

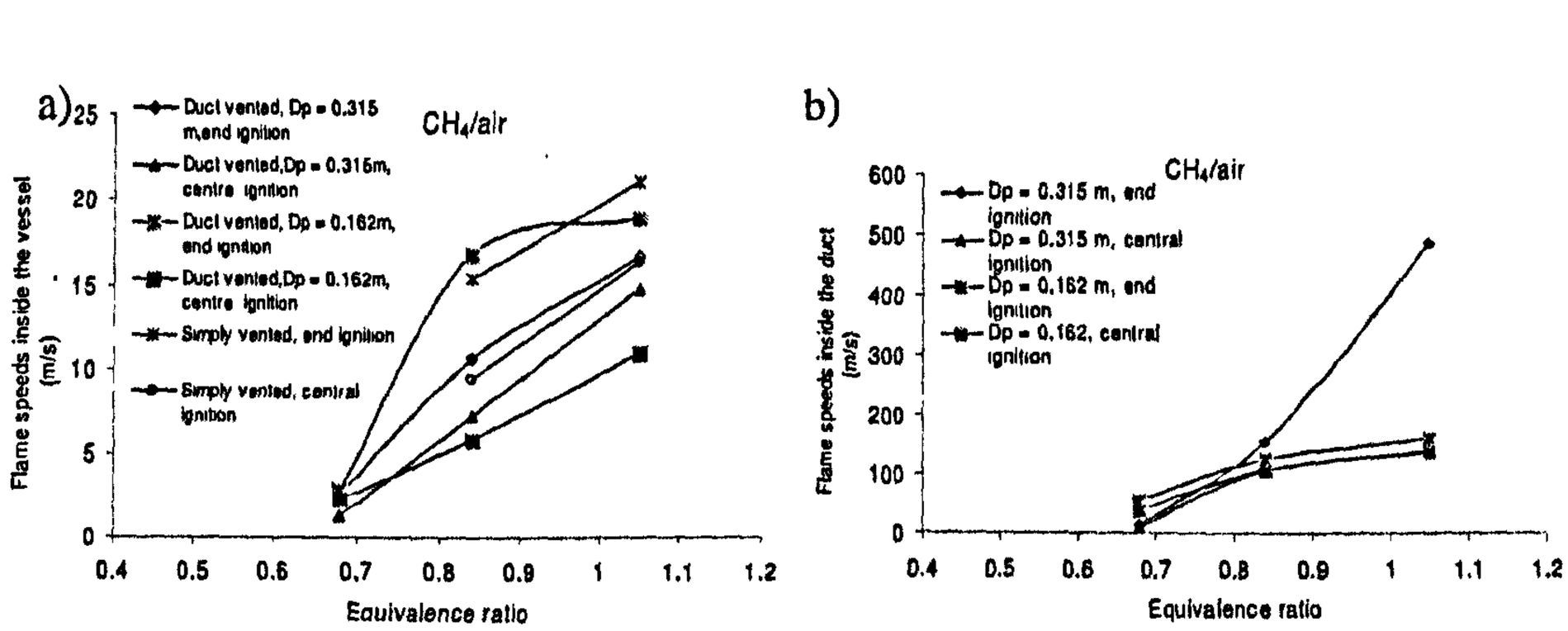

Figure 6.14 Average flame speeds measured (a) in second half of the vessel (between T_1 and T_3 as in Fig.2.3b) and (b) in the vent duct (between T_4 and T_9) as a function of equivalence ratio for methane/air.

The flame speeds in the main vessel approaching the vent were considerably higher than for spherical laminar flame speeds. This was due to two effects: firstly, self acceleration of the flame through the cellular flame front mechanism and secondly, the suction effect

of the vent discharge on the flame shape which would draw the flame expansion preferentially in the direction of the vent (Kasmani, Andrews, Phylaktou and Willacy, 2007a, Kasmani, Andrews, Phylaktou and Willacy, 2007b). These effects were both higher for end ignition as the distance to the vent was double that for central ignition and hence the two effects were enhanced. This was the main reason why the end ignition gave the highest overpressures compared with central ignition.

The flame speeds inside the duct were similar for both duct diameters, apart from the equivalence ratio at $\Phi = 1.08$ where the highest flame speeds of 490 m/s experienced at L/D = 3.18. The larger vent duct created a flow expansion from the vena contraction at the inlet vent to the duct wall. This flow expansion creates a pressure loss that is the source of the turbulence that accelerates the flame which is larger when there is a larger flow expansion. For the present geometry, the unburnt gas dynamic head pressure loss in terms of the vent area dynamic head, was 0.47 for the 0.162 m vent pipe and 1.27 for the 0.315 m diameter vent pipe. This produced more turbulence and a greater flame acceleration of the flame inside the larger vent pipe, as shown in Fig. 6.14. Also the lower mean velocities in the larger pipe would enable a flame to propagate in regions where there was local turbulent quenching in the smaller vent pipe (Kasmani, Andrews, Phylaktou and Willacy, 2007a, Kasmani, Andrews, Phylaktou and Willacy, 2007b) and this would increase the back pressure, as found experimentally. For leaner mixtures the velocities were much lower and the turbulence generation was significantly lower as this is proportional to the square of velocity. Hence, the effect of the vent pipe was much lower for the slower burning leaner mixtures.

However, the trend for leaner concentration results in lower flame speeds in the duct seems not applicable in the case of hydrogen/air explosion. As illustrated in Fig. 6.15, the flame speeds inside the duct was higher for all equivalence ratio for vent duct the same size as the vent compared to 0.315 m diameter duct for end ignition and marking its highest value at 484 m/s. This high flame speeds are due to the comparatively fast flame from the vessel due to large flame area effect. Study by Aung et al (Aung, Hassan and Faeth, 1997) showed that hydrogen at lower equivalence ratio $0.3 < \Phi < 0.6$ are in unstable preferential-diffusion conditions where developed chaotically irregular flame surfaces.

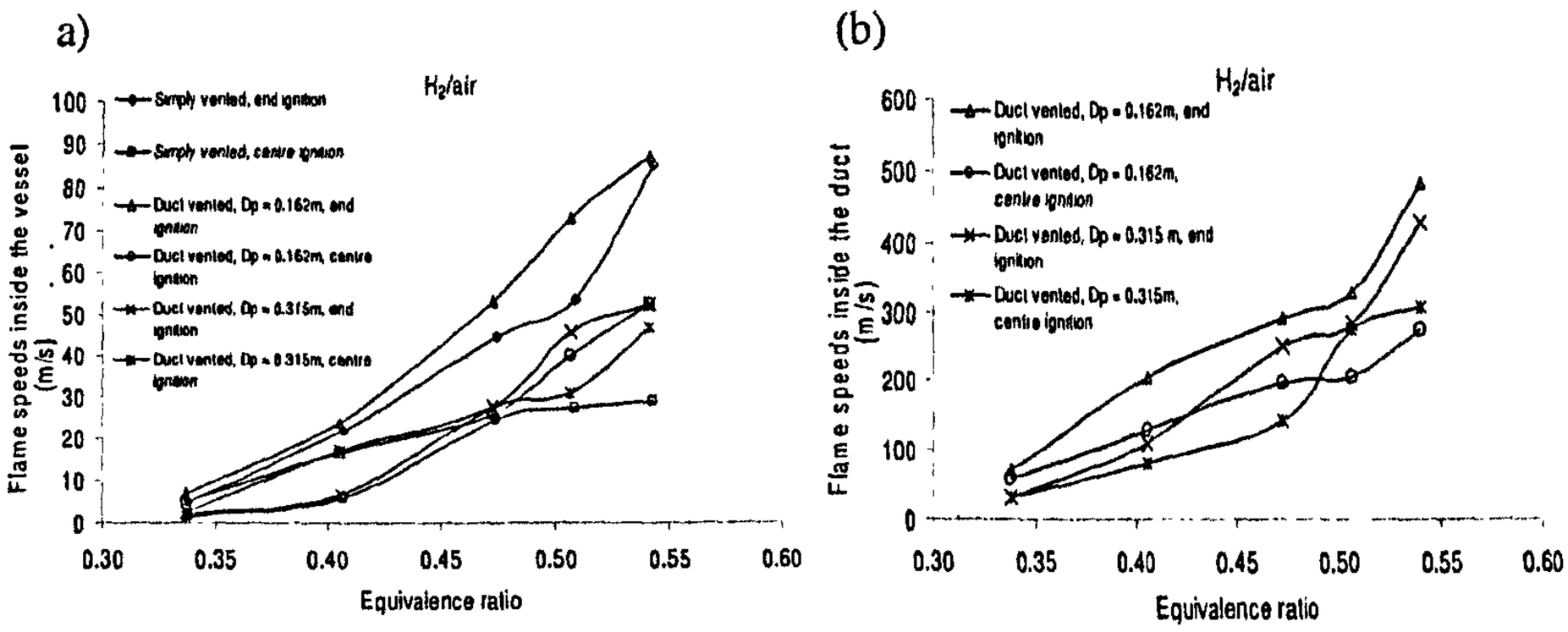

Figure 6.15 Flame speeds measured a) in second half of the vessel (between T_1 and T_3 as in Fig.2.3b) and b) inside the duct (between T_4 and T_9) as a function of equivalence ratio for hydrogen/air

The results agreed that Markstein no, Ma ≈ -1 at $\Phi = 0.3$ with neutral conditions (Ma = 0) at $\Phi = 0.7$. Markstein number is a physiochemical parameter that expresses the response of a flame to stretching. At low Ma no, all spherically expanding flames are intrinsically unstable with no stabilizing influence due to thermodiffusive effect (Bradley and Harper, 1994). As the flame is stretched, it begins to weaken and recede downstream due to the reduced local burning speed. This pattern continues to develop in time until the flame sheet finally breaks (Bell, Cheng, Day and Shepherd, 2007). Flame stretch influences laminar burning velocities through preferential diffusion of heat and mass. Within the thin-flameless regime, this can cause the instability of the flame surface depending upon the sign of the Markstein number. If the Markstein number is negative, the laminar burning velocity increases as the flame stretch increases with the following equation,

$$S_{L\infty}/S_L = 1 + MaKa \tag{6.2}$$

where $S_{L\infty}$ is the value of laminar burning velocity when the flame stretch, K = 0, SL is the laminar burning velocity, Ka is the Karlovitz number and Ma is the Markstein number given by equations as below respectively,

$$Ka = K\delta_D / S_L \tag{6.3}$$

$$\delta_D = D_u / S_L \tag{6.4}$$

$$Ma = L / \delta_D \tag{6.5}$$

The parameters stated in the equations are represented as;

K = flame stretch

δ_D = characteristic of flame thickness

D_u = mass diffusivity

L = Markstein length

Dimensionless Karlovitz and Markstein numbers are defined to characterise flame stretch and the response of a flame to stretch. For unstable condition, finite levels of stretch cause flame temperatures to be higher than for the unstretched flame (roughly 1550 K for the stretched flame with respect to 1400K for unstretched flame) (Aung, Hassan and Faeth, 1997). Perturbation of lean, premixed hydrogen flame induces a growing instability that evolves towards a cellular structure in corresponding to the increase of flame temperature, forming cracks or cusps in the flame surface and this cross-cracking develops until eventually the flame surface becomes completely cellular. This condition then promotes faster reaction rates and thus higher laminar burning velocities for the stretched flame. This is associated with a marked increase in flame speeds and this condition agreed with the experiment results showed. The schlieren cine photograph in Fig. 6.16 shows the cellular flame development during explosion of H_2/air mixtures at $\Phi = 0.26$.

Even though P_{max} for larger duct pipe at centre ignition exhibited highest value (refer to Fig.6.7), but yet the flame speeds inside the vessel and the duct disagreed with the result as $P_{max} \alpha S_u^3$. These results apparently showed that for centre ignition, the link between the vessel and duct pipe seems to be independent at some point, where the final value of P_{max} depends on the substantial amount of unburnt gases left inside the vessel as been postulated by others (Ferrara, Willacy, Phylaktou, Andrews, Benedetto, Salzano, Russo, 2008, Ponizy and Leyer, 1999a, 1999b).

A similar effect would occur for smaller K or larger vent diameters. The vent flow velocities would be reduced, lower turbulence levels in the pipe would be generated and lower overpressure increases due to the use of a vent would occur. It is significant that much of the published work on vent pipes, which all shows a large increase in the overpressure compared with a free vent discharge, was all carried out with relatively large values of K. More works on vent pipes has been carried out for dust explosions, but generally with K > 10. It is considered that in view of the limited experimental data on the impact of a vent duct on the overpressure for gaseous explosion and the potential importance of K and mixture reactivity (which determines the vent flow velocity) that more works is required to understand this type of venting phenomena and to provide more reliable venting design guidance.

6.3 Pressure loss and unburnt gas velocity

As mentioned earlier in Section 6.1, the pressure loss prior to the duct pipe entrance (indicated as $\Delta P_{2\text{-}3}$) and inside the pipe ($\Delta P_{3\text{-}6}$), will be used to calculate the unburnt gas velocity prior to duct entrance as well as the gas velocity inside the duct to ascertain the enhanced burning rate due to turbulisation and enhanced pressure drops due to the geometry are playing the important role to the final pressure inside the vessel. This can then leads to the comparison of the pressure loss for the vent pipe as being the same as the vent orifice and larger vent pipe. This simple analysis can be evaluated using;

$$\Delta P_{total} = \Delta P_{in} + \Delta P_{duct} + \Delta P_{out} = \frac{1}{2}\rho S_g{}^2 (Kin + 4f\frac{L}{D} + \sum_i N_i + K_{out}) \qquad (6.6)$$

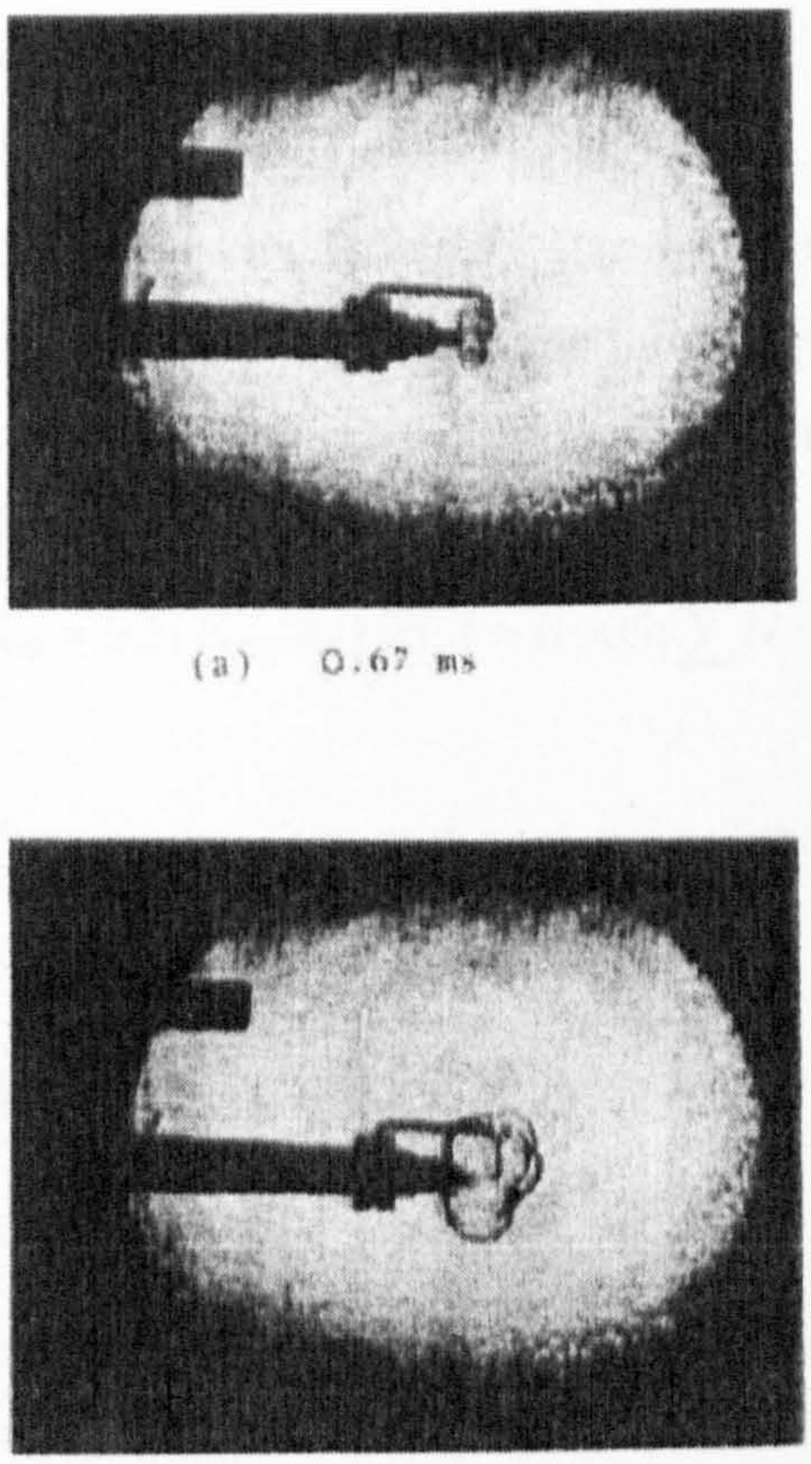

(a) 0.67 ms

(b) 2.51 ms

(c) 11.69 ms

(d) 20.04 ms

(e) 40.92 ms

(f) 59.29 ms

Figure 6.16 Schlieren cine photographs of cellular flame development during explosion of H_2/air mixture, Φ = 0.26. Reproduced from Bradley and Harper (Bradley and Harper, 1994).

K_{in} and K_{out} are respectively the pressure loss coefficients for sudden flow area restriction/enlargement (in the case of a flow to larger pipe from the vessel) and sudden flow area enlargement (pipe to dump vessel). f is the friction factor for he flow inside the duct evaluated from Darcy-Weisbach equation, Ni is the velocity heads lost in fittings (in this present case for duct pipe of 0.162m, one gate valve and two couplings in the duct; values reported in (Ferrara, Willacy, Phylaktou, Andrews, Benedetto and Salzano, 2005) was used. Below is the list of parameter values used;

$K_{in} = 0.5$; $K_{out} = 0.95$; $f = 0.005$; $\sum N_i = 0.25$

The pressure drop at the entrance of the duct pipe can be expressed as,

$$\Delta P_{in} = K\frac{1}{2}\rho S_g{}^2 \tag{6.7}$$

The actual value of K is strongly dependent on the geometry of the component considered. It may also be dependent on the fluid properties. That can be said,

$$K = \phi(geometry, \mathrm{Re}) \tag{6.8}$$

where Re is the pipe Reynolds number given by $\mathrm{Re} = \rho S_g D/\mu$. For many practical applications, the Re no is large enough so for the flow inside the pipe where inertia effect is more dominated rather than the viscous effects, is usually found that the pressure drops and head losses correlate directly with the dynamic pressure. Thus in most cases, the loss coefficients for components are a function of geometry only as Eq. 6.8 will be $K = \phi(geometry)$ (Munson, Young and Okiishi, 2006). Meanwhile, for pressure loss inside the pipe,

$$\Delta P_{duct} = \frac{1}{2}\rho S_g{}^2(4f\frac{L}{D} + \sum_i N_i) \tag{6.9}$$

From Eq.6.6, 6.7 and 6.9, unburnt gas velocity on each phase can be evaluated and determined as listed in Table 6.2.

Table 6.2 Calculated unburnt gas velocity at the duct entrance, inside the duct pipe and at the duct pipe exit for studied fuel/air mixtures.

Fuel/air	Pipe diameter, D_p (m)	Ignition position	Φ	S_g at duct entrance (m/s)	S_g inside the duct (m/s)	S_g exit (m/s)
CH_4/air	0.315	End	0.8	158.9	415.6	145.4
			1.05	251.0	942.3	357.5
		Centre	0.8	60.8	236.0	83.1
			1.05	95.4	769.6	222.2
	0.162	End	0.8	129.3	573.9	305.5
			1.05	235.8	634.2	367.5
		Centre	0.8	59.0	399.3	167.7
			1.05	103.6	501.5	232.7
C_3H_8/air	0.315	End	0.8	70.2	225.5	84.3
			1.0	305.2	823.5	320.3
			1.375	260.4	1437.5	505.95
		Centre	0.8	55.1	169.5	47.8
			1.0	166.7	548.7	177.6
			1.375	113.6	1379.7	333.1
	0.162	End	0.8	138.4	425.8	245.7
			1.0	254.1	686.7	429.4
			1.375	243.8	671.3	429.1
		Centre	0.8	69.0	206.9	113.9
			1.0	109.3	559.0	365.4
			1.375	109.3	443.4	296.4
C_2H_4/air	0.315	End	0.8	260.1	879.1	331.3
		Centre	0.8	111.4	1574.5	200.5
	0.162	End	0.8	207.7	562.1	508.1
		Centre	0.8	150.1	436.2	372.9
H_2/air	0.315	End	0.54	246.9	1470.2	313.6
		Centre	0.54	145.9	1820.5	391.9
	0.162	End	0.54	268.4	688.9	554.3
		Centre	0.54	132.2	434.0	252.1

From the tabulated data above (table 6.2), some interesting conclusions can be drawn. The high S_g at the duct entrance causes the restricted flow to the duct pipe and this eventually leading to the chocked flow (sonic venting) due to the higher turbulent field in the initial of the duct entrance. This high jet flame velocities produce remarkably high velocities of unburned gases inside the duct where 0.315 m diameter duct pipe, marking to attain highest S_g inside the pipe for rich concentration for methane/air and propane/air with respect with 0.162 m diameter duct pipe at the same concentrations. Interestingly, the very high S_g inside the pipe observed for H_2/air at $\Phi = 0.54$ for both ignitions in the case larger pipe diameter which is $S_g > 1400$ m/s. This high unburnt gas velocity reflects to the high flame speeds if the relationship of $S_f = S_g + S_u$ is used. At $\Phi = 0.54$, S_u is 1.0 m/s (Andrews and Bradley, 1973) and from the mentioned relationship, S_f inside the duct is 1471 m/s and 1821 m/s for end and centre ignition respectively. This high flame speeds inside the duct is very close to the CJ-velocity of 1970 m/s (Dorofeev, Bezmelnitsin and Sidorov, 1995) which the onset of detonation condition. From this, turbulence inducing elements can lead to a significant acceleration of the flame front inside the vessel due to the backflow and flame instabilities and consequently, to more intense mixing of unburned mixtures still present inside the vessel and thus, rapid rise in final pressure in the vessel. Due to the abovementioned condition, it is clear that venting at larger duct pipe diameter at lean concentration i.e. 16 % for hydrogen/air and rich concentrations for low burning velocity mixtures i.e. 5.5 % propane/air are less effective in reducing the peak pressure inside the vessel in comparison with the narrow duct pipe attached.

From this analysis, it can be confirmed that the high unburnt gas velocity inside the duct induced a very high turbulent level and thus a severe secondary explosion inside the duct. The secondary explosion in the duct which in turns affects the residual combustion in the main vessel and shows more violent for end ignition as shown in Fig. 6.4 and 6.5. However, the higher intensity of the secondary explosion does not affect literally in practise the final pressure inside the vessel in the case of central ignition especially for high burning velocities mixtures i.e. hydrogen/air and ethylene/air. It is postulated by others (Ferrara, Willacy, Phylaktou, Andrews, Benedetto, Mkpadi, 2005, Ferrara, Willacy, Phylaktou, Andrews, Benedetto, Salzano, Russo, 2008, Ponizy and Leyer,

1999b) that chemical contribution i.e. mixture reactivity left inside the vessel plays an important role to the pressure rise inside the test vessel as shown in Fig. 6.6 and 6.7.

6.4 Concluding remarks

Enlarged vent ducts, i.e. ducts with areas greater than the vent area gave vent overpressures similar to those for free vents for lean mixtures, but for the maximum reactivity mixture (Φ =1.08 for methane/air and Φ = 1.375 for propane/air) P_{max} was similar to that with a vent duct the same diameter as the vent.

The cause of the large increase in overpressure for both ducts in the case of rich concentration for methane and propane/air mixtures was due to the high induced unburnt gas velocity into the vent and inside the vent duct itself. For the present K = 16.4, this condition created near sonic flow conditions at the vent vena contraction. The arrival of the flame in the vent created sonic flow in the vent duct and the high back pressure created a reverse flow into the explosion vessel. This high turbulent flow accelerates the combustion of remaining unburnt mixture and this further accelerates the flow in the duct creating the peak overpressure.

It can be said that the ignition position plays an important role in determining the final pressure inside the vessel in which end ignition gave highest P_{max} for methane/air and propane/air in all cases. However, for high burning velocity mixtures i.e. hydrogen/air, the trend is seems not to have a good agreement where central ignition gave highest P_{max} with a profoundly 'spike detonation' peak. The major finding is the occurrence of auto-ignition at the unburned pocket of mixtures trapped inside the vessel and it contributes a significant role in the hydrogen/air explosion development but not in methane/air. It then can be postulated that with central ignition, the bigger quantity of fresh mixtures left for the residual combustion in the vessel is the main contribution of the high magnitude of 'spike detonation' pressure in comparison with the pressure peak attained at end ignition inside the vessel.

The present design correlations for explosion vents and vent ducts, which are based on very limited experimental data, do not predict the present results and their reliability for small vessel volumes with high K is in doubt. Further work is required in the area of the

impact of K, mixture reactivity and static burst pressure on vent design with vent discharge ducts attached if more reliable design guidance is to be given.

CHAPTER 7

CONCLUSIONS AND RECOMMENDATIONS FOR FUTURE WORKS

7.0 Summary of major findings

7.1. General effects of venting explosions

The initial project was to compile and collect all published experimental data available for different gas reactivity in venting explosion in order to investigate the validity of the published venting correlations in relation to the venting practicality. Although abundant data and several excellent reviews are available, there are no universally agreed correlations for guidance on the selection of vent areas. The most used and recommended correlation for venting gas deflagration is adopted by NFPA 68 (NFPA68, 2002) for low and high-strength enclosures based on the works of Swift-Epstein (Swift, 1983) and Bartknecht (Bartknecht, 1993) respectively. It is found that the correlation derived by Bartknecht (Bartknecht, 1993) have been shown to be under predicted most of the data presented. It can be said that the failure of the Bartknecht's correlation is due to the assumption of the same vent area is required irrespective of the volume. Further, most of the vessels involved in Bartknecht's correlation were large where there is suspected that self-acceleration may occur during the vented explosion and this parameter did not be taken into account in an appropriate manner. However, it is recommended that the validity and limitation of Swift's equation (Swift, 1983) can be extended to wider range for $P_{red} > 200$ mbar providing the parameter P_v is added into the equation.

The mass burning rate of the spherical flame propagation equation and incompressible flow equation were used in order to correlate the P_{red} and A_v for venting design purpose. From this theory, two methods were derived namely as Method 1 and Method 2. The equation given respectively as,

$$m_b = A_s S_u \rho_u = C_d \varepsilon A_v (2\rho_u P_{red})^{0.5} \tag{7.1}$$

$$m_b = A_s S_g \rho_u = A_s S_u (E-1)\rho_u = C_d \varepsilon A_v (2\rho_u P_{red})^{0.5} \tag{7.2}$$

It can be recommended that Method 2 gives reasonably good agreement with most of the experimental data and the use of S_g term to describe the unburnt gas displaced by the flame which gives approximately ~6 times the mass flow rate suggests it gives close estimation on P_{red} in relation with practical application in comparison by with S_u term

used in Method 1. The net effect is as S_g is close to the flame speed, S_f in value, the approach is only slightly lower vent mass flow rate than that based on S_f.

A significant flame self acceleration effect for subsonic venting was shown for K<~5 and this effect is similar to vent induced turbulence and could be accounted by the β term in the burning velocity equation. The turbulence enhancement predicted based on Bartknecht's equation and proposed Method 2 was in a good agreement with β derived from tabulated experimental data. It can be said that the β derived was perfectly reasonable value for β used by other works (Munday, 1963, Pasman, Groothuizen and Gooijer, 1974, Yao, 1974). However, the flame experiences deceleration effect in larger volumes when pressure is high in larger K and this effect has never been highlighted previously. It is postulated that at high K and P_{red} with sonic venting during the explosions, the self-acceleration is likely to have already occurred at the smaller volumes.

It can be suggested that the use of K term is more suitable to be applied on cubic and spherical vessel for L/D = 2 but failed to give satisfactory results for non-cubic vessels. The A_s/A_v term is more favourable to correlate the influence of vessel's geometries for non-cubic vessels. The data and figures shown in this work also illustrated that P_{red} exponent of 0.5 in the subsonic flow regime and unity in sonic flow regime are supported by the experimental data. The main data scatter is due to the additional influence of volume. The use of P_{red} exponent of 0.582 in Bartknecht's equation compromises between subsonic and sonic flow regime which gave most of the data scattered outside the line.

7.1.1 Comparison of theory and experimental results

Experiments in two different cylindrical vessel volumes in this present study have been used to identify the physics and dynamics mechanisms responsible for the generation of the pressure peaks, in particular on the occurrence of the deflagration-to-detonation in simply vented explosions. Generally, end ignition gives higher P_{max} compared to central ignition in hydrocarbon/air mixtures. For end ignition, the flame is allowed to propagate in one direction, leading to more elongated flame towards the vent and hence, increase in mass burning rate and high flame speed. Self-acceleration is expected to be one of the

important features for the increase in P_{max} magnitude which occurred in Test vessel 1 in comparison with P_{max} in Test vessel 2 at the same equivalence ratio. This is justified by the reversed calculation done using Method 2 equation. It shown that about 80-90 % of flame area has been occupying the vessel total surface area. It is confirmed the observation reported by McCann et al (McCann, Thomas and Edwards, 1985). In their work, they said that the flame cellularity (self-acceleration) appeared in earlier stage in larger volume and this give significant effect on the overpressure inside the vessel. For smaller vessel i.e. 0.0065 m^3, experiments have shown that the presence of pressure oscillation, coupling with the induced turbulence by the vent flow, increased the P_{max}. For centrally ignited explosion, the increased intensity of the flame cellularity during flame propagation produces accelerating flame front which later interact with the vessel wall. Due to the rapid deceleration of the flame front as it approach the vessel wall, it results on the strong rare fraction waves which triggering further combustion of a large amount of unburnt gases left inside the vessel and lead to a significant P_{max} inside the vessel for reactive gas/air mixtures as shown on ethylene/air and hydrogen/air mixtures.

Auto-ignition is the main factor of the appearance of spiky pressure traces on hydrogen/air and ethylene/air in the test vessels. It can be said that fast turbulent mixing of the combustion products and reactants initiates the 'hot spot' or auto-ignition centre leading to the transition to detonation explosion.

7.1.2 Duct vented gas explosion

The high overpressure due to the addition of a vent duct, in a 0.2 m^3 cylindrical vessel with an L/D of 2 and K of 16.4, occurs after the flame has exited the vent duct, but is not due to an external explosion. There is found that substantial amount of unburnt gases left inside the vessel after the vent bursts is the leading factor in increase of P_{max} for high burning velocity mixtures at centrally ignited. The associate gas velocities ahead of the flame create high unburnt gas flows conditions at entry to the vent and this give rise to high back pressures.

As P_v increases, the distance of normal spherical flame propagation increases and there is a further reduction in acceleration distance. This initially reduces the overpressure at low P_v. The effect of the vent burst pressure is to increase the flow velocity in the duct

when the vent burst, as the flame has had more time to grow upstream of the vent and this gives a higher vent duct flow velocity once the vent cover bursts. The effect of the vent burst pressure is complex and non-linear and was not represented by the linear effect in the correlation of Bartknecht (Bartknecht, 1993) used in NFPA 68 (NFPA68, 2002).

The greater self acceleration of flames due to cellular flame development for propane relative to methane is shown in the results. Propane has a very strong influence of equivalence ratio on the flame speeds and overpressures, especially for rich mixtures where the highest flame speeds and overpressures are exhibited for Φ = 1.35. It cannot be assumed that the mixture with the highest laminar burning velocity, measured on small diameter flames with no cellular flames, is the mixture with the worst case explosion hazards. For gases such as propane that have a strong cellular flame development the worst case explosion hazard will be for rich mixtures, where this effect is maximized. In the present work this was Φ = 1.35 for propane. For methane the vented overpressure occurred at the same mixture strength as that for the maximum laminar burning velocity, but the cellular flames did contribute to the higher flame speeds and overpressures. This is because for methane rich mixtures do not have greater cellularity. At lean concentration (low equivalence ratio), high burning velocities mixtures exhibit a detonation spike in the pressure traces inside the vessel even though the behaviour of secondary explosion (burn-up) and pressure drops at the duct entrance reproduce what have been observed in methane/air and propane/air mixtures well after the flame has left the vessel-duct assembly.

Enlarged vent ducts, i.e. ducts with areas greater than the vent area gave vent overpressures similar to those for free vents for lean mixtures, but for the maximum reactivity mixture (Φ =1.08 for methane/air and Φ = 1.375 for propane/air) P_{max} was similar to that with a vent duct the same diameter as the vent.

The cause of the large increase in overpressure for both ducts for rich concentration in low burning velocity mixtures was due to the high induced unburnt gas velocity into the vent and inside the vent duct. For K = 16.4, this condition created near sonic flow conditions at the vent vena contraction. The arrival of the flame in the vent created sonic flow in the vent duct and the high back pressure created a reverse flow into the

explosion vessel. This high turbulent flow accelerates the combustion of remaining unburnt mixture and this further accelerates the flow in the duct creating the peak overpressure.

It can be said that the ignition position play an important role in determining the final pressure inside the vessel where end ignition gave highest P_{max} with respect to central ignition for methane/air and propane/air in all cases. End ignition gives greater distance towards the vent and hence, the flame acceleration continuous over twice the distance as for the central ignition. However, for high burning velocity mixtures i.e. hydrogen/air, the trend is seems not to have a good agreement with central ignition gave highest P_{max} with a profoundly 'spike detonation' peak. The major finding is the occurrence of auto-ignition at the unburned pocket of mixtures trapped inside the vessel which eventually playing a significant role in the hydrogen/air explosions but not in methane/air. It then can be postulated that at central ignition, the bigger quantity of fresh mixtures left inside the vessel marked as the main contribution of the high magnitude of 'spike detonation' pressure in comparison with the pressure peak attained at end ignition inside the vessel.

7.2 Recommendation for the future work

From the discussion on the important parameters affecting the pressure development in vented gas explosion, some conclusions have been highlighted. The practicality of Bartknecht's correlation is only in good agreement with experimental results for K<~ 5 as shown in Chapter 3 and this equation has been adopted by NFPA 68 (NFPA68, 2002) and European Standard (2007). From simply vented experiment, the Bartknecht's and Swift's equations gave gross estimation in comparison with the experimental results obtained with both 0.2 and 0.0065 m^3 cylindrical vessel. In the discussion, it is also postulated that self-acceleration plays a major role in an increase of P_{red} in vented gas explosion for large volume. It is also found that vessel's shape/geometry influencing the final P_{red} inside the vessel. In order to validate this indicated dependence and to improve the prediction of current vented gas correlations, experiments involving lower K in cylindrical and spherical vessels at bigger scale could be carried out in the present test facility i.e. V = 1 m^3 in spherical vessel and 5 m^3 in cylindrical vessel. This is also to

validate and quantify the A_s/A_v term to P_{max} in venting design instead of K for non-cubic vessel.

The present design correlations for explosion vents and with vent ducts, which are based on very limited experimental data, do not predict the present results and their reliability for small vessel volumes with high K is in doubt. In order to justify the reliability and applicability of the current design correlation on this subject matter, more work on smaller vessel with high K with different mixture reactivity are needed. The use of $P_{dynamic}$ instead of P_v is more favourable in order to correlate the influence of vent cover to Pmax, dP/dt and flame speeds. It is recommended to use commercial vent cover for future work in order for vent cover inertia effect to be taken into account.

The experimental results gave variation of mixture reactivity and it observed that hydrogen/air and ethylene/air (high burning velocity mixtures) behaved differently with propane/air and methane/air (low burning velocity mixtures). At certain condition, detonation spike is detected in the tests for hydrogen/air and ethylene/air. It is interesting to study other high burning velocity mixtures such as butane and pentene as they are both has higher laminar burning velocity than propane/air and propensity for flame cell cellularity is likely to occur at lower concentrations. Further, both mixtures are given little attention on its behaviour and mechanism in venting gas explosion.

Camera and Schlieren recordings could be fitted inside the test facility in order to get more precise information regarding the mechanism developed during vented gas explosion. Further work is required in the area of the impact of K, mixture reactivity and static burst pressure on vent design with vent discharge ducts attached if more reliable design guidance is to be given.

Further, the essential role of substantial amount of unburnt gas left trapped inside the vessel that has been discussed in detail could be benefited from the application of CFD (Computational Fluid Dynamics) modelling. Previous CFD modelling (Ferrara, Benedetto, Salzano and Russo, 2006) showed that the main mechanism affecting the pressure rise during gas explosion in duct-vented vessel is the violent combustion that occurs in the initial section of the pipe which also been one of the major factors discussed in this project. However, more quantitative predictions for a more realistic

model of gas flow need to be introduced in order to take into account the fluid dynamic effect and the dynamics of flame propagation and associated pressure and temperature during the vented gas explosion. Further, to mitigate the severity of unburnt gas velocity at the duct, the use of flame arrester at the vena contracta region would be the solution to minimise the intensification of secondary explosion inside the vessel and hence, less physical back flow to the vessel, decreasing the final overpressure inside the vessel.

REFERENCES

RERERENCES

European Standard: Gas explosion venting guidance EN 14994:2007.

Abdel Gayed, R. G. & Bradley, D. (1981) A two-eddy theory of premixed turbulent flame propagation. *Trans Proceedings of Royal Society of London,* A 301, 1-25.

Andrews, G. E. (2004) *Course notes on gas and dust explosion protection design,* University of Leeds, United Kingdom.

Andrews, G. E. & Bradley, D. (1972) Determination of burning velocity: A critical review. *Combustion and Flame,* 18, 133.

Andrews, G. E. & Bradley, D. (1973) Determination of burning velocity by double ignition in a closed vessel. *Combustion and Flame,* 20, 77.

Andrews, G. E., Bradley, D. & Lwakabama, S. B. (1975) Turbulence and turbulent flame propagation-a critical appraisal. *Combustion and Flame,* 24, 285-304.

Anthony, E. J. (1978) The use of venting formula in the design and protection of building and industrial plant from damage by gas or vapor explosions. *Journal of Hazardous Materials,* 2, 23-49.

Aung, K. T., Hassan, M. I. & Faeth, G. M. (1997) Flame stretch interactions of laminar premixed hydrogen/air flames at normal temperature and pressure. *Combustion and Flame,* 109, 1-24.

Bartknecht, W. (1985) Effectiveness of explosion venting as a protective measure for silos. *Plant/Operational progress,* 4, 4-12.

Bartknecht, W. (1993) *Explosions-schultz,* Berlin, Springer-Verlag.

Bartknecth, W. (1981) *Explosions course prevention protection,* Berlin,New York, Springer-Verlag.

Bell, J. B., Cheng, R. K., Day, M. S. & Shepherd, I. G. (2007) Numerical simulation of lewis number effects on lean premixed turbulent flames. *Proceedings of the Combustion Institute,* 31, 1309-1317.

Bradley, D. (1999) Self acceleration of flames. *2nd Fire and Explosions Hazards Seminar.*

Bradley, D., Cresswell, T. M. & Puttock, J. S. (2001) Flame acceleration due to flame-induced instabilities in large scale explosions. *Combustion and Flame,* 124, 551-559.

Bradley, D., Emerson, D. R. & Gu, X. J. (2003) Modes of reaction front propagation from hot spots. *Combustion and Flame,* 133, 63-74.

Bradley, D. & Harper, C. M. (1994) The development of instabilities in laminar explosion flames. *Combustion and Flame,* 99, 562-572.

Bradley, D., Hicks, R. A., Haq, M. Z., Lawes, M., Sheppard, C. G. W. & Woolley, R. (2003) Turbulent burning velocity, burned gas distribution and associated flame surface definition. *Combustion and Flame,* 133, 415-430.

Bradley, D., Lau, A. K. C. & Lawes, M. (1992) Flame stretch rate as a determinant of turbulent burning velocity. *Phil.Trans.R.Soc.Lond.(A),* 338, 359-387.

Bradley, D. & Mitcheson, A. (1978a) The venting of gaseous explosions in spherical vessel (I) Theory. *Combustion and Flame,* 32, 221-236.

Bradley, D. & Mitcheson, A. (1978b) The venting of gaseous explosions in spherical vessels (II)-theory and experiment. *Combustion and Flame,* 32, 237-255.

Bradley, D., Sheppard, C.G.W., Woolley, R., Greenhalgh, D.A. & Lockett, R.D. (2000) The development and structure of flame instabilities and cellularity at low Markstein numbers in explosion. Combustion and Flame, 122, 195-209.

Buckland, I. G. (1980) Explosions of gas layers in a room size chamber. *7th International Symposium in Chemical Process Hazards with special reference to plant design.* Manchester, I.Chem.E.Symposium Series No.58.

Burgoyne, J. H. & Wilson, M. J. G. (1960) The relief of pentene vapor-air explosion in vessels. *I.Chem.E.Symposium on Chemical Process Hazards,* 25.

BS 1042, Part 1: Section 1.5: Measurement of fluid flow in closed conduits. pressure differential devices (1997)

Canu, P., Rota; R. & Carra, S. (1990) Vented gas deflagrations a detailed mathematical model tuned on a large set of experimental data. *Combustion and Flame,* 80, 49-64.

Chippett, S. (1984) Modelling of vented deflagrations. *Combustion and Flame,* 55, 127-140.

Chow, S. K., Cleaver, R. P., Fairweather, M. & Walker, D. G. (2000) An experimental study of vented explosions in a 3:1 aspect ratio cylindrical vessel. *Trans IChemE,* Vol 78, Part B, 425-433.

Clark, D. P. & Smoot, L. D. (1985) Model of accelerating coal dust flames. *Combustion and Flame,* 62, 255-269.

Clarke, A. (2002) Calculation and consideration of the lewis number for explosion studies. *Trans. IChemE,* 80, Part B, 135-140.

Cooper, M. G., Fairweather, M. & Tite, J. P. (1986) On the mechanism of pressure generation in vented explosions. *Combustion and Flame,* 65, 1-14.

Cousins, E. W. & Cottons, P. E. (1951) Design closed vessels to withstand internal explosions. *Chemical Engineering,* 58, 133.

Cubbage, P. A. & Marshall, M. R. (1972) Pressures generated in combustion chambers by the ignition of air-gas mixtures. *I.Chem.E Symposium Series No.33,* 33, 24-31.

Cubbage, P. A. & Marshall, M. R. (1974) Explosion relief protection for industrial plant of intermediate strength. *I.Chem.E.Symposium Series No.39a.*

Cubbage, P. A. & Simmonds, W. A. (1955) An investigation of explosion reliefs for industrial drying ovens. I-top reliefs in box ovens, London, The Gas Council: Research Communication GC23.

Cubbage, P. A. & Simmonds, W. A. (1957) An investigation of explosion reliefs for industrial drying ovens. II-back reliefs in box ovens: Reliefs in conveyor ovens, London, The Gas Council: Research Communication GC34.

DeGood, R. & Chartrathi, K. (1991) Comparative analysis of tests work studying factors influencing pressures developed in vented deflagrations. *Journal of Loss Prevention in the Process Industries,* 4, 297-304.

DeHaan, J. D., Crowhurst, D., Hoare, D., Bensilum, M. & Shipp, M. P. (2001) Deflagration involving stratified heavier than air vapor/air mixtures. *Fire Safety Journal,* 36, 693-710.

Donat, C. (1977) Pressure relief as used in explosion protection. *Journal of Loss Prevention in the Process Industries,* 11, 87-92.

Dorofeev, S. B., Bezmelnitsin, A. V. & Sidorov, V. P. (1995) Transition to detonation in vented hydrogen-air explosions. *Combustion and Flame,* 103, 243-246.

Eckhoff, R. K. (1991) *Dust explosions in the process industries,* Oxford, Butterworth-Heinemann.

Ellis, d. C. O. C. (1928) Flame movement in gaseous explosiove mixtures. *Fuel,* 7, 5-12.

Fairweather, M., Hargrave, G. K., Ibrahim, S. S. & Walker, D. G. (1999) Studies of premixed flame propagation in explosion tubes. *Combustion and Flame,* 116, 504-518.

Ferrara, G., Willacy, S.K., Phylaktou, H.N., Andrews, G.E., Benedetto, A.D., Salzano, E., Russo, G. (2008) Venting of gas explosion through relief ducts: Interaction between internal and external explosion. Journal of Hazardous Materials, In press accepted manuscript

Ferrara, G., Benedetto, A. D., Salzano, E. & Russo, G. (2006) CFD analysis of gas explosions vented through relief pipes (article in press). *Journal of Hazardous Materials*.

Ferrara, G., Willacy, S. K., Phylaktou, H. N., Andrews, G. E., Benedetto, A. D. & Mkpadi, M. C. (2005) Duct vented propane-air explosions with central and rear ignition. *IAFSS*.

Ferrara, G., Willacy, S. K., Phylaktou, H. N., Andrews, G. E., Benedetto, A. D. & Salzano, E. (2005) Venting of premixed gas explosions with a relief pipe of the same area as the vent. *Proceedings of the European Combustion Meeting 2005*.

Franzini, J. B. & Finnemore, E. J. (1994) *Fluid mechanics with engineering applications*, New York, The McGraw-Hill Companies Inc.

Gardner, C. L. (1998) Turbulent combustion in obstacle-accelerated gas explosions-the influence of scale. Thesis. *Department of Fuel and Energy*. University of Leeds.

Gostintsev, Y. A., Istratov, A. G. & Shulenin, V. (1989) Self-similar propagation of a free turbulent flame in mixed gas mixtures. *Combustion, Explosion & Shock Waves (Translated from Fizika Goreniyai Vzryva, Vol 24, No.5, pp. 63-70, Sept 1988)*, 563-569.

Groff, E. G. (1982) The cellular nature of confined spherical propane-air flames. *Combustion and Flame*, 48, 51-62.

Gu, X. J., Emerson, D. R. & Bradley, D. (2003) Modes of reaction front propagation from hot spots. *Combustion and Flame*, 133, 63-74.

Harris, G. F. P. (1967) The effect of vessel size and degree of turbulence on gas phase explosion pressures in closed vessels. *Combustion and Flame*, 11, 17-25.

Harris, G. F. P. & Briscoe, P. G. (1967) The venting of pentane vapour-air explosions in a large vessel. *Combustion and Flame*, 11, 329-338.

Harris, R. J. (1983) The investigation and control of gas explosions in buildings and heating plant, London, E&F N Spon Ltd.

Harris, R. J. & Wickens, M. J. (1989) Understanding vapour cloud explosions-an experimental study. 55th Autumn Meeting, The Institution of Engineers.

Harrison, A. J. & Eyre, J. A. (1987) External explosions as a result of explosion venting. *Combustion, Science and Technology*, 52, 91-106.

Hey, M. (1991) Pressure relief of dust explosions through large diameter ducts and effects of changing the position of ignition source. *Journal of Loss Prevention in the Process Industries*, 4, 217-222.

Iida, N., Kawaguchi, O. & Sato, G. T. (1985) Premixed flame propagation into a narrow channel at a high speed, part i: Flame behaviours in the channel. *Combustion and Flame,* 60, 245.

Istratov, A. G. & Librovich, V. B. (1969) Computing the speed of the normal propagation of a flame in a mixture of hydrogen and chlorine. *Astronautica Acta,* 14, 453-467.

Kasmani, R. M., Andrews, G. E., Phylaktou, H. N. & Willacy, S. K. (2007a) Influence of static burst pressure and ignition position on duct-vented gas explosions. *5th International Seminar on Fire and Explosion Hazards.* Edinburgh.

Kasmani, R. M., Andrews, G. E., Phylaktou, H. N. & Willacy, S. K. (2007b) Vented gas explosion in a cylindrical vessel with a vent duct. *European Combustion Meeting 2007.* Chania, Crete.

Kasmani, R. M., Willacy, S. K., Phylaktou, H. N. & Andrews, G. E. (2006) Self-accelerating gas flames in large vented explosions that are not accounted for in current vent design. *Proceedings of the 2nd International Conference on Safety and Environment in Process Industry.* Naples, Italy.

Kordylewski, W. & Wach, J. (1988) Influence of ducting on explosion pressure: Small scale experiments. *Combustion and Flame,* 71, 51-61.

Kumar, R. K., Bowles, E. M. & Mintz, K. J. (1992) Large-scale dust explosion experiments to determine the effects of scaling on explosion parameters. *Combustion and Flame,* 89, 320-332.

Kumar, R. K., Dewit, W. A. & Greig, D. R. (1989) Vented explosion of hydrogen-air mixtures in a large volume. *Combustion, Science and Technology,* 66, 251-266.

Kumar, R. K., Skraba, T. & Greig, D. R. (1987) Vented combustion of hydrogen-air mixtures in large volumes. *Nuclear Engineering and Design,* 99, 305-315.

Lee, J. H. S. & Guirao, C. M. (1982) Pressure development in closed and vented vessels. *Plant/Operational progress,* 1, 75-85.

Lees, F. P. (1996) Loss prevention in the process industries: Hazard identification, assessment and control, London, Butterworth-Heinemann.

Liebman, I., Corry, J. & Perlee, H. E. (1970) Flame propagation in layered methane/air system. *Combustion, Science and Technology,* 1, 257-267.

Lunn, G. (1992) Dust explosion prevention and protection. Part 1- venting, Institute of Chemical Engineers.

Lunn, G., Crowhurst, D. & Hey, M. (1988) The effect of vent ducts on the reduced explosion pressures of vented dust explosions. *Journal of Loss Prevention in Process Industries,* 1, 182-196.

Maisey, H. R. (1965) Gaseous and dust explosion venting- Part 1. *Chemical and Process Engineering*, 527-535.

Markstein, G. H. (1964) Nonsteady flame propagation, New York, Macmillan.

McCann, D. P. J., Thomas, G. O. & Edwards, D. H. (1985) Gasdynamics of vented explosions part i: Experimental studies. *Combustion and Flame,* 59, 233-250.

Moen, I. O., Bjerketvedt, D., Jenssen, A. & Thibault, P. A. (1985) Transition to detonation in a large fuel-air cloud (brief communication). *Combustion and Flame,* 61, 285-291.

Moen, I. O., Lee, J. H. S., Hjertager, B. H., Fuhre, K. & Eckhoff, R. K. (1982) Pressure development due to turbulent flame propagation in large-scale methane-air explosions. *Combustion and Flame,* 47, 31-52.

Molkov, V., Dobashi, R., Suzuki, M. & Hirano, T. (2000) Venting of deflagrations: Hydrocarbon-air and hydrogen-air systems. *Journal of Loss Prevention in the Process Industries,* 13, 397-409.

Molkov, V. V. (1994) Venting of deflagrations: Dynamic of the process in systems with a duct and receiver. *Proceedings of the 4th International Symposium on Fire Safety Science*, 1245-1254.

Molkov, V. V. (1995) Theoretical generalization of international experimental data on vented gas explosion dynamics. *Physics of Combustion and Explosions*, 165-181.

Molkov, V. V. (1999) Explosion safety engineering: NFPA 68 and improved vent sizing technology. *Interflam 1999, Proceedings of the 8th International Fire Science Conference.* Edinburgh.

Molkov, V. V. (2001) Unified correlations for vent sizing of enclosures at atmospheric and elevated pressures. *Journal of Loss Prevention in the Process Industries,* 14, 567-574.

Molkov, V. V., Baratov, A. & Korolchenko, A. (1993) Dynamics of gas explosions in vented vessels: Review and progress. *Progress in Astronautics and Aeronautics,* 154, 117-131.

Molkov, V. V., Dobashi, R., Suzuki, M. & Hirano, T. (1999) Modelling of vented hydrogen-air deflagrations and correlations for vent sizing. *Journal of Loss Prevention in the Process Industries,* 12, 147-156.

Molkov, V. V., Grigorash, A. V., Eber, R. M. & Makarov, D. V. (2004) Vented gaseous deflagrations: Modelling of hinged inertial vent covers. *Journal of Hazardous materials,* A116, 1-10.

Molkov, V. V., Grigorash, A. V., Eber, R. M., Tamanini, F. & Dobashi, R. (2004) Vented gaseous deflagrations with inertial vent covers: State-of-the-art and progress. *Process Safety Progress,* 23, 29-36.

Molkov, V. V., Korolchenko, A. & Alexandrov, S. (1997) Venting of deflagrations in buildings and equipment: Universal correlation. *Fire Safety Science-proceedings of the 5th International Symposium*, 1249-1260.

Molkov, V. V. & Nekrasov, V. P. (1981) Dynamics of gas combustion in a constant volume in the presence of exhaust. *Balashika. Translated from Fizika Goreniya i Vzryva,* 17, 17-24.

Munday, G. (1963) The calculation of venting areas for pressure relief of explosions in vessel. *Proceedings of Symposium on Chemical Process Hazards with Special Reference to Plant Design Series No.15.* Manchester, The Institution of chemical Engineers.

Munson, B. R., Young, D. F. & Okiishi, T. H. (2006) *Fundamentals of fluid mechanics: Fifth edition*, John Wiley and Sons Inc.

Nagy, J. & Verakis, H. C. (1983) *Development and control of dust explosions,* New York, Marcel Dekker Inc, New York and Basel.

NFPA68 (2002) Nfpa 68: Guide for venting of deflagrations: 2002. National Fire Protection Association.

Ng, H. D. & Lee, J. H. L. (2007) Comments on explosion problems for hydrogen safety. *Jounal of Loss of Prevention in Process Safety.*

Pasman, H. J., Groothuizen, T. M. & Gooijer, H. d. (1974) Design of pressure relief vents. *Loss Prevention and Safety Promotion in the Process Industries: Edited by C.H.Buschmann*, 185-189.

Phylaktou, H. N. & Andrews, G. E. (1991) Gas explosions in long closed vessels. *Combustion Science and Technology,* 77, 27-39.

Phylaktou, H. N., Andrews, G. E. & Herath, P. (1990) Fast flame speeds and rate of pressure rise in the initial period of gas explosions in large l/d cylindrical enclosures. *Journal of Loss of Prevention in Process Safety,* 3, 355-364.

Phylaktou, H. N., Foley, M. & Andrews, G. E. (1993) Explosions in a tube with a 90° bend. *Journal of Loss of Prevention in Process Safety,* 6, 21-29.

Ponizy, B. & Leyer, J. C. (1999a) Flame dynamics in a vented vessel connected to a duct: 1.Mechanism of vessel-duct interaction. *Combustion and Flame,* 116, 259-271.

Ponizy, B. & Leyer, J. C. (1999b) Flame dynamics in a vented vessel connected to a duct: 2.Influence of ignition site, membrane rupture and turbulence. *Combustion and Flame,* 116, 272-281.

Ponizy, B. & Veyssiere, B. (2000) Mitigation of explosions in a vented vessel connected to a duct. *Combustion, Science and Technology,* 158, 167-182.

Pritchard, D. K., Allsopp, J. A. & Eaton, G. T. (1995) Gas explosion venting in elongated enclosures. 1-12.

Rasbash, D. J. (1986) Quantification of explosion parameters for combustible fuel-air mixtures. *Fire Safety Journal,* 11, 113-125.

Rasbash, D. J., Drysdale, D. D. & Kemp, N. (1976) Design of an explosion relief system for a building handling liquefied fuel gases. *I.Chem.E.Symposium Series No.47,* 145-156.

Razus, D. M. & Krause, U. (2001) Comparison of empirical and semi-empirical calculation methods for venting of gas explosion. *Fire Safety Journal,* 36, 1-23.

Runes, E. (1972) Explosion venting. *Plant Operations & Loss Prevention,* 6, 63-71.

Russo, P. & Benedetto, A. D. (2007) Effects of a duct on the venting of explosions-critical review. *Trans IChemE, Part B (Process Safety and Environmental Protection),* 85(B1), 9-22.

Searby, G. & Quinard, J. (1990) Direct and indirect measurements of Markstein numbers in premixed flames. *Combustion and Flame,* 82, 298-311.

Simpson, L. L. (1986) Equations for the VDI and Bartknecht nomograms. *Plant /Operations Progress,* 8, 49-51.

Siwek, R. (1996) Explosion venting technology. *Journal of Loss Prevention in the Process Industries,* 9, 81-90.

Solberg, D. M., Pappas, J. A. & Skramstad, E. (1980) Observations of flame instabilities in large scale vented gas explosions. *18th International Symposium on Combustion.* University of Waterloo, Canada, Det Norske Veritas.

Starke, R. & Roth, P. (1986) An experimental investigation of flame behaviour during cylindrical vessel explosions. *Combustion and Flame,* 66, 249-259.

Swift, I. (1983) Gaseous combustion venting- a simplified approach. 4th International Symposium on Loss Prevention and Safety promotion in the Process Industries, 3, F21-F37.

Swift, I. (1984) Venting deflagrations-theory practice. *Plant/Operational progress,* 3, 89-93.

Swift, I. & Epstein, M. (1987) Performance of low pressure explosion vents. *Plant/Operations progress,* 6, 98-105.

Tamanini, F. (2000) Partial volume deflagration characteristics of explosions in layered fuel/air mixtures. *International Seminar on Fire and Explosion Hazards of Substances.*

Tamanini, F. & Fisher, M. (2003) Mixed-mode venting of dust explosions. *4th International Seminar on Fire and Explosion Hazards.* Londonderry.

Thorne, P. F., Rogowski, Z., W & Field, P. (1983) Performance of low inertia explosion reliefs fitted to a 22m3 cubical chamber. IN ENGINNER, T. I. O. C. (Ed.) *4th Int. Sym. on Loss Prevention and Safety Promotion in the Process Industries (Series no.82).* Harrogate, England, The Institute of Chemical Engineers.

Tseng, L. K., Ismail, M. A. & Faeth, G. M. (1993) Laminar burning velocities and Markstein numbers of hydrocarbon/air flame. *Combustion and Flame,* 95, 410-426.

Ural, E. A. (1993) A simplified method for predicting the effect of ducts connected to explosion vents. *Journal of Loss Prevention in the Process Industries,* 6, 3-10.

Wingerden, C. J. M. & Zeeuwen, J. P. (1983a) On the role of acoustically driven flame instabilities in vented gas explosions and their elimination. *Combustion and Flame,* 51, 109-111.

Wingerden, C. J. M. & Zeeuwen, J. P. (1983b) Venting of gas explosions in large rooms. 4tn International Symposium on Loss Prevention and Safety Promotion in the Process Industries.

Yao, C. (1974) Explosion venting of low-strength equipment and structures. *Journal of Loss Prevention in the Process Industries,* 8, 1-9.

Zalosh, R. (1995) Review of gas deflagration venting models. 1st International Fire and Explosion Hazards of Substances and Venting of Deflagrations, 79-87.

Zalosh, R. G. (1980) Gas explosion tests in room-size vented enclosures. *Loss Prevention,* 13, 98-110.

APPENDIX

Table A.2 List of the published experimental data for vented gas explosions.

Methane-air

Conc. vol %)	V (m3)	A_s (m2)	Vessel shape	L/D ratio	Ignition	P_v (barg)	P_{red} (barg)	A_v, expt (m2)	Sources
10.4	0.2	1.93	Rec	1.5	Centre	0.03	0.01	0.0473	R.G.Zalosh. K=4. Vent cover is aluminium
10.4	0.2	1.93	Rec	1.5	Centre	0.03	0.02	0.0315	R.G.Zalosh. K=6. Vent cover is aluminium
10.4	0.2	1.93	Rec	1.5	Centre	0.03	0.06	0.0172	R.G.Zalosh. K=11. Vent cover is aluminium
10.4	0.2	1.93	Rec	1.5	Centre	0.03	0.21	0.00675	R.G.Zalosh. K=28. Vent cover is aluminium
10.4	0.2	2.01	Rec	1	Centre	0.03	0.03	0.054	R.G.Zalosh. K=5.8. Vent cover is aluminium
10.4	0.2	2.01	Rec	1	Centre	0.03	0.06	0.031	R.G.Zalosh. K=10. Vent cover is aluminium
10.4	0.2	2.01	Rec	1	Centre	0.03	0.21	0.016	R.G.Zalosh. K=20. Vent cover is aluminium
10.4	0.2	2.01	Rec	1	Centre	0.03	0.69	0.0077	R.G.Zalosh. K=41. Vent cover is aluminium
10.4	0.2	2.08	Rec	1	Centre	0.03	0.03	0.045	R.G.Zalosh. K=5.8. Vent cover is aluminium
10.4	0.2	2.08	Rec	1	Centre	0.03	0.04	0.033	R.G.Zalosh. K=8. Vent cover is aluminium
10.4	0.2	2.08	Rec	1	Centre	0.03	0.14	0.015	R.G.Zalosh. K=18. Vent cover is aluminium
10.4	0.2	2.08	Rec	1	Centre	0.03	0.48	0.0069	R.G.Zalosh. K=38. Vent cover is aluminium
NR	0.4	3.25	Rec	1	Centre	0	0.043	0.3	Cubbage and Simmonds I: Top reliefs in box oven. W(Ib/ft^2)= activation pressure
NR	0.4	3.25	Rec	1	Centre	0.002	0.08	0.3	Cubbage and Simmonds I: Top reliefs in box oven. W(Ib/ft^2)= activation pressure
NR	0.4	3.25	Rec	1	Centre	0.003	0.1	0.3	Cubbage and Simmonds I: Top reliefs in box oven. W(Ib/ft^2)=

									activation pressure
NR	0.4	3.25	Rec	1	Centre	0.004	0.13	0.3	Cubbage and Simmonds 1: Top reliefs in box oven. W(lb/ft^2)= activation pressure
10.4	0.6	4.38	Rec	1.5	Centre	0.03	0.03	0.0652	R.G.Zalosh. K=6. Vent cover is aluminium
10.4	0.6	4.38	Rec	1.5	Centre	0.03	0.05	0.049	R.G.Zalosh. K=8. Vent cover is aluminium
10.4	0.6	4.38	Rec	1.5	Centre	0.03	0.76	0.036	R.G.Zalosh. K=11. Vent cover is aluminium
10.4	0.6	4.38	Rec	1.5	Centre	0.03	0.36	0.0098	R.G.Zalosh. K=40. Vent cover is aluminium
9.5	1.0	5.5	Cylinder	1.554	Centre	0.16	1.0	0.1	P.F.Thorne et al. Polyethylene 130um.K=4.0.Ignition at the center of rear wall
9.5	1.0	5.5	Cylinder	1.554	Centre	0.32	2.0	0.05	S.Chippett
9.5	1.0	6.0	Cubic	1	Centre	0.1	0.2	0.36	Bartknecht(Abb.2.223a)
9.5	1.0	6.0	Cubic	1	Centre	0.2	0.2	0.36	Bartknecht(Abb.2.223(a))
9.5	1.0	6.0	Cubic	1	Centre	0.2	0.4	0.36	Bartknecht(Abb.2.223b)
9.5	1.0	6.0	Cubic	1	Centre	0.5	0.64	0.36	Razus et al
9.5	1.0	6.0	Cubic	1	Centre	0.5	0.8	0.36	Bartknecht(Abb.2.223b)
9.5	1.0	6.0	Cubic	1	Centre	0.8	0.9	0.36	Bartknecht(Abb.2.223(a))
9.5	1.0	6.0	Cubic	1	Centre	1.0	1.2	0.36	Bartknecht(Abb.2.223b)
9.5	1.0	6.0	Cubic	1	Centre	1.0	1.3	0.36	Bartknecht(Abb.2.223(a))
9.5	1.0	6.0	Cubic	1	Centre	1.5	1.7	0.36	Bartknecht(Abb.2.223(a))
9.5	1.0	6.0	Cubic	1	Centre	2.0	2.4	0.36	Bartknecht(Abb.2.223(a))
9.5	1.0	6.0	Cubic	1	Centre	0.1	0.43	0.3	Razus et al
9.5	1.0	6.1	Cylinder	1.55	Centre	0.18	0.5	0.3	Paper as vent cover. One peak pressure.1st peak is taken as P_{red}. Pasman,H.J et al
9.5	1.0	6.1	Cylinder	1.55	Centre	0.20	0.1	0.3	Mylar as vent cover. Double peak pressure.1st peak is taken as P_{red}. Pasman,H.J et al
9.5	1.0	6.0	Cubic	1	Centre	0.2	0.77	0.3	Razus et al
9.5	1.0	6.0	Cubic	1	Centre	0.5	0.59	0.3	Razus et al
9.5	1.0	6.0	Cubic	1	Centre	0.5	0.5	0.26	Bartknecht(Abb.2.224(b))
9.5	1.0	6.0	Cubic	1	Centre	0.2	0.5	0.22	Bartknecht(Abb.2.224(b))
9.5	1.0	6.0	Cubic	1	Centre	0.1	0.5	0.2	Bartknecht(Abb.2.224(b))
9.5	1.0	6.0	Cubic	1	Centre	0.1	0.84	0.2	Razus et al

9.5	1.0	6.1	Cylinder	1.55	Centre	0.18	1.2	0.2	Paper as vent cover. One peak pressure. Pasman,H.J et al
9.5	1.0	6.1	Cylinder	1.55	Centre	0.20	0.1	0.2	Mylar as vent cover. Double peak pressure.2nd peak is taken as P_{red}. Pasman,H.J et al
9.5	1.0	6.0	Cubic	1	Centre	0.2	1.48	0.2	Razus et al
9.5	1.0	6.0	Cubic	1	Centre	0.5	1.11	0.2	Razus et al
9.5	1.0	6.0	Cubic	1	Centre	0.1	1.0	0.16	Bartknecht(Abb.2.223(a))
9.5	1.0	6.0	Cubic	1	Centre	0.2	1.7	0.16	Bartknecht(Abb.2.223b)
9.5	1.0	6.0	Cubic	1	Centre	0.2	1.8	0.16	Bartknecht(Abb.2.223(a))
9.5	1.0	6.0	Cubic	1	Centre	0.5	1.2	0.16	same as above
9.5	1.0	6.0	Cubic	1	Centre	0.5	1.4	0.16	Razus et al
9.5	1.0	6.0	Cubic	1	Centre	0.8	1.3	0.16	Bartknecht(Abb.2.223(a))
9.5	1.0	6.0	Cubic	1	Centre	1.0	1.4	0.16	Bartknecht(Abb.2.223(a))
9.5	1.0	6.0	Cubic	1	Centre	1.0	1.5	0.16	Bartknecht(Abb.2.223b)
9.5	1.0	6.0	Cubic	1	Centre	1.5	2.0	0.16	Bartknecht(Abb.2.223(a))
9.5	1.0	6.0	Cubic	1	Centre	2.0	2.5	0.16	Bartknecht(Abb.2.223(a))
9.5	1.0	6.0	Cubic	1	Centre	0.5	2.0	0.12	Bartknecht(Abb.2.224(b))
9.5	1.0	6.0	Cubic	1	Centre	0.1	1.4	0.1	Razus et al
9.5	1.0	6.0	Cubic	1	Centre	0.2	2.0	0.1	Bartknecht(Abb.2.224(b))
9.5	1.0	6.0	Cubic	1	Centre	0.2	2.19	0.1	Razus et al
9.5	1.0	6.1	Cylinder	1.55	Centre	0.20	1.0	0.1	Mylar as vent cover. Double peak pressure.Pasman,H.J et al
9.5	1.0	6.0	Cubic	1	Centre	0.5	1.95	0.1	Razus et al
9.5	1.0	6.0	Cubic	1	Centre	0.1	2.0	0.08	Bartknecht(Abb.2.224(b))
9.5	1.0	6.1	Cylinder	1.55	Centre	0.20	2.0	0.05	Mylar as vent cover.One peak pressure.Pasman,H.J et al
9.5	1.0	6.0	Cubic	1	Centre	0.1	1.8	0.04	Bartknecht(Abb.2.223b)
9.5	1.0	6.0	Cubic	1	Centre	0.2	2.6	0.04	Bartknecht(Abb.2.223(a))
9.5	1.0	6.0	Cubic	1	Centre	0.2	2.8	0.04	Bartknecht(Abb.2.223b)
9.5	1.0	6.0	Cubic	1	Centre	0.5	3.2	0.04	Bartknecht(Abb.2.223b)
9.5	1.0	6.0	Cubic	1	Centre	0.5	3.4	0.04	Bartknecht(Abb.2.223(a))
9.5	1.0	6.0	Cubic	1	Centre	0.8	3.4	0.04	Bartknecht(Abb.2.223(a))
9.5	1.0	6.0	Cubic	1	Centre	1.0	2.8	0.04	Bartknecht(Abb.2.223(a))
9.5	1.0	6.0	Cubic	1	Centre	1.5	2.6	0.04	Bartknecht(Abb.2.223(a))
9.5	1.0	6.0	Cubic	1	Centre	2.0	3.0	0.04	Bartknecht(Abb.2.223(a))
10	1.9	7.4	Sphere	1	Centre	2.9	9.3	0.0993	S.Chippett.
10	1.9	7.4	Sphere	1	Centre	3.5	11.2	0.0993	S.Chippett. Turbulent with 2 fan.

10	1.9	7.4	Sphere	1	Centre	4.5	10.2	0.0993	S.Chippett.
10	1.9	7.4	Sphere	1	Centre	6.0	10.0	0.0993	S.Chippett.
10	1.9	7.4	Sphere	1	Centre	2.8	19.8	0.0324	S.Chippett.
10	1.9	7.4	Sphere	1	Centre	3.0	20.4	0.0324	S.Chippett.
10	1.9	7.4	Sphere	1	Centre	5.2	21.1	0.0324	S.Chippett.
NR	2.8	12.46	Rec	1.8	Centre	0	0.014	1.14	Cubbage and Simmonds I: Top reliefs in box oven. W(lb/ft^2)= activation pressure
NR	2.8	12.46	Rec	1.8	Centre	0.002	0.034	1.14	Cubbage and Simmonds I: Top reliefs in box oven. W(lb/ft^2)= activation pressure
NR	2.8	12.46	Rec	1.8	Centre	0.005	0.066	1.14	Cubbage and Simmonds I: Top reliefs in box oven. W(lb/ft^2)= activation pressure
10	3.8	11.8	Sphere	1	Centre	2.8	15.8	0.0993	S.Chippett. Turbulent with 2 fan.
10	3.8	11.8	Sphere	1	Centre	2.9	15.4	0.0993	S.Chippett.
10	3.8	11.8	Sphere	1	Centre	3.5	17.9	0.0993	S.Chippett.
10.5	11.2	31.54	Rec	0.9	Centre	0.03	0.5	2.25	R.G.Zalosh.P2 is taken. Aluminium foil as a membrane
10.5	11.2	31.54	Rec	0.9	Centre	0.03	0.3	0.77	R.G.Zalosh.P2 is taken. Aluminium foil as a membrane
10	22.0	47.11	Cubic	1	Centre	0.012	0.016	7.85	P.F.Thorne et al. Polyethylene 130μm: K=1
10	22.0	47.11	Cubic	1	Centre	0.03	0.04	3.41	P.F.Thorne et al. Polyethylene 130μm; K=2.3
10	22.0	47.11	Cubic	1	Centre	0.05	0.02	3.41	P.F.Thorne et al. Polyethylene 130μm; K=2.3: Ignition at the centre of front wall
10	22.0	47.11	Cubic	1	Centre	0.05	0.07	3.41	P.F.Thorne et al. Polyethylene 130μm; K=2.3: Ignition at the centre of rear wall
10	22.0	47.11	Cubic	1	Centre	0.05	0.06	3.41	P.F.Thorne et al. Fibreboard 12.5μm; K=2.3
10	22.0	47.11	Cubic	1	Centre	0.05	0.16	3.41	P.F.Thorne et al. Polyester 50μm; K=2.3
10	22.0	47.11	Cubic	1	Centre	0.04	0.07	1.96	P.F.Thorne et al. Polyethylene 130μm; K=4.0
10	22.0	47.11	Cubic	1	Centre	0.05	0.11	1.96	P.F.Thorne et al. Polyethylene 130μm; K=4.0: Ignition at the

									centre of rear wall
10	22.0	47.11	Cubic	1	Centre	0.09	0.6	0.98	P.F.Thorne et al. Fibreboard 12.5µm; K=8.0
10.0	26.6	56.1	Rec	1	Centre	0.02	0.07	0.50	Buckland (G.A.Lunn book)
10.0	26.6	56.1	Rec	1	Centre	0.06	0.11	0.50	Buckland (G.A.Lunn book)
10.0	26.6	56.1	Rec	1	Centre	0.06	0.05	0.50	Buckland (G.A.Lunn book)
10.0	26.6	56.1	Rec	1	Centre	0.07	0.06	0.50	Buckland (G.A.Lunn book)
10.0	26.6	56.1	Rec	1	Centre	0.04	0.11	0.40	Buckland (G.A.Lunn book)
10.0	26.6	56.1	Rec	1	Centre	0.07	0.11	0.40	Buckland (G.A.Lunn book)
10.0	26.6	56.1	Rec	1	Centre	0.02	0.10	0.25	Buckland (G.A.Lunn book)
10.0	26.6	56.1	Rec	3	Centre	0.07	0.07	0.52	Buckland (G.A.Lunn book)
10.0	26.6	56.1	Rec	4	Centre	0.08	0.13	0.63	Buckland (G.A.Lunn book)
10.0	26.6	56.1	Rec	2	Centre	0.09	0.07	0.40	Buckland (G.A.Lunn book)
10.0	26.6	56.1	Rec	1	Centre	0.09	0.22	0.20	Buckland (G.A.Lunn book)
10.0	26.6	56.1	Rec	1	Centre	0.12	0.22	0.20	Buckland (G.A.Lunn book)
10.0	26.6	56.1	Rec	1	Centre	0.007	0.08	0.13	Buckland (G.A.Lunn book)
10.0	26.6	56.1	Rec	1	Centre	0.04	0.06	0.13	Buckland (G.A.Lunn book)
9.5	30.0	57.93	Cubic	1	Centre	0.1	0.1	3.9	Bartknecht(Abb.2.222).F= n x DN1000
9.5	30.0	57.93	Cubic	1	Centre	0.1	0.2	3.4	Bartknecht(Abb.2.222).F= n x DN1000
9.5	30.0	57.93	Cubic	1	Centre	0.1	0.4	2.5	Bartknecht(Abb.2.222).F=n x DN800
9.5	30.0	57.93	Cubic	1	Centre	0.1	0.5	2.0	Bartknecht(Abb.2.222).F=n x DN800
9.5	30.0	57.93	Cubic	1	Centre	0.1	1.0	1.5	Bartknecht(Abb.2.222).F=n x DN800
9.5	30.0	57.93	Cubic	1	Centre	0.1	0.9	1.4	Bartknecht(Abb.2.222).F=n x DN600
9.5	30.0	57.93	Cubic	1	Centre	0.1	1.4	1.0	Bartknecht(Abb.2.222).F=n x DN800
9.5	30.0	57.93	Cubic	1	Centre	0.1	1.88	0.85	Bartknecht(Abb.2.222).F=n x DN600
9.5	30.0	57.93	Cubic	1	Centre	0.1	2.2	0.8	Bartknecht(Abb.2.222).F= n x DN1000
9.5	30.0	57.93	Cubic	1	Centre	0.1	2.6	0.5	Bartknecht(Abb.2.222).F=n x DN800
9.5	30.0	57.93	Cubic	1	Centre	0.1	3.7	0.3	Bartknecht(Abb.2.222).F=n x DN600

10.5	34.0	66.12	Rec	2.7	Centre	0.03	1.6	3	R.G.Zalosh.P2 is taken. Aluminium foil as a membrane
10.5	34.0	66.12	Rec	2.7	Centre	0.03	2.2	3	R.G.Zalosh.P2 is taken. Aluminium foil as a membrane
10.5	34.0	66.12	Rec	2.7	Centre	0.03	1.3	2.25	R.G.Zalosh.P2 is taken. Aluminium foil as a membrane
10.5	34.0	66.12	Rec	2.7	Centre	0.03	0.9	2.25	R.G.Zalosh.P2 is taken. Aluminium foil as a membrane
10.5	34.0	66.12	Rec	2.7	Centre	0.03	1.6	2.25	R.G.Zalosh. A 0.91-m diameter and 2.7m long tank and an array of 2.5cm pipes suspended from ceiling is placed in the enclosures.
10.5	34.0	66.12	Rec	2.7	Centre	0.03	1.7	1.86	R.G.Zalosh.2nd vent panel bent open 25%

Propane/air

Conc. (vol %)	V (m^3)	A_s (m^2)	Vessel shape	L/D ratio	Ignition	P_v (barg)	P_{red} (barg)	A_v,expt (m^2)	Source
5.00	0.029	0.6	Cylinder	2.32	Centre	0.103	0.19	0.034	P.F.Thorne et al
5.0	0.03	0.61	Vessel	1.54	Center	4.8	10.9	0.055	Cousin & Cottons(1951).
5.0	0.03	0.61	Vessel	1.54	Center	29.0	32.1	0.055	Cousin & Cottons(1951).
5.0	0.03	0.61	Vessel	1.54	Center	33.1	33.1	0.055	Cousin & Cottons(1951).
5.0	0.03	0.61	Vessel	1.54	Center	16.4	20.7	0.055	Initial pressure is 45 psig(3.10 barg)
5.0	0.03	0.61	Vessel	1.54	Center	16.6	23.4	0.021	Cousin & Cottons(1951).
5.0	0.03	0.61	Vessel	1.54	Center	4.8	15.2	0.021	Cousin & Cottons(1951).
5.0	0.03	0.61	Vessel	1.54	Center	24.8	30.3	0.021	Cousin & Cottons(1951).
5.0	0.03	0.61	Vessel	1.54	Center	4.8	22.1	0.011	Cousin & Cottons(1951).
5.0	0.03	0.61	Vessel	1.54	Center	18.6	29	0.011	Cousin & Cottons(1951).
5.0	0.03	0.61	Vessel	1.54	Center	29	33.1	0.011	Cousin & Cottons(1951).
5.0	0.085	1.134	Tank	2.3	Centre	1.5	2.8	0.0417	Cousin & Cottons(1951)
5.0	0.085	1.134	Tank	2.3	Centre	8.0	8.6	0.0417	Cousin & Cottons(1951)
5.0	0.085	1.134	Tank	2.3	Centre	10.6	11.9	0.0417	Cousin & Cottons(1951)
5.0	0.085	1.134	Tank	2.3	Centre	0.0	0.1	0.0408	Cousin & Cottons(1951)
5.0	0.085	1.134	Tank	2.3	Centre	1.8	5.3	0.0161	Cousin & Cottons(1951)
5.0	0.085	1.134	Tank	2.3	Centre	7.0	8.9	0.0161	Cousin & Cottons(1951)
5.0	0.085	1.134	Tank	2.3	Centre	12.7	13.3	0.0161	Cousin & Cottons(1951)

5.0	0.085	1.134	Tank	2.3	Centre	0.0	1.1	0.0135	Cousin & Cottons(1951)
5.0	0.085	1.134	Tank	2.3	Centre	1.6	6.5	0.0080	Cousin & Cottons(1951)
5.0	0.085	1.134	Tank	2.3	Centre	5.9	9.6	0.0080	Cousin & Cottons(1951)
5.0	0.085	1.134	Tank	2.3	Centre	11.9	13.7	0.0080	Cousin & Cottons(1951)
5.0	0.085	1.134	Tank	2.3	Centre	0.0	2.0	0.0060	Cousin & Cottons(1951)
5.0	0.085	1.134	Tank	2.3	Centre	0.0	2.7	0.0036	Cousin & Cottons(1951)
5.20	0.17	1.9	Rec	1.5	Centre	0.03	0.021	0.07	R.G.Zalosh
5.20	0.17	1.9	Rec	1.5	Centre	0.03	0.028	0.07	R.G.Zalosh
5.20	0.17	1.9	Rec	1.5	Centre	0.03	1.55	0.0525	R.G.Zalosh
5.20	0.17	1.9	Rec	1.5	Centre	0.03	0.048	0.0525	R.G.Zalosh
5.20	0.17	1.9	Rec	1.5	Centre	0.03	1.32	0.0438	R.G.Zalosh
5.20	0.17	1.9	Rec	1.5	Centre	0.03	0.0276	0.035	R.G.Zalosh
5.20	0.17	1.9	Rec	1.5	Centre	0.03	0.344	0.0314	R.G.Zalosh
4.60	0.17	1.9	Rec	1.5	Centre	0.03	0.028	0.0314	R.G.Zalosh
5.20	0.17	1.9	Rec	1.5	Centre	0.03	0.037	0.0314	R.G.Zalosh
5.20	0.17	1.9	Rec	1.5	Centre	0.03	0.28	0.0314	R.G.Zalosh
5.20	0.17	1.9	Rec	1.5	Centre	0.03	0.66	0.0314	R.G.Zalosh
5.20	0.17	1.9	Rec	1.5	Centre	0.03	1.61	0.0263	R.G.Zalosh
6.00	0.17	1.9	Rec	1.5	Centre	0.03	0.03	0.0175	R.G.Zalosh
5.20	0.18	2.0	Rec	1	Centre	0.03	0.055	0.0525	R.G.Zalosh
5.20	0.18	2.0	Rec	1	Centre	0.03	0.26	0.0525	R.G.Zalosh
5.20	0.18	2.0	Rec	1	Centre	0.03	0.05	0.0525	R.G.Zalosh
5.20	0.18	2.0	Rec	1	Centre	0.03	0.74	0.0525	R.G.Zalosh
5.20	0.18	2.0	Rec	1	Centre	0.03	0.05	0.0525	R.G.Zalosh
5.20	0.18	2.0	Rec	1	Centre	0.03	0.052	0.0525	R.G.Zalosh
5.20	0.18	2.0	Rec	1	Centre	0.03	0.052	0.0525	R.G.Zalosh
5.20	0.18	2.0	Rec	1	Centre	0.03	0.083	0.035	R.G.Zalosh
5.20	0.18	2.0	Rec	1	Centre	0.03	0.57	0.035	R.G.Zalosh
4.80	0.65	2.9	Cylinder	1.198	Centre	0.86	2.75	0.0993	P.F.Thorne et al
4.80	0.65	2.9	Cylinder	1.198	Centre	0.86	3.14	0.073	P.F.Thorne et al
4.80	0.65	2.9	Cylinder	1.198	Centre	0.72	5.59	0.0324	P.F.Thorne et al
4.80	0.65	2.9	Cylinder	1.198	Centre	0.65	5.22	0.0182	P.F.Thorne et al
4.80	0.65	2.9	Cylinder	1.198	Centre	0.65	5.31	0.0182	P.F.Thorne et al
4.5	0.77	5.0	Cubic	1	Center	0.049	0.01	0.52	Yao
4.5	0.77	5.0	Cubic	1	Center	0.0686	0.021	0.52	Yao
4.5	0.77	5.0	Cubic	1	Center	0.0196	0.0103	0.52	Yao
4.5	0.77	5.0	Cubic	1	Center	0.0924	0.0171	0.29	Yao
4.5	0.77	5.0	Cubic	1	Center	0.063	0.035	0.29	Yao

4.5	0.77	5.0	Cubic	1	Center	0.06	0.03	0.20	Yao
4.5	0.77	5.0	Cubic	1	Center	0.1096	0.175	0.16	Yao
4.5	0.77	5.0	Cubic	1	Center	0.1078	0.1848	0.16	Yao
5.00	0.77	5.0	Cubic	1	Centre	0.0	0.05	0.29	Razus et al
4.5	0.79	5.7	Cylinder	1	Center	0.0938	0.0595	0.85	Yao
4.5	0.79	6.7	Cylinder	1	Center	0.043	0.0203	0.85	Yao
4.5	0.79	4.7	Cylinder	1	Center	0.04	0.056	0.59	Yao
4.5	0.79	6.7	Cylinder	1	Center	0.0	0.0175	0.53	Yao
4.5	0.79	6.7	Cylinder	1	Center	0.0	0.0286	0.30	Yao
4.5	0.79	6.7	Cylinder	1	Center	0.0	0.04	0.21	Yao
4.5	0.79	4.7	Cylinder	1	Center	0.108	0.08	0.06	Yao
4.00	1.0	6.0	Cubic	1	Centre	0.1	0.14	0.6	Razus et al
4.00	1.0	6.0	Cubic	1	Centre	0.1	0.32	0.4	Razus et al
4.02	1.0	1.0	Cubic	1	Centre	0.1	0.28	0.38	Bartknecht data(Abb.2.219)
5.00	1.0	4.8	Sphere	1	Centre	0.2	0.3	0.355	Donat
5.00	1.0	4.8	Sphere	1	Centre	0.1	0.3	0.31	C.Donat(1973)
5.00	1.0	4.8	Sphere	1	Centre	0.22	0.52	0.301	C.Donat(1973)
5.00	1.0	4.8	Sphere	1	Centre	0.2	0.5	0.3	Donat
4.02	1.0	1.0	Cubic	1	Centre	0.5	0.5	0.3	Bartknecht(Abb.2.224(b))
4.02	1.0	1.0	Cubic	1	Centre	0.2	0.5	0.259	Bartknecht(Abb.2.224(b))
5.00	1.0	4.8	Sphere	1	Centre	0.1	0.5	0.25	C.Donat(1973)
4.02	1.0	1.0	Cubic	1	Centre	0.1	0.5	0.24	Bartknecht(Abb.2.224(b))
4.02	1.0	1.0	Cubic	1	Centre	0.1	0.55	0.23	Bartknecht data(Abb.2.219)
5.00	1.0	4.8	Sphere	1	Centre	0.2	1	0.21	Donat
4.00	1.0	6.0	Cubic	1	Centre	0.1	1	0.2	Razus et al
5.00	1.0	4.8	Sphere	1	Centre	0.5	1	0.195	C.Donat(1973)
5.00	1.0	4.8	Sphere	1	Centre	0.52	1.02	0.195	Donat
4.02	1.0	1.0	Cubic	1	Centre	0.1	0.92	0.18	Bartknecht data(Abb.2.219)
5.00	1.0	4.8	Sphere	1	Centre	0.1	1	0.15	C.Donat(1973)
5.00	1.0	4.8	Sphere	1	Centre	0.2	1.5	0.145	Donat
5.00	1.0	4.8	Sphere	1	Centre	0.22	1.52	0.145	C.Donat(1973)
4.02	1.0	1.0	Cubic	1	Centre	0.5	2.0	0.1	Bartknecht(Abb.2.224(b))
5.00	1.0	4.8	Sphere	1	Centre	0.5	1.5	0.12	C.Donat(1973)
4.02	1.0	1.0	Cubic	1	Centre	0.2	2.0	0.1	Bartknecht(Abb.2.224(b))
4.02	1.0	1.0	Cubic	1	Centre	0.1	1.9	0.1	Bartknecht data(Abb.2.219)
4.02	1.0	1.0	Cubic	1	Centre	0.1	2.0	0.1	Bartknecht(Abb.2.224(b))
5.00	1.0	4.8	Sphere	1	Centre	0.2	2	0.095	Donat
5.00	1.0	4.8	Sphere	1	Centre	0.1	1.5	0.09	C.Donat(1973)

5.00	1.0	4.8	Sphere	1	Centre	0.5	2	0.085	C.Donat(1973)
5.00	1.0	4.8	Sphere	1	Centre	0.2	2.5	0.07	Donat
5.00	1.0	4.8	Sphere	1	Centre	0.5	2.5	0.065	C.Donat(1973)
5.00	1.0	4.8	Sphere	1	Centre	0.52	2.52	0.065	C.Donat(1973)
4.02	1.0	6.0	Cubic	1	Centre	0.1	2.4	0.055	Bartknecht data(Abb.2.219)
5.00	1.0	4.8	Sphere	1	Centre	0.1	2	0.045	C.Donat(1973)
5.00	1.7	6.9	Sphere	1	Centre	0.52	1.02	0.308	Harris and Briscoe
5.00	1.7	6.9	Sphere	1	Centre	0.22	1.52	0.156	Harris and Briscoe
5.00	1.7	6.9	Sphere	1	Centre	0.22	0.52	0.139	Harris and Briscoe
5.00	1.7	6.9	Sphere	1	Centre	0.52	2.52	0.139	Harris and Briscoe
4.02	2.0	9.5	Cubic	1	Centre	0.1	0.29	0.33	Bartknecht(Abb.2.224(b))
4.02	2.0	9.5	Cubic	1	Centre	0.1	0.55	0.26	Bartknecht(Abb.2.224(b))
4.02	2.0	9.5	Cubic	1	Centre	0.1	1	0.17	Bartknecht(Abb.2.224(b))
4.02	2.0	9.5	Cubic	1	Centre	0.1	2.1	0.12	Bartknecht(Abb.2.224(b))
5.00	2.6	11.91	Rec	2.3	Centre	0.096	0.199	0.56	R.DeGood/K.Chatrathi: Study of factors affecting Pred.
5.00	2.6	11.91	Rec	2.3	Bottom	0.103	0.159	0.56	R.DeGood/K.Chatrathi: Study of factors affecting Pred.
5.00	2.6	11.91	Rec	2.3	Centre	0.1	0.235	0.56	R.DeGood/K.Chatrathi: Study of factors affecting Pred.
5.00	2.6	11.91	Rec	2.3	Centre	0.1	0.314	0.56	R.DeGood/K.Chatrathi: Study of factors affecting Pred.
5.00	2.6	11.91	Rec	2.3	Centre	0.086	0.185	0.56	R.DeGood/K.Chatrathi: Study of factors affecting Pred.
5.00	2.6	11.91	Rec	2.3	Centre	0.086	0.311	0.56	R.DeGood/K.Chatrathi: Study of factors affecting Pred.
5.00	2.6	11.91	Rec	2.3	Centre	0.086	0.385	0.56	R.DeGood/K.Chatrathi: Study of factors affecting Pred.
5.00	2.6	11.91	Rec	2.3	Bottom	0.086	1.007	0.56	R.DeGood/K.Chatrathi: Study of factors affecting Pred.
5.00	2.6	11.91	Rec	2.3	Centre	0.086	0.215	0.56	R.DeGood/K.Chatrathi: Study of factors affecting Pred.
5.00	2.6	11.91	Rec	2.3	Centre	0.93	0.241	0.56	R.DeGood/K.Chatrathi: Study of factors affecting Pred.
5.00	2.6	11.91	Rec	2.3	Centre	0.9	0.172	0.56	R.DeGood/K.Chatrathi: Study of factors affecting Pred.
5.00	2.6	11.91	Rec	2.3	Centre	0.9	0.16	0.56	R.DeGood/K.Chatrathi: Study of factors affecting Pred.
5.00	2.6	11.91	Rec	2.3	Centre	0.9	0.144	0.56	R.DeGood/K.Chatrathi: Study of

									factors affecting Pred.
5.00	2.6	11.91	Rec	2.3	Centre	0.103	0.262	0.56	R.DeGood/K.Chatrathi: Study of factors affecting Pred.
5.00	2.6	11.91	Rec	2.3	Centre	0.103	0.26	0.56	R.DeGood/K.Chatrathi: Study of factors affecting Pred.
5.00	2.6	11.91	Rec	2.3	Centre	0.103	0.156	0.56	R.DeGood/K.Chatrathi: Study of factors affecting Pred.
5.00	2.6	11.91	Rec	2.3	Centre	0.11	0.246	0.56	R.DeGood/K.Chatrathi: Study of factors affecting Pred.
5.00	2.6	11.91	Rec	2.3	Centre	0.103	0.334	0.56	R.DeGood/K.Chatrathi: Study of factors affecting Pred.
5.00	2.6	11.91	Rec	2.3	Centre	0.103	0.325	0.56	R.DeGood/K.Chatrathi: Study of factors affecting Pred.
5.00	2.6	11.91	Rec	2.3	Centre	0.103	0.29	0.56	R.DeGood/K.Chatrathi: Study of factors affecting Pred.
5.00	2.6	11.91	Rec	2.3	Centre	0.103	0.441	0.56	R.DeGood/K.Chatrathi: Study of factors affecting Pred.
5.00	2.6	11.91	Rec	2.3	Centre	0.103	0.282	0.54	R.DeGood/K.Chatrathi: Study of factors affecting Pred.
5.00	2.6	11.91	Rec	2.3	Centre	0.1	0.3	0.54	R.DeGood/K.Chatrathi: Study of factors affecting Pred.
5.00	10.0	22.5	Sphere	1	Centre	0.2	0.3	2.18	C.Donat(1973)
5.00	10.0	22.5	Sphere	1	Centre	0.1	0.3	2.1	C.Donat(1973)
5.00	10.0	22.5	Sphere	1	Centre	0.2	0.5	1.7	C.Donat(1973)
5.00	10.0	22.5	Sphere	1	Centre	0.1	0.5	1.5	C.Donat(1973)
5.00	10.0	22.5	Sphere	1	Centre	0.5	1	1.21	C.Donat(1973)
5.00	10.0	22.5	Sphere	1	Centre	0.2	1	1.07	C.Donat(1973)
5.00	10.0	22.5	Sphere	1	Centre	0.1	1	0.8	C.Donat(1973)
5.00	10.0	22.5	Sphere	1	Centre	0.5	1.5	0.79	C.Donat(1973)
5.00	10.0	22.5	Sphere	1	Centre	0.2	1.5	0.74	C.Donat(1973)
5.00	10.0	22.5	Sphere	1	Centre	0.5	2	0.56	C.Donat(1973)
5.00	10.0	22.5	Sphere	1	Centre	0.1	1.5	0.55	C.Donat(1973)
4.02	10.0	4.6	Cubic	1	Centre	0.1	0.24	0.49	Bartknecht(Abb.2.219)
5.00	10.0	22.5	Sphere	1	Centre	0.2	2	0.47	C.Donat(1973)
5.00	10.0	22.5	Sphere	1	Centre	0.5	2.5	0.42	C.Donat(1973)
5.00	10.0	22.5	Sphere	1	Centre	0.1	2	0.4	C.Donat(1973)
4.02	10.0	4.6	Cubic	1	Centre	0.1	0.32	0.4	Bartknecht(Abb.2.219)
4.02	10.0	4.6	Cubic	1	Centre	0.1	0.39	0.38	Bartknecht(Abb.2.219)
5.00	10.0	22.5	Sphere	1	Centre	0.2	2.5	0.37	C.Donat(1973)

4.02	10.0	4.6	Cubic	1	Centre	0.1	0.52	0.32	Bartknecht(Abb.2.219)
5.00	10.0	22.5	Sphere	1	Centre	0.1	2.5	0.3	C.Donat(1973)
4.02	10.0	4.6	Cubic	1	Centre	0.1	0.69	0.28	Bartknecht(Abb.2.219)
4.02	10.0	4.6	Cubic	1	Centre	0.1	0.9	0.2	Bartknecht(Abb.2.219)
4.02	10.0	4.6	Cubic	1	Centre	0.1	2.8	0.1	Bartknecht(Abb.2.219)
4.02	10.0	27.8	Cubic	1	Centre	0.1	2.9	0.052	Bartknecht(Abb.2.219)
4.05	11.0	28.3	Cylinder	1.25	Rear	0.05	0.09	1.36	P.F.Thorne et al
4.3	22.0	47.11	Cubic	1	Centre	0.02	0.025	7.85	P.F.Thorne et al
4.3	22.0	47.11	Cubic	1	Centre	0.04	0.2	3.41	P.F.Thorne et al
4.3	22.0	47.11	Cubic	1	Centre	0.09	0.19	3.41	P.F.Thorne et al
4.3	22.0	47.11	Cubic	1	Centre	0.04	0.2	1.96	P.F.Thorne et al
4.3	22.0	47.11	Cubic	1	Centre	0.05	0.25	1.96	P.F.Thorne et al
4.3	22.0	47.11	Cubic	1	Centre	0.2	0.55	1.96	P.F.Thorne et al
4.5	25.0	53.9	Rec	`1	Center	0.0	0.025	7.70	Bromma(Sweden)
6.0	25.0	53.9	Rec	`1	Center	0.0	0.01	6.20	Bromma(Sweden)
5.00	30.0	46.7	Sphere	1	Centre	0.5	0.5	3.48	C.Donat(1973)
5.00	30.0	46.7	Sphere	1	Centre	0.1	0.3	3	C.Donat(1973)
5.00	30.0	46.7	Sphere	1	Centre	0.2	0.3	2.7	C.Donat(1973)
5.00	30.0	46.7	Sphere	1	Centre	0.1	0.5	2.25	C.Donat(1973)
5.00	30.0	46.7	Sphere	1	Centre	0.2	0.5	2.03	C.Donat(1973)
5.00	30.0	46.7	Sphere	1	Centre	0.5	1	1.88	C.Donat(1973)
5.00	30.0	46.7	Sphere	1	Centre	0.1	1	1.5	C.Donat(1973)
5.00	30.0	46.7	Sphere	1	Centre	0.2	1	1.35	C.Donat(1973)
5.00	30.0	46.7	Sphere	1	Centre	0.5	1.5	1.35	C.Donat(1973)
5.00	30.0	46.7	Sphere	1	Centre	0.2	1.5	0.97	C.Donat(1973)
5.00	30.0	46.7	Sphere	1	Centre	0.5	2	0.97	C.Donat(1973)
5.00	30.0	46.7	Sphere	1	Centre	0.1	1.5	0.9	C.Donat(1973)
5.00	30.0	46.7	Sphere	1	Centre	0.2	2	0.72	C.Donat(1973)
5.00	30.0	46.7	Sphere	1	Centre	0.5	2.5	0.72	C.Donat(1973)
5.00	30.0	46.7	Sphere	1	Centre	0.1	2	0.6	C.Donat(1973)
5.00	30.0	46.7	Sphere	1	Centre	0.2	2.5	0.53	C.Donat(1973)
5.00	30.0	46.7	Sphere	1	Centre	0.1	2.5	0.45	C.Donat(1973)
4.02	30.0	9.7	Cubic	1	Centre	0.1	0.2	0.4	Bartknecht(Abb.2.219)
4.02	30.0	9.7	Cubic	1	Centre	0.1	0.6	0.2	Bartknecht(Abb.2.219)
4.02	30.0	9.7	Cubic	1	Centre	0.1	0.75	0.175	Bartknecht(Abb.2.219)
4.02	30.0	9.7	Cubic	1	Centre	0.1	1.1	0.17	Bartknecht(Abb.2.219)
4.02	30.0	9.7	Cubic	1	Centre	0.1	1.7	0.1	Bartknecht(Abb.2.219)
4.02	30.0	57.9	Cubic	1	Centre	0.1	2.1	0.069	Bartknecht(Abb.2.219)

4.45	30.4	61.4	Rec	0.363	Centre	0.4	0.7	0.58	P.F.Thorne et al
4.3	35.0	67.4	Rec	1.14	Center	0.1	0.18	2.1	Solberg et al(1980)
4.3	35.0	67.4	Rec	1.14	Front	0.1	0.19	2.1	Solberg et al(1980)
4.3	35.0	67.4	Rec	1.14	Rear	0.1	0.1	2.1	Solberg et al(1980)
4.3	35.0	67.4	Rec	1.14	Front	0.1	0.3	1.6	Solberg et al(1980)
4.3	35.0	67.4	Rec	1.14	Rear	0.1	0.18	1.6	Solberg et al(1980)
4.3	35.0	67.4	Rec	1.14	Center	0.1	1.05	1.1	Solberg et al(1980)
4.3	35.0	67.4	Rec	1.14	Front	0.1	0.71	1.1	Solberg et al(1980)
4.3	35.0	67.4	Rec	1.14	Rear	0.1	0.72	1.1	Solberg et al(1980)
5.00	35.0	67.4	Rec	1.415	Near vent	0.0	0.75	1	P.F.Thorne et al
5.00	35.0	67.4	Rec	1.415	Centre	0.0	1.37	1	P.F.Thorne et al
4.3	35.0	67.4	Rec	1.14	Center	0.1	1.55	0.53	Solberg et al(1980)
4.3	35.0	67.4	Rec	1.14	Front	0.1	1.68	0.53	Solberg et al(1980)
6.0	40.0	73.7	Rec	`1	Center	0.0137	0.0299	8.48	Bromma(Sweden)
6.0	40.0	73.7	Rec	`1	Center	0.0196	0.0295	8.48	Bromma(Sweden)
5.0	60.0	74.2	Sphere	1	Centre	0.5	0.5	5.22	C.Donat(1973)
5.0	60.0	74.2	Sphere	1	Centre	0.1	0.3	4.8	C.Donat(1973)
5.0	60.0	74.2	Sphere	1	Centre	0.2	0.5	3.76	C.Donat(1973)
5.0	60.0	74.2	Sphere	1	Centre	0.1	0.5	3	C.Donat(1973)
5.0	60.0	74.2	Sphere	1	Centre	0.5	1	2.22	C.Donat(1973)
5.0	60.0	74.2	Sphere	1	Centre	0.1	1	1.2	C.Donat(1973)
4.0	60.0	92.0	Cubic	1	Centre	0.1	1.5	0.69	Bartknecht(Abb.2.219)
4.0	60.0	92.0	Cubic	1	Centre	0.1	0.4	0.22	Bartknecht(Abb.2.219)
4.0	60.0	92.0	Cubic	1	Centre	0.1	0.6	0.18	Bartknecht(Abb.2.219)
4.0	60.0	92.0	Cubic	1	Centre	0.1	1	0.14	Bartknecht(Abb.2.219)
6.0	70.0	107.0	Rec	`1	center	0.0	0.0785	12.31	Bromma(Sweden)
6.0	70.0	107.0	Rec	1	Center	0.0196	0.0348	12.31	Bromma(Sweden)
6.0	200.0	215.5	Rec	`1	Center	0.055	0.06	30.81	Bromma(Sweden)
6.0	200.0	215.5	Rec	`1	Center	0.0294	0.033	30.81	Bromma(Sweden)
6.0	200.0	215.5	Rec	`1	Center	0.0098	0.018	30.81	Bromma(Sweden)
6.0	200.0	215.5	Rec	`1	Center	0.029	0.0343	30.81	Bromma(Sweden)
6.0	200.0	215.5	Rec	`1	Center	0.0549	0.0588	30.81	Bromma(Sweden)
6.0	200.0	215.5	Rec	`1	Center	0.049	0.0637	18.19	Bromma(Sweden)
4.0	203.8	218.2	Rec	1.951	centre	0.0	0.03	21.58	P.F.Thorne et al
4.0	203.8	218.2	Rec	1.951	Centre	0.0	0.06	17.3	P.F.Thorne et al
5.2	0.17	1.9	Rec	0.3	Center	0.036	0.046	0.05	Zalosh

5.2	0.17	1.9	Rec	0.3	Center	0.036	0.0386	0.05	Zalosh
5.2	0.17	1.9	Rec	0.3	Center	0.036	0.05	0.05	Zalosh
5.2	0.17	1.9	Rec	0.3	Center	0.036	0.069	0.05	Zalosh
5.2	0.17	1.9	Rec	0.3	Center	0.036	0.0365	0.08	Zalosh
5.2	0.17	1.9	Rec	0.3	Center	0.036	0.0552	0.08	Zalosh
5.2	0.17	1.9	Rec	0.3	Center	0.036	0.0621	0.08	Zalosh
5.2	0.17	1.9	Rec	0.3	Center	0.036	0.0483	0.10	Zalosh
5.2	0.17	1.9	Rec	0.3	Center	0.036	0.0552	0.10	Zalosh
5.2	0.18	2.0	Rec	1	Center	0.036	0.103	0.05	Zalosh
5.2	0.18	2.0	Rec	1	Center	0.036	0.089	0.05	Zalosh
5.2	0.18	2.0	Rec	1	Center	0.036	0.0965	0.05	Zalosh
5.2	0.18	2.0	Rec	1	Center	0.036	0.0965	0.05	Zalosh
5.2	0.18	2.0	Rec	1	Center	0.036	0.112	0.05	Zalosh
5.2	0.18	2.0	Rec	1	Center	0.036	0.112	0.05	Zalosh
5.2	0.18	2.0	Rec	1	Center	0.036	0.104	0.05	Zalosh
5.2	0.18	2.0	Rec	1	Center	0.036	0.0896	0.03	Zalosh
5.2	0.18	2.0	Rec	2	Center	0.036	0.105	0.03	Zalosh
5.0	81.00	117.9	Rec	1	Center	0.014	0.049	18.72	Howards and Karabinis.
5.0	81.00	117.9	Rec	2	Center	0.0252	0.0462	18.72	Howards and Karabinis.
5.0	81.00	117.9	Rec	3	Center	0.0735	0.1008	18.72	Howards and Karabinis.
5.0	81.00	117.9	Rec	4	Center	0.0351	0.0469	18.72	Howards and Karabinis.
5.0	81.00	117.9	Rec	5	Center	0.0336	0.035	18.72	Howards and Karabinis.
5.0	81.00	117.9	Rec	6	Center	0.0136	0.043	18.72	Howards and Karabinis.
5.0	81.00	117.9	Rec	7	Center	0.0189	0.0679	18.72	Howards and Karabinis.
5.0	81.00	117.9	Rec	8	Center	0.014	0.021	18.72	Howards and Karabinis.

Town gas/ air

Conc. (vol %)	V (m^3)	As (m^2)	Vessel shape	L/D ratio	Ignition	P_v (barg)	P_{red} (barg)	Av,expt (m^2)	Sources
25	0.23	2.25	Rec	1	Center	0.0008	0.11	0.37	Cubbage & Simmonds
25	0.23	2.25	Rec	1	Center	0.0008	0.12	0.37	Cubbage & Simmonds
25	0.23	2.25	Rec	1	Center	0.001	0.13	0.37	Cubbage & Simmonds
25	0.23	2.25	Rec	1	Center	0.0014	0.14	0.37	Cubbage & Simmonds
25	0.23	2.25	Rec	1	Center	0.0012	0.13	0.3	Cubbage & Simmonds
25	0.23	2.25	Rec	1	Center	0.00096	0.14	0.3	Cubbage & Simmonds
25	0.23	2.25	Rec	1	Center	0.0017	0.18	0.3	Cubbage & Simmonds
25	0.23	2.25	Rec	1	Center	0.0017	0.19	0.3	Cubbage & Simmonds

25	0.23	2.25	Rec	1	Center	0.00072	0.16	0.21	Cubbage & Simmonds
25	0.23	2.25	Rec	1	Center	0.001	0.22	0.21	Cubbage & Simmonds
25	0.23	2.25	Rec	1	Center	0.0013	0.26	0.21	Cubbage & Simmonds
25	0.23	2.25	Rec	1	Center	0.00019	0.08	0.092	Cubbage & Simmonds
25	0.23	2.25	Rec	1	Center	0.00072	0.19	0.092	Cubbage & Simmonds
25	0.23	2.25	Rec	1	Center	0.00086	0.24	0.092	Cubbage & Simmonds
10	1.47	7.76	Rec	4.48	Center	0.0005	0.01	0.84	Cubbage & Simmonds
15	1.47	7.76	Rec	4.48	Center	0.0005	0.029	0.84	Cubbage & Simmonds
20	1.47	7.76	Rec	4.48	Center	0.0005	0.069	0.84	Cubbage & Simmonds
25	1.47	7.76	Rec	4.48	Center	0.0005	0.096	0.84	Cubbage & Simmonds
30	1.47	7.76	Rec	4.48	Center	0.0005	0.041	0.84	Cubbage & Simmonds
35	1.47	7.76	Rec	4.48	Center	0.0005	0.022	0.84	Cubbage & Simmonds
25	1.47	7.76	Rec	4.48	Center	0.0008	0.069	0.84	Cubbage & Simmonds
25	1.47	7.76	Rec	4.48	Center	0.001	0.131	0.84	Cubbage & Simmonds
25	1.47	7.76	Rec	4.48	Center	0.003	0.248	0.84	Cubbage & Simmonds
25	2.8	11.92	Rec	1.3	Center	0.0012	0.076	1.24	Cubbage & Simmonds
25	2.8	11.92	Rec	1.3	Center	0.0013	0.083	1.24	Cubbage & Simmonds
25	2.8	11.92	Rec	1.3	Center	0.0026	0.141	1.24	Cubbage & Simmonds
25	2.8	11.92	Rec	1.3	Center	0.0005	0.041	1.14	Cubbage & Simmonds
25	2.8	11.92	Rec	1.3	Center	0.0014	0.086	1.14	Cubbage & Simmonds
25	2.8	11.92	Rec	1.3	Center	0.002	0.124	1.14	Cubbage & Simmonds
25	2.8	11.92	Rec	1.3	Center	0.0026	0.15	1.14	Cubbage & Simmonds
25	2.8	11.92	Rec	1.3	Center	0.0006	0.076	0.84	Cubbage & Simmonds
25	2.8	11.92	Rec	1.3	Center	0.001	0.103	0.84	Cubbage & Simmonds
25	2.8	11.92	Rec	1.3	Center	0.002	0.14	0.84	Cubbage & Simmonds
25	2.8	11.92	Rec	1.3	Center	0.0006	0.034	0.62	Cubbage & Simmonds
25	2.8	11.92	Rec	1.3	Center	0.0007	0.09	0.62	Cubbage & Simmonds
25	2.8	11.92	Rec	1.3	Center	0.0014	0.17	0.62	Cubbage & Simmonds
25	2.8	11.92	Rec	1.3	Center	0.0007	0.103	0.47	Cubbage & Simmonds
25	2.8	11.92	Rec	1.3	Center	0.001	0.124	0.47	Cubbage & Simmonds
25	2.8	11.92	Rec	1.3	Center	0.001	0.131	0.47	Cubbage & Simmonds
25	2.8	11.92	Rec	1.3	Center	0.0012	0.152	0.47	Cubbage & Simmonds
25	1.0	6.00	Cubic	1	Center	0.1	0.5	0.26	Bartknecht(Abb.2.224(b))
25	1.0	6.00	Cubic	1	Center	0.2	0.5	0.28	Bartknecht(Abb.2.224(b))
25	1.0	6.00	Cubic	1	Center	0.5	0.5	0.32	Bartknecht(Abb.2.224(b))
25	1.0	6.00	Cubic	1	Center	0.1	2.0	0.12	Bartknecht(Abb.2.224(b))
25	1.0	6.00	Cubic	1	Center	0.2	2.0	0.13	Bartknecht(Abb.2.224(b))
25	1.0	6.00	Cubic	1	Center	0.5	2.0	0.15	Bartknecht(Abb.2.224(b))

Hydrogen/air

Conc. (vol %)	V (m^3)	A_s (m^2)	Vessel shape	L/D ratio	Ignition	P_v (barg)	P_{red} (barg)	$A_{v,expt}$ (m^2)	Sources
40	0.03	0.004	Vessel	1.54	Centre	4.8	22.1	0.011	Cousin & Cottons. Initial P= 45 psig (3.1 barg)
40	0.03	0.004	Vessel	1.54	Centre	11.2	25.5	0.011	Cousin & Cottons. Initial P= 45 psig (3.1 barg)
40	0.03	0.004	Vessel	1.54	Centre	25.5	28.5	0.011	Cousin & Cottons. Initial P= 45 psig (3.1 barg)
40	0.03	0.004	Vessel	1.54	Centre	4.8	12.4	0.021	Cousin & Cottons. Initial P= 45 psig (3.1 barg)
40	0.03	0.004	Vessel	1.54	Centre	11.7	22.1	0.021	Cousin & Cottons. Initial P= 45 psig (3.1 barg)
40	0.03	0.004	Vessel	1.54	Centre	24.1	27.6	0.021	Cousin & Cottons. Initial P= 45 psig (3.1 barg)
40	0.03	0.004	Vessel	1.54	Centre	4.8	11.7	0.055	Cousin & Cottons. Initial P= 45 psig (3.1 barg)
40	0.03	0.004	Vessel	1.54	Centre	11	16.5	0.055	Cousin & Cottons. Initial P= 45 psig (3.1 barg)
40	0.03	0.004	Vessel	1.54	Centre	22.8	25.4	0.055	Cousin & Cottons. Initial P= 45 psig (3.1 barg)
40	0.03	0.004	Vessel	1.54	Centre	28.3	28.8	0.055	Cousin & Cottons. Initial P= 45 psig (3.1 barg)
40	0.085	1.134	Tank	2.3	Centre	0	3.1	0.14	Cousin & Cottons. Initial P= 0 psig
40	0.085	1.134	Tank	2.3	Centre	0	2.6	0.26	Cousin & Cottons. Initial P= 0 psig
40	0.085	1.134	Tank	2.3	Centre	0	1.2	0.72	Cousin & Cottons. Initial P= 0 psig
40	0.085	1.134	Tank	2.3	Centre	1.6	9.2	0.008	Cousin & Cottons. Initial P= 15 psig
40	0.085	1.134	Tank	2.3	Centre	5.9	11	0.008	Cousin & Cottons .Initial P= 15 psig
40	0.085	1.134	Tank	2.3	Centre	11.9	12.6	0.008	Cousin & Cottons. Initial P= 15 psig
40	0.085	1.134	Tank	2.3	Centre	1.8	7.9	0.0161	Cousin & Cottons. Initial P= 15 psig
40	0.085	1.134	Tank	2.3	Centre	7	10.3	0.0161	Cousin & Cottons. Initial P= 15

									psig
40	0.085	1.134	Tank	2.3	Centre	11	11.9	0.0161	Cousin & Cottons. Initial P= 15 psig
40	0.085	1.134	Tank	3.3	Centre	1.5	4.6	0.0417	Cousin & Cottons. Initial P= 15 psig
40	0.085	1.134	Tank	4.3	Centre	6.5	8.2	0.0417	Cousin & Cottons. Initial P= 15 psig
40	0.085	1.134	Tank	5.3	Centre	10.6	11.8	0.0417	Cousin & Cottons. Initial P= 15 psig
40	0.22	0.5	Drum	1.41	Centre	0	4.5	0.09	Cousin & Cottons. Initial P= 0 psig
40	0.22	0.5	Drum	1.41	Centre	0	2.8	0.23	Cousin & Cottons. Initial P= 0 psig
40	0.22	0.5	Drum	1.41	Centre	0	1.5	0.43	Cousin & Cottons. Initial P= 0 psig
40	0.4	5.8	Pipe	22.1	Centre	0	4	0.05	Cousin & Cottons. Initial P= 0 psig
40	0.4	5.8	Pipe	22.1	Centre	0	2.9	0.09	Cousin & Cottons. Initial P= 0 psig
40	0.4	5.8	Pipe	22.1	Centre	0	2.6	0.2	Cousin & Cottons. Initial P= 0 psig
40	0.4	5.8	Pipe	22.1	Centre	0	1.3	0.69	Cousin & Cottons. Initial P= 0 psig
NR	0.95	4.673	Cylinder	2	Centre	0.075	1.3	0.2	Razus et al
NR	0.95	4.673	Cylinder	2	Centre	0.135	0.4	0.3	Razus et al
20	1	6	Cubic	1	Centre	0.1	0.5	0.34	Bartknecht(Abb.2.224(b))
20	1	6	Cubic	1	Centre	0.1	2	0.159	Bartknecht(Abb.2.224(b))
20	1	6	Cubic	1	Centre	0.2	0.5	0.36	Bartknecht(Abb.2.224(b))
20	1	6	Cubic	1	Centre	0.2	2	0.16	Bartknecht(Abb.2.224(b))
20	1	6	Cubic	1	Centre	0.5	2	0.18	Bartknecht(Abb.2.224(b))
10	6.37	16.6	Sphere	1	Centre	0.1	0.3	0.64	R.K.Kumar et.al.(1989)
10	6.37	16.6	Sphere	1	Centre	0.1	0.9	0.2	R.K.Kumar et.al.(1989)
10	6.37	16.6	Sphere	1	Centre	0.1	1.7	0.071	R.K.Kumar et.al.(1989)
20	6.37	16.6	Sphere	1	Centre	0.1	3.4	0.64	R.K.Kumar et.al.(1989)
20	6.37	16.6	Sphere	1	Centre	0.1	4.2	0.2	R.K.Kumar et.al.(1989)
20	6.37	16.6	Sphere	1	Centre	0.1	4.8	0.071	R.K.Kumar et.al.(1989)
12	6.37	16.6	Sphere	1	Centre	0.1	1	0.64	R.K.Kumar et.al.(1989)
12	6.37	16.6	Sphere	1	Centre	0.1	2	0.2	R.K.Kumar et.al.(1989)
12	6.37	16.6	Sphere	1	Centre	0.1	2.5	0.071	R.K.Kumar et.al.(1989)

14	6.37	16.6	Sphere	1	Centre	0.1	1.6	0.64	R.K.Kumar et.al.(1989)
14	6.37	16.6	Sphere	1	Centre	0.1	4.9	0.2	R.K.Kumar et.al.(1989)
14	6.37	16.6	Sphere	1	Centre	0.1	5.1	0.071	R.K.Kumar et.al.(1989)
16	6.37	16.6	Sphere	1	Centre	0.1	2.2	0.64	R.K.Kumar et.al.(1989)
16	6.37	16.6	Sphere	1	Centre	0.1	3.4	0.2	R.K.Kumar et.al.(1989)
16	6.37	16.6	Sphere	1	Centre	0.1	3.6	0.071	R.K.Kumar et.al.(1989)
18	6.37	16.6	Sphere	1	Centre	0.1	3	0.64	R.K.Kumar et.al.(1989)
18	6.37	16.6	Sphere	1	Centre	0.1	3.9	0.2	R.K.Kumar et.al.(1989)
18	6.37	16.6	Sphere	1	Centre	0.1	5.1	0.071	R.K.Kumar et.al.(1989)

Acetone/air

Conc. (vol %)	V (m3)	As (m2)	Vessel shape	P_v (barg)	Pred (barg)	$A_{v,exp}$ $_t(m^2)$	Sources
3.0	0.008	0.19	Sphere	0	1.17	0.00013	Proceeding of 1st & 2nd Sym. On Comb.Inst.
3.0	0.008	0.19	Sphere	0	0.48	0.00051	Proceeding of 1st & 2nd Sym. On Comb.Inst.
3.0	0.008	0.19	Sphere	0	0.14	0.002	Proceeding of 1st & 2nd Sym. On Comb.Inst.
3.0	0.008	0.19	Sphere	0	0.034	0.0082	Proceeding of 1st & 2nd Sym. On Comb.Inst.
3.0	0.008	0.19	Sphere	0	0.034	0.018	Proceeding of 1st & 2nd Sym. On Comb.Inst.
3.0	0.008	0.19	Sphere	0	0.034	0.031	Proceeding of 1st & 2nd Sym. On Comb.Inst.
3.0	0.008	0.19	Sphere	0	0.034	0.0016	Proceeding of 1st & 2nd Sym. On Comb.Inst.
3.0	0.008	0.19	Sphere	0	0.034	0.0036	Proceeding of 1st & 2nd Sym. On Comb.Inst.
4.0	0.008	0.19	Sphere	0	2.76	0.00013	Proceeding of 1st & 2nd Sym. On Comb.Inst.
4.0	0.008	0.19	Sphere	0	1.38	0.00051	Proceeding of 1st & 2nd Sym. On Comb.Inst.
4.0	0.008	0.19	Sphere	0	0.48	0.002	Proceeding of 1st & 2nd Sym. On Comb.Inst.
4.0	0.008	0.19	Sphere	0	0.17	0.0082	Proceeding of 1st & 2nd Sym. On Comb.Inst.
4.0	0.008	0.19	Sphere	0	0.034	0.018	Proceeding of 1st & 2nd Sym. On Comb.Inst.
4.0	0.008	0.19	Sphere	0	0.034	0.031	Proceeding of 1st & 2nd Sym. On Comb.Inst.
4.0	0.008	0.19	Sphere	0	0.17	0.0016	Proceeding of 1st & 2nd Sym. On Comb.Inst.
4.0	0.008	0.19	Sphere	0	0.034	0.0036	Proceeding of 1st & 2nd Sym. On Comb.Inst.
5.0	0.008	0.19	Sphere	0	4.48	0.00013	Proceeding of 1st & 2nd Sym. On Comb.Inst.
5.0	0.008	0.19	Sphere	0	3.1	0.00051	Proceeding of 1st & 2nd Sym. On Comb.Inst.
5.0	0.008	0.19	Sphere	0	0.83	0.002	Proceeding of 1st & 2nd Sym. On Comb.Inst.
5.0	0.008	0.19	Sphere	0	0.28	0.0082	Proceeding of 1st & 2nd Sym. On Comb.Inst.
5.0	0.008	0.19	Sphere	0	0.1	0.018	Proceeding of 1st & 2nd Sym. On Comb.Inst.
5.0	0.008	0.19	Sphere	0	0.0344	0.031	Proceeding of 1st & 2nd Sym. On Comb.Inst.
5.0	0.008	0.19	Sphere	0	0.34	0.0016	Proceeding of 1st & 2nd Sym. On Comb.Inst.
5.0	0.008	0.19	Sphere	0	0.1	0.0036	Proceeding of 1st & 2nd Sym. On Comb.Inst.

5.5	0.008	0.19	Sphere	0	3.38	0.00051	Proceeding of 1st & 2nd Sym. On Comb.Inst.
5.5	0.008	0.19	Sphere	0	0.97	0.002	Proceeding of 1st & 2nd Sym. On Comb.Inst.
5.5	0.008	0.19	Sphere	0	0.31	0.0082	Proceeding of 1st & 2nd Sym. On Comb.Inst.
5.5	0.008	0.19	Sphere	0	0.14	0.018	Proceeding of 1st & 2nd Sym. On Comb.Inst.
5.5	0.008	0.19	Sphere	0	0.034	0.031	Proceeding of 1st & 2nd Sym. On Comb.Inst.
5.5	0.008	0.19	Sphere	0	0.41	0.0016	Proceeding of 1st & 2nd Sym. On Comb.Inst.
5.5	0.008	0.19	Sphere	0	0.14	0.0036	Proceeding of 1st & 2nd Sym. On Comb.Inst.
4.907	0.022	0.374	Cylinder	0.100	0.680	0.680	Molkov et al: Venting of Deflagration: HC-air and H2-air system
4.907	2.000	7.677	Cylinder	0.150	2.270	2.270	Molkov et al: Venting of Deflagration: HC-air and H2-air system
4.907	0.022	0.374	Cylinder	0.200	0.500	0.500	Molkov et al: Venting of Deflagration: HC-air and H2-air system
4.907	0.022	0.374	Cylinder	0.230	0.480	0.480	Molkov et al: Venting of Deflagration: HC-air and H2-air system
4.907	2.000	7.677	Cylinder	0.750	3.170	3.170	Molkov et al: Venting of Deflagration: HC-air and H2-air system
4.907	0.760	4.027	Cylinder	1.900	3.300	3.300	Molkov et al: Venting of Deflagration: HC-air and H2-air system
5.5	8.056	0.319	Cylinder	0.000	0.070	3.653	G.A Lunn
5.5	8.056	0.319	Cylinder	0.000	0.100	2.734	G.A Lunn
5.5	8.056	0.319	Cylinder	0.000	0.175	1.818	G.A Lunn
5.5	8.056	0.319	Cylinder	0.000	0.315	0.909	G.A Lunn

Table A.2 List of published experimental data for vented gas explosion with a presence of duct pipe.

Fuel	L (m)	D (m)	L/d	A_v (m^2)	V (m^3)	P_v (bar)	P_{red} (bar)	Ignition	P_{red} without vent (bar)	Souces
Propane/air	0.6	0.016	37.5	0.000201	0.00366	1.01	2.46	End	Not measured	Ponizy and Leyer
4.0%	0.6	0.021	28.6	0.000346	0.00366	1.01	2.18	End	Not measured	Ponizy and Leyer
	0.6	0.036	16.7	0.001017	0.00366	1.01	2.28	End	Not measured	Ponizy and Leyer
	1.1	0.016	68.8	0.000201	0.00366	1.01	2.81	End	Not measured	Ponizy and Leyer
	1.1	0.021	52.4	0.000346	0.00366	1.01	2.46	End	Not measured	Ponizy and Leyer
	1.1	0.036	30.6	0.001017	0.00366	1.01	2.93	End	Not measured	Ponizy and Leyer
	2.6	0.016	162.5	0.000201	0.00366	1.01	2.93	End	Not measured	Ponizy and Leyer
	2.6	0.021	123.8	0.000346	0.00366	1.01	2.56	End	Not measured	Ponizy and Leyer
	2.6	0.036	72.2	0.001017	0.00366	1.01	2.93	End	Not measured	Ponizy and Leyer
	1.7	0.036	47.2	0.001017	0.00366	1.01	3.02	Central	Not measured	Ponizy and Leyer
	1.7	0.036	47.2	0.001017	0.00366	1.31	3.17	Central	Not measured	Ponizy and Leyer
	1.7	0.036	47.2	0.001017	0.00366	1.92	3.67	Central	Not measured	Ponizy and Leyer
	1.7	0.036	47.2	0.001017	0.00366	3.31	4.38	Central	Not measured	Ponizy and Leyer
	1.7	0.036	47.2	0.001017	0.00366	1.01	2.77	End	Not measured	Ponizy and Leyer
	1.7	0.036	47.2	0.001017	0.00366	1.33	2.89	End	Not measured	Ponizy and Leyer
	1.7	0.036	47.2	0.001017	0.00366	1.84	2.82	End	Not measured	Ponizy and Leyer

Propane/air											
5.0%	1	0.8446	1.2	0.56	2.6	1.11	1.2	Central	1.212	DeGood Chartrathi	a
	2	0.8446	2.4	0.56	2.6	1.11	1.32	Central	1.212	DeGood Chartrathi	a
	3	0.8446	3.6	0.56	2.6	1.11	1.4	Central	1.212	DeGood Chartrathi	a
	3	0.8446	3.6	0.56	2.6	1.11	2.02	Bottom	1.16	DeGood Chartrathi	a
Acetone/air											
5.0%	25	0.5	50.0	0.19625	10	1.11	5.11	Central	Not measured	Molkov (1993)	
	25	0.5	50.0	0.19625	10	1.06	3.81	Central	Not measured	Molkov (1993)	
	4	0.2	20.0	0.0314	2	1.16	5.31	Central	Not measured	Molkov (1993)	
	10	0.2	50.0	0.0314	2	1.16	6.21	Central	Not measured	Molkov (1993)	
	10	0.38	26.3	0.113354	2	1.16	3.16	Central	Not measured	Molkov (1993)	
	1.83	0.05	36.6	0.001963	0.027	1.21	6.01	Central	1.7	Molkov (1993)	
	2.35	0.05	47.0	0.001963	0.027	1.26	5.41	Central	1.7	Molkov (1993)	
	2.35	0.05	47.0	0.001963	0.027	1.26	4.51	Central	Not measured	Molkov (1993)	
	2.35	0.05	47.0	0.001963	0.027	2.66	2.91	Central	Not measured	Molkov (1993)	
	1.83	0.05	36.6	0.001963	0.027	2.43	5.41	Central	Not measured	Molkov (1993)	
Methane/air											
9.5%	0.11	0.1129	1.0	0.01	0.00564	1.01	1.11	Not available	1.092	McCann (1985)	
	0.3	0.1129	2.7	0.01	0.00564	1.01	1.2	Not available	1.092	McCann (1985)	
	0.52	0.1129	4.6	0.01	0.00564	1.01	1.18	Not available	1.092	McCann (1985)	